



**HAL**  
open science

# Thermal and thermo-mechanical behavior of energy piles

Van-Tri Nguyen

► **To cite this version:**

Van-Tri Nguyen. Thermal and thermo-mechanical behavior of energy piles. Géotechnique. Université Paris-Est, 2017. English. NNT : 2017PESC1160 . tel-02003027

**HAL Id: tel-02003027**

**<https://pastel.hal.science/tel-02003027>**

Submitted on 1 Feb 2019

**HAL** is a multi-disciplinary open access archive for the deposit and dissemination of scientific research documents, whether they are published or not. The documents may come from teaching and research institutions in France or abroad, or from public or private research centers.

L'archive ouverte pluridisciplinaire **HAL**, est destinée au dépôt et à la diffusion de documents scientifiques de niveau recherche, publiés ou non, émanant des établissements d'enseignement et de recherche français ou étrangers, des laboratoires publics ou privés.

# UNIVERSITÉ — — PARIS-EST

Thèse présentée pour obtenir le grade de

**Docteur de l'Université Paris-Est**

discipline : Géotechnique

par

**Van Tri NGUYEN**

**Thermal and thermo-mechanical behavior of energy piles**

*Soutenue le 18 Décembre 2017 devant le jury composé de :*

Mme. Farimah MASROURI	Université de Lorraine	Rapporteur
M. Frédéric COLLIN	Université de Liège	Rapporteur
M. Panagiotis KOTRONIS	Ecole Centrale de Nantes	Examineur
M. Sébastien BURLON	IFSTTAR	Examineur
M. Jean-Michel PEREIRA	École des Ponts ParisTech	Co-directeur de thèse
M. Anh Minh TANG	École des Ponts ParisTech	Directeur de thèse



# ACKNOWLEDGEMENTS

Working at CERMES is really a good opportunity for me. Experimental researches are based on good ideas and equipment setup process, and success is the result of the cooperation among persons who involved in the project.

First of all, I would like to extend my sincere gratitude and appreciation to my adviser, Dr. Anh Minh Tang, for this continuous support, leadership, constructive guidance, and friendship.

I am grateful to my thesis co-advisor, Prof. Jean-Michel Pereira, for being friendly, supportive and guidance that he has given me during my years at ENPC.

I would like to express my gratitude to the members of my examination committee, Prof. Farimah MASROURI, Prof. Frédéric COLLIN, Prof. Panagiotis KOTRONIS and Dr. Sébastien BURLON for all of their guidance through his process,

I would like to thank all the persons in Technical Team for helping me to set up experiments, your discussions and administrative support.

I thank to all of my excellent colleagues in “Equipe CERMES”, my deep appreciation for the support you have offered me on my project.

I want to express my appreciation and thanks to all my Vietnamese friends at ENPC, Manh Huy Tran, Van Giai Tran, Vinh Phuc Tran, ... for your kind help and encouragement.

Finally, I would especially like to thank my family, my parents, my wife and my sons, which has been extremely supportive of me throughout my study period.



## **ABSTRACT**

The thermal and thermo-mechanical behavior of energy piles is investigated by various approaches: laboratory measurement on small soil samples, physical modeling on small-scale pile, experiments on real-scale pile, and analytical/numerical calculations. First, the thermal conductivity of unsaturated loess is measured simultaneously with moisture content and suction. The results show a unique relationship between thermal conductivity and moisture content during a wetting/drying cycle while a clear hysteresis loop can be observed on the relationship between thermal conductivity and suction. Second, thermal tests are performed on a full-scale experimental energy pile to observe heat transfer at the real scale. Third, an analytical solution is proposed to simulate conductive heat transfer from an energy pile to the surrounding soil during heating. The above-mentioned tasks related to the thermal behavior are then completed by studies on the thermo-mechanical behavior of energy piles. On one hand, experiments are performed on a small-scale pile installed either in dry sand or in saturated clay. Thirty thermal cycles, representing thirty annual cycles, are applied to the pile under various constant pile head loads. The results show irreversible pile head settlement with thermal cycles; the settlement is higher at higher pile head load. In addition, the irreversible thermal settlement is the most significant during the first cycles; it becomes negligible at high number of cycles. On the other hand, the experimental work with small-scale pile is completed with numerical calculations by using the finite element method. This approach is first validated with the results on small-scale pile prior to be used to predict the results of full-scale experiments.

**Keywords:** energy pile, physical model, full-scale experiment, conductive heat transfer, thermo-mechanical behavior, finite element method, analytical method, thermal conductivity.

## RESUME

Le comportement thermique et thermo-mécanique des pieux énergétiques est étudié par plusieurs approches : mesures au laboratoire sur des éprouvettes de sol, modélisation physique en modèle réduit, expérimentations sur pieu en vraie grandeur, et calculs numériques/analytiques. D'abord, la conductivité thermique d'un loess à l'état non saturé est mesurée en fonction de la teneur en eau et de la succion. Les résultats montrent une relation univoque entre la conductivité thermique et la teneur en eau pendant un cycle d'humidification/séchage alors qu'une boucle d'hystérésis est observée pour la relation entre la conductivité thermique et la succion. Deuxièmement, des essais thermiques sont réalisés sur un pieu énergétique expérimental en vraie grandeur pour étudier le transfert thermique à l'échelle réelle. Troisièmement, une solution analytique est proposée pour simuler la conduction thermique d'un pieu énergétique vers le sol environnant pendant un chauffage. Les tâches mentionnées ci-dessus concernant le comportement thermique sont ensuite complétées par des études sur le comportement thermo-mécanique des pieux énergétiques. D'un côté, des expérimentations sont réalisées sur un modèle réduit de pieu installé dans un sable sec ou dans une argile saturée. Trente cycles thermiques, représentant trente cycles annuels, sont appliqués au pieu sous différentes charges axiales en tête. Les résultats montrent un tassement irréversible avec les cycles thermiques ; ce tassement est plus important sous une charge axiale plus grande. De plus, le tassement est plus marqué pendant les premiers cycles thermiques et devient négligeable pour les cycles suivants. De l'autre côté, les travaux expérimentaux sur le modèle réduit de pieu sont complétés par les calculs numériques utilisant la méthode des éléments finis. Cette approche est d'abord validée avec les résultats obtenus sur le pieu modèle avant d'être utilisée pour prédire les résultats des expérimentations en vraie grandeur.

**Mots-clés :** pieu énergétique, modèle physique, expérimentation en vraie grandeur, transfert thermique conductif, comportement thermo-mécanique, méthode des éléments finis, méthode analytique, conductivité thermique.

## LIST OF PUBLICATIONS

- **Nguyen, V.T.**, Tang, A.M., Pereira, J.M. 2017. Long-term thermo-mechanical behavior of energy pile in dry sand. *Acta Geotechnica*, 12(4):pp.729-737.
- **Nguyen, V.T.**, Heindl, H., Pereira, J.M., Tang, A.M., and Frost, D., 2017. Water retention and thermal conductivity of a natural unsaturated loess. *Géotechnique Letters*, 7(4): pp.286-291.
- **Nguyen, V.T.**, Tang, A.M., Pereira, J.M. 2017. An analytical analysis of conductive heat transfer for energy pile. *Energy and Buildings*, (under review).
- **Nguyen, V.T.**, Wu, N., Gan, Y., Pereira, J.M., and Tang, A.M., 2017. Long term behavior of energy pile in saturated clay: numerical and physical modeling. *Environmental Geotechnics*, (under review).
- **Nguyen, V.T.**, Tang, A.M., Pereira, J.M. 2017. Long term thermo-mechanical behavior of energy pile in dry sand. *Proceeding of the first International Conference on Geomechanics and Geoenvironmental Engineering* (ISBN 978-0-6480147-5-1).
- **Nguyen, V.T.**, Tang, A.M., Pereira, J.M. 2017. Effect of thermal cycles on the mechanical behavior of a model energy pile in dry sand. *The 6<sup>th</sup> International Conference on Coupled THMC Processes in Geosystem* (Paris, France).
- Tang, A.M., Yavari, N., **Nguyen, V.T.**, Hassen G., Pereira, J.M., Vasilescu, R., Kotronis, P., and Housse, P.J, 2017. Experimental studies on the thermo-mechanical behavior of energy piles in clay. *Proceeding of the 19<sup>th</sup> International Conference on Soil Mechanics and Geotechnical Engineering* (Seoul, Korea), pp. 3467-3470.
- **Nguyen, V.T.**, Tang, A.M., Pereira, J.M., 2017. Conductive heat transfer analysis of energy pile. *Proceeding of the 4<sup>th</sup> Congrès International de Géotechnique-Ouvrages-Structures* (HCM city, Vietnam), pp. 685-693.
- **Nguyen, V.T.**, Tang, A.M., Pereira, J.M., 2016. Thermo-mechanical behavior of energy pile in physical model. *The 4<sup>th</sup> International Conference on Advances in Mining and Tunneling* (Hanoi, Vietnam).
- **Nguyen, V.T.**, Tang, A.M., Pereira, J.M., 2016. Thermo-mechanical behavior of small-scale energy pile in dry sand. *Proceeding of the 1<sup>st</sup> International Conference on Energy Geotechnics* (Kiel, Germany), pp. 577-584.
- **Nguyen, V.T.**, Tang, A.M., Pereira, J.M. 2015. Thermo-active geostructures in tropical climate countries. *Proceeding of the 3<sup>th</sup> International Conference CIGOS "New challenges in Civil Engineering"* (Paris, France), pp. 037-59.
- **Nguyen, V.T.**, Tang, A.M., Pereira, J.M 2014. Challenges to the use of Energy geostructures in Vietnam. *The 3<sup>th</sup> International Conference on Advances in Mining and Tunneling* (Hanoi, Vietnam).



# TABLE OF CONTENT

- GENERAL INTRODUCTION ..... 1
  
- PART I. HEAT TRANSFER IN THE CONTEXT OF ENERGY PILE..... 4**
  
- CHAPTER 1: LITERATURE REVIEW ..... 5
  - 1.1 Introduction ..... 5
  - 1.2 Thermo-active geostructure ..... 9
    - 1.2.1 GSHP system operation ..... 9*
    - 1.2.2 Ground temperature and soil thermal properties ..... 10*
  - 1.3 Heat conduction analysis ..... 12
  - 1.4 Conclusions ..... 21
  
- CHAPTER 2: THERMAL CONDUCTIVITY OF UNSATURATED SOIL ..... 23
  - 2.1 Introduction ..... 23
  - 2.2 Material and experimental method ..... 23
  - 2.3 Results and discussion ..... 25
  - 2.4. Conclusions ..... 31
  
- CHAPTER 3: FULL-SCALE EXPERIMENT ON ENERGY PILE..... 32
  - 3.1 Introduction ..... 32
  - 3.2 Site description ..... 32
  - 3.3 Description of the experimental setup ..... 38
    - 3.3.1 Pile installation ..... 38*
    - 3.3.2 System for controlling pile temperature and monitoring soil/pile temperatures..... 41*
  - 3.4 Experimental results ..... 42
  - 3.5 Conclusions ..... 47
  
- CHAPTER 4: CONDUCTIVE HEAT TRANSFER ANALYSIS..... 48
  - 4.1 Introduction ..... 48
  - 4.2 Proposed analytical model..... 50
  - 4.3 Validation of the proposed solution..... 56
  - 4.4 Conclusions ..... 59

**PART II. THERMO-MECHANICAL BEHAVIOR OF ENERGY PILE ..... 60**

CHAPTER 5: REVIEW OF THE THERMO-MECHANICAL BEHAVIOR ON ENERGY PILE ..... 61

5.1 Introduction ..... 61

5.2 Experimental studies on the thermo-mechanical behavior of energy pile..... 61

5.3 Numerical studies on the thermo-mechanical behavior of pile ..... 67

5.4 Behavior of soil and soil-pile interface under thermal loading ..... 72

5.5 Long term behavior of geothermal pile ..... 73

5.6 Conclusions.....81

CHAPTER 6: INVESTIGATION ON THE LONG-TERM BEHAVIOR BY PHYSICAL MODELING..... 82

6.1 Introduction ..... 82

6.2 Description of the pile model ..... 82

6.3 Experiments in dry sand ..... 84

6.3.1 Experiment setup ..... 84

6.3.2 Short-term behavior ..... 86

6.3.3 Long-term behavior ..... 95

6.3.4 Discussion ..... 103

6.4 Experiments in saturated clay ..... 105

6.4.1 Experiment setup ..... 105

6.4.2 Test program ..... 109

6.4.3 Creep behavior (test A1)..... 110

6.4.4 Thermo-mechanical behavior ..... 110

6.4.5 Discussion ..... 115

6.5 Conclusions ..... 115

CHAPTER 7: NUMERICAL MODELING OF ENERGY PILE..... 117

7.1 Introduction ..... 117

7.2 Fully coupled analysis of Thermo-Hydro-Mechanical behavior..... 117

7.2.1 *Water mass balance* ..... 118

7.2.2 *Mechanical behaviour* ..... 119

7.2.3 *Energy balance* ..... 120

7.3 Two dimensions finite element model..... 120

7.3.1 *Modeling of small-scale energy pile in saturated clay* ..... 120

7.3.2 <i>Modeling of full-scale energy piles: a case study</i> .....	130
7.4 Conclusion .....	141
GENERAL CONCLUSIONS AND PERSPECTIVES .....	143
REFERENCES .....	145



# LIST OF NOTATIONS

$A$	$m^2$	Cross section
$A_{eq}$	$m^2$	Equivalent cross section
$COP$	-	Coefficient of Performance of the Ground source heat pump system
$c$	$J/(kg \cdot ^\circ C)$	Specific heat capacity
$C_g$	-	Convective heat transfer coefficient
$EER$	-	Energy Efficiency Ratio of the Ground source heat pump system
$e$	-	Void ratio
$Ei(x)$	-	Exponential integral function
$E$	MPa	Young's modulus
$F_0$	-	Fourier number
$G$ -function	-	Temperature response function of borehole/pile
$H$	m	Length of heat source
$H_\alpha$	-	Hankel function
$I_0$	-	Modified Bessel function of the first kind of zero order
$I_p$	-	Plasticity index
$J_i$	-	Bessel function of the first kind of order $i$
$J_w$	$kg/(s \cdot m^2)$	Mass flux of water in liquid phase
$J_v$	$kg/(s \cdot m^2)$	Mass flux of water in vapour phase
$K_0$	-	Modified Bessel function of the second kind of zero order
$k$	m/s	Permeability
$m$	kg	Mass of material
$N_c$	-	Number of cycles
$O(x^3)$	-	Infinitesimal function
$P$	N	Force
$q$	W/m	Inlet or outlet heat flow rate per unit length
$Q$	W	Heat flow rate
$r$	m	Distance from heat source center
$r_b$	m	Diameter of borehole/pile
$r_M$	m	Distance from point M
$r_e$	m	Pipe radius
$R_b$	K/W	Thermal resistance of borehole/pile
$R, \theta$	-	Cylindrical coordinates
$s$	-	Complex variable
$SPF$	-	Seasonal Performance Factor of the Ground source heat pump system
$S_r$	%	Degree of saturation
$\Delta T$	$^\circ C$	The change of temperature

$T_b$	°C	Temperature of borehole/pile
$T_s$	°C	Temperature of soil
$T_0$	°C	Initial temperature
$t$	s	Elapsed time
$t_s$	s	Time at which the heat exchange reaches its steady state
$v$	m <sup>3</sup> /h	Water flow rate
$w$	%	Water content
$w_p$	-	Plastic limit
$w_l$	-	Liquid limit
$z$	m	Depth
$Y_i$	-	Bessel function of the second kind of order $i$
$\alpha$	m <sup>2</sup> /s	Thermal diffusivity
$\alpha_c$	-	Coefficient of thermal expansion/contraction
$\alpha_n$	-	Creep rate
$\lambda$	W/(m.K)	Thermal conductivity
$\lambda_p$	W/(m.K)	Thermal conductivity of pile
$\lambda_s$	W/(m.K)	Thermal conductivity of soil
$\beta$	-	Exponent of convergence rate
$(R, \theta, \varphi)$	-	Spherical coordinate
$\gamma$	-	Euler's constant (=0.5772)
$\rho$	kg/m <sup>3</sup>	Density of the material
$\rho_d$	kg/m <sup>3</sup>	Dry unit mass
$\mu$	-	Dynamic viscosity
$\delta$	mm	Displacement
$\chi$	-	Experimental factor that depends on degree of saturation
$\varepsilon_T$	-	Thermal strain
$\varepsilon_M$	-	Mechanical strain
$\underline{\underline{\sigma}}$	-	Total stress tensor
$\underline{\underline{\sigma'}}$	-	Effective stress tensor
$\underline{\underline{m}}$	-	The identity tensor
$\underline{\underline{M}}$	-	Strain-stress tensor
$\underline{\underline{\varepsilon}}$	-	Total strain tensor
$\underline{\underline{\varepsilon_T}}$	-	Thermal strain tensor
$\underline{\underline{B_{DT}}}$	-	Tensor of drained linear thermal expansion coefficient
$\underline{\underline{J_c}}$	-	Heat flux conduction

## GENERAL INTRODUCTION

Energy piles, or heat exchanger piles, have a dual function: *(i)* providing support for overhead structures as conventional foundation; *(ii)* exchanging heat with the ground for the purpose of heating and/or cooling the building. Energy piles have been used in some European countries during the last two decades. This technique has gained encouraging efficiencies in the use of renewable energy in modern cities and contributed to the reduction of CO<sub>2</sub> emission. However, the implementation of this technique is not homogeneous across countries due to the lack of design standards.

Many studies have been performed in the recent years to investigate on the thermo-mechanical behavior of energy piles. The results evidenced the effects of temperature change on the pile-soil interaction and the mobilized resistance of piles.

Besides, the energetic efficiency of energy pile also depends on the heat exchange condition between pile and surrounding soil. Heat exchange rate of energy pile is strongly affected by the saturation conditions of the surrounding soil. Heat transfer models between pile and surrounding soil have been developed and these models focus on the most relevant process: heat conduction.

Although the large amount of research work done has helped shed light on the problem, more questions have been raised. In the present work, the thermo-mechanical behavior of energy pile in the long-term performance is investigated. In addition, identification of heat transfer problems in heterogeneous media is also considered in this work. Studying the effect of saturated conditions of soil on the thermal parameters will help to better assess the heat transfer between pile and surrounding soil.

The thesis is organized in two parts. The first part focuses on heat transfer in the context of energy pile and includes four chapters.

The Chapter 1 focuses on the literature review. The functioning of thermo-active geostructure is first presented. Secondly, heat conduction models used for heat exchanger borehole and energy pile are analyzed.

The Chapter 2 presents an experimental study on thermal conductivity of unsaturated soil. Suction, volumetric moisture content and thermal conductivity of a loess sample were measured simultaneously during the application of wetting/drying cycles to the sample. The results show a one-to-one approximately linear relationship between thermal conductivity and volumetric moisture content during the wetting/drying paths.

The Chapter 3 presents a full-scale experiment performed with an experimental energy pile. The pile was subjected to heating, cooling and recovery phases respectively. The results show that, with a heat flow rate of 60 W/m, temperature of pile increased from 12°C to 35 °C after 23 days of heating and decreased to 7 °C after one week of cooling.

In the Chapter 4, an analytical solution of the heat transfer in surrounding soil is proposed based on the approach of Laplace transform method and also the contour integral method. The analytical solution is then validated by numerical model and the field test data. This solution allows the determination of heat transfer of energy pile in the very short time scales (minutes or less).

The second part of the thesis focuses on the thermo-mechanical behavior of energy pile and includes three chapters (chapters 5 – 7).

A review on the thermo-mechanical behavior of energy pile is shown in the Chapter 5. Existing studies on energy piles are first analyzed following the approaches used: experimental or numerical. Afterward, the behavior of soil and soil-pile interface under thermo-mechanical loading is presented. Finally, the long-term behavior of energy pile is shown.

The Chapter 6 presents an investigation into the long-term behavior of energy pile by using physical modeling. A small-scale model was used to study the thermo-mechanical behavior of energy pile. Experiments have been done in dry sand and then in saturated clay. Thirty heating/cooling cycles (representing thirty years of seasonal temperature changes of energy piles) were applied to the model pile under various constant pile head loads ranging from 0 to 60 % of pile resistance. The results show that thermal cycles under constant head load induce irreversible settlement of the pile head and that the irreversible settlement of the pile head is higher at a higher pile head load.

The Chapter 7 presents the numerical modeling of thermo-mechanical behavior of energy pile in clay. The finite element method (Plaxis 2D) was used with coupled thermo-hydro-mechanical analysis. The experiments performed with small-scale pile in clay were first simulated, allowing to better interpreting the experiments and validating the numerical method. Secondly, a full-scale thermo-mechanical experiment was simulated. The results will be used as a scoping calculation for future experiments that will be performed on the full-scale experimental energy piles.

# **PART I. HEAT TRANSFER IN THE CONTEXT OF ENERGY PILE**

## CHAPTER 1: LITERATURE REVIEW

### 1.1 Introduction

A thermo-active geostructure is a system that consists of conventional geostructures (*e.g.* pile foundation, tunnel lining, diaphragm wall, *etc.*) and individual or several pipe circuits (high-density polyethylene pipes, HDPE) in order to enable heat exchange with the surrounding ground (Fig. 1.1). This system is a part of the Ground Source Heat Pump (GSHP) System that is usually used for heating and/or cooling purpose for buildings (Fig. 1.2). Generally, the GSHP system includes a heat pump and two circuits, and operates like a reverse refrigerator. A heat pump is a machine or device that transfers heat from one location to another using mechanical work. The two circuits, the first one embedded in the geostructures and the second one embedded in structures on the surface, are connected via a heat pump.

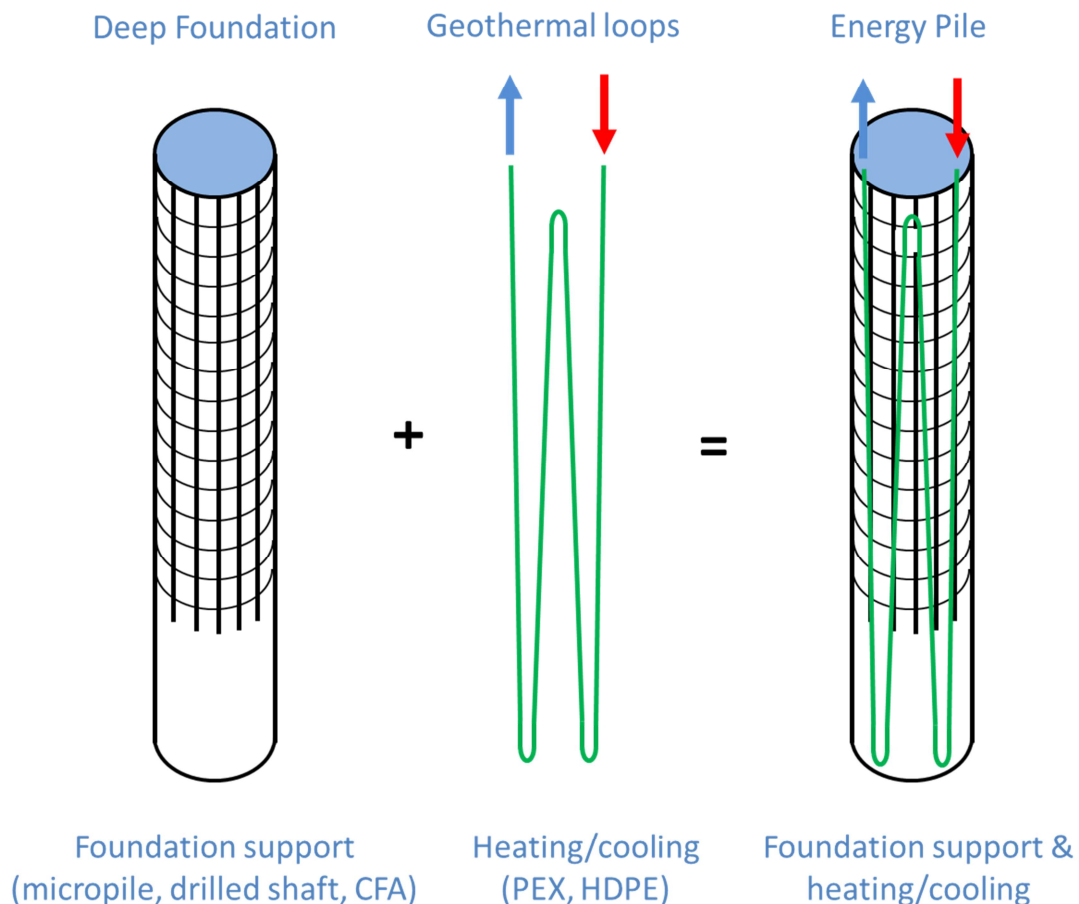


Fig. 1.1 Energy piles - dual purpose elements (after Olgun & McCartney, 2014)

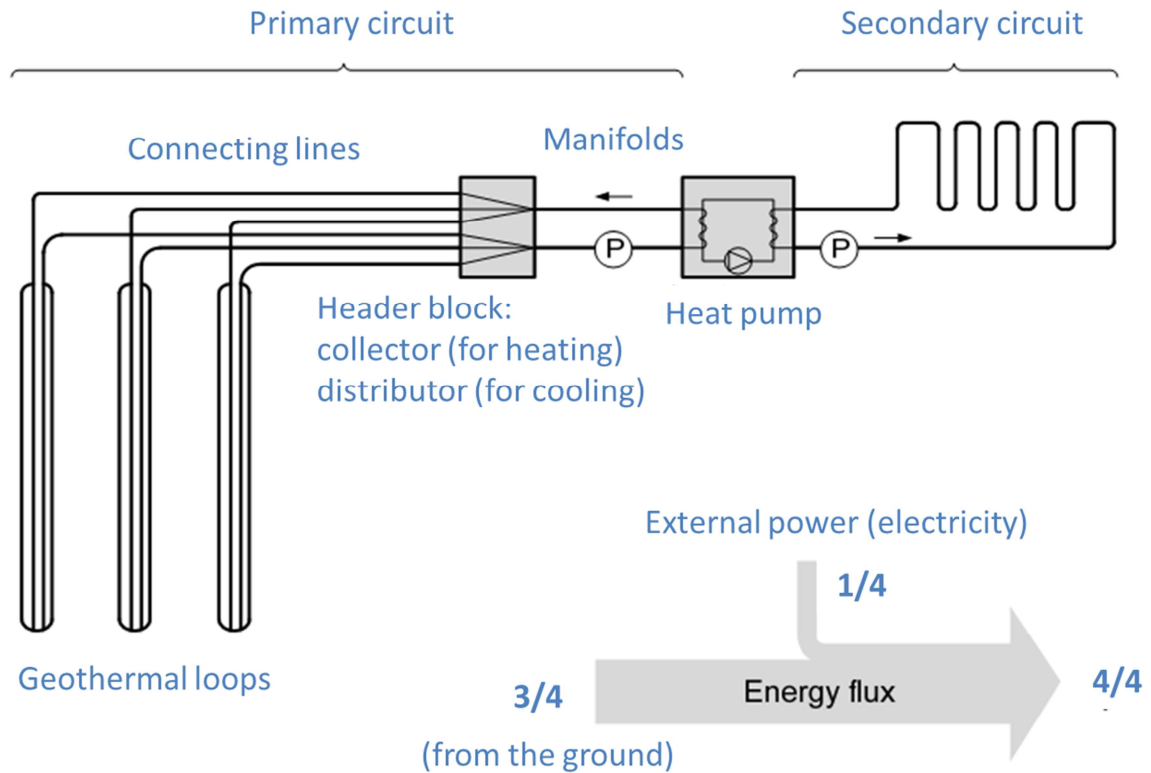


Fig. 1.2 Scheme of a Ground Source Heat Pump with energy piles and method of energy delivery (after Brandl, 2006)

Thermo-active geostructures have been used since the 1980s in Europe as pile foundations and then as diaphragm walls in Austria. This technology provides a clean energy source contributing to reduce the conventional energy sources consumption and reduce CO<sub>2</sub> emissions. Currently, this system has been widely applied in developed countries (*e.g.* USA, Austria, Switzerland, England, Australia, *etc.*) in the forms of energy pile foundations, energy tunnels, heat exchanger anchors for thermo-active tunnels, energy walls, *etc.* Table 1.1 shows that numerous thermo-active geostructures have been built since 2000. Most of them are located in Europe and other developed countries, which are characterized by a temperate climate. Among these structures, energy pile is the most used. Besides, energy tunnels, heat exchanger anchors and other geostructures tend to be used more widely in the exploitation of ground source heat, as some leading energy projects in Austria, the UK, Switzerland and Germany (Franzius & Pralle, 2011; Mimouni *et al.*, 2013; Nicholson *et al.*, 2013; Payne *et al.*, 2010). As shown in Table 1.1, energy obtained from thermo-active geostructures contributes significantly to the total energy for air conditioning of buildings. The GSHP system associated to thermo-active geostructures can thus be used to supply energy independently for buildings, and/or combined with other conventional energy sources.

Table 1.1 Examples of thermo-active geostructures applications

Project	Country	Year	Energy (MWh/year)	Type of structure	Climate	References
Dock Midfield Zurich Terminal Airport	Switzerland	2003	1170 (cooling)	306 energy piles	Temperate	(Adam & Markiewicz, 2009; Pahud & Hubbuch, 2007)
Condominium Great morning, Einsiedeln	Switzerland	2011	262 (heating)	270 energy piles	Temperate	Data from www.enercret.com
Lainzer Tunnel	Austria	2004	-	Heat exchanger anchors, Tunnel lining	Temperate	(Adam & Markiewicz, 2009; Pahud & Hubbuch, 2007;)
Uniqa Tower, Vienna	Austria	2003	468 (heating) 530 (cooling)	7800 m <sup>2</sup> diaphragm wall	Temperate	Data from www.enercret.com
Vienna Metro line	Austria	-	-	Energy lining elements, floor slabs	Temperate	(Franzius & Pralle, 2011)
Hotel Sofitel, Viena	Austria	2010	960 (heating) 600 (cooling)	100 energy piles and 253 m diaphragm wall	Temperate	Data from www.enercret.com
STRABAG Headquarters, Vienna	Austria	2003	840 (heating) 1450 (cooling)	245 energy piles and 6000 m <sup>2</sup> of floor plate layout	Temperate	Data from www.enercret.com
Omega-Computers and Peripherals, Vienna	Austria	2012	104 (heating) 84 (cooling)	3100 m <sup>2</sup> of floor plate layout	Temperate	Adapted from www.enercret.com
Dalham Hall Stud, Newmarket	Great Britain	2008	288 (heating) 80 (cooling)	147 energy piles	Temperate	Data from www.enercret.com
The Keble College, Oxford	Great Britain	2002	133 (heating)	83 energy piles	Temperate	Data from www.enercret.com
Hospital Valle Belbo, Nizza Monferrato	Italia	2010	341 (heating) 318 (cooling)	450 energy piles	Temperate	Data from www.enercret.com
European Central Bank, Frankfurt	Germany	2009	290 (heating) 176 (cooling)	72 energy piles	Temperate	Data from www.enercret.com
Office Building Timber Port, Hamburg	Germany	2011	1170 (heating) 967 (cooling)	770 energy piles	Temperate	Data from www.enercret.com
Financial Building, Wuxi	China	2011	4140 (heating) 5600 (cooling)	513 energy piles	Tropical monsoon	Data from www.enercret.com
People's hospital, Yangzhou	China	2014	8260 (heating) 6740 (cooling)	434 energy piles	Tropical monsoon	Data from www.enercret.com
Samsung Electronics, Seoul	Korea	1997	-	11150 m <sup>2</sup> of floor plate layout	Temperate	Data from www.enercret.com

Whereas, in tropical climate countries and specially in the emerging economies - BRICS (Brazil, Russia, India, China and South Africa), energy geostructures use is still limited and does not exploit its huge potential (Zhang *et al.*, 2011). According to the International Energy Agency (IEA) in 2005, the world's top five CO<sub>2</sub> emitting countries (USA, China, Russia, Japan and India) accounted for 55% of global energy-related CO<sub>2</sub> emissions (Resch *et al.*, 2008). Note that three out of the top five carbon dioxide emitters are emerging economies (Sadorsky, 2009; Bodas Freitas *et al.*, 2012). Among several environmental pollutants, carbon dioxide represents about 58.8% of the greenhouse gases that cause climate change (The World Bank, 2007; Pao & Tsai, 2010). Although China and India are ranked in the top five countries to develop renewable energy, so far, the development of thermo-active geostructures in these countries is still limited.

Actually, in temperate and cold climates the thermo-active geostructures can be used for both cooling and heating demands. The seasonal ground temperature remains relatively constant below a depth of 10÷15 m and values between 10°C and 15°C to a depth of about 50 m (Brandl, 2006; Yasukawa *et al.*, 2009). In tropical and also hot dry climate zones, the thermo-active geostructures systems may play a leading role to provide cooling dominated energy for the building. But this ground heat exchanger system is not easy to achieve in some regions. Actually, the ground temperature may increase due to the GSHP system operation, which in turn affects the long-term performance of the GSHP system. However, literature review in the recent years show that there is still a possibility to use GSHP systems in tropical and hot dry climate regions (Yasukawa *et al.*, 2009; Uchida *et al.*, 2011; De Moel *et al.*, 2010; Bourne-Webb *et al.*, 2009; He & Lam, 2006; Nicholson *et al.*, 2013). The main reasons are the following: (i) the thermo-active geostructures have better heat transfer characteristics than conventional borehole systems; (ii) there is no need for additional land; and (iii) there is no need for drilling of holes to install heat exchangers.

Moreover, this system can be combined with outdoor systems such as solar panel on the roof (plate heat exchanger) or nocturnal cooling radiator, cooling tower or domestic hot water production device to reduce the heat rejected into the ground, namely a hybrid GSHP system (Man *et al.*, 2009; Man *et al.*, 2011; Sagia *et al.*, 2012). This makes sense if wasted heat can be used to keep ground thermal balance in the cooling load operation period and to increase the coefficient of performance of the GSHP system.

In this chapter, heat transfer aspects related to thermo-active geostructure are first reviewed (section 1.2). Secondly, an overview on the heat conduction analysis related to energy pile is

presented (section 2.2.). That provides a general background for the works done in the Part I of this thesis that focuses on the heat transfer in the context of energy pile.

## 1.2 Thermo-active geostructure

### 1.2.1 GSHP system operation

GSHP system is one of the fastest growing applications of renewable energy in the world, with annual increases of 10 % in about 30 countries in the last decades (Curtis *et al.*, 2005). Some of the main advantages of GSHP system can be listed as follows (Curtis *et al.*, 2005; Omer, 2008; Permchart & Tanatvanit, 2009; Ozgener & Hepbasli, 2007; Brandl, 2006):

- Saves fossil fuel energy and reduce CO<sub>2</sub> emissions,
- Highly reliable (few moving parts, no exposure to weather),
- Not noisy and no unsightly outdoor unit is needed,
- More efficient than air source heat pumps,
- Uses electricity only to transfer heat, and does not generate it by the burning fuel or using electric resistance elements.

To evaluate the performance of the GSHP system in the heating mode, the Coefficient of Performance (*COP*) is used. *COP* is the heating capacity of the unit divided by its electrical input (Brandl, 2006):

$$COP = \frac{\text{Energy output after heat pump [kW]}}{\text{Energy input for operation [kW]}} \quad (1.1)$$

The ISO 13256-1 standard recommends that *COP* must be higher than 3.3, and should be greater than or equal to 4 for economic reasons (Mimouni *et al.*, 2013). To ensure this condition for heating mode, ground temperature should not be lower than 0÷5°C and the output temperature in the secondary circuit should not exceed 35÷45°C.

In the cooling mode, to evaluate the performance of the GSHP system, the Energy Efficiency Ratio (*EER*) is used. *EER* is defined as cooling capacity of the unit divided by its electrical input (AHRI, 1998).

$$EER = \frac{\text{Output cooling energy [Btu]}}{\text{Input electrical energy [W.h]}} \quad (1.2)$$

As recommended by the American Refrigerant Institute (ARI), *EER* should be in the range of 10 to 18.6 (Inalli & Esen, 2005), and after the ISO 13256-1 standard *EER* value must be greater than or equal to 14.1.

In the areas where both heating and cooling are needed, in winter the GSHP system provides heat for buildings and cools down the ground, and *vice versa* in summer. However, at the beginning of cold season, heating demand is not important while the ground temperature is high. Reversely, at the beginning of hot season, cooling demand is low while the ground temperature is low. The *COP* and *EER* values change then constantly depending on the ground temperature and the buildings' demand. Accordingly, the ratio of the usable energy output of the system to the energy input to the system is known as the seasonal performance factor (*SPF*) (Brandl, 2006).

$$SPF = \frac{\text{Usable energy output of energy system [kWh]}}{\text{Energy input of the energy system [kWh]}} \quad (1.3)$$

This important factor is necessary to evaluate the seasonal variations of the *COP* and *EER*. *SPF* is dependent on the heat pump, local climatic conditions, and also on the other energy consuming elements (Brandl, 2006; Mimouni *et al.*, 2013).

### ***1.2.2 Ground temperature and soil thermal properties***

The knowledge of the ground temperature plays an important role for the design of thermo-active geostructures. Low-temperature soil can be used to cool down the building in summer, while high-temperature soil is suitable to heat the building in winter. But in the regions with year-round high atmospheric temperature, if the soil temperature is high the application of GSHP system is not suitable (Pouloupatis *et al.*, 2011). The ground temperature distribution is affected by the following factors (Farouki, 1986; Popiel *et al.*, 2001; Florides & Kalogirou, 2005; Omer, 2008; Singh *et al.*, 2011; Pouloupatis *et al.*, 2011; Akrouch *et al.*, 2013):

- Climatic factors (air temperature, wind, solar radiation, air humidity, rainfall, *etc.*)
- Structure and physical properties of the ground
- Ground surface cover (snow, trees, *etc.*)

These properties have strong effects on the capacity of the ground to transfer heat and of the geostructure to exchange heat. Besides, the ground temperature-depth relationship can be separated into three different zones around the thermo-active geostructure as follows (Popiel *et al.*, 2001; Wang & Qi, 2008; Nguyen *et al.*, 2017):

- *Surface zone*: (0 ÷ 1 m depth), subsurface mostly absorbs heat from solar radiation throughout the year. In most regions, poorly shaded landscapes may contribute to high temperatures in soils.
- *Shallow zone*: (1 ÷ 10 m depth), where soil temperature is almost constant and approximately equals to the average air temperature, but still affected by the seasonal temperature fluctuation.
- *Deep zone*: (> 10 m depth), ground temperature is constant throughout the year.

The three main forms of heat transfer process in soils are conduction, convection and radiation. Among them, convection and radiation generally have relatively small or negligible effects, however they may have a noticeable influence in certain situations (*e.g.* in regions with high groundwater flow) (Rees *et al.*, 2000). Heat conduction due to temperature gradient is the most relevant process associated with heat transfer in soils (Farouki, 1986; GSHP Association, 2012). The most important thermal properties of soil are thermal conductivity and volumetric heat capacity, which are key for the design of thermo-active geostructure systems (GSHP Association, 2012). The thermal conductivity of soils and rocks is in the range of 0.2 W/(m.K) to 5 W/(m.K). This value is controlled by the structure and physical properties of soil and rock with the solid particles being the most conductive, followed by water and then air. As the thermal conductivity is highly dependent on soil's density and water content, wet or saturated soils have higher (about five times) thermal conductivity than dry soil (Riederer *et al.*, 2007). In addition, volumetric heat capacity of soil also depends on the water and air contents. When soil temperature changes over time, assessment of the ability to diffuse heat as well as to store thermal energy in the ground is done by using the thermal diffusivity, which is defined as the ratio of the thermal conductivity to the volumetric heat capacity of the ground. Thus, soil thermal properties have an important role in the design of heat exchanger geostructures (Brandl, 2006; De Moel *et al.*, 2010; Omer, 2008; GSHP Association, 2012; Suryatriyastuti *et al.*, 2012; Mattsson *et al.*, 2008):

- The thermal conductivity of soil acts as a standard value to design the number of heat exchanger piles as required to provide energy for building;
- Dry or unsaturated soil with smaller thermal conductivity may require deeper energy piles foundation and larger area of the heat exchanger;
- Depending on soil properties and depth of boreholes, 1 kW heating in saturated soil needs from 20÷35m<sup>2</sup> (and in dry soil from 35÷50m<sup>2</sup>) of surface of concrete structures in contact with soil or groundwater.

In addition, in areas with existence of groundwater flow, the effect of thermal conduction and also advection in the soil contributes to accelerate the process of heat extracted from/rejected to the soil around heat exchangers and it affects the sustainable operation of GSHP system.

Studies on heat exchange between energy piles and the ground in unsaturated state showed that the heat exchange rate of energy pile is strongly affected by the saturation conditions of the surrounding soil (Yun & Santamarina, 2008; Thomas & Rees, 2009; Choi *et al.*, 2011; Dong *et al.*, 2015; Akrouch *et al.*, 2015). Choi *et al.*, (2011) indicated that the heat exchange rate of energy pile in unsaturated soil (water table at the pile's toe) is 40% smaller than that in fully saturated soil (water table at the ground surface). Thomas & Rees (2009) showed that that heat exchange rate of a raft foundation located 10 m above the water table was 35% smaller than the case where it was located below the water table.

### 1.3 Heat conduction analysis

In the range of vertical heat exchanger borehole and energy pile, heat is diffused from the pipes into the concrete and then to the surrounding soil. As mentioned above, heat conduction is the most relevant process associated with heat transfer in soil and pile. Therefore, various analytical and numerical solutions have been proposed to simulate the conductive heat transfer of heat exchanger pile.

Analytical models (Jaeger, 1944; Carslaw, 1947; Zeng *et al.*, 2002; Lamarche & Beauchamp, 2007; Bandos *et al.*, 2009; Man *et al.*, 2010; Bozis *et al.*, 2011; Li & Lai, 2012a and 2012b; Akrouch *et al.*, 2015), for simplicity, have been developed with the following general assumptions: heat transfer is purely conductive; the surrounding medium is homogeneous and infinite or semi-infinite; the initial temperature is homogenous; the influence of ground surface temperature is ignored; a constant heat flow is applied at the pipe boundaries and the vertical heat transfer can be neglected. Most of the analytical heat transfer models have been developed mainly for borehole ground heat exchanger system (GHE).

The existing analytical models of heat transfer can be divided into two groups: the first one is applicable for homogeneous media and the second one for composite media. Most of these models are only valid after a certain time of operation and they are generally suitable for long-term heat exchanger performance. It means that temperature of borehole reaches a steady state as soon as the heat exchanger system is activated. This is acceptable when the diameter of heat exchanger borehole is much smaller than its length, as well as the instantaneous heat

transfer is not much of interest. However, energy pile has larger diameter and smaller length than those of a borehole. As a result, heat transfer inside the pile takes a longer time to reach the steady state, and pile often has different thermal properties from the surrounding soil.

Based on the theory of infinite line source model, Carslaw & Jaeger (1959) developed a 1-D solution of heat transfer in homogeneous media (equation 1.4), under constant heat flow condition. This model is relatively simple and it can be used to estimate the soil temperature around a heat exchanger borehole quickly.

$$\Delta T = \frac{q}{4\pi\lambda} \int_{\frac{r^2}{4\alpha t}}^{\infty} \frac{e^{-u}}{u} du = -\frac{q}{4\pi\lambda} E_i \left( -\frac{r^2}{4\alpha t} \right) \quad (1.4)$$

$$\text{with: } E_i(x) = \int_x^{\infty} \frac{e^{-u}}{u} du$$

For a small value of  $x$ :

$$E_i(-x) = \gamma + \ln(x) - x + \frac{1}{4}x^2 + O(x^3) \quad (1.5)$$

This exponential integral  $E_i$  is expressed as a logarithmic function that was validated by Abramowitz & Stegun (1972). In this solution,  $\Delta T$  is the change of temperature,  $\lambda$  is the soil thermal conductivity (W/mK),  $\alpha$  is the soil thermal diffusivity ( $\text{m}^2/\text{s}$ ),  $r$  is the distance from heat source,  $q$  is the heat flow rate (W/m),  $\gamma = 0.5772$  is Euler's constant,  $t$  is the elapsed time of heating operation and  $O(x^3)$  is the infinitesimal function.

Eskilson (1987) developed a 2-D analytical solution for a finite line source model. This model is applied for the case a borehole having a limit length, in which temperature of the surrounding soil depends on those of the line source and on the surface. This latter considers only the heat transfer from the borehole's wall to the surrounding soil. Temperature at the borehole's wall is assumed to be constant over the depth and depends only on time. The solution of Carslaw & Jaeger (1959) on temperature of borehole  $T_b$  can be expressed in another way as follows:

$$T_b = q \cdot R_b(t) \quad (1.6)$$

The thermal resistance of soil  $R_b(t)$  can be taken approximately as follows:

$$R_b(t) = \frac{1}{4\pi\lambda} \left[ \ln \left( \frac{4\alpha t}{r_b^2} \right) - \gamma \right] \quad (1.7)$$

To apply the model to the borehole/pile with a diameter  $r_b$  and a finite length  $H$ , the author suggested that  $t$  must satisfy the inequality:  $\frac{5r_b^2}{\alpha} < t < \frac{t_s}{10}$ . Where the lower limit is necessary for the use of a line source at  $r = 0$ . In case of conventional borehole/pile, this lower limit corresponds to a few hours. And  $t_s = \frac{H^2}{9\alpha}$  is the time in which the heat exchange reaches its steady state that varies between several days to years. In a larger time, 3D problems should be considered. The results show that, when the heat exchange does not reach the steady state, temperature response function depends only on the dimensionless variables  $\frac{r_b}{H}$  and  $\frac{t}{t_s}$ . The thermal resistance is then expressed in G-function as follows:

$$R_b(t) = \frac{1}{2\pi\lambda} G\left(\frac{t}{t_s}, \frac{r_b}{H}\right) \quad (1.8)$$

Here, G-function is also called temperature response function of the borehole's wall.

In general:

$$G\left(\frac{t}{t_s}, \frac{r_b}{H}\right) = \begin{cases} \ln\left(\frac{H}{2r_b}\right) + \frac{1}{2} \ln\left(\frac{t}{t_s}\right); & \frac{5r_b^2}{\alpha} < t < t_s \\ \ln\left(\frac{H}{2r_b}\right) & ; t > t_s \end{cases} \quad (1.9)$$

$$(1.10)$$

The G-function, shown in equation (1.9), is used to determine the wall's temperature of a single borehole. For example, by using this G-function measured with a conventional borehole (0.11 m in diameter, and 110 m long;  $\lambda = 3.5$  W/(m.K) and  $\alpha = 1.62 \cdot 10^{-6}$  m<sup>2</sup>/s) Eskilson (1987) found that the steady state is reached after 26 years. That is why this solution (equation 1.9) is often used in practice. However, in the case of energy pile, with a larger diameter and much smaller length than heat exchanger borehole, the steady state is obtained after several days to one year (Bozis *et al.*, 2011). It can be seen that, these G-functions are only suitable with long-term heat transfer problems and with a borehole having a small diameter.

Practically, the heat exchange rate of the ground heat exchanger system changes hourly and depends on the energy requirements of the building. This change directly affects the *COP* of the system. Study of Yavuzturk & Spitler (1999) shows that the temperature fluctuation in

short term typically varies up to  $5.6 \div 10^\circ\text{C}$  over a given day. Therefore, prediction of short-term temperature exchange allows determining exactly the building's energy consumption.

Yavuzturk & Spitler (1999) have extended the application of Eskilson's G-functions to simulate the short-time response of heat conduction exchanger borehole by using a 2-D numerical model. This is the first solution, related to the problem of transient heat of heat exchanger borehole, which considers different thermal properties between the borehole and surrounding soil. Later, Zeng *et al.* (2002) proposed a 2-D model of a finite line heat source that represents the effect of heat transfers along the axis of the vertical borehole and the temperature at the ground surface. This model is used to determine the temperature outside the finite length of heat exchanger borehole, in short-time operation (equation 1.11a).

$$\Delta T(r, z, t) = \frac{q}{4\pi\lambda} \int_0^H \left\{ \frac{\operatorname{erfc}\left(\frac{\sqrt{r^2 + (z-z')^2}}{2\sqrt{\alpha t}}\right)}{\sqrt{r^2 + (z-z')^2}} - \frac{\operatorname{erfc}\left(\frac{\sqrt{r^2 + (z-z')^2}}{2t}\right)}{\sqrt{r^2 + (z+z')^2}} \right\} dz' \quad (1.11a)$$

with  $\operatorname{erfc}$  is the complementary error function, commonly denoted  $\operatorname{erfc}(z)$ , is an entire function defined by:

$$\operatorname{erfc}(z) = \frac{2}{\pi} \int_z^\infty e^{-t^2} dt \quad (1.11b)$$

At longer time, the transient solution becomes:

$$\Delta T(r, z, t) = \frac{q}{4\pi\lambda} \ln \left[ \frac{\sqrt{(H-z)^2 + \varphi^2} + H - z}{\sqrt{(H-z)^2 + \varphi^2} + H + z} \cdot \frac{2z^2 + 2z\sqrt{\varphi^2 + z^2} + \varphi^2}{\varphi^2} \right] \quad (1.12)$$

where,  $H$  is the depth of the borehole,  $z$  is the depth, and  $\varphi$  is the radial coordinate.

Base on the 1-D solution of Carslaw & Jaeger (1959), Bozis *et al.* (2011) analyzed heat transfer of an energy pile with  $2n$  heat pipes and a constant injection heat flow per pipe. The authors have proven that the temperature at the pile center is dependent neither on the number of pipes nor on the pipes' diameter. Actually, it depends on the total injection heat flow at a given time, the distance with the pipes and also the pile thermal properties.

In contrast to the line source model with the heat source located in the center of borehole/pile, when the heat sources are close to the pile edge and distributed as a hollow cylinder shape, the temperature response model behaves as a cylinder model (Fig. 1.3).

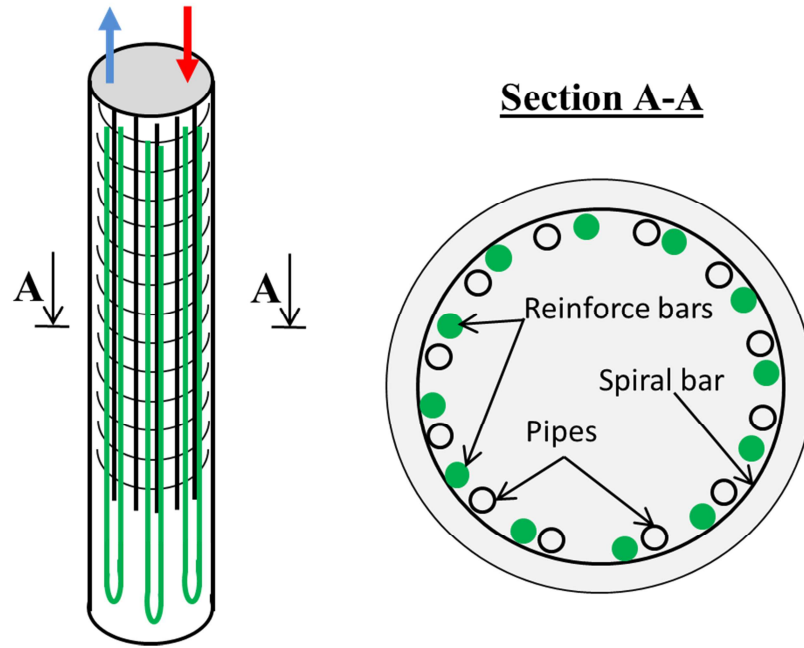


Fig. 1.3 The arrangement of pipes close to the pile edge

Therefore, a heat transfer model with cylindrical geometry is necessary to simulate more accurately the heat transfer in this case. Based on the complex variable theory and the Laplace transform method, Carslaw & Jaeger (1947) also developed an exact solution for the problem of the infinite hollow cylinder heat source (equation 1.13).

$$\Delta T = \frac{\dot{q}}{\lambda r_0 \pi^2} \int_0^{\infty} (e^{-\alpha u^2 t} - 1) \frac{J_0(ur) Y_1(ur_0) - J_1(ur_0) Y_0(ur)}{J_1^2(ur_0) + Y_1^2(ur_0)} \frac{du}{u^2} \quad (1.13)$$

Here,  $J_i$  and  $Y_i$  are Bessel functions of the first and second kinds of order  $i$ .

Recently, Man *et al.* (2010) have developed new cylinder surface source models by assuming that the material inside and outside the surface is homogeneous. By using the Green's function method, they found the expression of soil temperature in 1-D model as follows:

$$\Delta T(r, \tau) = \frac{q_l}{4\pi\lambda} \int_0^{\tau} \frac{1}{\tau - \tau'} \exp\left[-\frac{r^2 + r_0^2}{4\alpha(\tau - \tau')}\right] \cdot I_0\left[\frac{rr_0}{2\alpha(\tau - \tau')}\right] d\tau' \quad (1.14)$$

The 2-D model that represents the simultaneous influence of a finite cylindrical heat source and the boundary ground surface is showed in equation (1.15).

$$\Delta T(r, z, \tau) = \frac{q_l}{\rho c} \int_0^\tau \int_0^h \frac{1}{8\sqrt{\pi\alpha(\tau-\tau')}} I_0 \left[ \frac{rr_0}{2\alpha(\tau-\tau')} \right] \left\{ \exp \left[ -\frac{r^2 + r_0^2}{4\alpha(\tau-\tau')} \right] - \exp \left[ -\frac{r^2 + r_0^2 + (z' + z)^2}{4\alpha(\tau-\tau')} \right] \right\} dz' d\tau' \quad (1.15)$$

where  $I_0(x) = \frac{1}{\pi} \int_0^\pi \exp(x \cos \varphi) d\varphi$  is the modified Bessel function of the first kind of zero order.

For heat transfer models that consider different thermal properties between the pile and the surrounding soil, Lamarche & Beauchamp (2007) presented a closed-form solution of transient heat inside a heat exchanger borehole. An equivalent pipe is placed in the center of borehole and this equivalent pipe is considered as an infinite cylindrical heat source. Heat mass capacity of fluid inside the pipe is ignored and the pipe's temperature is supposed to be uniform. Equation (1.16) shows the transient heat function of the borehole.

$$\Delta T = \frac{\dot{q}}{\lambda_{soil}} \frac{4\tilde{\lambda}}{\pi^4 \delta^2} \int_0^\infty (1 - e^{-\alpha u^2 t}) \frac{Y_0(u\tilde{r}) J_1(u) - J_0(u\tilde{r}) Y_1(u)}{\phi^2 + \psi^2} \frac{du}{u^4} \quad (1.16)$$

where

$$\phi = Y_1(\beta) [Y_0(\beta\delta\gamma) J_1(\beta\delta) - Y_1(\beta\delta\gamma) J_0(\beta\delta) \tilde{\lambda}\gamma] - J_1(\beta) [Y_0(\beta\delta\gamma) Y_1(\beta\delta) - Y_1(\beta\delta\gamma) Y_0(\beta\delta) \tilde{\lambda}\gamma]$$

$$\psi = J_1(\beta) [J_0(\beta\delta\gamma) Y_1(\beta\delta) - J_1(\beta\delta\gamma) Y_0(\beta\delta) \tilde{\lambda}\gamma] - Y_1(\beta) [J_0(\beta\delta\gamma) J_1(\beta\delta) - J_1(\beta\delta\gamma) J_0(\beta\delta) \tilde{\lambda}\gamma]$$

$$\tilde{\lambda} = \lambda_{soil} / \lambda_{pile}; \quad \tilde{r} = r / r_e; \quad \delta = r_p / r_e$$

where  $r$  is the distance from the heat source,  $r_e$  the pipe radius, and  $r_p$  the pile radius. The advantage of this model is that it allows analyzing heat transfer inside borehole in a very short time.

Li & Lai (2012a) has also developed a solution for a continuous line source model in composite media (equations 1.17 & 1.18). This solution is developed from the solution of an instantaneous line source in composite media of Jaeger (1944). This new model uses the superposition method to solve the problem with multiline sources inside the pile. The temperature response function is then expressed as a G-function; this concept was first proposed by Eskilson (1987).

$$G_1(F_0, R, \theta) = \frac{1}{2\pi\lambda_1} \sum_{n=-\infty}^{+\infty} \cos n(\theta - \theta') \int_0^{+\infty} [1 - \exp(-v^2 F_0)] \frac{J_n(vR) J_n(vR') (\varphi g - \psi f)}{v(\varphi^2 + \psi^2)} dv \quad (1.17)$$

$$G_2(F_0, R, \theta) = \frac{1}{\pi^2 \lambda_2} \sum_{n=-\infty}^{+\infty} \cos n(\theta - \theta') \int_0^{+\infty} [1 - \exp(-v^2 F_0)] \frac{J_n(vR') [\psi J_n(\alpha v R) - \varphi Y_n(\alpha v R)]}{v^2 (\varphi^2 + \psi^2)} dv \quad (1.18)$$

where  $F_0$  is the Fourier number,  $R$  and  $\theta$  are the coordinates of the line source in the cylindrical coordinates, and  $\lambda_1$  and  $\lambda_2$  are thermal conductivities of pile and soil, respectively.

$$\begin{aligned} \varphi &= \alpha \lambda J_n(v) J_n'(\alpha v) - J_n'(v) J_n(\alpha v) \\ \psi &= \alpha \lambda J_n(v) Y_n'(\alpha v) - J_n'(v) Y_n(\alpha v) \\ f &= \alpha \lambda Y_n(v) J_n'(\alpha v) - Y_n(v) J_n(\alpha v) \\ g &= \alpha \lambda Y_n(v) Y_n'(\alpha v) - Y_n'(v) Y_n(\alpha v) \end{aligned} \quad (1.19)$$

where  $J_n$  and  $Y_n$  are Bessel functions of the first and second kinds of order  $n$ ;  $\alpha = \sqrt{\alpha_1/\alpha_2}$ , where  $\alpha_1$  and  $\alpha_2$  are thermal diffusivities of pile and soil, respectively;  $\lambda = \lambda_2/\lambda_1$ .

In case of pile with a U-pipe source, the G-function inside the borehole is:

$$G_1(F_0, R_p, R') = \frac{1}{2\pi\lambda_1} \sum_{m=-\infty}^{+\infty} \int_0^{+\infty} [1 - \exp(-v^2 F_0)] \frac{J_{2m}(vR_A) + J_{2m}(vR_B)}{2} \frac{J_{2m}(vR') (\varphi g - \psi f)}{v(\varphi^2 + \psi^2)} dv \quad (1.20)$$

In case of double U-tubes:

$$G_1(F_0, R_p, R') = \frac{1}{2\pi\lambda_1} \sum_{l=-\infty}^{+\infty} \int_0^{+\infty} [1 - \exp(-v^2 F_0)] \frac{J_{4l}(vR_A) + J_{4l}(vR_B)}{2} \frac{J_{4l}(vR') (\varphi g - \psi f)}{v(\varphi^2 + \psi^2)} dv \quad (1.21)$$

where,  $R_A$  and  $R_B$  are dimensionless radial coordinates, values of  $n$  in definitions equation (1.19) equal  $2m$  and  $4l$ ;

It can be seen that this model refers to the presence of thermal properties of two materials. However, the solution is relatively complex and each type of U-tubes configuration requires a different G-function. This solution is only applicable for the short-term performance of the ground heat exchanger system.

Besides, Li & Lai (2012b) have developed cylindrical-surface and spiral-line sources solutions for the thermal pile with finite length (equation 1.22). The model considers anisotropic medium around the heat source. The comparison between the cylindrical-surface and spiral-line sources shows that the temperature of both models has similar values at the pile wall. The effect of anisotropic medium around the pile is found negligible in the short-term period of pile heating or cooling.

$$\Delta T = \frac{q_l b}{4\pi\sqrt{\lambda_x\lambda_y}} \int_0^{2n\pi} \left[ \frac{1}{d} \operatorname{erfc}\left(\frac{d}{2\sqrt{\alpha_z t}}\right) - \frac{1}{d'} \operatorname{erfc}\left(\frac{d'}{2\sqrt{\alpha_z t}}\right) \right] d\beta \quad (1.22)$$

with

$$d = \sqrt{\kappa_{zx} (r \cos \varphi - r' \cos \beta)^2 + \kappa_{zy} (r \sin \varphi - r' \sin \beta)^2 + (z - b\beta)^2}$$

$$d' = \sqrt{\kappa_{zx} (r \cos \varphi - r' \cos \beta)^2 + \kappa_{zy} (r \sin \varphi - r' \sin \beta)^2 + (z + b\beta)^2}$$

In the majority of the existing models, the solutions are usually represented in symbolic functions form and therefore solving them must be done by numerical integration methods, by using programs like Matlab, Maple, Maxima, *etc.* These models are called semi-analytical solutions. Practically, the results obtained from the analytical solution have an excellent accuracy but the existing heat transfer solutions, used for transient heat in heterogeneous medium, are usually represented in complex forms. For these reasons, empirical models are also considered. Actually, empirical models are often expressed as simple mathematical forms and give approximate results when compared with analytical models.

Loveridge & Powrie (2013b) have developed empirical solutions that were based on the 2-D finite element analyses of Loveridge & Powrie (2012a) and the analytical solution of Man *et al.* (2010). The ground temperature response functions (G-functions) were obtained by fitting the numerical simulations. Advantages of these new G-functions are that they consider typical geometries of heat exchanger piles (*e.g.* pile sizing, pipes arrangement and the relative thermal properties of pile and soil). In addition, they allow estimating heat storage inside the pile and soil in both short- and long-term operations. For the short-term behavior of ground temperature response, the G-function is based on 2D simulation and it can only be validated within the timescale of  $F_0 = 0.1 \div 10$ . In which  $F_0 = \alpha t / r_p^2$  is the Fourier number. Equation (1.23) is the proposed ground temperature response function that is based on the simplified line source model. Equation (1.24) is based on simplified solid cylinder model.

$$G = \frac{1}{2} [\ln(4F_0) - \gamma] \quad (1.23)$$

and

$$\ln\left(\frac{G}{2}\right) = -2.321016 + 0.499615 \ln(F_0) - 0.027243 [\ln(F_0)]^2 - 0.00525 [\ln(F_0)]^3 + 0.000264311 [\ln(F_0)]^4 + 0.00006873912 [\ln(F_0)]^5 \quad (1.24)$$

It can be said that this model is simpler than the analytical model of Li & Lai (2012a). For the long-term behavior, the ground temperature response is based on the 3D simulation. That means the model mentioned the influence of temperature on the ground surface when the pile has short length. The G-function for this case is showed in the Fig. 1.4, where the empirical G-function is fitted with eight curves that are represented for four aspect ratios ( $AR$ ) of 15, 25, 33 and 50; and each aspect ratio has been simulated with only the upper and lower bound scenarios. After Loveridge & Powrie (2013b) the upper bound solution corresponds to piles with pipes situated near the pile edge of cross section and thermal conductivity of pile is larger than that of soil. The lower bound solution corresponds to piles with pipes situated in the center and thermal conductivity of pile is smaller than that of soil. The authors have also indicated that, in case of the lower bound the response tends to get closer to the line source model, and inversely the response of the upper bound will moves closer to the solid cylindrical model.

Equation (1.25) shows the G-functions for the upper bound solution with  $F_0 > 0.1$ , and lower bound solution with  $F_0 > 0.25$ .

$$G = a[\ln(F_0)]^7 + b[\ln(F_0)]^6 + c[\ln(F_0)]^5 + d[\ln(F_0)]^4 + e[\ln(F_0)]^3 + f[\ln(F_0)]^2 + g[\ln(F_0)]h \quad (1.25)$$

The result in the Fig 1.4 is a combination of 2-D and 3-D model, in which the ground temperature response is shown in both short- and long-terms. It can be seen that, with  $F_0 < 10$  there is only two distinguished curves that related to the lower and upper bound, the response is only governed by the pile's parameters (size, number of pipes and its arrangement) but not by the aspect ratio. However, in the long term,  $F_0 > 10$ , the response depends on the aspect ratio but the two bounds are close to each other. Especially, the ground temperature responses in four aspect ratios are equivalent and they are well fitted with the finite line source model.

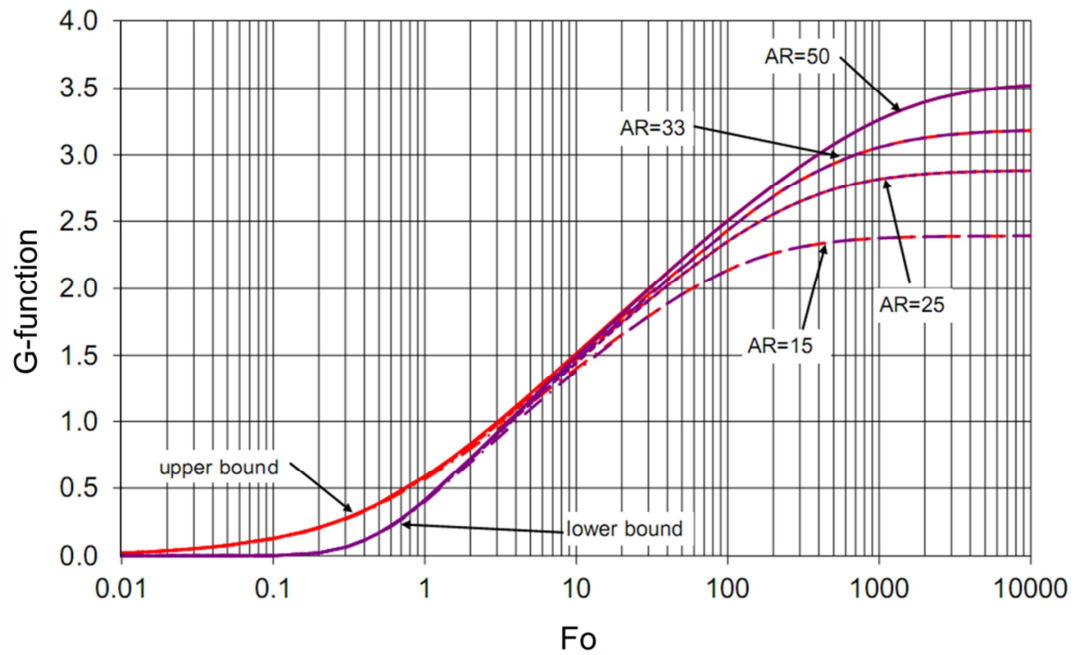


Fig. 1.4 Ground heat exchanger G-function for long-term operation, (after Loveridge & Powrie, 2013b)

Besides, finite element method (FEM) have been also used to analyze heat transfer problem of borehole and pile in composite media (Bauer *et al.*, 2011; Ghasemi-Fare & Basu, 2013; Ozudogru *et al.*, 2015). In general, this method is capable of simulating complex problems of heat exchanger piles in which the temperature response function is affected by a large number of parameters such as different thermal properties, pile sizes, number and distribution of heat pipes, timescale, *etc.* Meanwhile this is not possible with the analytical method. Although FEM is a powerful tool to solve different problems, it can be used to study the impact of various parameters on heat transfer. However, the finite element method is predominately used for research instead of being used as a design tool. Therefore, a simple analytical solution is always useful.

## 1.4 Conclusions

Thermo-active geostructure has been applied in various developed countries since the 1980s for heating and also cooling building. In general, the operation principles of thermo-active geostructure are similar to that of the GSHP system. In addition, the thermo-active geostructure can be used to supply energy independently or combined with other conventional energy sources for the buildings. However, unbalance heating and/or cooling loads in the long

term causes heat or cold accumulation in the ground, thus the *COP* of the system gradually reduces.

Practically, the heat exchange rate of energy pile is influenced by thermal conductivity of the surrounding soils. Soil density and water content are generally known as the major factors that influence the thermal conductivity. Therefore, thermal conductivity of soils is considered as an important parameter for the design of energy pile.

Among the existing analytical heat conduction models, the conventional models of heat conduction in pile and surrounding soil are applicable after a certain period of time when the process reaches its steady state. Recently, some models have been proposed to address the problem of transient heat but most of them are quite complex for the use as a simple design tool. Therefore, a simpler analytical heat transfer solution would be useful for the optimization of the energy pile design process.

## CHAPTER 2: THERMAL CONDUCTIVITY OF UNSATURATED SOIL

### 2.1 Introduction

A geological review of natural loess in Northern France shows that the thickness of loess deposits ranges between 3 to 8 m and is usually composed of less than 10 % sand and 10-25 % of clay particles (Antoine *et al.* 2003). The main features are characterized by: (i) a relative homogeneity, a high porosity and a low plasticity; and (ii) a natural unsaturated state even during winter periods (Antoine *et al.* 2003; Cui *et al.* 2004; Delage *et al.* 2005; Yang *et al.* 2008; Karam *et al.* 2009; Muñoz-Castelblanco *et al.* 2011, 2012a, 2012b). These authors have demonstrated that the mechanical properties of unsaturated loess are strengthened by suction, but that its open structure collapses upon wetting.

Several geotechnical applications require a good knowledge of the thermal properties of soils, including the thermal conductivity. One can cite, for instance, the energetic performance of thermo-active geostructures or the determination of the zone of thermal influence of buried underground cables and pipelines. In general, loess around the world has thermal conductivity values ranging between 0.15 to 2 W/(m.K) (Bidarmaghz *et al.* 2016). This quantity strongly depends on the soil moisture state: the higher the water content, the higher the thermal conductivity. The loess from Northern France has a high porosity and therefore the thermal conductivity can be significantly affected by seasonal wetting/drying cycles. In this chapter, moisture content, suction and thermal conductivity on an intact block of loess from Northern France are simultaneously measured to quantify the effect of moisture content and suction on the soil thermal conductivity.

### 2.2 Material and experimental method

A block soil sample was obtained from a depth of 1-m in Northern France (Muñoz-Castelblanco *et al.* 2011, 2012a, 2012b). The geotechnical properties of the sampled soil are showed in the Table 2.1.

Table 2.1. Geotechnical properties of sampled loess from Northern France (Muñoz-Castelblanco *et al.* 2011)

Natural water content $w$ (%)	14.4
Natural void ratio $e$	0.84
Dry unit mass $\rho_d$ ( $\text{Mg}/\text{m}^3$ )	1.45
Soil particle density $\rho_s$ ( $\text{Mg}/\text{m}^3$ )	2.67
Natural degree of saturation $S_r$ (%)	46
Natural suction (kPa)	40
Clay fraction ( $\% < 2 \mu\text{m}$ )	16
Plastic limit $w_p$	19
Liquid limit $w_l$	28
Plasticity index $I_p$	9

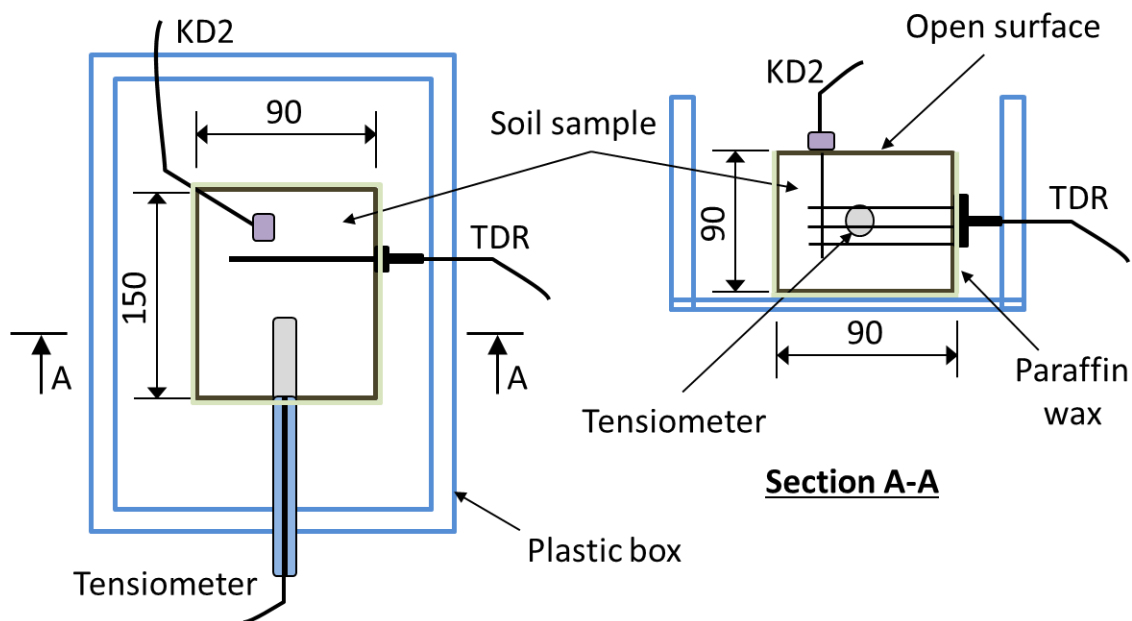


Fig. 2.1 Experimental setup

A rectangular prism (approximately 150 mm x 90 mm x 90 mm) is cut from an undisturbed block by using a hand saw. The weight of the soil sample and its water content are first measured. The soil sample is then coated with a thin layer of paraffin on its bottom and lateral surfaces to avoid moisture exchange with the atmosphere. A thin plastic wrap lid is used to cover the top surface. For wetting steps, the wrap lid on the top surface is removed and water

is sprayed onto the soil surface. For drying steps, the wrap lid is removed and the sample is dried by allowing water evaporation from the top surface. Moisture equilibrium within the sample is achieved by waiting for a few hours after each wetting or drying step, by covering the soil surface by the lid to avoid moisture exchange with the atmosphere. The moisture equilibrium is assumed to be reached when suction and moisture content do not change during a 1 hour period ( $< 1$  kPa for suction and  $< 1\%$  for moisture content).

Three sensors are carefully inserted inside the sample prior to wetting/drying: (i) a tensiometer (23 mm in diameter; accuracy equals 1 kPa) to measure the soil suction (Duong et al. 2013); (ii) a time-domain reflectometry (TDR) probe including three rods (80 mm length, 3 mm in diameter; accuracy equals 1%) to measure the soil volumetric moisture content; (iii) and a KD2-Pro probe (60 mm length and 1 mm in diameter; accuracy equals 0.1 W/(m.K)) to measure the soil thermal conductivity. Holes having dimensions similar to those of the sensors are drilled prior to the insertion of the sensors. That allows good contact between the sensors and the soil while minimizing the disturbance of its initial state. The tensiometer and the TDR probe are connected to the data logger system for automatic reading; the thermal conductivity is recorded manually.

### 2.3 Results and discussion

Fig. 2.2 shows the results obtained during the first 10 days where the sample was subjected to various wetting steps from its initial state. Actually, from its initial state with  $s = 40$  kPa and  $\theta = 18.7\%$ , adding water rapidly increases the moisture content to  $\theta = 23\%$ , but this value decreases progressively and stabilizes at  $\theta = 22\%$  after a few hours. At the same time, wetting induces a rapid decrease of the suction to 18 kPa, but suction increases progressively thereafter to 20 kPa. Such non-monotonic variations of moisture content and suction can also be observed in the subsequent wetting steps. That can be explained by the homogenization process of moisture inside the soil block that takes a few hours at high suction but more than 1 day at low suction (see Fig. 2.2a). From these results, equilibrated points were chosen at the end of each wetting step (vertical lines in Fig. 2.2a). As the thermal conductivity was recorded manually, such evolution during each wetting step could not be observed (see Fig. 2.2b). However, the thermal conductivity corresponding to the end of each wetting step was determined.

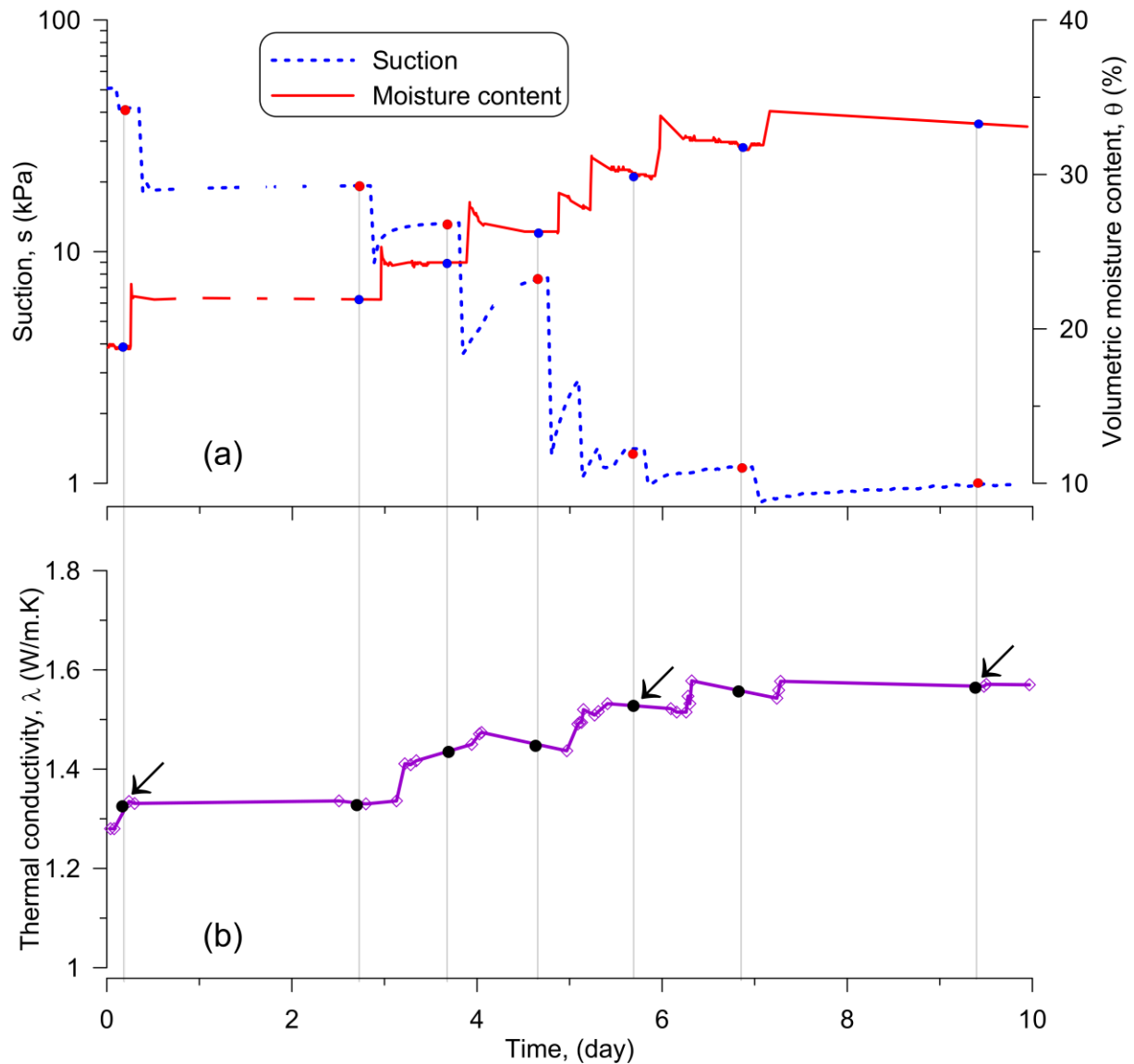


Fig. 2.2 Suction, moisture content and thermal conductivity in the wetting phase

Fig. 2.3 shows the results obtained during the subsequent drying path (from day 10 to 65). When the wrap lid is removed, water evaporation takes place and the moisture content decreases slowly (see Fig. 2.3a). Note that the non-monotonic variations in moisture content and suction are more obvious during the wetting than during the drying because water was sprayed onto the soil surface at the beginning of the wetting, while the drying took place progressively. As expected, drying induces a suction increase. The time to reach equilibrium is about one day at low suction but may take several days at high suction. The results obtained during this drying path allow for determining nine equilibrated points at the end of the drying steps (vertical lines shown in Fig. 2.3a). The soil thermal conductivity corresponding to these points was then determined from Fig. 2.3b.

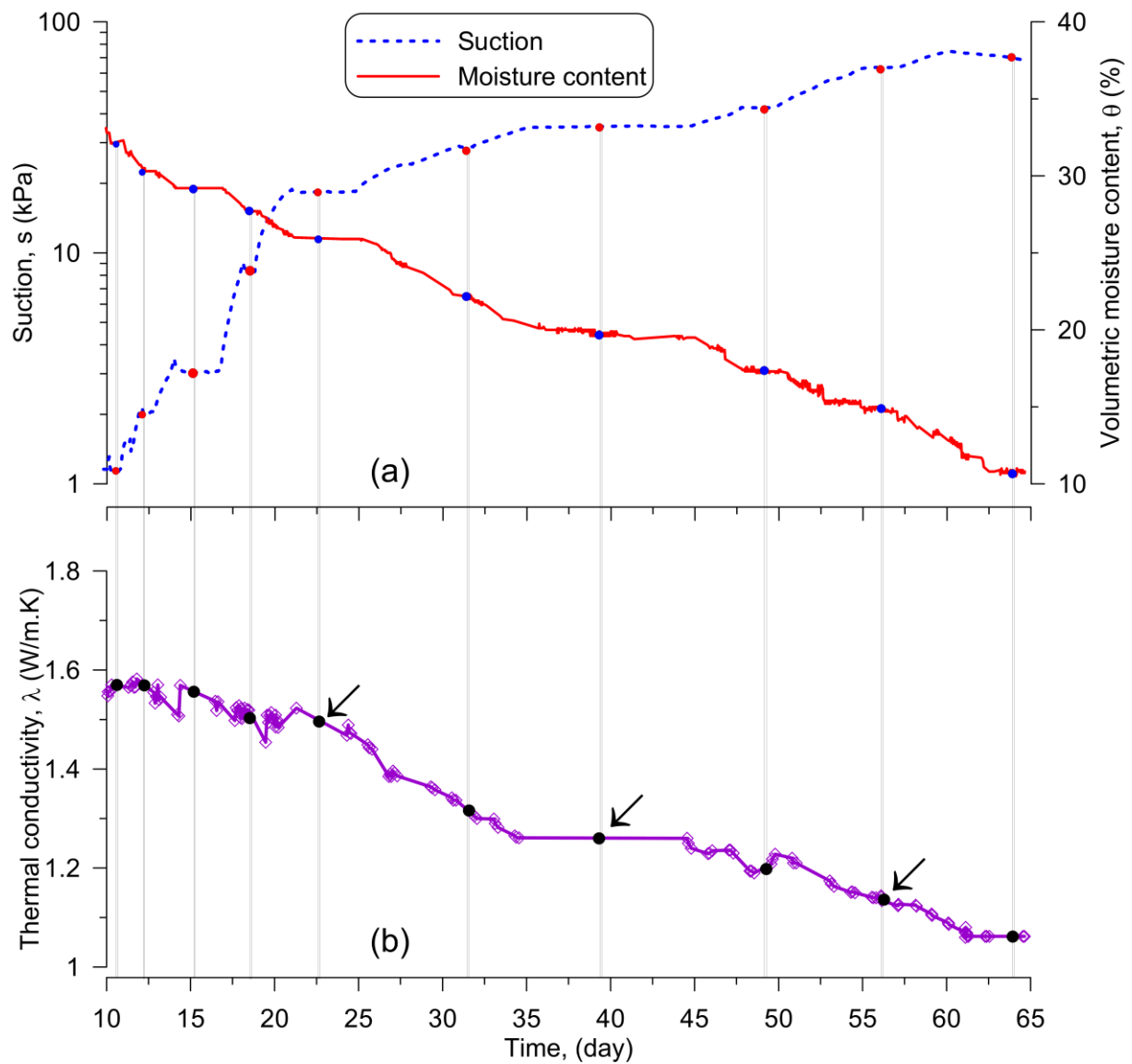


Fig. 2.3 Suction, moisture content and thermal conductivity in the drying phase

After the drying phase, the soil block was rewetted by steps. The result of this rewetting path (from day 65 to 90) is shown in Fig. 2.4. The rate of suction and moisture content variations versus elapsed time during this path is very similar to that observed during the initial wetting path. Eleven equilibrated points were determined along this path at the end of the wetting steps (Fig. 2.4a). The non-monotonic variations in moisture content and suction are more obvious during the wetting than during the rewetting because the quantity of water added to each step is generally more important in the wetting. The corresponding thermal conductivities were determined from Fig. 2.4b.

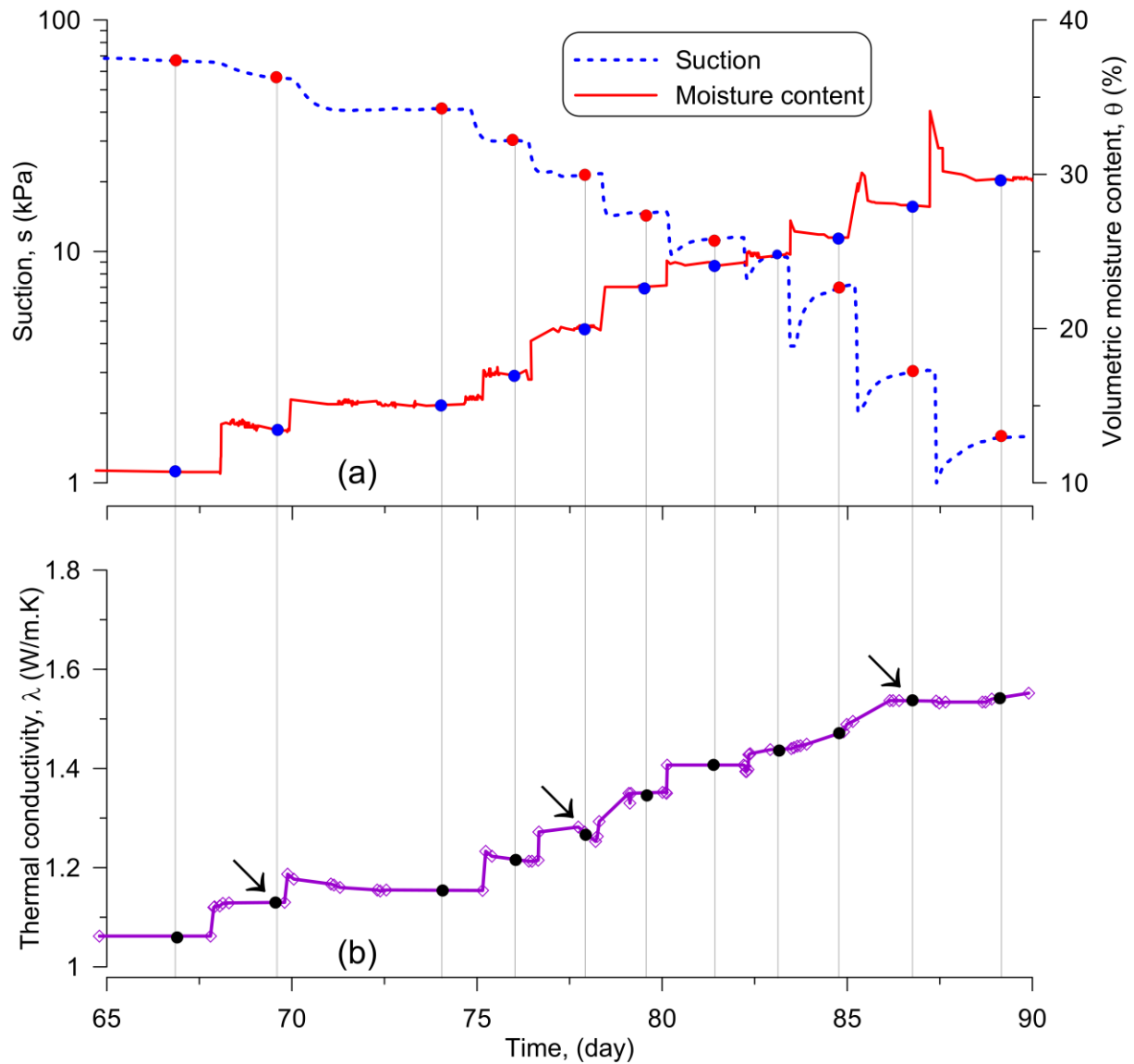


Fig. 2.4 Suction, moisture content and thermal conductivity in the re-wetting phase

The values of suction, moisture content and thermal conductivity corresponding to the end of drying or wetting steps (shown in Figures 2.2÷2.4) are plotted in Figure 2.5. Figure 2.5a shows the soil suction versus volumetric moisture content and degree of saturation. From the initial state, when the degree of saturation is increased to 0.8, soil suction is decreased to 1 kPa. The subsequent drying path decreases the degree of saturation to 0.3 and increases the soil suction to 70 kPa. The drying curve is located above the wetting curve. Finally, the rewetting curve is located below the drying path and approaches the wetting curve at suctions lower than 10 kPa.

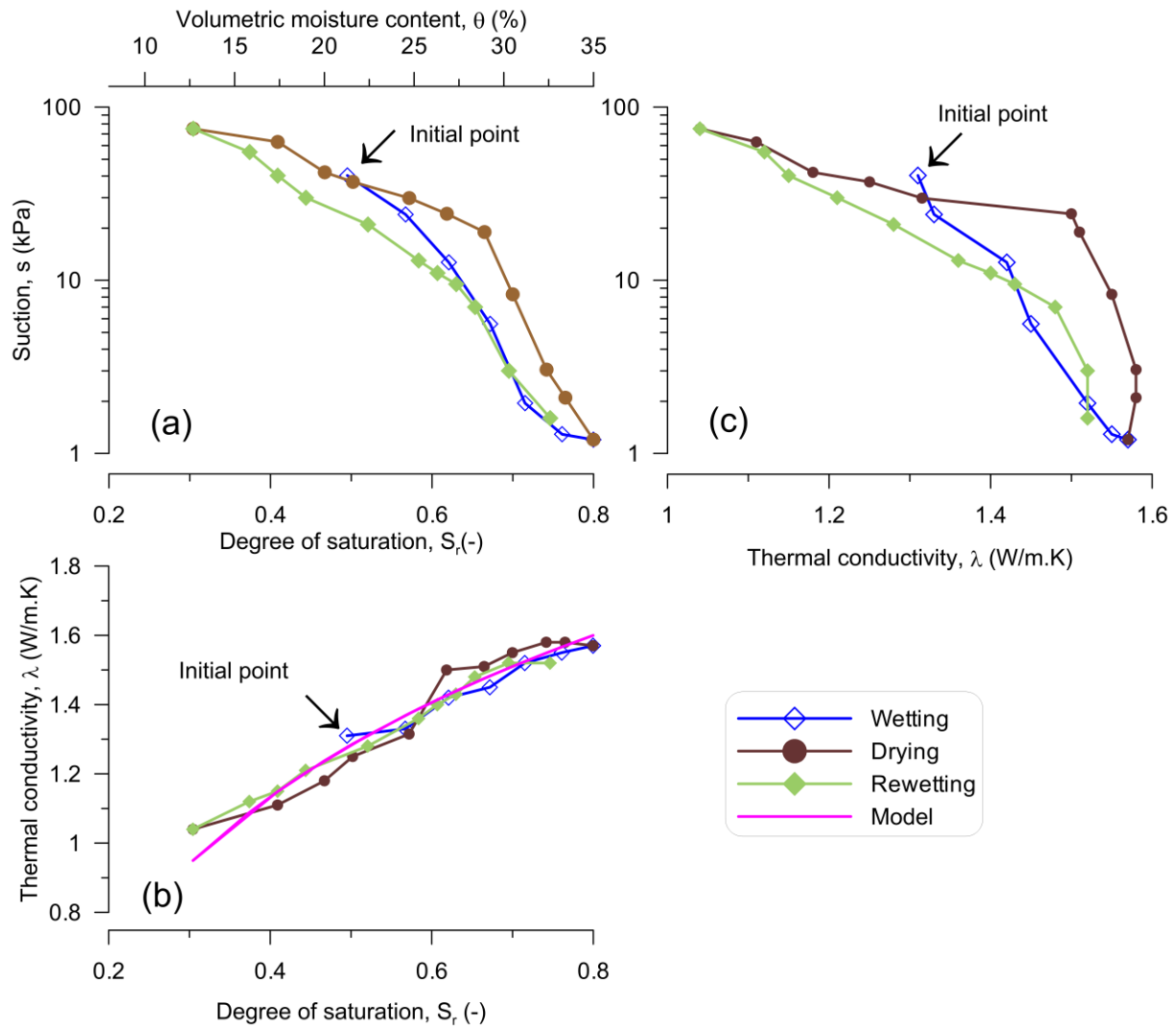


Fig. 2.5 Relationships between thermal conductivity, suction and degree of saturation

When plotting the thermal conductivity as a function of suction (Fig. 2.5c), a hysteresis loop is observed, quite similar to the water retention curve. However, when the thermal conductivity is plotted versus the degree of saturation, an almost linear one-to-one relationship is obtained (Fig. 2.5b). Thermal conductivity increases from 1.0 W/(m.K), at  $S_r = 0.3$ , to 1.6 W/(m.K) at  $S_r = 0.8$ .

For further analyses, the model proposed by Johansen (1975) was used to calculate the thermal conductivity of soil from the degree of saturation. According to Farouki (1986), the method developed by Johansen (1975) is applicable for unfrozen fine-grained soils at  $S_r > 0.2$ . The thermal conductivity ( $\lambda$ ) is expressed as:  $\lambda = (\lambda_{sat} - \lambda_{dry})(1 + \log_{10} S_r) + \lambda_{dry}$ , where  $\lambda_{sat}$  and  $\lambda_{dry}$  are the thermal conductivities in saturated and dry states, respectively.

- For saturated unfrozen soils:  $\lambda_{sat} = \lambda_s^{(1-n)} \lambda_w^n$ , where  $n$  is the porosity and  $\lambda_w$  is the

thermal conductivity of water,  $\lambda_w = 0.57 \text{ W/(m.K)}$ . The thermal conductivity of the solids  $\lambda_s$  is calculated using the equation:  $\lambda_s = \lambda_q^q \lambda_o^{1-q}$ , where  $\lambda_q$  is the thermal conductivity of quartz ( $\lambda_q = 7.7 \text{ W/(m.K)}$ ),  $\lambda_o$  is the thermal conductivity of other minerals ( $\lambda_o = 2.0 \text{ W/(m.K)}$ ) and  $q$  is the quartz content.

- For dry soils:  $\lambda_{dry} = (0.135\rho_d + 64.7)/(\rho_s - 0.947 \rho_d)$ , where the dry unit mass,  $\rho_d$ , and the unit mass of the solids,  $\rho_s$ , are expressed in  $\text{kg/m}^3$  and  $\lambda_{dry}$  is expressed in  $\text{W/(m.K)}$ .
- It can be seen in the Figure 2.5b that the model can predict correctly the relation between the thermal conductivity and the degree of saturation by using a quartz content of 60%. This value is in the same range as that mentioned previously by Antoine *et al.* (2003).

It can be seen in the Fig. 2.5b that the model can predict correctly the relation between the thermal conductivity and the degree of saturation by using quartz content of 60%. This value is in the same range as that mentioned previously by Antoine *et al.* (2003).

The experimental set-up used in this study is quite similar to that used by Smits *et al.* (2013) to investigate the thermal properties of sand. In the present work, wetting and drying were applied in steps in order to ensure moisture equilibrium at each step. This procedure was necessary because the hydraulic conductivity of loess is much lower than sand. The soil-water-retention curves obtained are similar to those obtained by Muñoz-Castelblanco *et al.* (2012b) on the same soil (for suction smaller than 100 kPa) but using other techniques (filter paper and high-capacity tensiometer).

In this work, the wetting/drying paths do not correspond to the main wetting/drying paths, which start from a dry state of fully saturated state, respectively. For this reason, analysis on air-entry value or degree of hysteresis (as that performed by Ng *et al.*, 2016) could not be done. Following the conceptual model proposed by Lu & Dong (2015), the soil-water-retention curves obtained in the present work correspond to two regimes: capillary and funicular. The hysteresis observed in the soil-water-retention curve in these regimes can be explained by the combined effects of ink-bottle, contact-angle and entrapped air (Pham *et al.*, 2005; Ng *et al.*, 2016).

Besides, it is well known that the soil thermal conductivity depends on various parameters such as degree of saturation, microstructure, water distribution, density, etc. (see Farouki, 1986; Tang *et al.* 2008; Guan *et al.* 2009; Dong *et al.* 2015; Usowicz *et al.* 2016). In this study, it was assumed that wetting/drying cycles change neither the density nor the

microstructure of the loess. At a given degree of saturation, soil suction on a drying path is higher than that on a wetting path. That means the water distributions between the two states are different. However, a unique relationship was found between thermal conductivity and water degree of saturation. These results suggest that the effect of water distribution on soil thermal conductivity is less significant than those of the other factors.

## 2.4. Conclusions

The relationship between moisture content, suction and thermal conductivity under wetting/drying paths has been investigated for loess from Northern France. The following conclusions can be drawn:

- ❖ Water-retention curve and thermal conductivity of intact loess can be obtained by simultaneous measurement of moisture content, suction and thermal conductivity on a single soil sample.
- ❖ The thermal conductivity varies between 1.0 and 1.6 W/(m.K) when the degree of saturation increases from 0.3 to 0.8. In this range, a unique relationship between these two quantities is observed during the wetting/drying paths.
- ❖ The relationship between suction and thermal conductivity is characterized by a clear hysteresis loop.
- ❖ At a given degree of saturation, soil suction corresponding to a drying path is higher than that of wetting path. That means the water distribution is different from one path to the other path. As a result, at first order, the thermal conductivity of loess in this study depends on the amount of water but not on its distribution within the soil microstructure in the suction range studied.

## CHAPTER 3: FULL-SCALE EXPERIMENT ON ENERGY PILE

### 3.1 Introduction

Two experimental full-scale energy piles were installed in 2010 (Fig. 3.1). The initial goal is to have two piles arranged side by side to ensure that they are in the same geological condition and have a similar bearing capacity. The first tests focus on the thermal behavior of the piles. The piles are heated and/or cooled to investigate the thermal response inside the pile as well as in the surrounding soil.

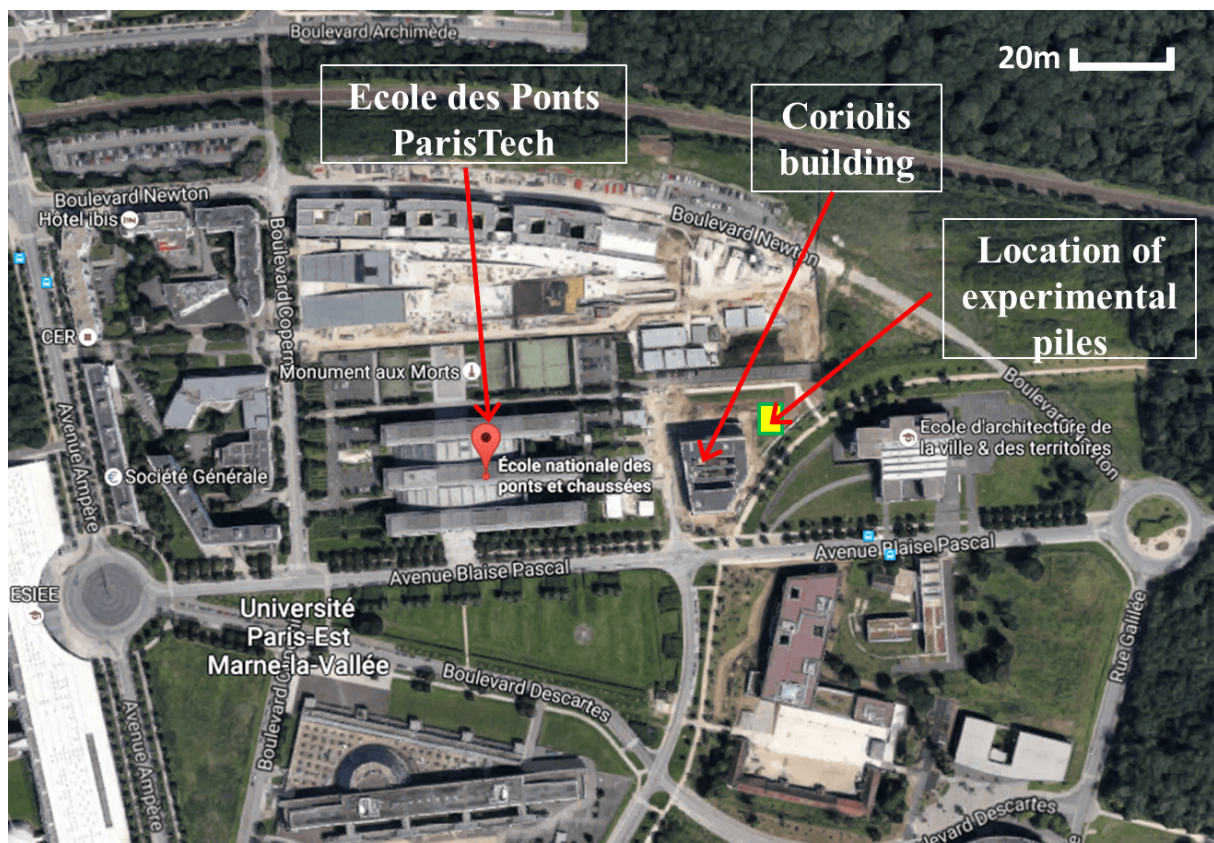


Fig. 3.1 Site location from Google Earth

### 3.2 Site description

The experiment piles were installed next to the Coriolis building at Ecole des Ponts ParisTech, and the piles were built at the same time with the foundation of this building. The

soil investigation for the construction of the Coriolis building can be found in Fondasol (2010). Four pressuremeter tests (PMT), following the French standard (NF P 94-110), have been done on the site and up to 20-m depth. The location of these test are shown in Fig. 3.2 (SP1-4).

The results obtained from the test SP1 are shown in Fig. 3.3 as an example. The profile of soil and the mechanical parameters of soil are represented. In which,  $E_M$  (MPa) is pressuremeter modulus;  $pf$  (MPa) is creep pressure;  $pl$  (MPa) is limited pressure;  $p_0$  (MPa) is horizontal stress of soil at the initial state,  $P_l^*$  (MPa) is the net limit pressure of soil ( $P_l^* = pl - p_0$ ) and  $P_f^*$  (MPa) is the net limit pressure of soil ( $P_f^* = pf - p_0$ ). The fill and silty layer is observed with 1.0-m thickness from the surface, the green clay distribute from 1.0-m to 8.0-m depth, the final is beige marl and white marl distribute from 8.0-m to 20.0-m depth. The silty layer has  $E_M = 15.6$  MPa,  $P_l^* = 0.74$  MPa,  $P_f^* = 0.4$  MPa; the green clay has  $E_M = 9.6 \div 16.3$  MPa,  $P_l^* = 0.59 \div 0.89$  MPa,  $P_f^* = 0.33 \div 0.52$  MPa; the beige marl has  $E_M = 18.5 \div 32.4$  MPa,  $P_l^* = 1.31 \div 2.35$  MPa,  $P_f^* = 0.7 \div 1.49$  MPa and the white marl has  $E_M = 30.7 \div 32.7$  MPa,  $P_l^* = 1.89 \div 2.25$  MPa,  $P_f^* = 1.10 \div 1.12$  MPa. It can be said that, the pile with 12-m depth mainly works within the green clay and partly in the beige marl.

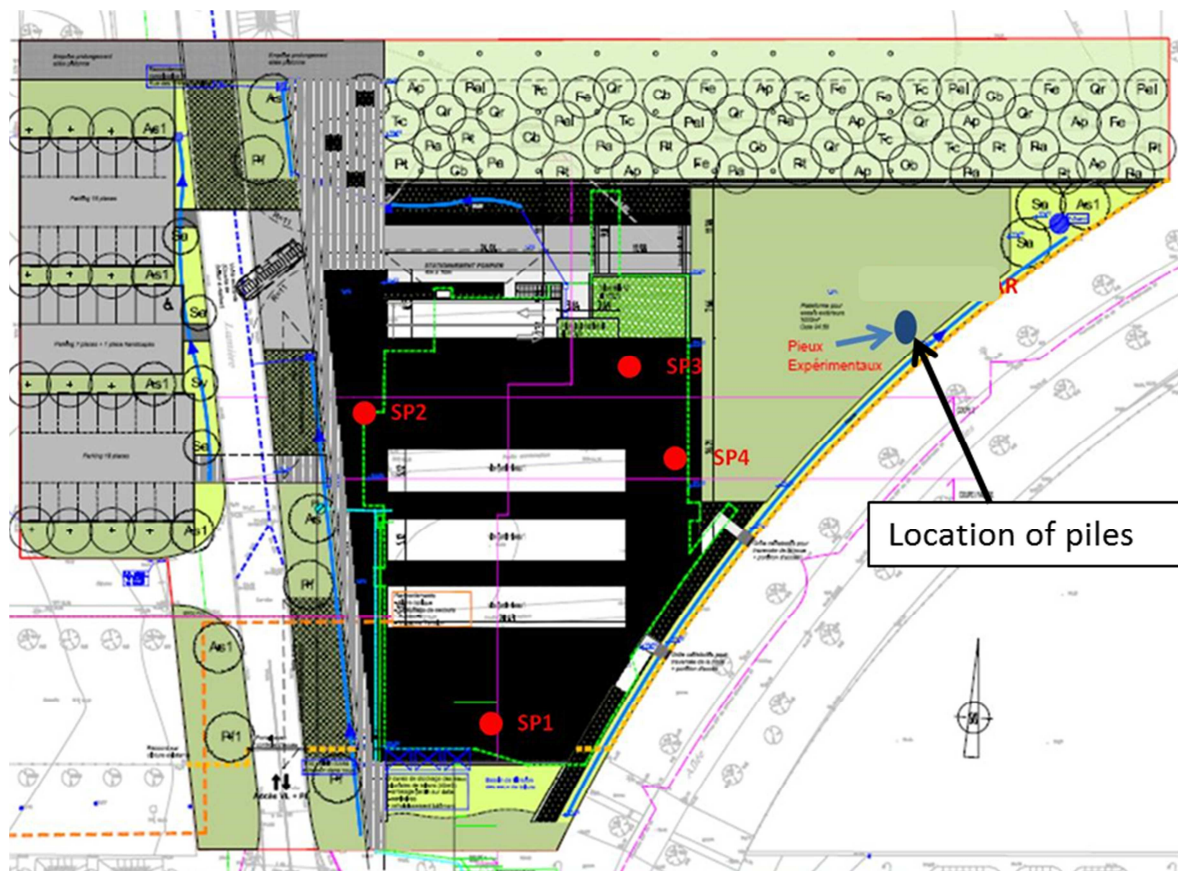


Fig. 3.2 Locations of pressuremeter tests.

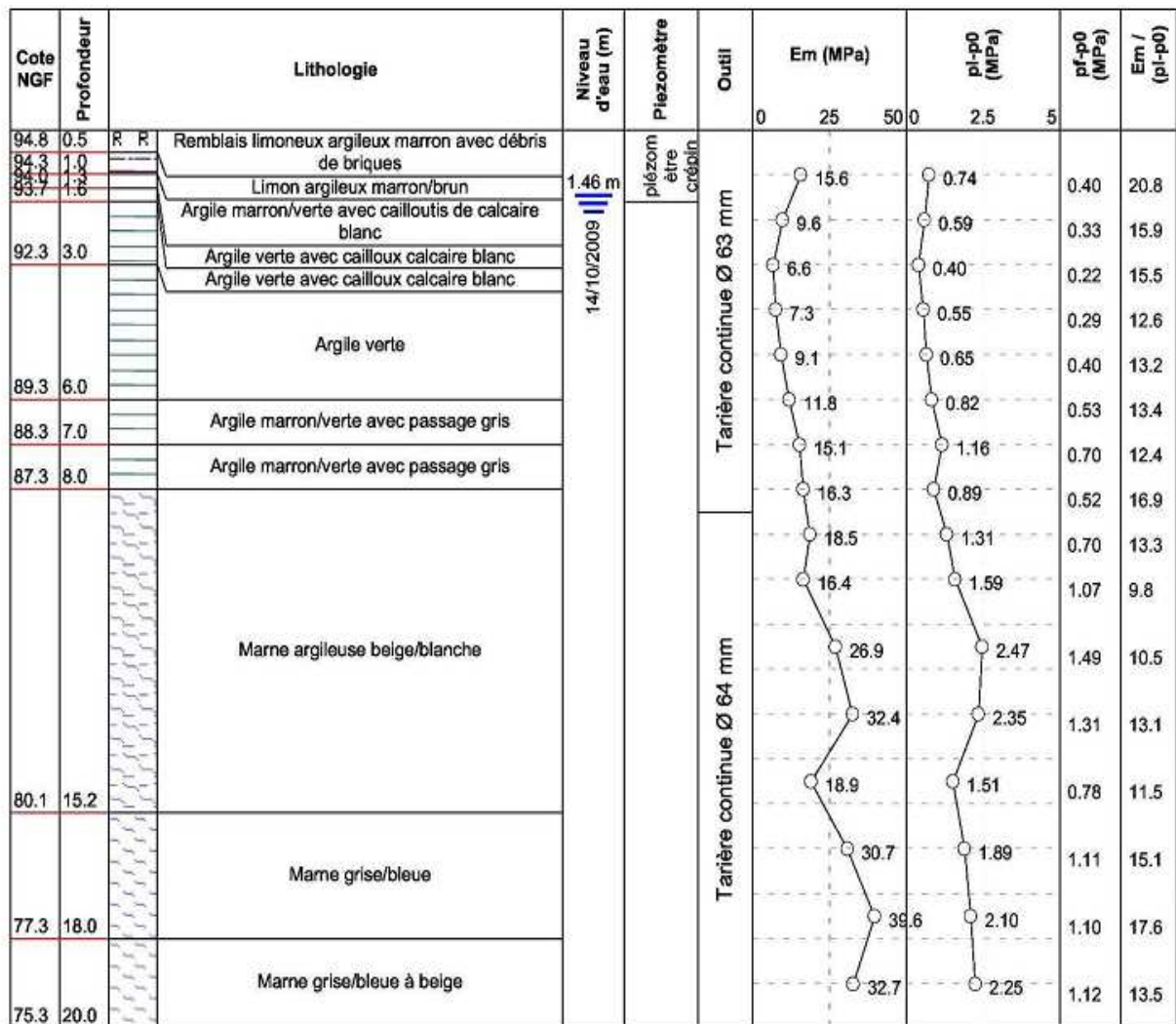


Fig. 3.3 Results of the pressuremeter test SP1

In Fig 3.4, the results of all the tests are plotted. It is observed that the values of  $Em$  and  $P_i^*$  by depth of all tests are relatively similar. The parameters increase with depth and depend on the type of soil. The values at lower part (from 8÷20-m depth) are twice larger than the one at the upper part (from 0÷8-m depth).

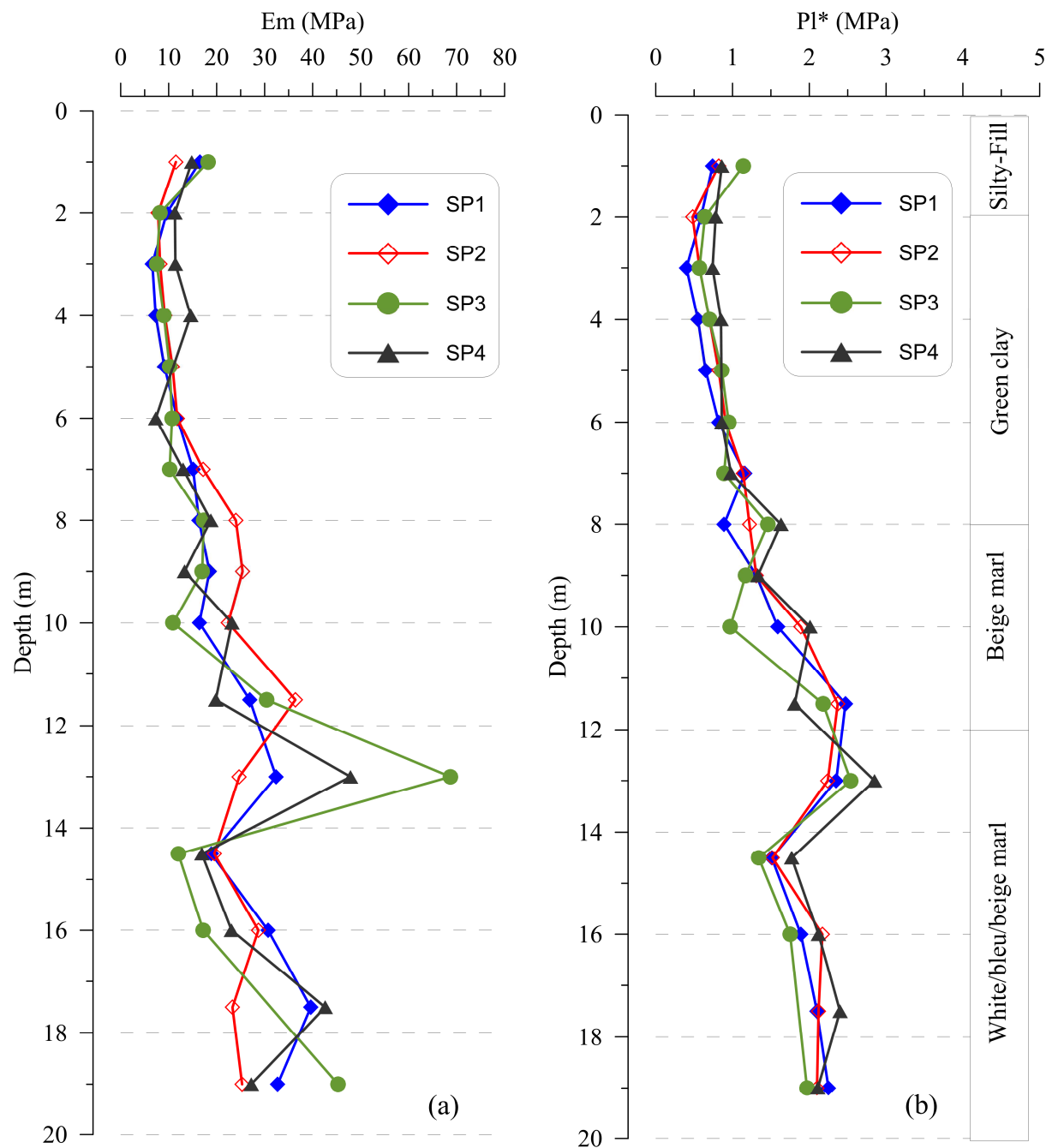


Fig 3.4. Pressuremeter test results, (a) pressuremeter modulus and (b) net limit pressure of soil

Based on the pressuremeter tests and borehole performed around the piles, the geological profile of the site is shown in Table 3.1. The piles are embedded in various soil layers: Fill, Silty clay, Green clay, Beige Marl, White Marl, successively. The pile toes touch the top of the White Marl layer situated at 12 m depth. Soil strength parameters (cohesion,  $c'$ , and angle of internal friction  $\phi'$ ) are measured from Consolidated Undrained (CU) triaxial tests and Direct shear tests (Fondasol, 2010). The thermal properties of soil (thermal conductivity,  $\lambda$ , and specific heat capacity,  $c_s$ ) are measured in laboratory. The soil hydraulic conductivity,  $k$ ,

was obtained by *in situ* infiltration test. The tip resistance ( $q_d$ ) of soil is measured by Dynamic Cone Penetration Test (DCPT) up to 9.0-m depth on site. The water table is at 4.0-m depth. It is to note that the parameters of fill layer are equal to the values of silty layer.

In the results of pressuremeter tests, the net limit pressure ( $P_l^*$ ) is defined as the failure pressure of soil at which the increase in volume of membrane equals to the initial volume of membrane in the borehole, the pressuremeter modulus ( $E_m$ ) is defined by the ratio of the increase in pressure by the increase in volume of membrane in the elastic phase.

Table 3.1 Geological profile and soil parameters

Profile	$\gamma$ (kN/m <sup>3</sup> )	$Pl^*$ (MPa)	$E_m$ (MPa)	$c'$ (kPa)	$\varphi'$ (°)	$\nu$	$q_d$ (MPa)	$\lambda$ (W/m/°C)	$c_s$ (J/kg/°C)	$k$ (m/s)
Fill 0.0-m ÷ 0.7-m	17	0.74÷1.14	11.5÷18.2	5	25	0.33	7÷15	1.0	1200	3E-5
Silty clay 0.7-m ÷ 2.0-m	18	0.74÷1.14	11.5÷18.2	5	25	0.33	7÷15	1.1	1150	1E-7
Green clay 2.0-m ÷ 8.0-m	18	0.5÷1.4	8.0÷18.8	30	22	0.33	3÷20	1.1	1150	4E-8
Beige marl 8.0-m ÷ 12.0-m	20	1.3÷2.4	18.0÷36.0	32	35	0.33	-	1.2	1000	1E-9
While/bleu/beige marl 12.0-m ÷ 20.0-m	20	1.3÷2.8	12.0÷68.0	32	35	0.33	-	1.2	1000	1E-9

### 3.3 Description of the experimental setup

#### 3.3.1 Pile installation

The cross-section of experimental piles is shown on the figure 3.7. The two piles have a diameter of 0.42 m and a length of 12 m. The distance between the piles' axis is 4.40 m. The reinforcement cage includes 5 longitudinal rebars  $\Phi 12$  and 60 rings of spiral bar  $\Phi 8$ . The piles were equipped with a heat exchanger W-tube (HDPE) that allows the circulation of a temperature-controlled fluid along the pile. There are three additional pipes embedded inside the pile to host temperature sensors at three depths, 1 m, 6 m and 11 m. That allows measuring the temperature at the pile's center, pile/soil interface and the middle point next to the steel cage.

The two experimental piles were installed by Continuous Flight Auger method (CFA). The pile installation consists of four main steps: (i) drilling a full length auger with a temporary plugged using a constant penetration rate and the auger being rotated so as to remove the soil; (ii) injecting concrete through the plugged system under pressure while extracting the auger; (iii) installing the reinforcement cage. The construction phases of pile are shown in figure 3.8.

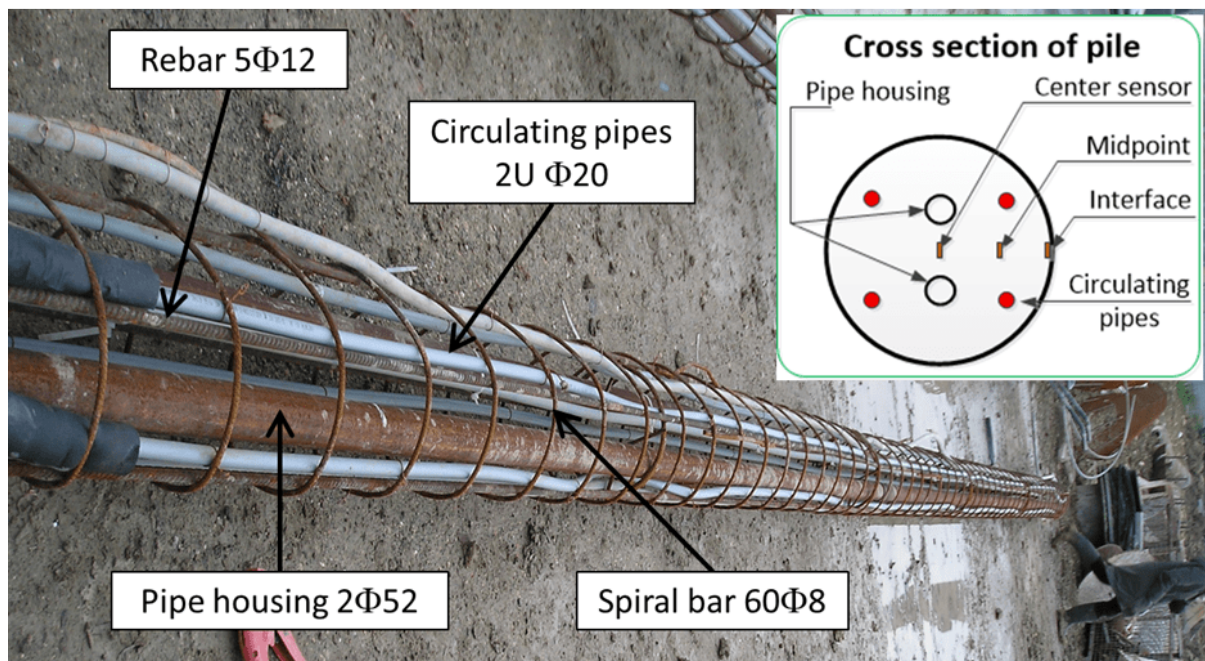


Fig. 3.7 Reinforcement cage of energy pile model



Fig. 3.8 Pile installation by Continuous Flight Auger (CFA) method: drilling & concrete casting (a); installing the reinforcement cage (b); work completed (c).

Fig. 3.9 shows the data recorded during the piles' installation. The diameter of the pile No. 1 at its top and bottom is slightly higher than at its center while the diameter of the pile No. 2 is quite uniform. Note that the pile diameter is estimated from the volume of concrete injected at each depth. The auger torque varies in range of 200÷400 bar during drilling. Its variation is related to the geological profile of the soils. In addition, the auger torque profiles obtained on the two piles are not similar. On the first pile (Fig. 3.9a), the torque in the green clay (from 2÷8 m) slightly changes while the torque in the marl layers (from 8÷12 m) is relatively uniform and equals to 200 bar. On the second pile (Fig. 3.9b), the torque in the green clay changes considerably while it slightly changes in the marl layers and equals to 400 bar. As a result, the torque in marl layers of the second pile is higher than that in the first pile and the torque in the green clay of the second pile is smaller than that in the first pile. The torque in the fill and silty clay layer (from 0÷2.0 m) is relatively high (400 bar) for both piles. This may be due to the presence of pebbles embedded in these soil layers. The pumping pressure of concrete is relatively uniform on the pile length. These results evidence that the ground is slightly heterogeneous; the geological profiles between the two piles can be slightly different from each other even if the distance between them is quite small (4.40 m). It is also in agreement with the result of pressuremeter tests (Fig 3.4.).

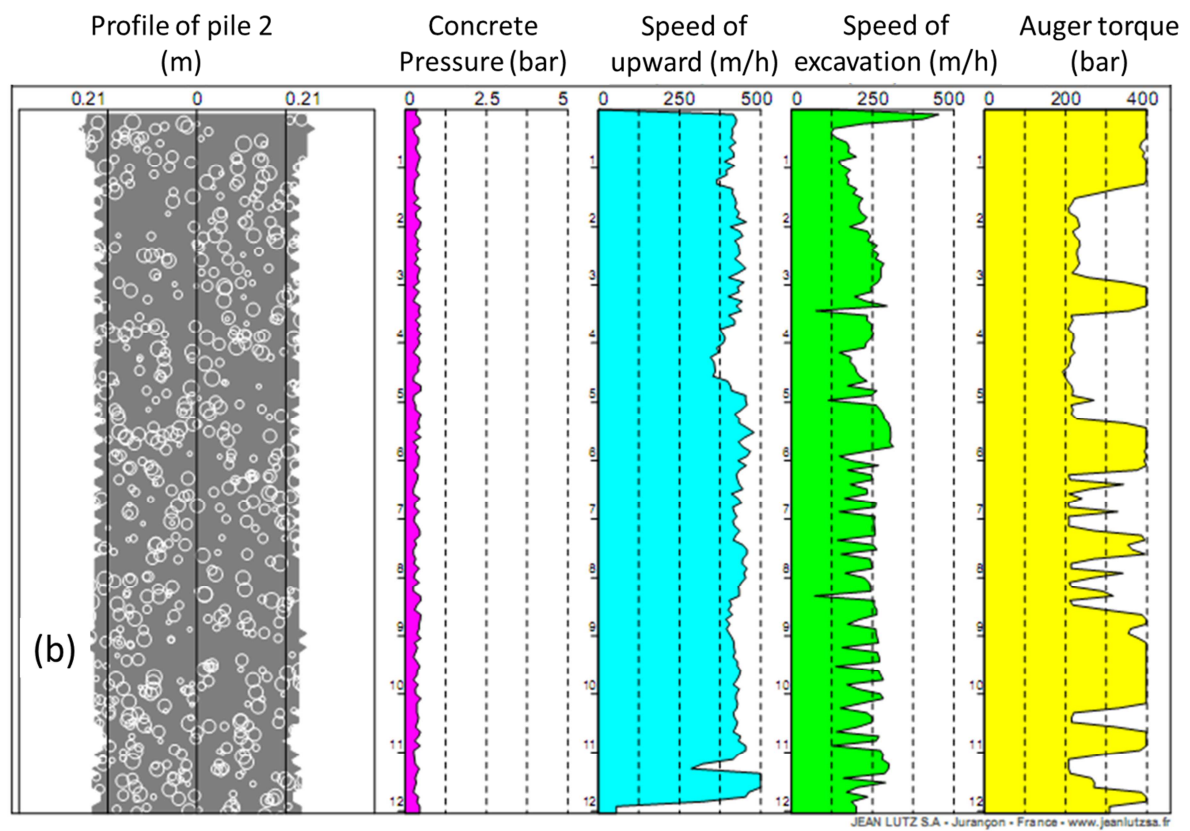
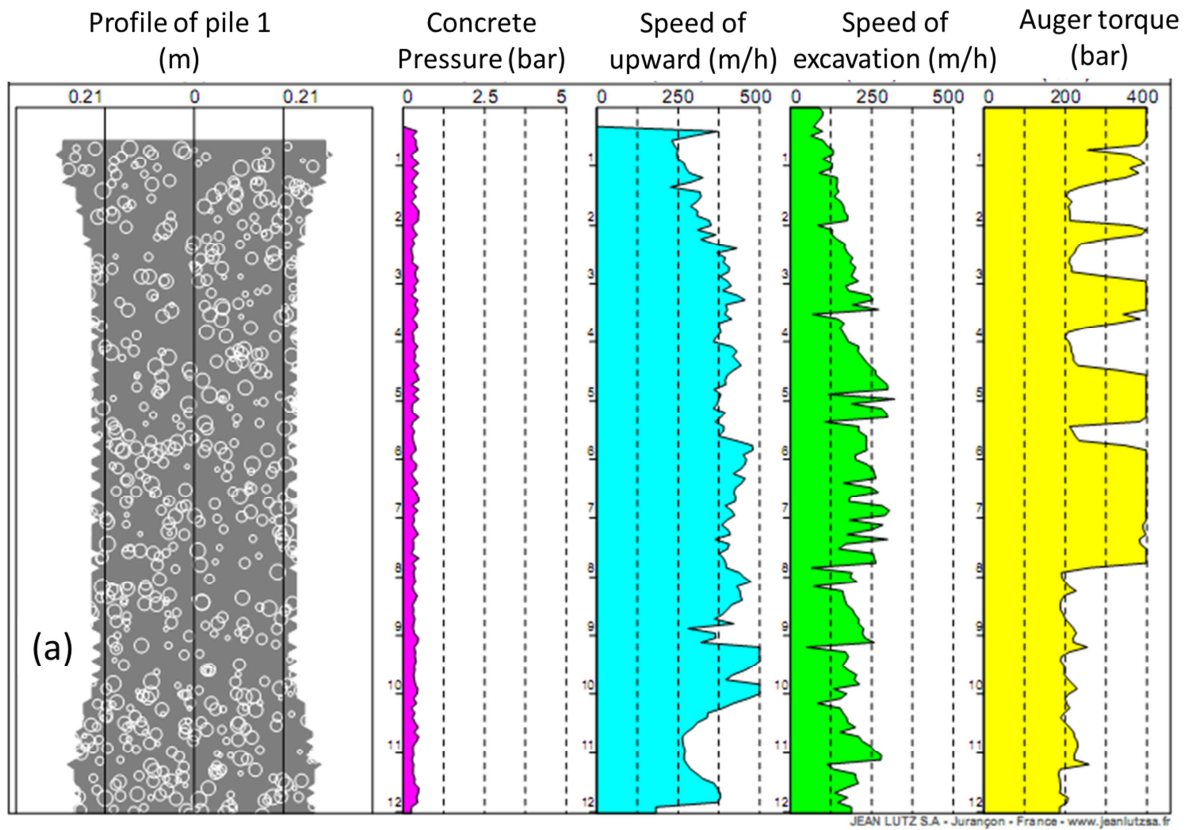


Fig. 3.9 Data recorded during the piles' installation: (a) Pile No. 1; (b) Pile No. 2.

### 3.3.2 System for controlling pile temperature and monitoring soil/pile temperatures

An overview of the experimental setup is shown in Fig. 3.10. To control the piles temperature, the W-tube is connected to a temperature-controlled bath. The flow rate of the fluid circulating in this tube is measured by a flow meter. Two temperature transducers (PT100) are used to measure the inlet and outlet fluid temperatures. The circulating fluid is a mixture of 80% water and 20% glycol to avoid freezing when temperature is negative.

The temperatures at different locations inside each pile are measured by 9 temperature transducers, which are embedded at three depths. Besides, two temperature transducers are installed in the surrounding soil at 6-m depth in order to measure temperature of soil at distances of 0.5 m and 1.0 m from the pile's axis. A data logger is used to record automatically data of all the sensors.

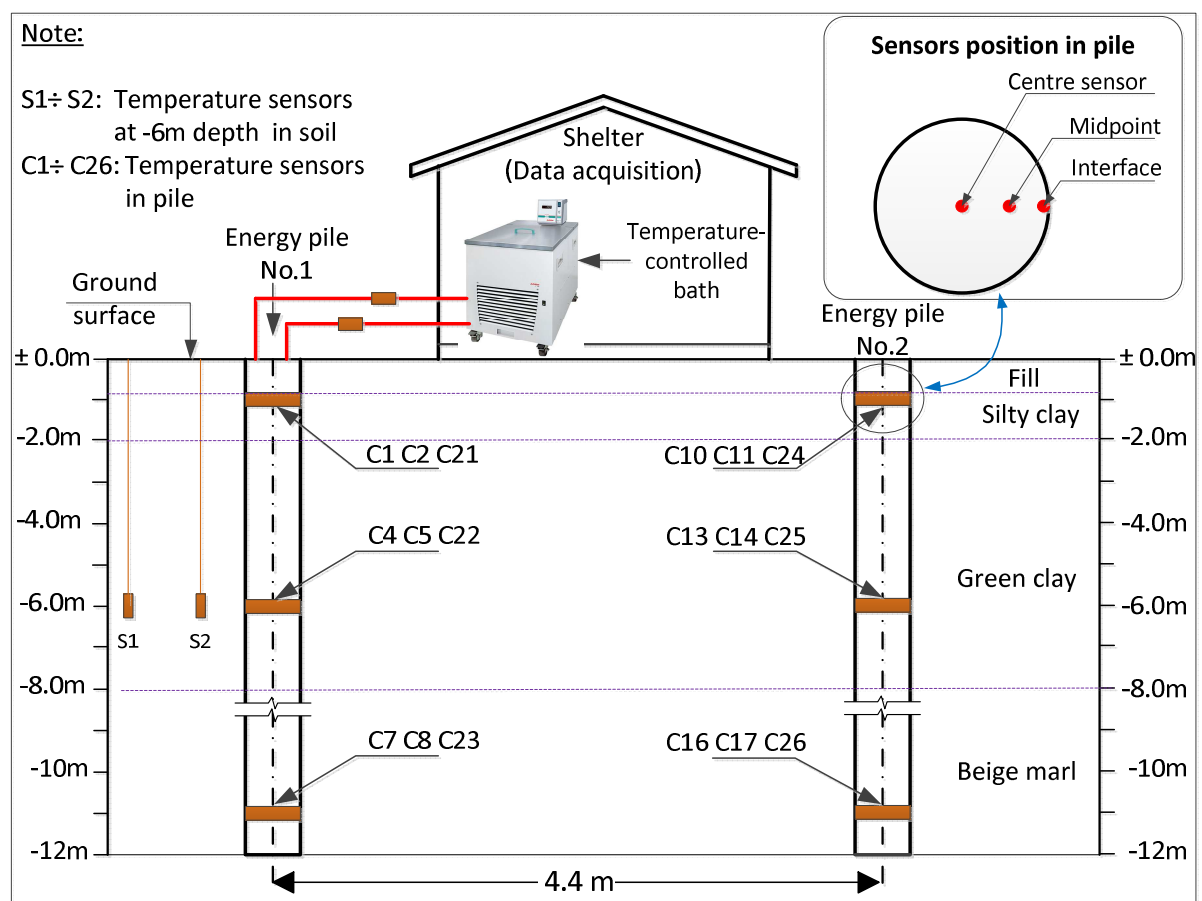


Fig. 3.10 Overview of the experimental setup

### 3.4 Experimental results

Heating/cooling tests have been firstly performed on the pile No. 1 in order to investigate the thermal behavior of the pile. In the first phase, the temperature of the temperature-controlled bath is fixed at 5 °C in order to cool down the pile. The results are shown in Fig. 3.11. Unfortunately, the soil and the fluid inlet/outlet temperatures are not available for this phase. Only the pile temperatures were recorded. Before the cooling phase, the average temperature of pile at 1-m depth equals to 18 °C while it equals to 12 °C at 6-m and 11-m depths. Actually, this phase has been performed during summer (July 2014) and the ground was being heated by the atmosphere. That can explain why the soil temperature close to the surface is higher than that at higher depths. The temperature recorded in the air during this period varies from 17 °C to 32 °C. In addition, it can be seen that the daily fluctuation of air temperature has a slight influence on the pile temperature.

In the cooling phase, temperatures of pile at 6-m and 11-m rapidly drop in the first day and reaches 9 °C after 4 days. Meanwhile, temperatures of pile at 1-m depth measured at the pile/soil interface and the midpoint drop from 18 °C to 12 °C, while that at the pile's center decreases until 10 °C. Note that, the sensor at pile-soil interface at 11-m depth is missing during the test due to a problem of electrical signal. At  $t = 13$  days, the pump was stopped and data was recorded for the recovery phase. Temperature of pile returns to the value equal to the initial temperature after 3 days in the recovery phase (Fig. 3.11).

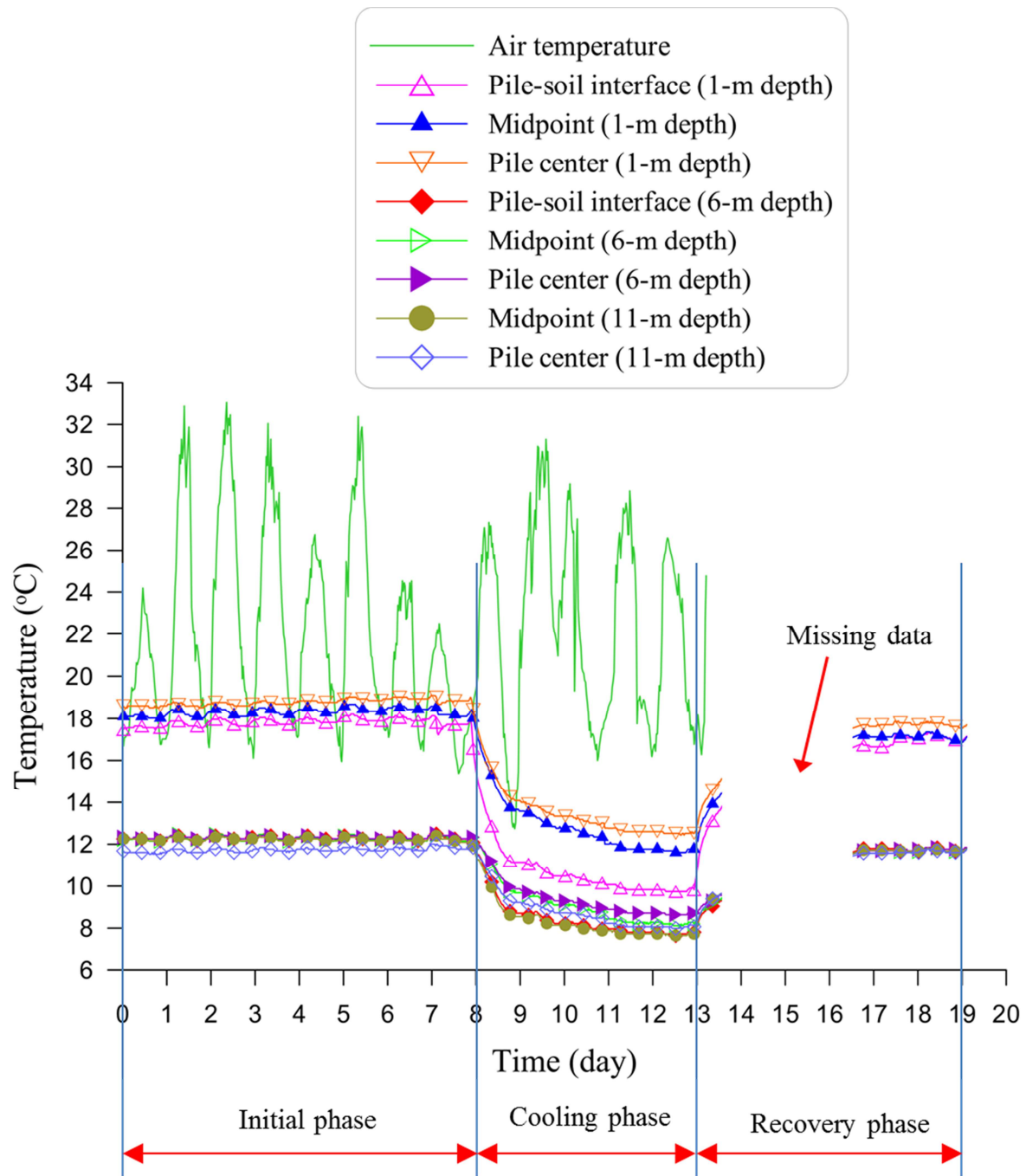


Fig. 3.11 Temperature of pile at different locations during the cooling phase

After the recovery phase, the pile was heated during 22 days by imposing the temperature of the bath at 40 °C. During this phase, temperatures of pile, soil and also inlet/outlet fluid were recorded (see Figs. 3.12, 3.13 and 3.14).

Fig. 3.12 shows that temperatures in the pile raise rapidly during the first 5 days of heating. After 5 days, these values increase with a lower rate and reach 30 ÷ 34 °C after 23 days. Temperature of pile is relatively uniform, with a difference of about 4 °C. This slight

heterogeneity in temperature can be explained on one hand by the initial temperature (12 °C at 6 and 11-m depths; 18 °C at 1-m depth) and the 3D distribution of heating pipes and temperature sensors (see the cross section in Fig. 3.7) on the other hand.

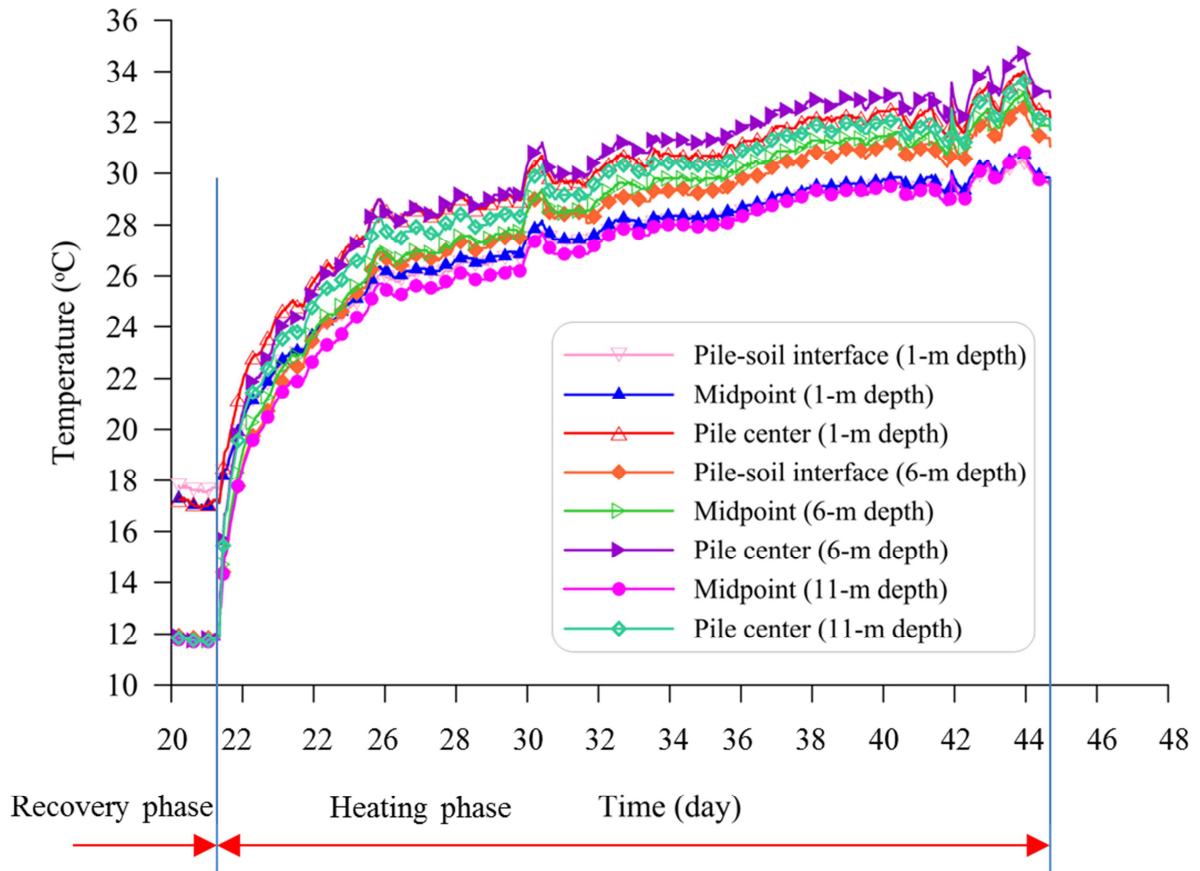


Fig. 3.12 Temperature of pile at different locations during the heating phase

The result related to the pile inlet and outlet temperatures are shown in Fig. 3.13. Note that even if the temperature of the bath was set at 40 °C, the inlet temperature took 23 days to reach this target. The results show that the fluid temperature decreases about 3 °C after circulating through the pile. With the flow rate measured by the flow meter and the thermal parameters of the fluid, the heat flow injected to the pile during this phase can be then estimated by the following equation:

$$Q = \rho \cdot c_p \cdot \Delta T \cdot v \quad (3.1)$$

where:  $\rho$  is density of the liquid ( $\text{kg/m}^3$ ),  $c_p$  is the specific heat capacity of liquid ( $\text{J/kg}^\circ\text{C}$ ),  $\Delta T$  is different temperature between inlet and outlet fluid ( $^\circ\text{C}$ ) and  $v$  is water flow rate measured by flow meter ( $\text{m}^3/\text{s}$ ).

The specific heat capacity of water-ethylene glycol heat transfer fluid is calculated from the specific heat capacities of water ( $c_{sw} = 4185 \text{ J/(kg}\cdot\text{°C)}$ ) and ethylene glycol ( $c_{sg} = 2460 \text{ J/(kg}\cdot\text{°C)}$ ). In the same way, the density of heat transfer fluid is determined from the densities of ethylene glycol ( $\rho_g = 1097 \text{ kg/m}^3$ ) and water ( $\rho_w = 1000 \text{ kg/m}^3$ ).

The heat flow injected to the pile during this phase is plotted versus elapsed time in Fig. 3.13. The average value equals to 740 W. Heat exchanger efficiency between pile and surrounding soil may be affected by the actual capacity of the pump during thermal loading. The average of heat exchange rate per unit length of pile is 60 W/m. This result is in accordance with the feasibility studies of energy foundations mentioned by Brandl (2006).

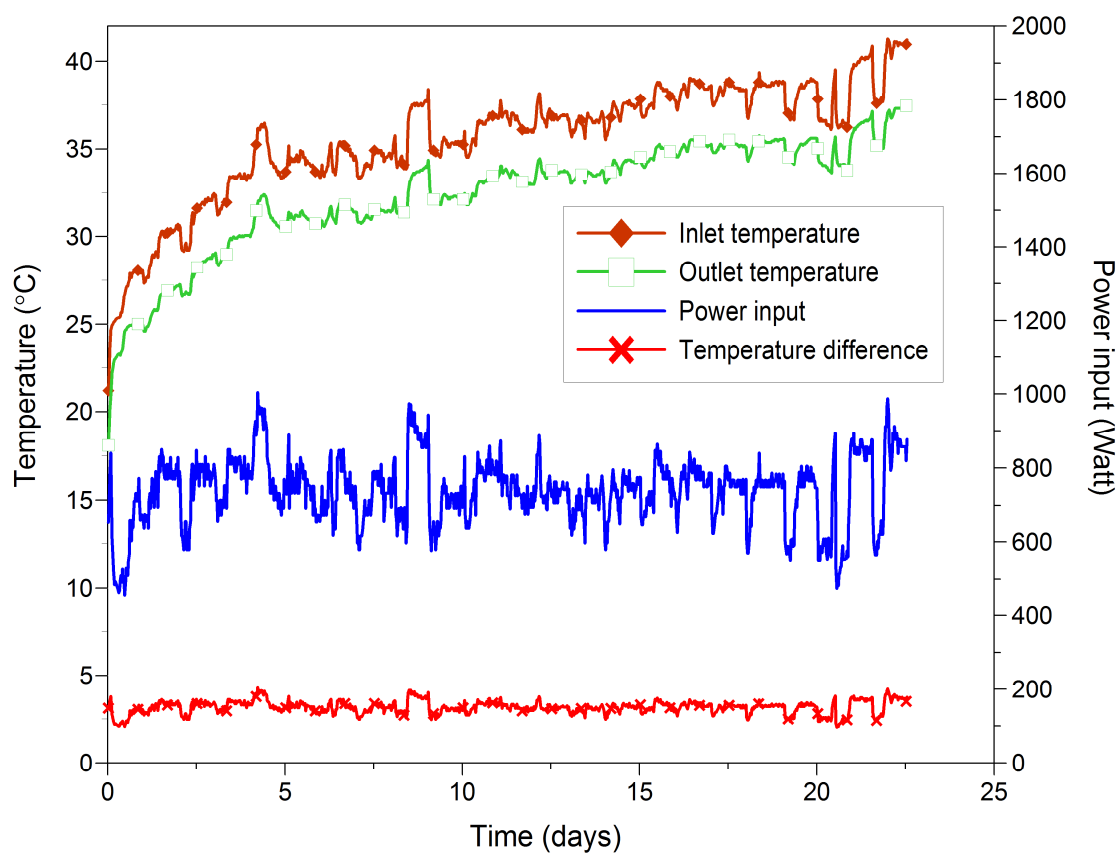


Fig. 3.13 Temperature of inlet and outlet fluid during heating phase

Results in Fig. 3.13 show that, in the natural state, temperature of pile between 6 and 11-m depth is similar and stable, it is unaffected by the temperature on the ground surface. Moreover, soil profile shows a homogeneous layer of green clay from  $-3.0 \div -10.0 \text{ m}$ . Thus temperature of pile and soil at 6.0-m depth is suitable to analyze temperature of the in-situ experiment during thermal loading. Fig. 3.14 shows the average pile temperature at 6-m depth and the temperatures measured in soil. The average temperature at 6-m depth of the

pile No. 2 is also plotted. The results show that the temperature of the pile No. 1 increases quickly during the first days and reaches 34 °C after 23 days. The soil temperatures measured at 0.5 and 1 m from the pile axis increase from 12.5 °C to 22 °C and 21 °C after this period, respectively. The temperature of the pile No. 2 is not influenced by the heating of the pile No. 1.

Fig. 3.15 shows temperature profile (temperature versus distance from the pile's axis) at different periods. It can be seen that the temperature of soil close to the pile No. 1 is strongly influenced by the pile temperature while that measured at 4.4 m (in the pile No. 2) is unchanged. That means the heating of the pile would influence the soil temperature at few meters around the pile.

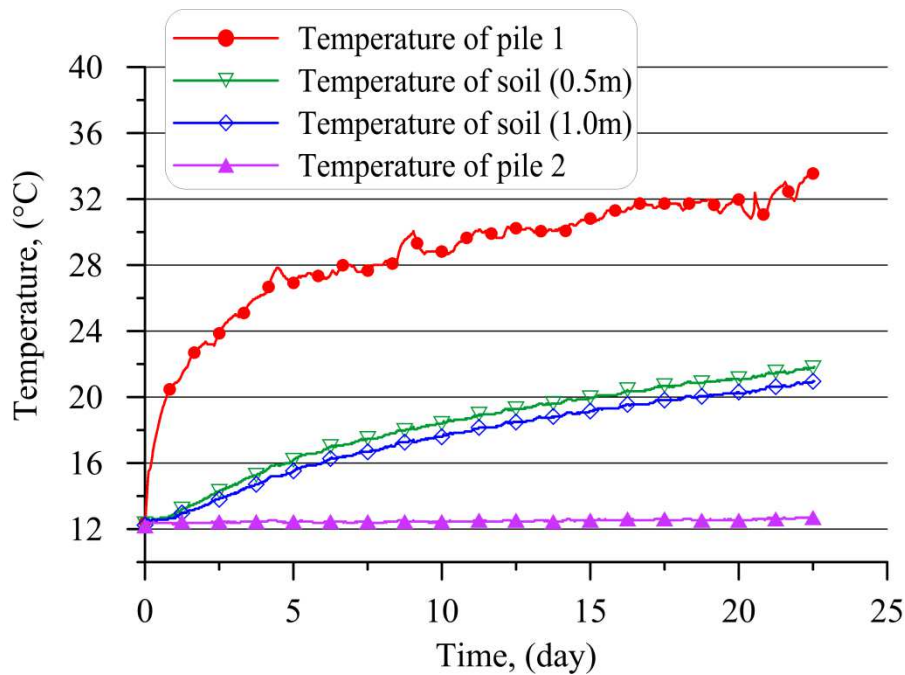


Fig. 3.14 Temperature of pile and soil at -6.0 m depth during the heating phase

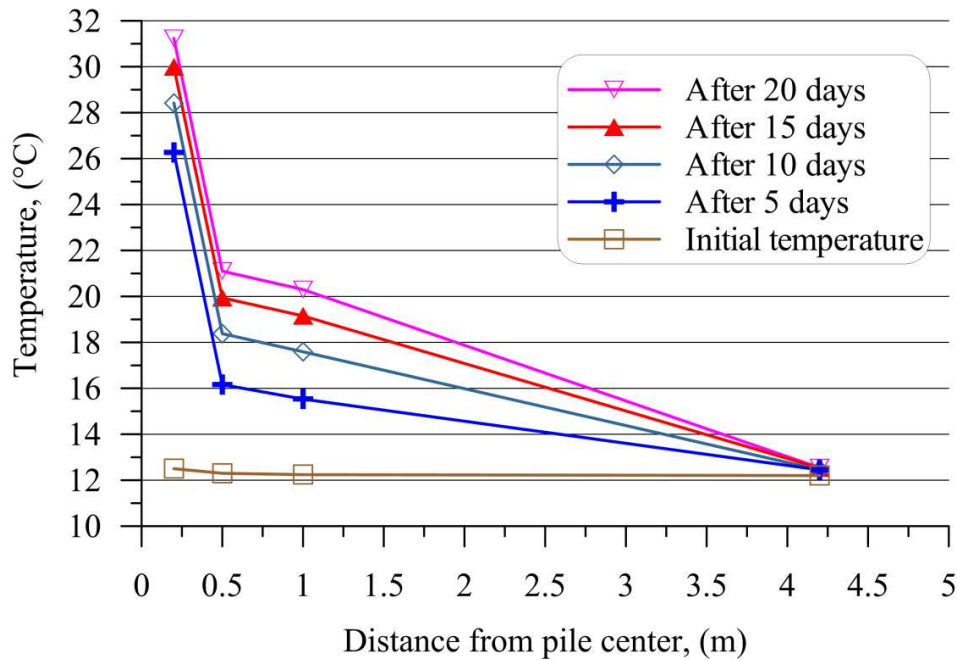


Fig. 3.15 Profile of temperature of soil around the pile at -6.0 m depth

### 3.5 Conclusions

Thermal tests have been performed on one full-scale experimental energy pile. The following conclusions can be drawn:

- ❖ Natural temperature of the ground from -6.0 m depths is constant (12 °C) and independent of air temperature.
- ❖ During a heating period, the heat flux injected to the pile per meter length is 60 W/m.
- ❖ It takes about 10 days to heat the pile up to 30 °C and in contrast it takes 5 days to cool down the pile down to 7 °C. This result is useful to program future tests that would be applied to these two piles to investigate its mechanical behavior under thermo-mechanical loads.

## CHAPTER 4: CONDUCTIVE HEAT TRANSFER ANALYSIS

### 4.1 Introduction

The literature review on analytical models for conductive heat transfer of vertical heat exchanger borehole (Chapter 1) shows that: (i) the majority of the models are firstly developed for calculating heat transfer in the long term, (ii) the conventional models often neglect heat capacity of the concrete pile by homogenizing environment of pile and surrounding soil, and (iii) temperature response inside the pile is considered at steady state thus the temperature of the system is only validated after a certain period of time. In contrast to the borehole, as energy piles have a higher diameter, it may take a considerable period of time to achieve thermal steady state. Furthermore, as the energy demand of the building changes within hours, the problem of heat transfer in the short time is really needed.

Besides, some advanced models have taken into account the effect of different thermal properties between pile and soil. These models considered also heat transfer in a short-term period. One of them is the analytical model of Li & Lai (2012b) where the authors developed the solution based on Jaeger's instantaneous line-source solution for a cylindrical composite medium. The solution is solved by Laplace transform method and expressed in form of Bessel functions (Jaeger, 1944). It can be said that this is a relatively general solution of transient heat model applied for energy pile. As can be, the solution requires a new G-function for any different configuration of fluid pipes. Meanwhile, study of Bozis *et al.* (2011) indicates that, if the pile and surrounding soil are assumed homogeneous and the total inlet heat flow is constant, the temperature at the pile center does not depend on the number of fluid pipes. By using the principle of superposition, temperature at any point M is expressed as follows (see Fig 4.1):

$$T_M(r_M, t) = T_0 + \frac{q}{4\pi\lambda} E_1\left(\frac{r_M^2}{4\alpha t}\right) \quad (4.1)$$

With  $E_1(x) = \int_x^\infty e^{-u}/u du$  is the exponential integral;  $q$  is the heat flow imposed into the pile (W/m),  $r_M$  is the distance from the point M to the heat sources,  $\lambda$  is the thermal conductivity (W/m.K) and  $\alpha$  is the thermal diffusivity (m<sup>2</sup>/s).

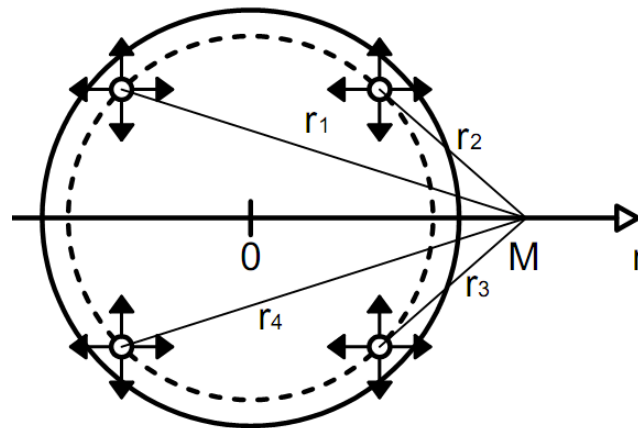


Fig. 4.1 Distribution of fluid pipes on the pile's cross section (Bozis *et al.*, 2011)

Although the solution is simple, this model does not consider the effect of different thermal properties between pile and soil. In addition, it can be applied only after a certain period since the beginning of heating,  $t > 5 r_b^2/\alpha$ , with  $\alpha$  is soil thermal diffusivity and  $r_b^2$  is diameter of heat source. That period typically takes 1÷2 hours.

The solution of Lamarche & Beauchamp (2007) refers to an infinite line source located at the pile center. Two different cases have been mentioned: the first one corresponds to a given heat flow and the second one corresponds to a given fluid temperature. Heat transfer equation of pile and soil were determined independently based on the initial and boundary conditions, in which the temperature at the pile-soil interface is continuous and the temperature functions refer to thermal properties of both pile and soil. However, only the heat transfer function inside the pile has been identified (see equation 1.16 in Chapter 1). This solution is found by using the Laplace transform method and also the contour integration analysis which is mentioned in the study of Carslaw & Jaeger (1940).

To sum up, with the constant inlet heat flow assumption, temperature of pile does not depend on the number of fluid pipes (after Bozis *et al.* 2011) and therefore the use of equivalent diameter pipe placed at the pile center as mentioned in the works of Lamarche & Beauchamp (2007) can represent satisfactorily the temperature of pile. The solution of Li & Lai (2012a) is expressed in a more complex form than the model of an equivalent infinite line source that locates in the pile center (Lamarche & Beauchamp, 2007). Moreover, it depends on the configuration of fluid pipes.

In the present work, a new simplified function, which allows determining heat transfer in surrounding soil in short-term periods, is presented. This solution is based on simple hypothesis and using the technique proposed by Lamarche & Beauchamp (2007). In fact, fluid pipe diameter is often much smaller than the pile diameter so the thermal properties of the pipes can be ignored. Instead of using the solid cylindrical heat source as showed in the solution of Lamarche & Beauchamp (2007), in the present work, an infinitive source model located at the pile center is considered.

## 4.2 Proposed analytical model

The heat source is supposed to be located at the pile center (Fig. 4.2). The pile temperature is considered uniform and it only depends on time. Thus the problem is solved with the following assumptions:

- ❖ The heat source is an infinite line source;
- ❖ The heat transfer mechanism in pile and surrounding soil is purely conductive;
- ❖ The surrounding soil is a homogeneous and semi-infinite medium;
- ❖ Initial soil and pile temperatures is homogenous ( $T_0$ );
- ❖ A constant inlet mass flow rate is imposed to the heat source and heat transfer in the vertical direction is negligible;
- ❖ The pile has a very high thermal conductivity.

It is worth noting that the assumption that the initial temperature in soil and pile are homogeneous restricts the use of any analytical solution to monotonic temperature changes (either cooling or heating) making them unusable to model thermal cycles.

The initial temperature conditions are written as follows:

$$\begin{cases} 0 < r \leq r_p, T = T_{pile} \\ r_p \leq r < \infty, T = T_{soil} \\ t = 0, T_{pile} = T_{soil} = T_0 \end{cases} \quad (4.2)$$

and the boundary conditions are written as follows:

$$\begin{cases} r = r_p, T_{soil}(r, t) = T_{pile}(r, t) \\ r = \infty, T_{soil}(r, t) = T_0 \\ -\lambda_{soil} A \frac{dT_{soil}}{dr} \Big|_{r=r_p} = \dot{Q}_{soil}, [W] \end{cases} \quad (4.3)$$

where  $r_p$  is the radius of pile,  $\lambda_{soil}$  is the thermal conductivity of soil,  $A$  is the heat transfer area ( $m^2$ ) and  $\dot{Q}_{soil}$  is the inlet or outlet heat flow.

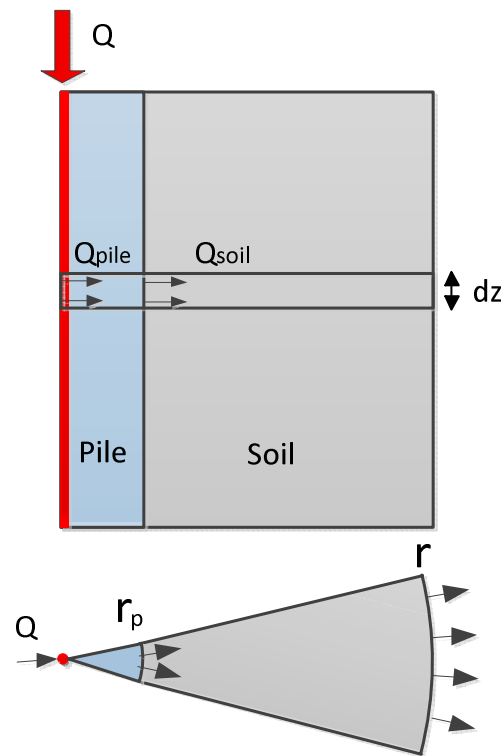


Fig. 4.2. Conductive heat transfer model

The heat transfer from the heat source to the surrounding soil can be solved by combining the heat energy balance and the heat conduction equations:

$$dQ = const, (J) \quad (4.4)$$

$$\frac{1}{\alpha} \frac{\partial T}{\partial t} = \frac{\partial^2 T}{\partial r^2} + \frac{1}{r} \frac{\partial T}{\partial r} \quad (4.5)$$

where,  $\alpha$  is the thermal diffusivity ( $m^2/s$ ).

By applying a constant heat flow along the entire length of the heat source, the energy balance can be expressed as follows:

$$\begin{aligned}\dot{Q} &= \text{const}, [W] \\ dQ &= dQ_{pile} + dQ_{soil}, [J]\end{aligned}\quad (4.6)$$

Combining the equations (4.3÷4.6) allows determining the temperature of the surrounding soil. For simplicity, denote  $T(r,t) = T_{soil} - T_0$ , where  $T(r,t)$  is the soil temperature in excess to the initial temperature; it varies with time and space.

The initial and boundary conditions for temperature of soil can be re-written as follows:

$$\begin{cases} t = 0 \Rightarrow T(r, t = 0) = 0 \\ r = r_p \Rightarrow T(r, t)|_{soil} = T(r, t)|_{pile} \\ r = \infty \Rightarrow T(r = \infty, t) = 0 \\ -\lambda_{soil} A \frac{dT(r, t)}{dr} \Big|_{r=r_p} = \dot{Q}_{soil}, [W] \end{cases}\quad (4.7)$$

The equation (4.6) can be represented as follows:

$$\dot{Q} - \left| -\lambda_{soil} A \frac{dT_{soil}}{dr} \right| = m_{pile} c_{pile} \frac{dT_{soil}}{dt}, \left[ \frac{J}{s} \right]\quad (4.8)$$

Considering conduction only, the heat transfer equation in soil can be written as follows:

$$\frac{1}{\alpha_{soil}} \frac{\partial T(r, t)}{\partial t} = \frac{\partial^2 T(r, t)}{\partial r^2} + \frac{1}{r} \frac{\partial T(r, t)}{\partial r}\quad (4.9)$$

where  $\alpha_{soil}$  is the soil thermal diffusivity,  $r$  is the distance from pile' surface.

Rewriting the heat transfer equation in Laplace's space:

$$\frac{d^2 \bar{T}}{dr^2} + \frac{1}{r} \frac{d\bar{T}}{dr} - q^2 \bar{T} = 0\quad (4.10)$$

where  $q^2 = s\alpha^1$  and  $s$  is a complex variable. A general solution of soil temperature is expressed as follows:

$$\bar{T}(r, s) = a_1 K_0(qr) + a_2 I_0(qr)\quad (4.11)$$

where  $I_0$  and  $K_0$  are the modified Bessel functions of the first and the second kinds, respectively.  $a_1, a_2$  are constants. From the temperature condition at the boundary,  $a_2$  equals to zero. The equation thus simplifies to:

$$\bar{T}(r, s) = a_1 K_0(qr) \quad (4.12)$$

By using the boundary conditions, the constant  $a_1$  of the equation can be found:

$$a_1 = \frac{\dot{Q}}{s} \frac{1}{m_{soil} c_{soil} s K_0(qr_p) + \lambda_{soil} A q K_1(qr_p)} \quad (4.13)$$

Thus

$$\bar{T}(r, s) = \frac{\dot{Q}}{s} \frac{K_0(qr)}{m_{soil} c_{soil} s K_0(qr_p) + \lambda_{soil} A q K_1(qr_p)} \quad (4.14)$$

The inverse Laplace transform of the solution is written as follows:

$$T(r, t) = \frac{1}{2\pi i} \int_{a-i\infty}^{a+i\infty} e^{st} \bar{T}(r, s) ds \quad (4.15)$$

This equation can be solved by the contour integration method. By using the Cauchy theorem, the inverse Laplace integration equation (4.15) can be expressed by the sum of the integral over a closed contour (Fig. 4.3), more details can be seen in the studies of Carslaw & Jaeger (1940) and Lamarche & Beauchamp (2007).

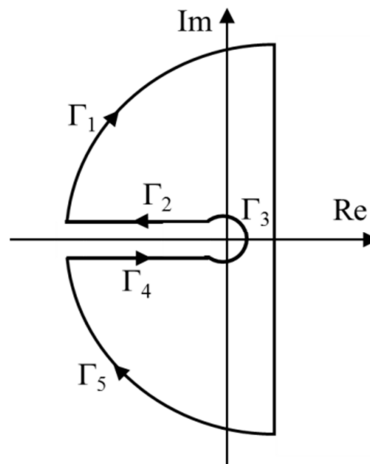


Fig. 4.3 Contour of integration

Thus, the equation (4.15) is then expressed in the closed contour form:

$$T(r, t) = \frac{1}{2\pi i} \int_{\Gamma=\Gamma_1+\Gamma_2+\Gamma_3+\Gamma_4+\Gamma_5} e^{st} \bar{T}(r, s) ds \quad (4.16)$$

The limits of the function under the integral in the contour  $\Gamma_2$  and  $\Gamma_4$  are infinite when the variable  $s$  tends to zero. This makes the integral on the closed contour divergent. The problem is then solved by examining the convergence of the derivative of the integral in equation (4.16):

$$\frac{\partial T(r, t)}{\partial t} = \frac{1}{2\pi i} \int_{\Gamma=\Gamma_1+\Gamma_2+\Gamma_3+\Gamma_4+\Gamma_5} e^{st} s \bar{T}(r, s) ds \quad (4.17)$$

Based on the studies of Carslaw & Jaeger (1940), when the radii of contour  $\Gamma_1$  and  $\Gamma_5$  tend to infinity the integral in these contours should be zero. By applying the Cauchy's integral for holomorphic function, the integral on the contour  $\Gamma_3$  equals zero. It can be easily deduced that the integral on the contour  $\Gamma_2$  and  $\Gamma_4$  should be convergent.

$$\int_{\Gamma_1, \Gamma_5} e^{st} s \bar{T}(r, s) ds = 0 \quad \text{when } R \rightarrow \infty \quad (4.18)$$

$$\int_{\Gamma_3} e^{st} s \bar{T}(r, s) ds = 0; \quad \text{due to } \lim_{s \rightarrow 0} f(s) \approx \lim_{s \rightarrow 0} [s \ln(s)] = 0 \quad (4.19)$$

Therefore, expression of equation (4.17) becomes:

$$T(r, t) = \int_0^t \frac{\partial T(r, t)}{\partial t} dt = \frac{\dot{q}}{2\pi i} \int_{\Gamma_2+\Gamma_4} (e^{st} - 1) \frac{K_0(qr)}{\pi r_p \left[ r_p \rho_{pile} c_{pile} s K_0(qr_p) + 2\lambda_{soil} q K_1(qr_p) \right]} s ds \quad (4.20)$$

The integration is now solved by change of variable method.

By using expression of Hankel function of the first kind for integral on the contour  $\Gamma_4$ :

$$H_\alpha^{(1)}(x) = J_\alpha(x) + iY_\alpha(x) \quad (4.21)$$

$$\text{with } -\pi < \arg(x) \leq \frac{\pi}{2} \Rightarrow K_\alpha(x) = \frac{\pi}{2} i^{\alpha+1} H_\alpha^{(1)}(ix)$$

$$\text{put } s = \alpha u^2 e^{-i\pi} \Rightarrow qr = ure^{-\frac{i\pi}{2}}; qr_p = ur_p e^{-\frac{i\pi}{2}} \text{ and } \frac{ds}{s} = 2 \frac{du}{u}$$

$$T(r, t) = \frac{\dot{q}}{\pi^2 r_p \lambda_{soil}} \frac{1}{i} \int_0^\infty (1 - e^{-\alpha u^2 t}) \frac{J_0(ur) + iY_0(ur)}{\left[ A_1 u J_0(ur_p) + A_2 J_1(ur_p) \right] + i \left[ A_1 u Y_0(ur_p) + A_2 Y_1(ur_p) \right]} u^2 du \quad (5.28)$$

Similarly for the integral on the contour  $\Gamma_2$ :

$$H_\alpha^{(2)}(x) = J_\alpha(x) - iY_\alpha(x) \quad (4.22)$$

$$\text{with } \frac{\pi}{2} < \arg(x) \leq \pi \Rightarrow K_\alpha(x) = \frac{\pi}{2} (-i)^{\alpha+1} H_\alpha^{(2)}(ix)$$

$$\text{put } s = \alpha u^2 e^{i\pi} \Rightarrow qr = ure^{\frac{i\pi}{2}}; qr_p = ur_p e^{\frac{i\pi}{2}} \text{ and } \frac{ds}{s} = 2 \frac{du}{u}$$

We obtain the conjugate of equation in contour  $\Gamma_4$ :

$$T(r, t) = -\frac{\dot{q}}{\pi^2 r_p \lambda_{soil}} \frac{1}{i} \int_0^\infty (1 - e^{-\alpha u^2 t}) \frac{J_0(ur) - iY_0(ur)}{\left[ A_1 u J_0(ur_p) + A_2 J_1(ur_p) \right] - i \left[ A_1 u Y_0(ur_p) + A_2 Y_1(ur_p) \right]} u^2 du \quad (4.23)$$

The final solution for soil temperature is then:

$$T_{soil}(r, t) = T_0 + \frac{\dot{q}}{\lambda_{soil}} \frac{2}{\pi^2 r_p} \int_0^\infty (1 - e^{-\alpha u^2 t}) \frac{Y_0(ur)\phi - J_0(ur)\psi}{\phi^2 + \psi^2} \frac{du}{u^2} \quad (4.24)$$

Temperature response function (G-function) of surrounding soil can be drawn:

$$G_{soil}(r, t) = \frac{2}{\pi^2 r_p \lambda_{soil}} \int_0^\infty (1 - e^{-\alpha u^2 t}) \frac{Y_0(ur)\phi - J_0(ur)\psi}{\phi^2 + \psi^2} \frac{du}{u^2} \quad (4.25)$$

where

$$\phi = A_1 u J_0(ur_p) + A_2 J_1(ur_p); \psi = A_1 u Y_0(ur_p) + A_2 Y_1(ur_p); A_1 = -r_p \tilde{\rho} \tilde{c}; A_2 = 2$$

$$\tilde{\rho} = \rho_{pile} / \rho_{soil}; \tilde{c} = c_{pile} / c_{soil}$$

$$(4.26)$$

The final solution of soil temperature shows that thermal property of pile (specific heat capacity) is mentioned in the solution. Thus the total inlet heat flow is used partially to heat the pile and the remaining part to heat up the surrounding soil. It can be seen that the

proposed solution (equation 4.25) is expressed in a simpler form when compared to the model of Li & Lai (2012a) (equation 1.18 in Chapter 1). In general, the integral of a function that is expressed under Bessel functions are not solved directly but rather through the support of numerical softwares such as Matlab, Maple, ...

### 4.3 Validation of the proposed solution

In this section, the analytical results (using MATLAB) are compared with the numerical calculation using the finite element method (Plaxis 2D Thermal, version 2016). A two dimensions axisymmetric model of unit length of pile and surrounding soil is used. Boundary of the semi-infinite surrounding soil is chosen large enough to neglect its impact on temperature changes. The finite element mesh is refined small enough until no variation is obtained for the results, in which the minimum size of the refined mesh is modeled for the soil and pile elements located near the heat source (Fig. 4.4). The initial temperature of pile and soil is constant and homogeneous. The heat flow is null at the surface, bottom and vertical sides. To avoid the effect of thermal expansion coefficient on the temperature (which is not accounted for in the proposed analytical solution), a very small thermal expansion coefficient is used in the numerical model. In addition, only conductive heat transfer is considered in the numerical model. The parameters, used for the numerical and the analytical calculations, are presented in the Table 4.1. Note that all the parameters of the model and also the thermal load program are similar with the full-scale experimental pile which is mentioned in the Chapter 3. To heat the pile, a constant rate of heat (60 W/m) is imposed along the pile on a cylindrical-surface with 0.32 m diameter (Fig. 4.4). Note that this rate of heat flow is similar to that measured from the full-scale experiment during heating.

Table 4.1. Parameters used for the calculations

Parameters	Pile	Soil
Dimensions: radius x length (m x m)	0.21 x 1.0	20.0x1.0
Thermal conductivity $\lambda$ (W/(m.K))	1.5	1.0
Specific heat capacity $c$ (kJ/kg/K)	1.1	1.0
Density $\rho$ (kg/m <sup>3</sup> )	2500.0	1800.0
Initial temperature $T_o$ (°C)	12.5	12.5

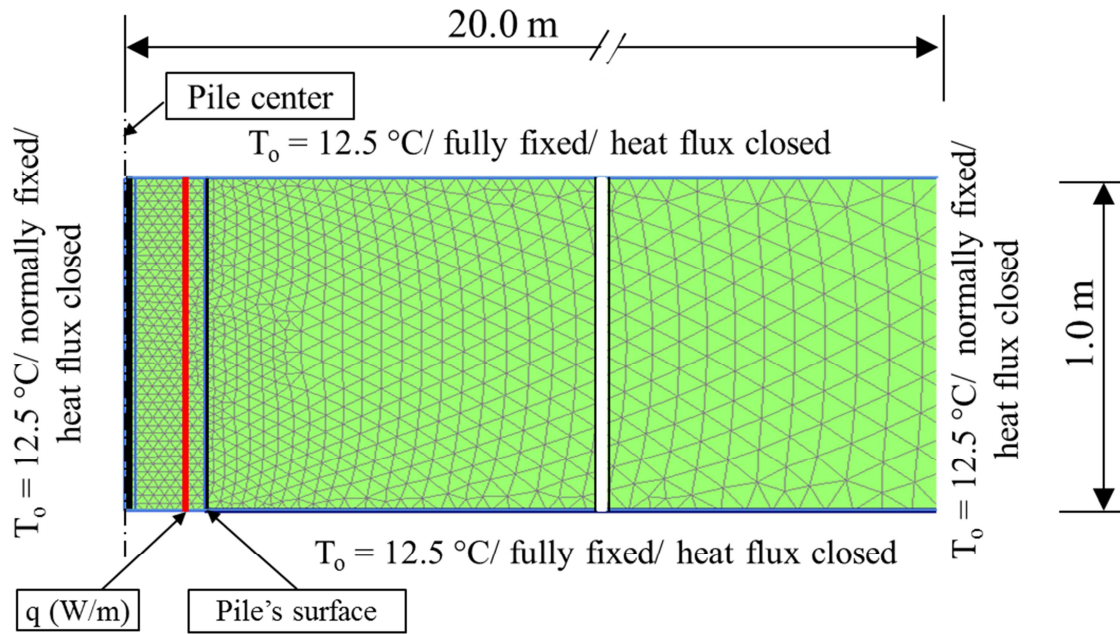


Fig. 4.4 Boundary and initial conditions

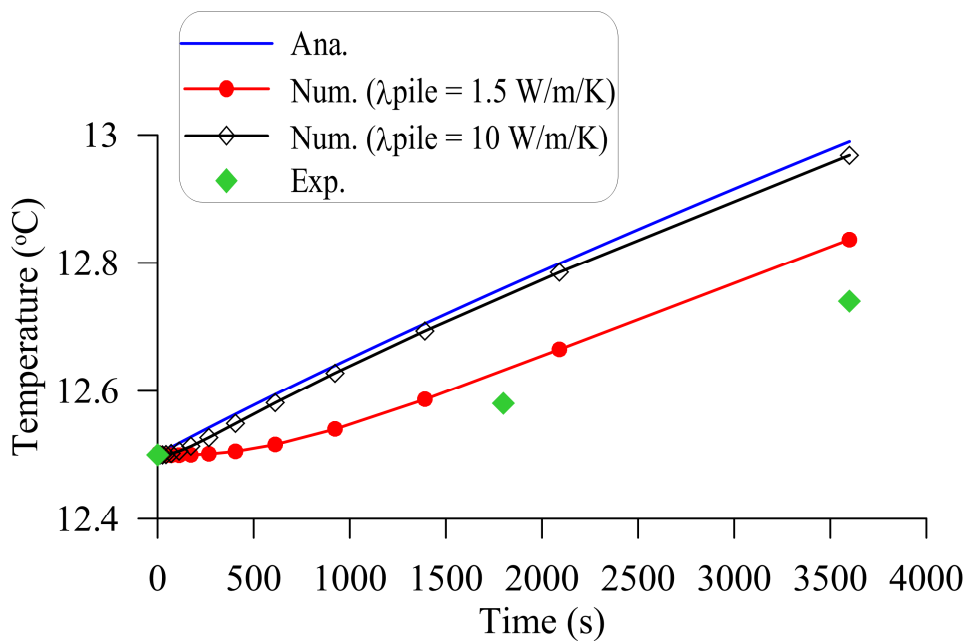


Fig. 4.5 Temperature at pile's wall versus elapsed time during the first hour of heating phase

Fig. 4.5 shows the pile temperature versus elapsed time during the first hour of heating phase. The analytical result (Ana.) is similar to the numerical (Num.) one when the thermal conductivity of the pile is set at 10 W/(m.K) (which is much higher than the real value, 1.5 W/(m.K)). When the real value of thermal conductivity is used for the numerical simulation, the rate of temperature increase is smaller than that obtained by the analytical calculation.

Note that, in the analytical model, the thermal conductivity of the pile is assumed to be very high.

Temperature of pile's surface in the experiment shows a smaller value compared to the model but closes to the numerical result. This can be explained by the effect of heat transfer between concrete and high density polyethylene (HDPE) tube which contains the water and transducer PT100 inside, in which the HDPE material has a smaller thermal conductivity compared to that of concrete.

Fig. 4.6 shows the temperature values obtained at the soil/pile interface (0.21 m from the pile axis) and at two distances from the pile axis (0.5 m and 1.0 m) versus elapsed time for the whole heating phase. In spite of the assumption of very high thermal conductivity of the pile in the analytical model, it can be seen that the results obtained by the numerical simulation and those by the analytical calculation are in good agreement for the whole heating phase (even if the thermal conductivity of the pile is set at  $1.5 \text{ W}/(\text{m}\cdot^\circ\text{C})$  in the numerical simulation). In addition, the temperatures at the pile's wall and at distance 0.5 m in surrounding soil are relatively similar with the experiment results. The discrepancies between experiment and models are negligible.

Fig. 4.7 shows the temperature versus the distance from the pile's axis at 23 days. Again, a good agreement between the analytical calculation and the numerical simulation can be observed. The experimental results are taken from the transducers (PT100) at position of pile's wall, 0.5 m and 1.0 m in surrounding soil, and 4.0 m at the wall of pile number 2. The experimental values are similar with those of the models, except for the value at 1.0 m.

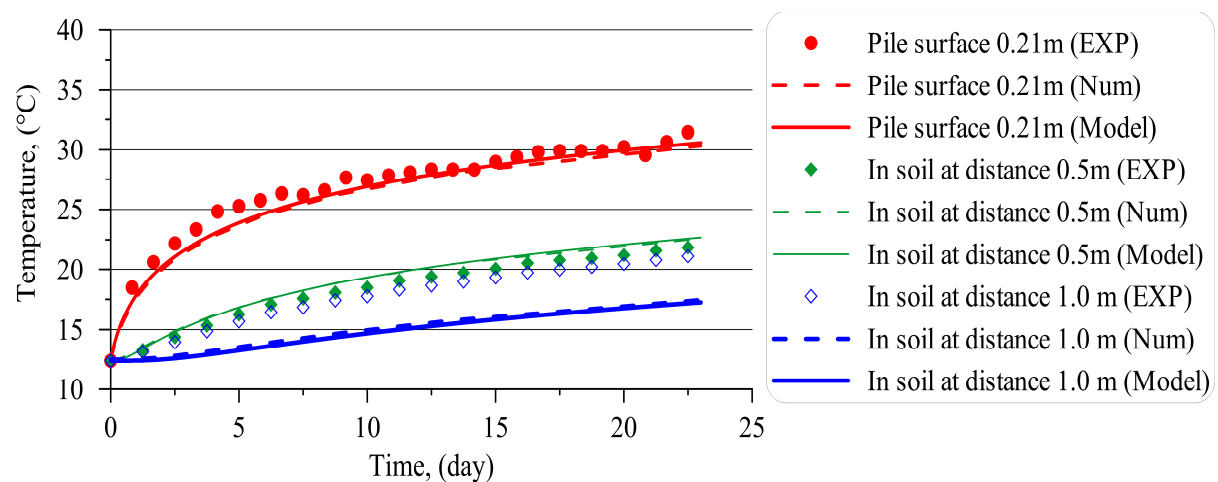


Fig. 4.6 Soil temperature at different distances from the pile axis during heating phase

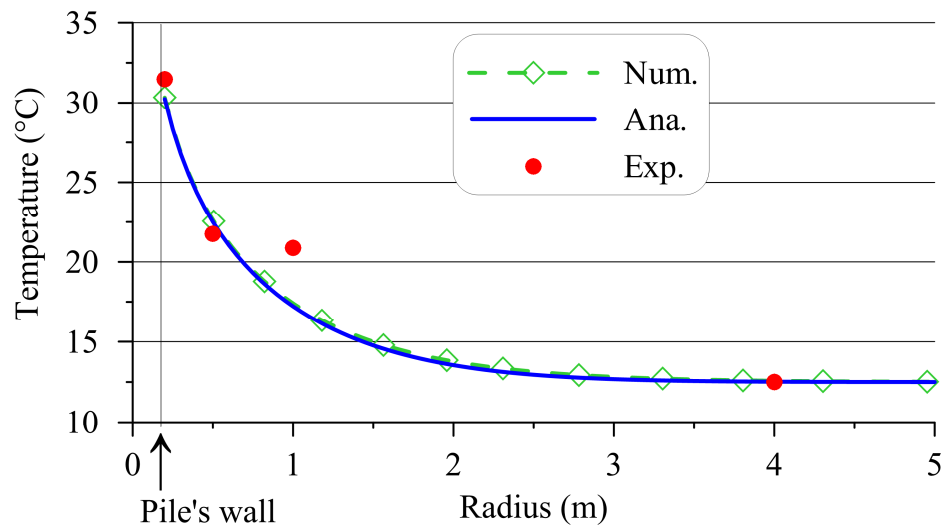


Fig. 4.7 Heat transfer in surrounding soil at the end of heating phase

#### 4.4 Conclusions

This paper presented a simple solution of heat conduction applied to energy pile. The different thermal properties of pile and surrounding soil are taken into account, and an unsteady state of heat conduction of energy pile is also considered in this solution. By using this solution, temperature change of pile and surrounding soil can be estimated during short- and long-term periods of heating or cooling of the GSHP system. Therefore, this solution can be considered as a useful tool to analyze energy consumption of GSHP system for the building.

In this work, based on the approach of Laplace transform method and also the contour integral method, an analytical solution of the heat transfer in soil surrounding a pile subjected to heating/cooling is proposed. Some hypotheses have been used in order to simplify the problem, among which the heat pipe is assumed as an infinite line source, heat flow is assumed to be constant throughout the heating or cooling period, heat transfer in pile and soil is purely conductive and especially the thermal parameters of pile and surrounding soil are considered different. Moreover, this solution is also used for short-term period.

This solution is expressed in a simpler form than the available solutions mentioned in the literature. In addition, this solution can replace the heat transfer solution inside the pile proposed by Lamarche & Beauchamp (2007) if the pile has a very high thermal conductivity. Thus, the temperature of pile and soil can be determined simultaneously by only one equation. The solution is then validated by comparing to numerical results obtained using the finite element method. Besides, the solution is able to predict with a good agreement the heat transfer of the experimental energy pile.

## **PART II. THERMO-MECHANICAL BEHAVIOR OF ENERGY PILE**

## **CHAPTER 5: REVIEW OF THE THERMO-MECHANICAL BEHAVIOR OF ENERGY PILE**

### **5.1 Introduction**

Variation of temperature of pile foundation can affect its mechanical response. Because of the lack of standards related to the energy pile design, the current design work is still based on the thermal free expansion condition of the pile. Another approach uses the thermal stress values obtained in the case of fully-restrained conditions (Boennec, 2009; Knellwolf & Laloui, 2011; GSHP Association, 2012). This conservative approach, therefore, over estimates the safety factor.

A quick review on the geothermal pile studies (Fromentin *et al.*, 1998; Bourne-Webb *et al.*, 2009; Laloui, 2011; Amatya *et al.*, 2012; McCartney & Murphy, 2012; Murphy *et al.*, 2013; Ng *et al.*, 2014; Wang *et al.*, 2014; Yavari *et al.*, 2014a and 2016a; Akrouch *et al.*, 2014; Di Donna & Laloui, 2015; Nguyen *et al.*, 2017) gives the following general conclusions: the pile's stress/strain behaviour is mainly reversible; temperature changes affect the pile's mobilized friction capacity due its thermal dilation/contraction. For more details, the existing studies on energy pile are presented and discussed in the following sections. The main aims of the review focus on the effect of thermal cycles on the thermo-mechanical behavior of energy pile.

### **5.2 Experimental studies on the thermo-mechanical behavior of energy pile**

Many studies have been carried out to investigate experimentally the thermo-mechanical behavior of energy piles. These studies include in situ full-scale experiments (Laloui *et al.*, 2006; Bourne-Webb *et al.*, 2009; Murphy *et al.*, 2013; Murphy & McCartney, 2014; Wang *et al.*, 2014; Akrouch *et al.*, 2014;) or laboratory small-scale experiments (Kalantidou *et al.*, 2012; Ng *et al.*, 2014; Stewart *et al.*, 2014; Stewart & McCartney, 2013; Yavari *et al.*, 2014a and 2016a; Nguyen *et al.*, 2017). The results evidence the effect of pile temperature variation on the soil/pile interaction. Actually, the temperature of energy piles can vary in the range of 5 °C to 40 °C and can thus induce stress changes along the pile and pile head movement.

These phenomena are the consequences of thermal dilation/contraction of pile and the soil/pile interface behavior.

Laloui *et al.* (2006) focuses on the behavior of in-situ energy pile subjected to heating/cooling under various weights of building stories. The result allows determining additional pile head load caused by heat load. The pile (25.8 m in length and 0.88 m in external diameter) was installed in the ground composed of four different types of soil. Mechanical load of about 0–1300 kN by the dead weight of a building under construction was measured at the pile head and the pile's temperature was varied between 15 °C and 22 °C. Pile head heave was observed during heating period. In addition, the thermal stress and friction mobilization of the pile increase with the temperature. For example when the pile works under a vertical stress of 1.3 MPa, an increase of temperature of 13.4 °C results in a thermal stress of 1.2 MPa at pile top and 2 MPa at pile toe (Fig. 5.1). The experiment results also show that for 1 °C of temperature rise, the additional axial thermal force is approximately 0.1 MPa. Thus the authors recommended that the additional value must be considered in the design of energy piles.

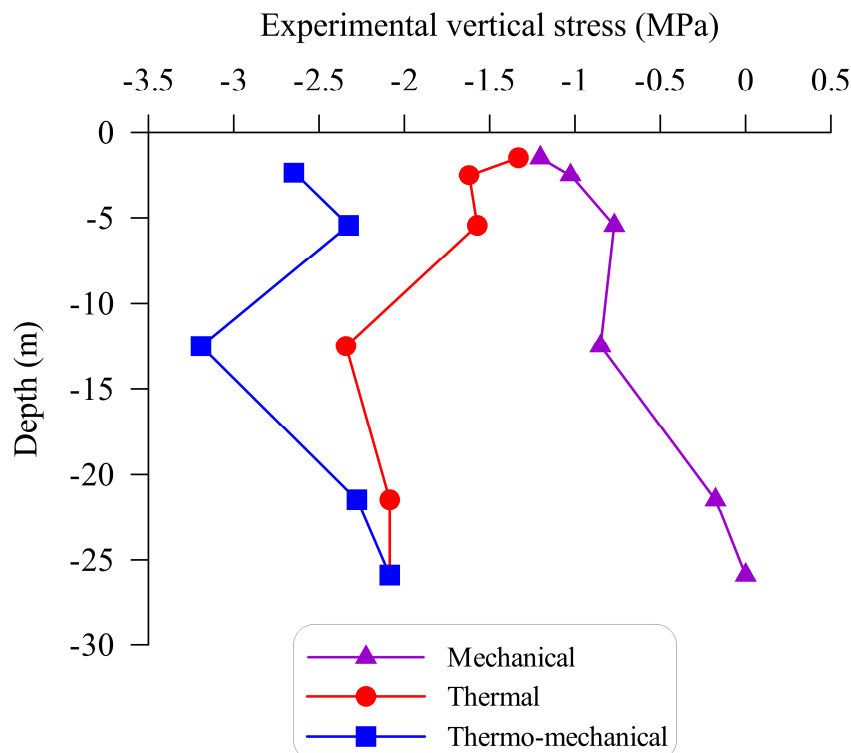


Fig. 5.1 Thermo-mechanical axial stress in an energy pile (after Laloui *et al.*, 2006)

Amatya *et al.* (2012) have summarized the in-situ experiments described by Laloui *et al.* (2006) and Bourne-Webb *et al.* (2009), and given a deeper understanding on the effect of

temperature changes to the behavior of energy pile. Firstly, to estimate the axial force of pile under thermal and thermo-mechanical loading, an analytical formulation can be derived from the total axial strain of the pile. This formula allows calculating separately the axial forces of pile due to the mechanical load and the thermal load as follows:

$$\varepsilon_{T\_Free} = \alpha_c \Delta T \quad (5.1)$$

$$\varepsilon_{Total} = \varepsilon_M + \varepsilon_{T\_Obs} \quad (5.2)$$

where  $\varepsilon_{T\_Free}$  is the free axial thermal strain of pile without any restraint;  $\alpha_c$  is the coefficient of thermal expansion/contraction of pile and  $\Delta T$  is the temperature change of pile;  $\varepsilon_{Total}$  is the total axial strain of pile under thermo-mechanical loading;  $\varepsilon_M$  is the strain due to the mechanical load; and  $\varepsilon_{T\_Obs}$  is the thermal strain observed from the test.

$$\varepsilon_{T\_Rstr} = \varepsilon_{T\_Free} - \varepsilon_{T\_Obs} \quad (5.3)$$

$\varepsilon_{T\_Rstr}$  is the restrained strain of the pile.

The axial thermal force of the pile without mechanical load can be then calculated:

$$P_T = -EA\varepsilon_{T\_Rstr} = -EA[\alpha_c \Delta T - \varepsilon_{T\_Obs}] \quad (5.4)$$

The total force of pile under thermo-mechanical loading thus equals:

$$P_{Total} = P_M + P_T = EA[\varepsilon_{Total} - \alpha_c \Delta T] \quad (5.5)$$

where  $E$  is the Young's modulus of the material, and  $A$  is the cross-sectional area of the pile.

In the case of no end restraint pile, as mentioned in the study of Bourne-Webb *et al.* (2009), the pile load is sustained mainly by the shaft friction. For the cooling phase, the pile contracts and both ends are free to move. The mobilized shaft friction prevents this movement and causes the restrained thermal strain. The shaft friction is considered to be positive over the upper half of the pile. This positive shaft friction has the same direction with that induced by the compressive head load. A negative shaft friction is distributed on the lower half of the pile. Conversely, when pile is heated, it is free to expand towards both ends. The mobilized shaft friction in the upper part is negative and it is positive in the lower part (Fig. 5.2). In the case of end restraint pile, the axial expansion/contraction of pile during heating/cooling is restrained at the pile head and toe, leading to additional axial stress. As a result, the axial

stress-strain state of pile is modified and depends on the relative stiffness of both ends restraints of the pile (Fig. 5.3).

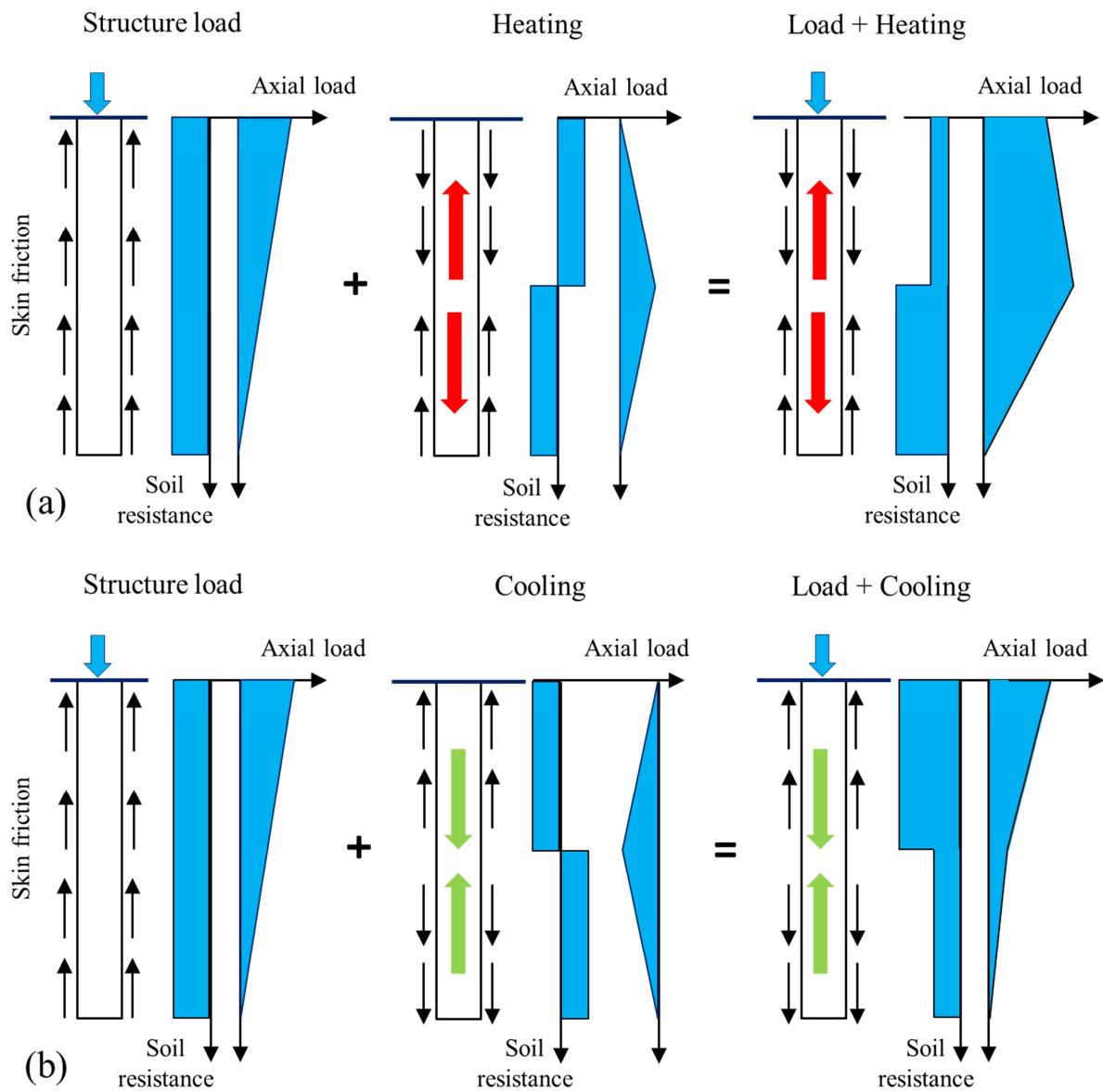


Fig. 5.2 Load transfer mechanisms for the pile subjected to thermo-mechanical loading; (a) heating and (b) cooling with no end restraint (redrawn after Bourn Webb *et al.*, 2009)

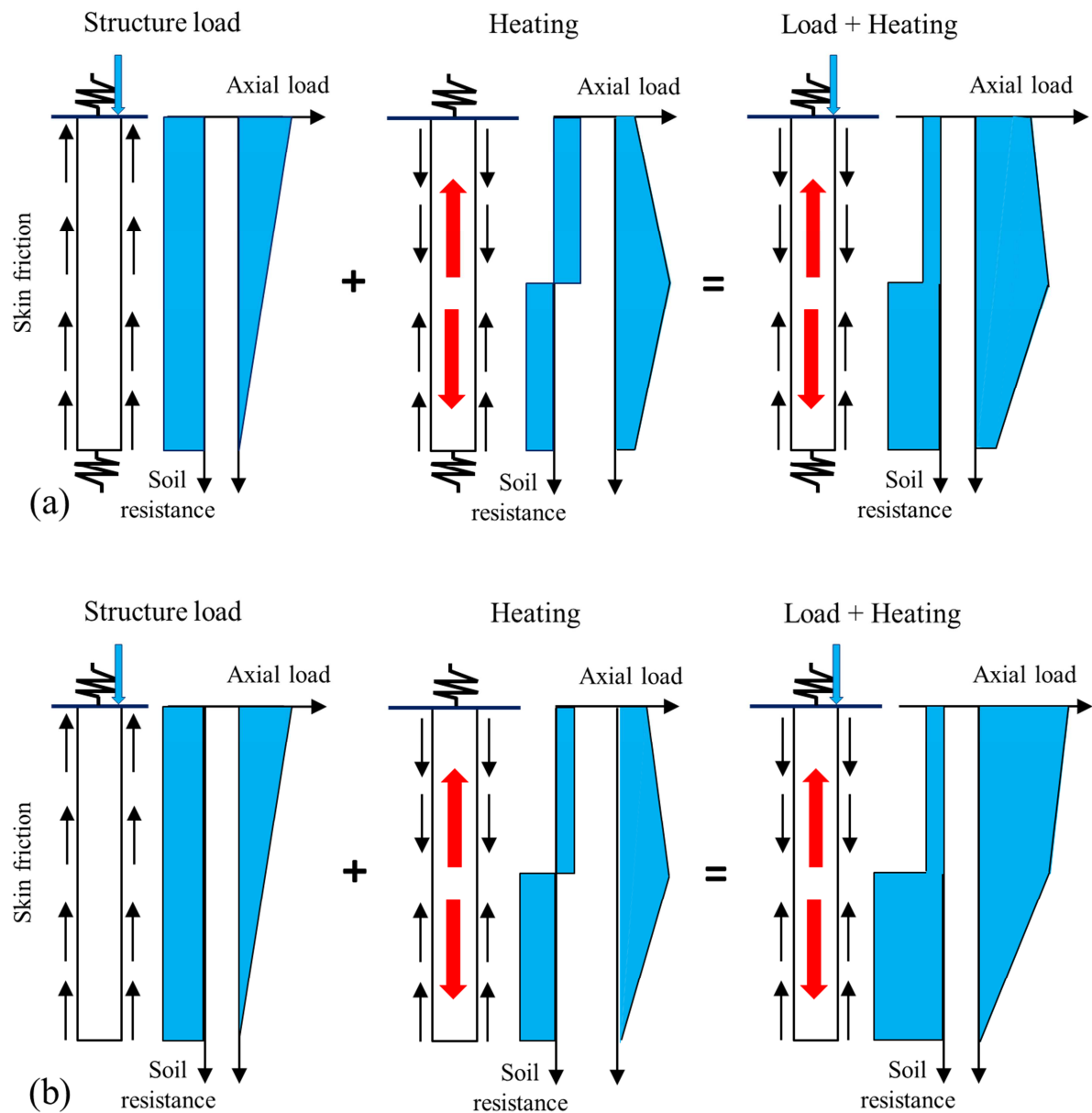


Fig. 5.3 Load transfer mechanisms for the pile subjected to thermo-mechanical loading; heating and cooling with end restraint (redrawn after Bourne Webb *et al.*, 2009): (a) both ends partially restrained; (b) top restrained and toe unrestrained; (redrawn after Bourn Webb *et al.*, 2009).

McCartney & Murphy (2012) tested two energy piles under a residential building in Denver, Colorado (USA). The two piles (0.91 m in diameter; 14.8 m and 13.4 m in length) were equipped with a conventional ground source heat pump system. The axial thermal strain due to the contraction/expansion of pile during cooling/heating period, respectively, shows a much smaller value than the acceptable limit of reinforced concrete (reference to the ACI 318-08 code). In another field test of energy pile of one-storey building, eight end-bearing

piles (0.61 m in diameter and 15.2 m in length) were installed in stiff sandstone (Murphy *et al.*, 2013). The results again confirm that the behavior of pile is thermo-elastic and the additional thermal stress and strain of pile (related to heating/cooling) are within the acceptable limits.

All the above experiments show that temperature changes induce adjustment of pile shaft resistance. Soil-pile interaction can be seen more clearly in the full-scale experiments of Wang *et al.* (2014) and Akrouch *et al.* (2014). In the test of Wang *et al.* (2014) the pile load was controlled by Osterberg cell which is installed beneath the pile tip. This device makes it easier to study the shaft resistance of pile wall thanks to the ability to push upward the pile. A pile (16.1 m in length and 0.6 m in diameter) was installed by solid auger bored drilling into very dense sand clay soil layers. The results show that the ultimate shaft resistance at 38 °C is higher than that at the initial state (17 °C); pile behavior is thermo-elastic. Akrouch *et al.* (2014) conducted an experiment on an in-situ pile (0.18 m in diameter and 5.50 m in length) under tension loading. The pile was embedded in very high plasticity clay. During the experiment, pile is initially loaded with a series of axial tension load, from 0 to 256 kN, with an increment of 50 kN. After 1 hour of each loading step the pile head load is maintained, and the pile is heated over a period of four hours with a temperature increase of 10÷15°C. The results show that the influence of increasing temperature on the soil-pile friction is negligible. However, the creep rate ratio between the thermo-mechanical load and the mechanical load is relatively large, of about 4.7 times.

Kalantidou *et al.* (2012) and Yavari *et al.*, (2014a) used physical model to study the effect of temperature change on the mechanical behavior of heat exchanger pile in dry sand. The results show that the response of pile head displacement is thermo-elastic when the pile works at low mechanical load (smaller than 30% of the pile resistance). During the thermal loading, displacement of pile is similar to the thermal expansion curve. At higher head load, the pile settles after thermal cycles. The same pile model was equally tested with saturated clay (Yavari *et al.*, 2016a). The results show that the pile head heaves during heating phase and settles in the following cooling phase. The thermally induced irreversible settlement was observed even at low head load (20% the ultimate capacity of pile). The irreversible settlement is larger under higher axial load (see Fig. 5.4).

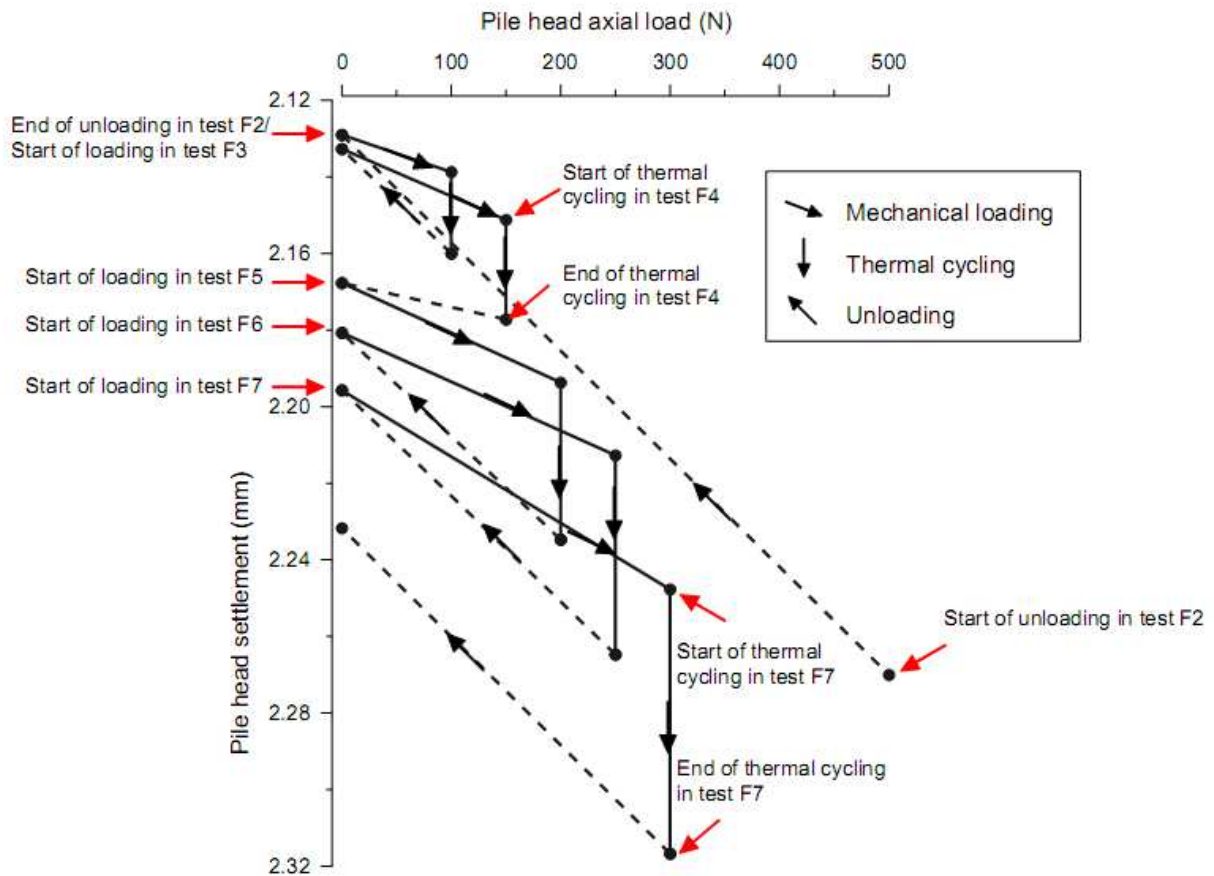


Fig. 5.4 Pile load - settlement curve obtained under thermo-mechanical load tests, (after Yavari *et al.*, 2016a)

### 5.3 Numerical studies on the thermo-mechanical behavior of pile

Besides the experimental studies, numerical method permits to optimize the design works, as well as to develop standard design tools. It is well known that, when pile works under thermo-mechanical load, the combination between the pile head load, the shaft resistance and the pile base resistance produces additional thermal stress within the pile. The thermal strains are the result of the balance between the thermal stress and the mobilized bearing resistances. Numerical methods can be used to predict this complex features. There are two methods that are usually used: load-transfer and finite element methods.

The load-transfer method was first developed by Coyle & Reese (1966). It is used to analyze the interaction between soil and pile, commonly called the  $t$ - $z$  method. This method is probably the most widely used technique to study the behavior of pile. This method refers to the modeling of the pile as a series of elements supported by discrete nonlinear springs, which represent the resistance of the soil in skin friction (Fig. 5.5a and 5.5b). The spring between the

elements represents pile axial stiffness, and the spring at the pile tip represents the end bearing resistance.

In the case of heat exchanger pile, modified load-transfer methods have been used to estimate axial load-settlement behavior of pile (Knellwolf *et al.*, 2011; Mimouni & Laloui, 2014; Pasten & Santamarina, 2014; Suryatriyastuti *et al.*, 2014). In these models, the pile's thermal expansion/contraction is taken into account. An additional spring located at the head was added to simulate the boundary conditions that depend on the building foundation (Fig. 5.5c). Thermal hardening and/or softening behavior of soil can be taken into account to investigate the cyclic degradation effects on pile shaft resistance. As well as mechanical model, an iterative approach has been used in order to ensure force equilibrium and compatibility between displacements of the elements.

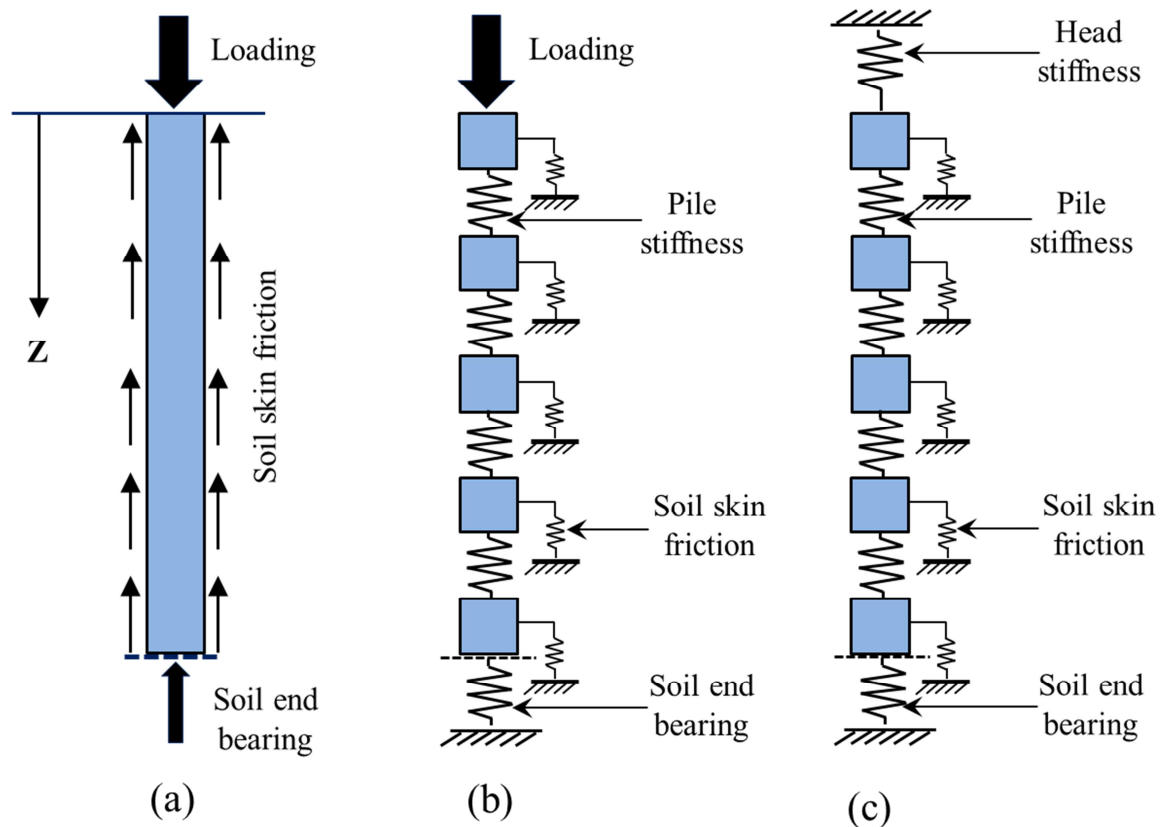


Fig. 5.5 Load transfer mechanisms in an axially loaded pile; (a) structure loading, (b) spring mass model under mechanical loading, (c) spring mass model under thermo-mechanical loading

Based on the load transfer method, Knellwolf *et al.*, (2011) presented a numerical study that allows determining the effect of temperature changes on the behavior of heat exchanger pile. The model was validated with the experiment results of in-situ energy pile at the l'École

Polytechnique Fédérale de Lausanne (EPFL) (Laloui *et al.*, 2006) and another undertaken at Lambeth College in London (Bourne-Webb *et al.*, 2009). The authors indicated that this method is adequate to analyze the thermo-mechanical behavior of energy pile. However they also recommended a careful analysis on the soil-pile-structure interaction due to the temperature changes.

The finite element method has been also used to predict the thermo-mechanical behavior of energy pile (Laloui *et al.*, 2006; Jeong *et al.*, 2014; Yavari *et al.*, 2014b; Olgun *et al.*, 2015; Di Donna & Laloui, 2015; Saggiu & Chakraborty, 2015; Ng *et al.*, 2016; Di Donna *et al.*, 2016; Rotta Loria & Laloui, 2016; Vieira & Maranhã, 2016). In general, the model is set up in three main steps: (i) initial geostatic equilibrium, (ii) application of the overlying structures load at the pile head (iii) and application of thermal loading. A 2D axisymmetric model is usually used to model the behavior of a single pile, while a 3D symmetric model is used for pile group.

In the study of Laloui *et al.*, (2006), a thermo-hydro-mechanical model was developed to predict the response of soil and pile under thermal, hydraulic and mechanical loading simultaneously. For the solid matrix (concrete pile and surrounding soil), a thermo-elasto-plastic behavior was used. The results showed that the model could predict correctly the behavior of energy pile observed from the in situ experiments. The heat transfer is mainly horizontal. When the pile works under only heating-cooling cycle, the pile head moves upward in the heating phase and moves downward in the cooling phase. However, the pile head displacement is not completely thermo-elastic. Actually, the soil-pile interface resistance restricts the dilation of the pile. The thermal stress inside the pile is then the result of the restricted displacement. When the pile works under thermo-mechanical loading, mechanical stress of pile decreases with the depth and the additional stress due to thermal loading distributed rather uniform along the pile length. The radial strain of pile under thermo-mechanical loading is negligible and therefore the pore water pressure and the effective stress of the surrounding soil remain almost constant.

In the study of Yavari *et al.*, (2014b), the thermal load of energy pile is modeled by imposing the volumetric thermal dilatation of pile concrete. The pile and soil are considered as isotropic linear elastic non-porous and isotropic linear elastic porous material, respectively. This decoupling method is then validated with the experimental results (see Figs. 5.6, 5.7 and 5.8). The results of pile head displacement and axial strain of pile show a good agreement between numerical and experimental results, the disparity is explained by the hypothesis of

homogeneous temperature profile of pile. The authors highlight that the mechanical behavior of pile is mainly influenced by the volumetric thermal dilation of pile, so that the thermal dilation of soil is less affected. It can be said that, this simple computation can allow simulating the mechanical behavior of energy pile under thermo-mechanical loading in terms of pile head displacement and axial strain at various depths.

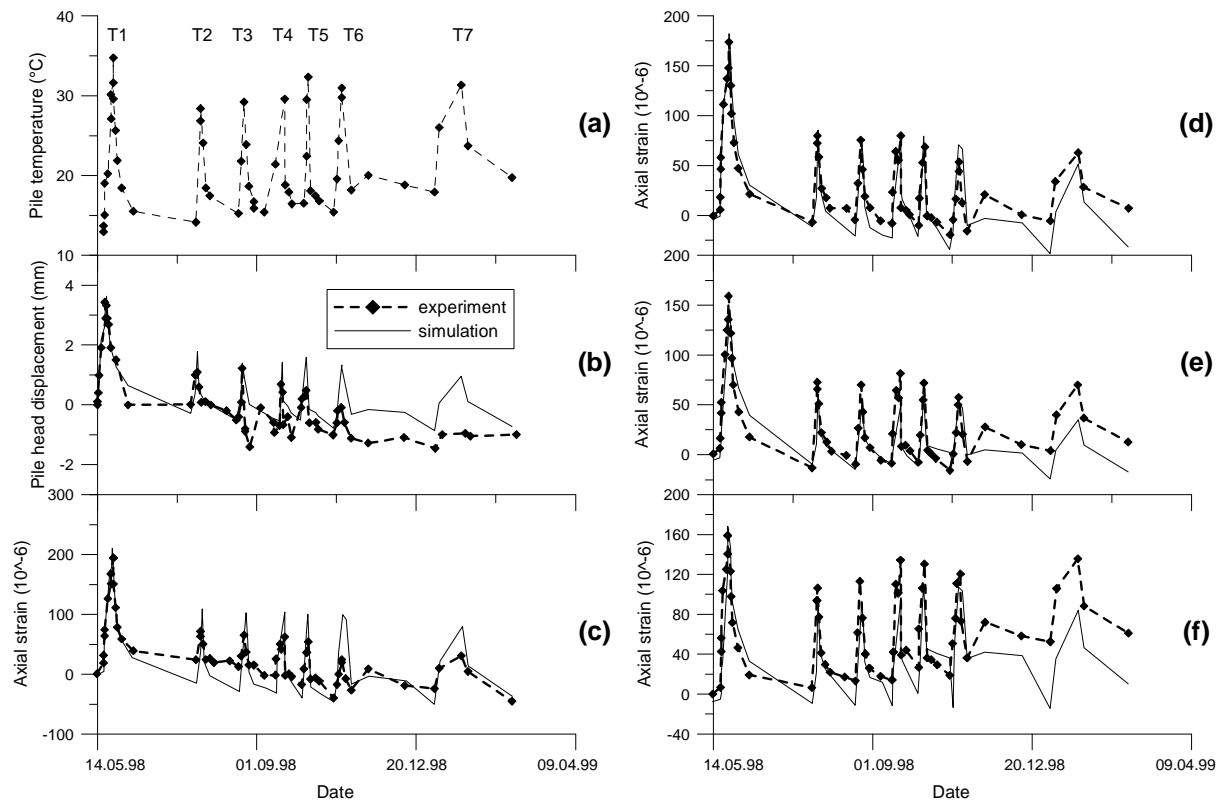


Fig. 5.6 Comparison between numerical results of Yavari *et al.* (2014b) with experimental results by Laloui *et al.*, (2003): (a) pile temperature; (b) pile head displacement; (c) axial strain at 2.5 m depth; (d) axial strain at 10.5 m depth; (e) axial strain at 16.5 m depth; (f) axial strain at 24.5 m depth

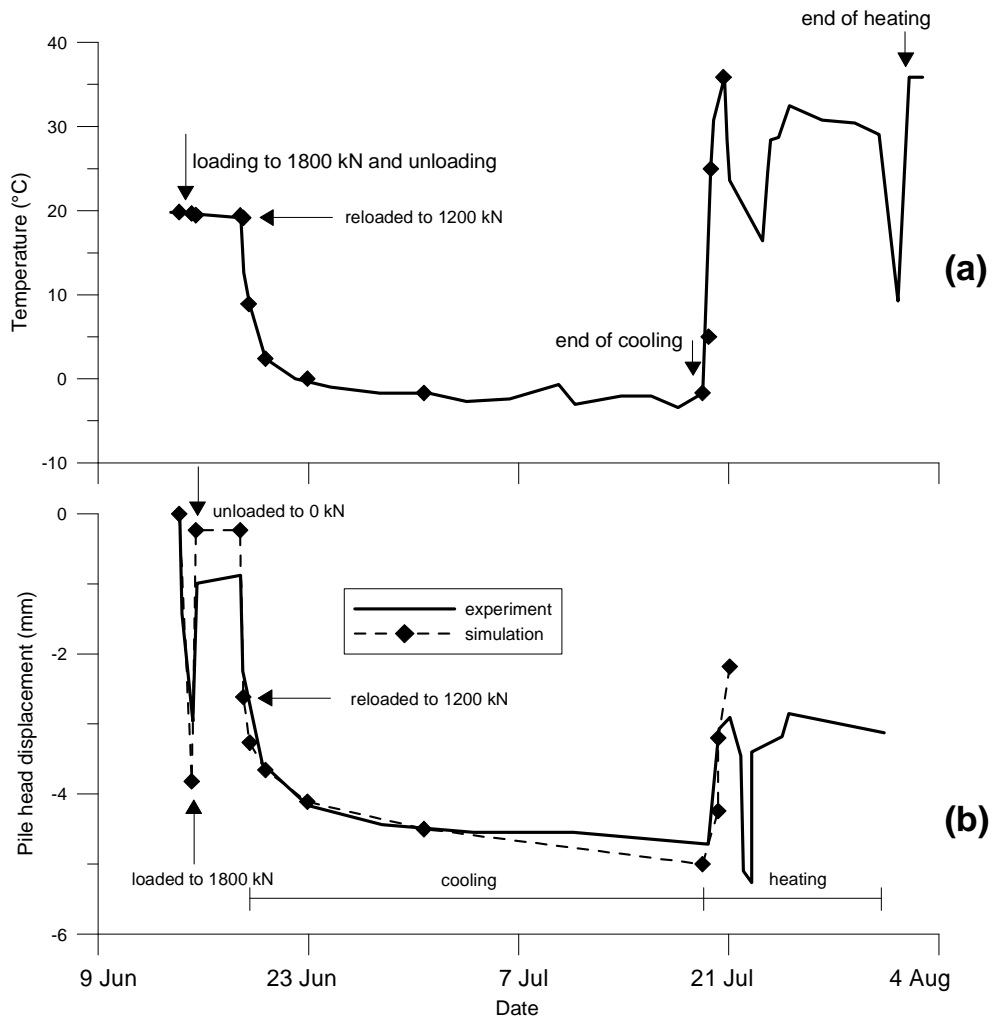


Fig. 5.7 Comparison between numerical results Yavari *et al.* (2014b) with experimental results by (Bourne-Webb *et al.*, 2009): (a) pile temperature; (b) pile head displacement

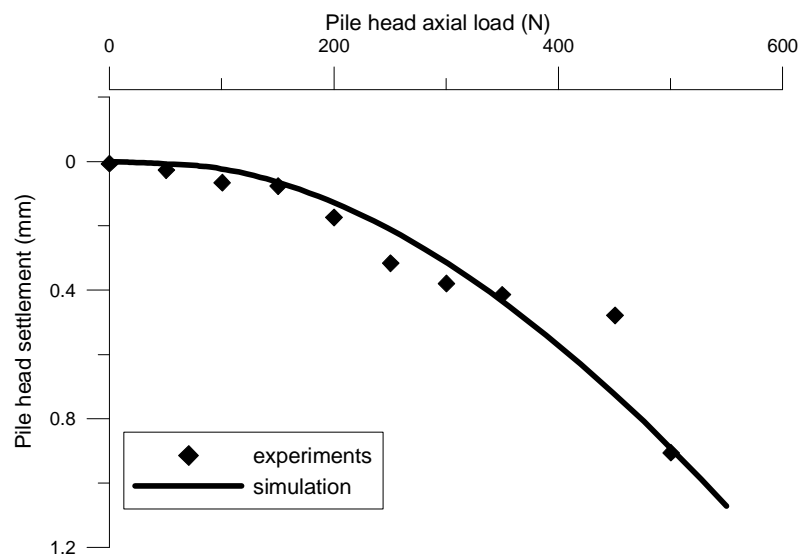


Fig. 5.8 Comparison between numerical results Yavari *et al.* (2014b) with experimental result by Kalantidou *et al.*, (2012)

#### 5.4 Behavior of soil and soil-pile interface under thermal loading

Soil-pile interface behavior plays an important role in the pile ultimate bearing capacity and also the pile load transfer characteristics. During thermal loading of energy pile, temperature exchange between energy pile and the surrounding will lead to soil heating or cooling. This can induce significant change of mechanical and physical behavior of soil and pile, especially the soil-pile interface.

The issues related to thermo-mechanical behavior of clays were summarized in the study of Modaressi & Laloui (1997), Laloui *et al.*, (2014) and Hong *et al.*, (2015). The thermo-mechanical response of clays mainly relates to their physical and chemical characteristics. Temperature change causes reversible dilation of soil and the magnitude of volumetric strains depends on the loading history of soil. Thermal consolidation induces irreversible strains. This phenomenon is usually obtained in normally consolidated soil whereas reversible strains are observed in highly over-consolidated soil (Baldi *et al.*, 1988; Hueckel & Baldi, 1990; Graham *et al.*, 2001; Sultan *et al.*, 2002; Abuel-Naga *et al.*, 2005; Cui *et al.*, 2000). In addition, experimental data on the drained heating clayed soil showed that the void ratio changes are related to rearrangement of particles and depend on thermal, stress history and recent stress history (Burghignoli *et al.*, 2000, Cekerevac & Laloui, 2004, Abuel-Naga *et al.*, 2007).

It can be concluded that there are two main features of thermal volumetric strain of clay soil: (i) the irreversible strain is related to the rearrangement of soil particles; (ii) and the reversible strain is related to the expansion of pore water and clay mineral particles and also the repulsive forces between particles of clay minerals.

Besides, temperature change can modify the shear strength of clay soil. The study of Hicher, (1974) on the Francisco clay shows that temperature increase reduces the soil friction angle, and so it reduces the soil shear strength. This is explained by the decrease of the viscosity of water. Similarly, studies of Baldi *et al.*, (1988) and Hueckel *et al.*, (2009) also mentioned an alteration of the physical properties such as adsorption forces in clay water. Study of Cekerevac & Laloui (2004) showed that the shear strength increased with an increase of temperature loading. The increase of shear strength in normally consolidated soils was observed slightly higher than in over-consolidated specimen. However, the friction angle at critical state is independent of the temperature variations.

Recently, in the experiment work of Yavari *et al.*, (2016b), shear behavior of soils and soil-concrete interface under various temperatures was investigated. Sandy soil, clay and clay-concrete interface were tested. The results show negligible effect of temperature on the shear strength parameters (friction angle and cohesion) of soil and soil-concrete interface. Besides, under shearing, sand and clay show a hardening behavior while the clay-concrete interface show a softening one. In addition, the peak shear strength of clay-concrete interface is smaller than that of clay soil. A similar experiment can be found in the study of Di Donna *et al.*, (2016) where direct shear tests were conducted under different temperatures (at 20 °C and 50 °C). The results show that the behavior of sand-concrete interface is not affected by the temperature variations. However, the shear strength of clay-concrete interface increases with heating while the friction angle of the interface slightly reduces at high temperature. This phenomenon can be explained by the thermal consolidation observed during drained heating.

Campanella & Mitchell (1968) has conducted experiments on clayed soil to investigate the behavior of soil under thermal cycles. Thermal cycles (temperature varying from 18 °C to 60 °C) were applied to the soil under constant stress conditions. The results show irreversible volumetric strain under this thermo-mechanical loading. After several thermal cycles, the medium becomes insensitive to the thermal loading. Since the soil structure achieves steady state, the temperature changes cause only reversible volume change of soil. A similar result can be found in the studies of Burghignoli *et al.*, (2000) on Italian clays and studies of Cekerevac & Laloui (2010) on saturated Kaolin clay.

### **5.5 Long term behavior of geothermal pile**

Commonly, energy pile foundation is often designed to be used along the lifetime of the building. The thermal exchange between the pile and surrounding soil depends on the annual energy needs of the building, heating mode in winter and cooling mode in summer. Therefore, energy pile foundation must undergo in general one heating-cooling cycle per year. During the long-term operation of the system, the stress state in the soil/pile system can be modified and the allowable displacement limit of pile can be exceeded. This will lead to damage to the overlying structures. In spite of various studies on the thermo-mechanical behavior of energy piles, few works have investigated their long-term behavior. Actually, to deal with this aspect, some studies investigated the mechanical behavior of energy piles under numerous thermal cycles, which represent the seasonal pile temperature variations.

Suryatriyastuti *et al.*, (2014) studied the behavior of a free- and restraint-head pile in very loose sand using the pile-soil load transfer approach. The proposed t-z function comprises a cyclic hardening/softening mechanism, which allows investigating the degradation of the soil/pile interface behavior during cyclic loading. This approach is then compared with a numerical simulation using the finite element method where the degradation of the soil-pile interface behavior under cyclic loading is considered. A simulation accounting for 12 thermal cycles shows a ratcheting of pile head settlement under a constant working load and a decrease in pile head load for the restraint-head pile (Fig. 5.9).

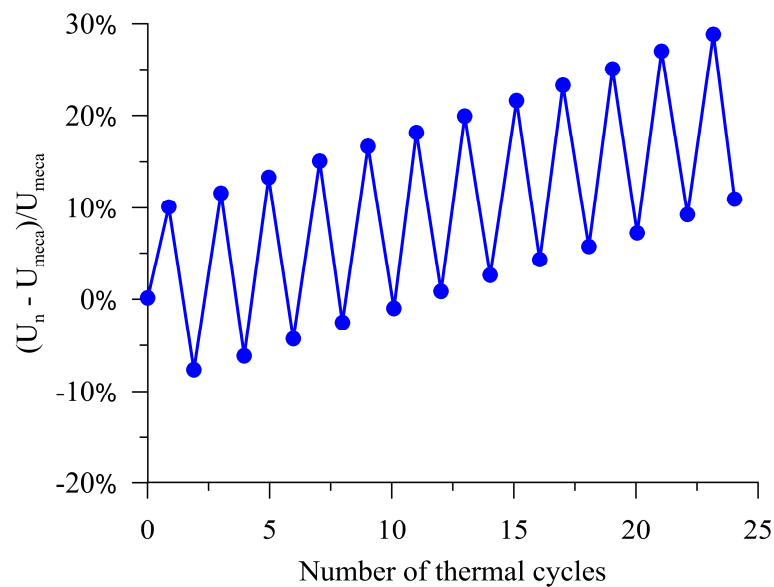


Fig. 5.9 Ratio of head displacement during thermal cycles:  $U_n$  is the displacement of pile in  $n$  cycles and  $U_{meca}$  is the displacement of pile due to mechanical load (Suryatriyastuti *et al.*, 2014)

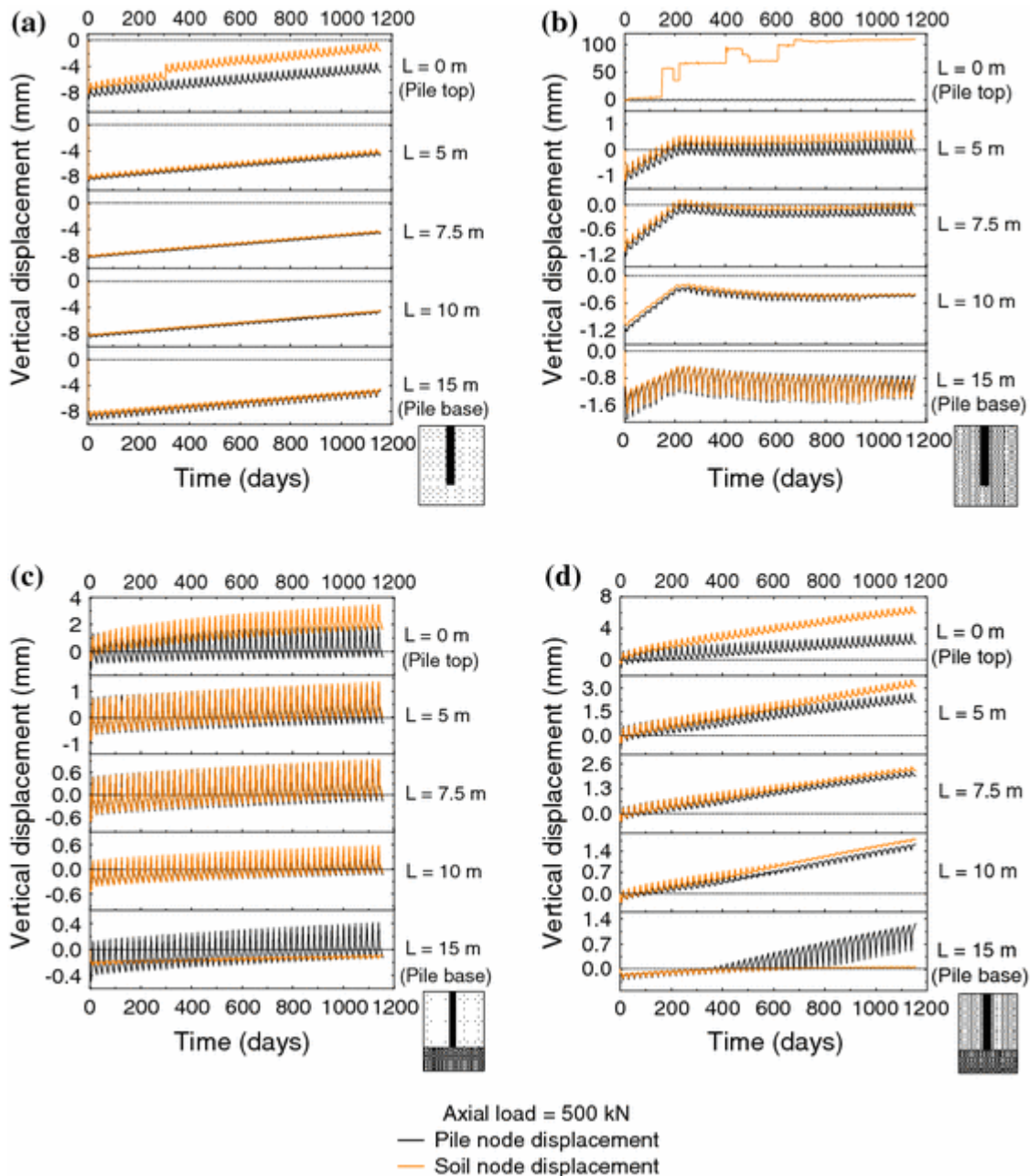


Fig. 5.10 Pile axial displacement versus time for floating and end bearing piles under thermo-mechanical load at vertical loading of 500 kN (Saggu & Chakraborty, 2015)

Saggu & Chakraborty (2015) investigated the behavior of a floating pile and an end-bearing pile in loose and dense sands under various thermal cycles by using the finite element method and nonlinear transient analyses (Figure 5.10). The thermal load applied to the pile was in the same temperature range as in the experiments of Laloui *et al.*, (2006), with a temperature amplitude of 21 °C. The result shows an important settlement of the pile after the first thermal cycle. The subsequent thermal cycles induced pile heave. This phenomenon can be seen clearly in the case of dense sand where the pile and soil go upward together after 50 cycles

(Fig. 5.10d). This is understandable because the pile and soil were progressively heated during 50 cycles. The pile shaft resistance in dense sand increased with the thermal cycles while this value did not change in case of loose sand. Actually in the dense sand, soil thermal expansion induced a larger horizontal stress and affected the mobilized shaft resistance of the pile. However, a parametric study showed a decreasing trend of the pile axial stress with thermal cycles.

A similar result can be found in the numerical study of Olgun *et al.*, (2015) where pile head displacement and axial stress were investigated under three different climatic conditions for 30 years. The model pile with 0.6 m diameter and 20 m length is embedded in a homogeneous and isotropic soil. The pile capacity is derived mainly from the mobilized shaft friction. As the demand for heating and cooling of each region is unbalanced, the long-term thermal performance will lead to an increase or a decrease in pile temperature over time. After 30 annual thermal cycles, even if the pile was progressively cooled, the axial stress of pile tended to increase. A decrease in axial stress was observed during heating process. This can be explained by the difference in the thermal dilation of the pile and soil during the thermal loading process. Figure 5.11 shows a higher displacement of pile head in Chicago comparing with the others in Charlotte and in Austin. This is explained by the progress of cooling down in the soil surrounding pile in Chicago while the progress of heating up occurs in soil surrounding the pile in Charlotte and in Austin.

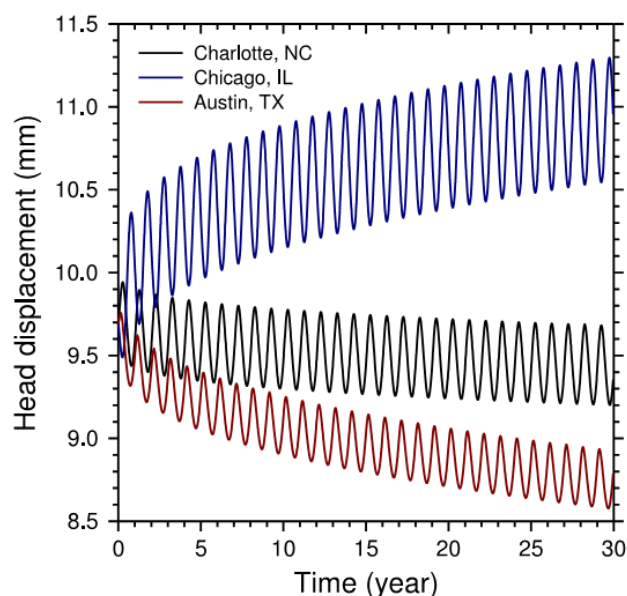


Fig. 5.11 Evolution of the pile head displacement under different temperature conditions (the pile tends to settle in Chicago climate, and heave in Austin and Charlotte climates), (after Olgun *et al.*, 2015)

Ng *et al.*, (2016) studied the horizontal stress change of soil element close to the pile when the pile is subjected to 50 heating-cooling cycles. The results show that the horizontal stress along the pile depth decreased with thermal cycles. In addition, the irreversible settlement of pile due to the decrease of the shaft resistance leads to the densification of soil below the pile toe and thus the decrease of the rate of pile's settlement.

Pasten & Santamarina (2014) also used a modified one-dimensional load transfer model to predict the long-term response of shaft- and end-bearing piles subjected to thermal cycles. The numerical modeling represented an energy pile with 1-m diameter and 20-m length subjected to 50 thermal cycles under constant static load. The temperature change along the pile length is considered uniform. The results show that, after one cycle, axial force of pile increases in the heating phase and decreases in the cooling phase. The axial force changes mainly occur in the middle of the pile, while it does not change at the two pile ends. Actually the displacement is free at both pile ends. The results on the irreversible settlement of floating pile during 50 thermal cycles indicated that, when the pile works under small head load, the accumulated settlement of pile is negligible. However, the irreversible settlement of pile increases under higher vertical load. The results (shown in Fig. 5.12) were then fitted with a simple exponential function that is represented in the equation (5.6).

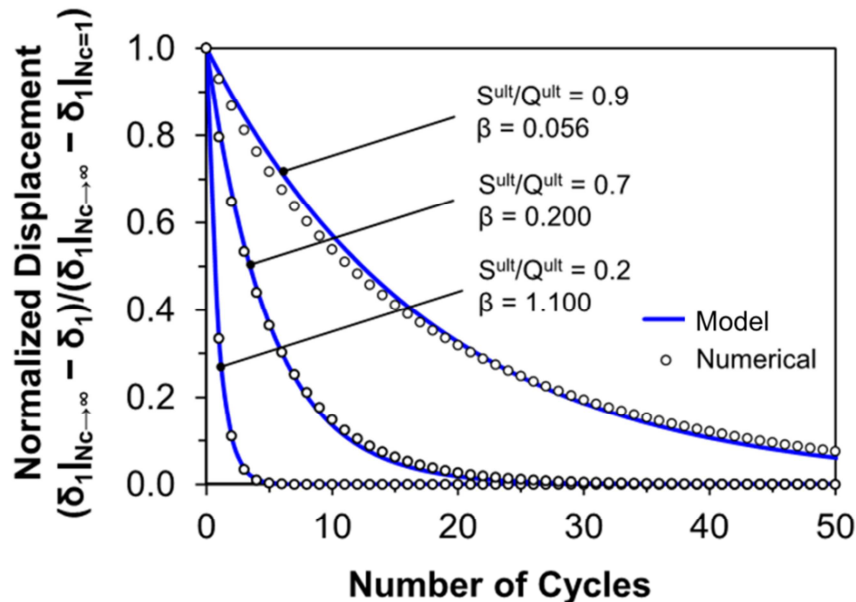


Fig. 5.12 Evolution of the normalized pile head settlement under various shaft-to-ultimate resistance ratios,  $S^{\text{ult}}/Q^{\text{ult}}$ ; (after Pasten & Santamarina, 2014)

$$\delta_1 = \delta_1|_{N_c \rightarrow \infty} + (\delta_1|_{N_c=1} - \delta_1|_{N_c \rightarrow \infty}) \exp(-\beta \cdot N_c) \quad (5.6)$$

where,  $\delta_1|_{N_c=1}$  is the head displacement for the static load,  $\delta_1|_{N_c \rightarrow \infty}$  is the asymptotic head displacement,  $\beta$  is the exponent of convergence rate,  $N_c$  is number of cycles.

Di Donna & Laloui (2015) modeled thermo-mechanical behavior of an energy pile during ten years. The study focuses on the estimation of the additional displacement of pile head and stress state of soil-pile interface. In addition, the evolution of volumetric total strain for different points of the surrounding soil was also studied. During the thermal loading, the temperature on the soil-pile interface changes in the range of 0 °C to 25 °C. The result indicates that heating-cooling cycles affect the soil volumetric strain. The majority of the plastic strain was obtained after the first cycle (Fig. 5.13a). A greater soil plastic strain was obtained at points located closer to the soil-pile interface, and only the point close to the pile shows a cyclic behavior with temperature change is not large enough to cause any variation. The results also showed displacement upwards during heating and downwards during cooling for the upper part of the pile, while the opposite occurs with the lower part (Fig. 5.13b). Analysis of vertical displacement at different depths showed that the significant displacement of pile occurs within the first cycle. After the first cycle, the displacement response of pile is thermo-elastic. Besides, the displacement along the pile's shaft also confirms the reversible response obtained at long term. The thermal cycles do not affect the pore water pressure. In addition the horizontal effective stress at pile-soil interface depends on the expansion/contraction of the pile during heating/cooling phase, respectively. Besides, thermal loading induced significant additional shear stress around the pile ends. But in the point located near the null point the influence of temperature is negligible. The axial stress obtained along the pile is consistent with the vertical displacement results as noted above; it increases in heating phase and decreases in cooling phase. The study emphasizes that the additional axial stress does not cause mechanical damage to the foundation structure.

Vieira & Maranhã (2016) investigated the behavior of a floating pile model in clay soil under different constant static loads and seasonal temperature variation during five years using finite element method. The soil is saturated and normally consolidated. The results indicate that when the pile works with a high factor of safety, its displacement is reversible during the thermal cycles. However, a low factor of safety induces an increase in axial stresses while the rate of irreversible settlement reduces with the number of cycles (Fig. 5.14).

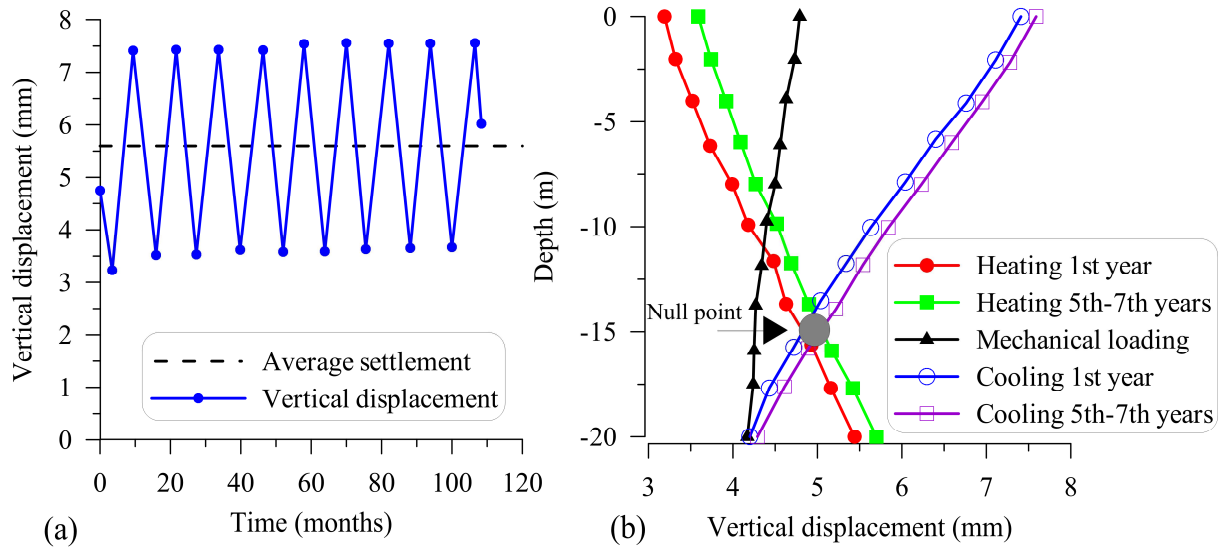


Fig. 5.13 Vertical displacement of pile (a) with time and (b) along the pile's length (Di Donna & Laloui, 2015)

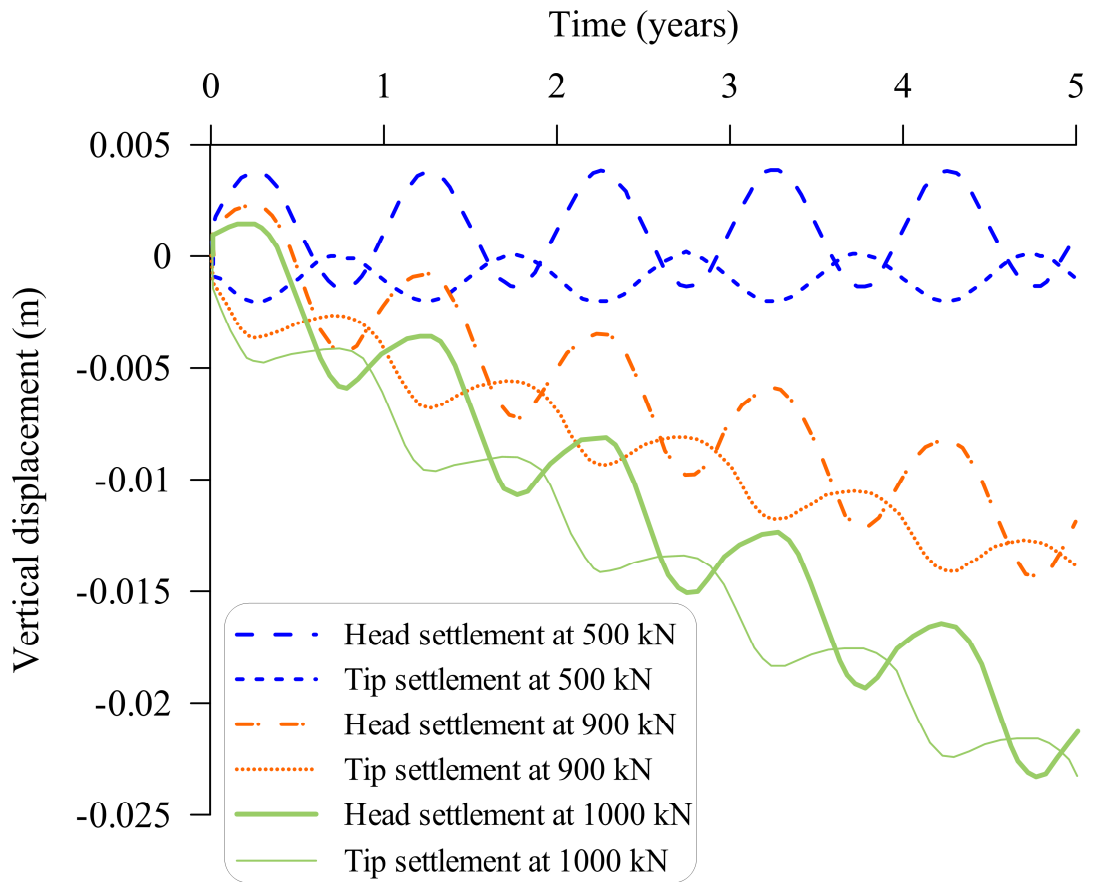


Fig. 5.14 Vertical displacement of pile versus 5 thermal cycles (Vieira & Maranhã, 2016)

Beside the numerical studies mentioned above, few experimental studies have been performed to investigate the long-term behavior of energy piles. Ng *et al.*, (2014) used centrifuge modeling to study the thermo-mechanical behavior of energy piles constructed in lightly and heavily over-consolidated clay under five thermal cycles. The results show that the most irreversible settlement of pile was observed in the first thermal cycle, and then in the following cycles the settlement increases with a lower rate. After 5 cycles the cumulative settlement was about 3.8% D (pile diameter) for a pile in the lightly over-consolidated clay, and 2.1% D in the case of heavily over-consolidated clay (Fig. 5.15).

Another centrifuge modeling of energy pile to investigate the long-term behavior under four thermal cycles can be found in the study of Stewart & McCartney (2013). An end bearing pile, installed in unsaturated silt worked under a constant head load and four thermal cycles. The thermal axial stress-strain behavior of pile was observed in consistency with the results of in-situ experiments performed by Laloui *et al.*, (2006), Bourne-Webb *et al.*, (2009) and McCartney & Murphy (2012). During four thermal cycles, the profiles of axial stress, displacement and strain of pile did not change significantly.

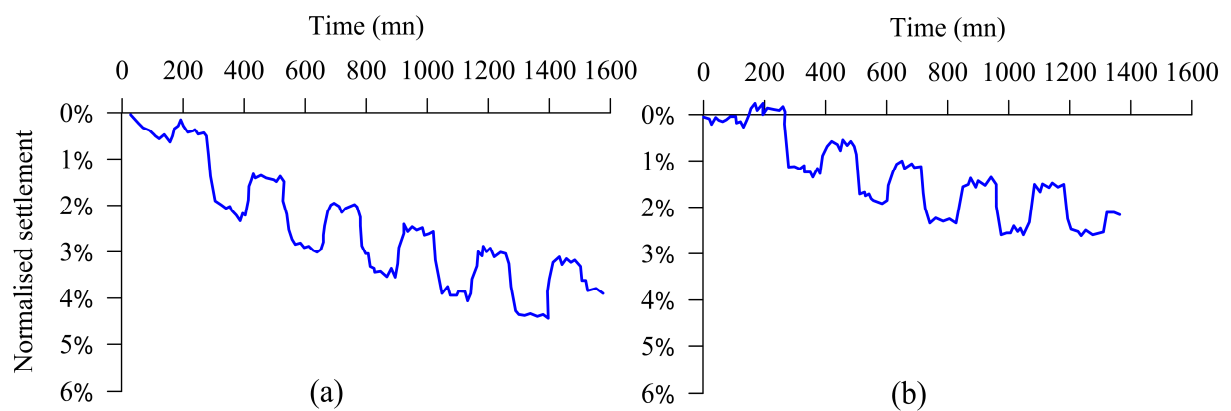


Fig. 5.15 Normalized displacement of pile (a) in highly overconsolidated clay and (b) in heavily over-consolidated clay (Ng *et al.*, 2014)

## 5.6 Conclusions

Energy pile is increasingly applied in the buildings, especially in European countries where the temperature conditions of the shallow ground are most suitable for this system. Studies on the behavior of energy pile show that temperature changes can modify its mechanical behavior.

The ultimate bearing capacity of pile increases when heated. In addition, heating can increase the axial stress along the pile and vice versa cooling causes the decrease of this axial stress. The additional thermal axial stress of pile can be calculated by decoupling the thermo-mechanical behavior. Actually, heating induces the thermal expansion of the pile and modifies the stress distribution along the pile. That can induce afterward irreversible settlement of the pile under low factor of safety. This has been clearly pointed out in the studies on the behavior of pile in short term.

Studies on the long term behavior of energy pile have shown that the irreversible settlement of pile is mainly obtained in the first thermal cycles. In the subsequent thermal cycles, the displacement of pile can be characterized by either thermo-elastic, shakedown or ratcheting behavior. That means, the displacement of pile can be reversible, irreversible with settlement decreasing and reaching stability or irreversible with a constant cyclic displacement rate, respectively. The cyclic displacement rate of pile is highly dependent on the load level of pile head as well as the behavior of pile-soil interface.

To sum up, the selection of an appropriate working load of pile as well as amplitude of temperature cycle plays an important role for the use of energy pile during the lifetime of the building. The above results are mainly derived from numerical simulation studies, while studies based on experimental works are limited. Thus, experimental studies on a small-scale energy pile will be presented in the following chapter. Its results are then interpreted in the last chapter by numerical simulation to further clarify the behavior of energy pile under thermal cycles.

---

## CHAPTER 6: INVESTIGATION ON THE LONG-TERM BEHAVIOR BY PHYSICAL MODELING

### 6.1 Introduction

In this chapter, a small-scale model was used to study the thermo-mechanical behavior of energy pile. This method allows to easily evaluating the effect of different variables in soil conditions and loading. Experiments have been done in dry sand and then in saturated clay. The model pile and the installation procedure is similar to those used by Yavari *et al.*, (2014a) with the model pile installed in dry sand; and Yavari *et al.*, (2016a) in saturated clay. When compared with these previous works, the present work focuses on the long-term behavior. The long-term performance refers to the actual working conditions of energy pile under the impact of seasonal temperature change. It means pile is heated in summer for cooling the building and vice versa it is cooled in winter for the heating demand. One heating/cooling cycle corresponds then to one year of operation. In this study, the long-term performance of pile was modeled for a period of 30 years and the thermo-mechanical behavior of pile during this period was observed.

### 6.2 Description of the pile model

The pile model is made of an aluminum tube with internal and external diameters equal to 18 mm and 20 mm, respectively. The length of the tube is 800 mm and the tube is sealed at the bottom. The tube head is open in order to introduce the heating-cooling system inside the tube. The tube is equipped with five axial strain gauges distributed on its surface (Fig. 6.1). The external surface of the tube was coated with sand to imitate the roughness of a full-scale bored pile (Fig. 6.2). More details about the pile model can be seen in Yavari (2014).

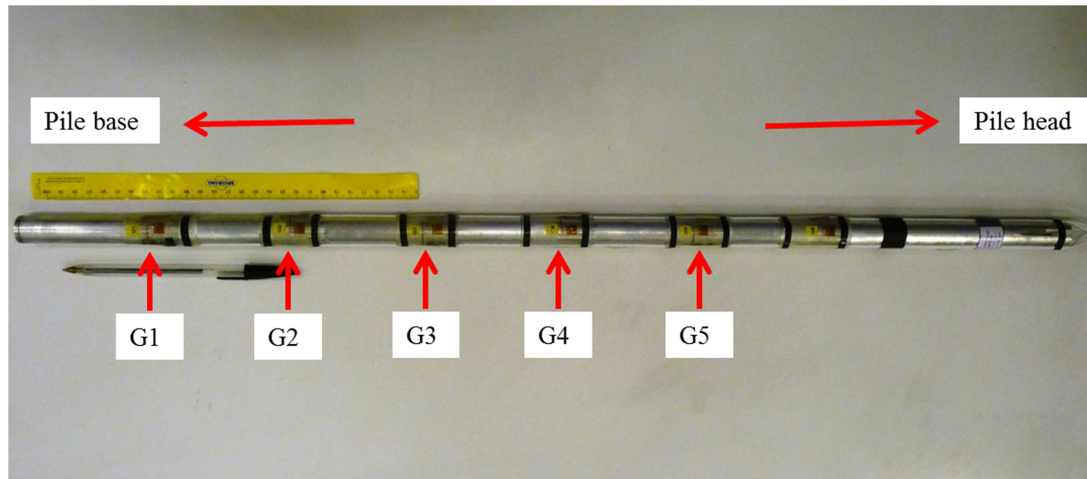


Fig. 6.1 The model pile before coating with sand on the surface (after Yavari, 2014)

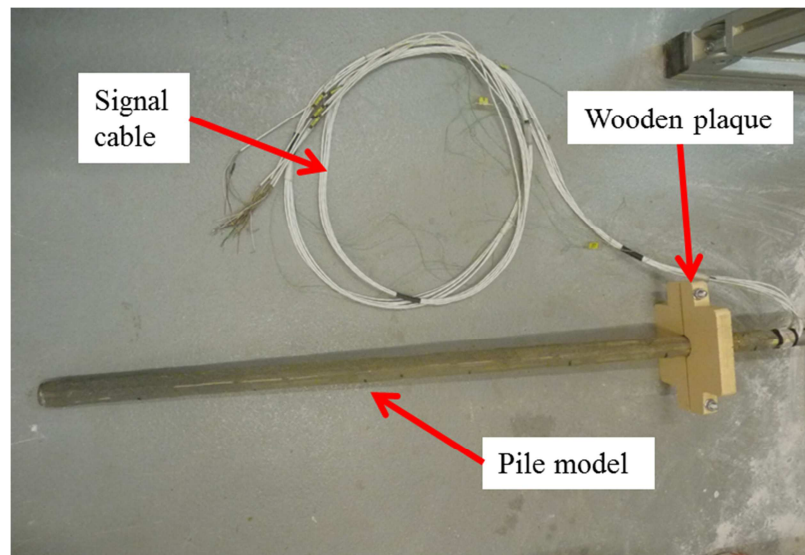


Fig. 6.2 Pile model after coating with sand on the surface

To calibrate the axial strain gauges, the pile was first kept upright and fixed. A series of constant load with an increment of 50 N was then applied on the pile head (from 0 N to 200 N). Results show in Fig. 6.3 evidence that all axial strains increase linearly with axial load. In addition, the axial strain gauges were also tested with pile temperature variation of about 1 °C. The results indicated that the increase of pile temperature induced small change in the signal even if the axial load was maintained constant. This data allow correcting the calibration curve during thermo-mechanical loading in the experiments.

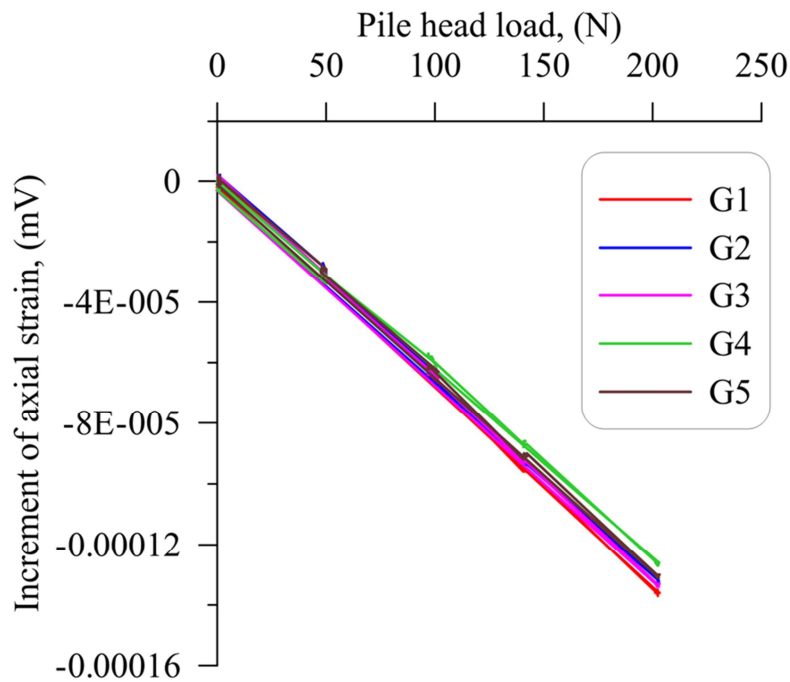


Fig. 6.3 Linear evolution of strain gauges

## 6.3 Experiments in dry sand

### 6.3.1 Experiment setup

The pile model was installed in a dry sand sample of 548 mm inner diameter and 900 mm height (Figs. 6.4 & 6.5). The sand used in this study (Fontainebleau sand) has the following physical properties: particle density  $\rho_s = 2.67 \text{ Mg/m}^3$ ; maximal void ratio  $e_{max} = 0.94$ ; minimal void ratio  $e_{min} = 0.54$ ; and median grain size  $D_{50} = 0.23 \text{ mm}$ .

The installation process began with the compaction of the first two 100-mm-thick layers, then two layers of 50 mm in thickness. The pile was then installed at its position inside the soil container and fixed by a steel bar attached to the top surface of the soil container. Finally, other sand layers of 100 mm in thickness were compacted around the pile. The soil was compacted manually, by using a wooden tamper, at a unit weight of  $15.1 \text{ kN/m}^3$ .

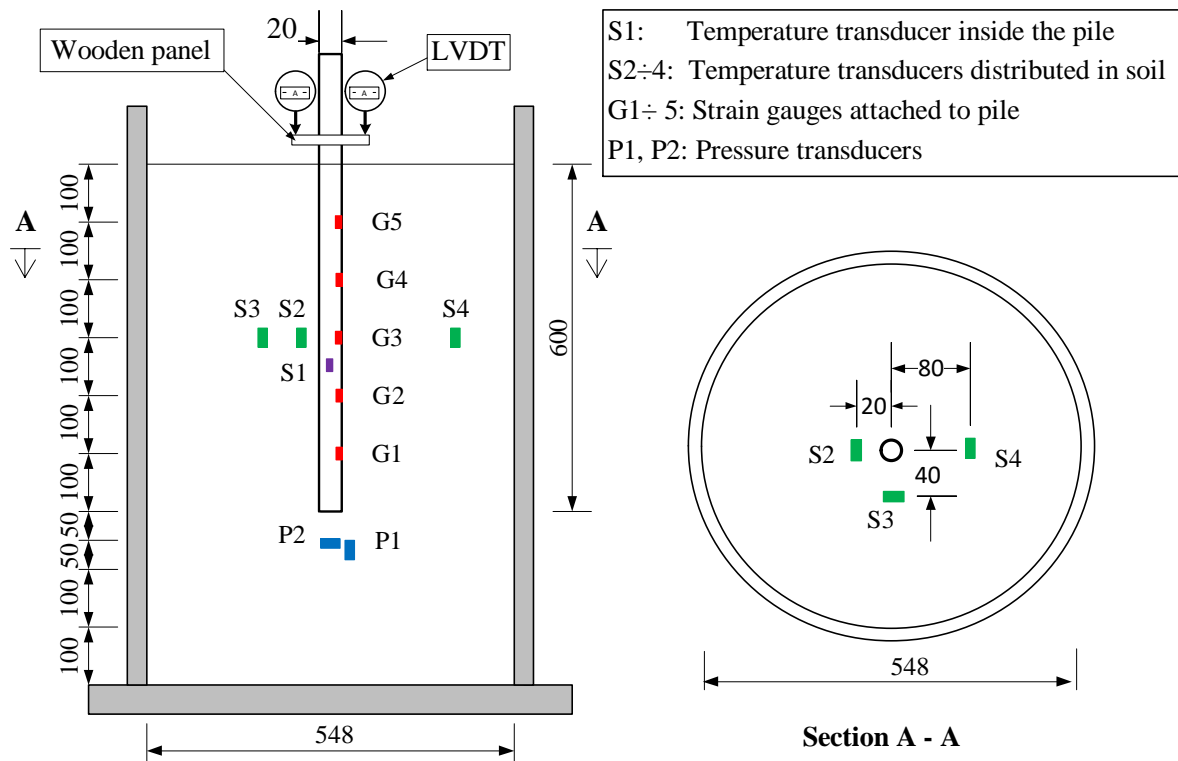


Fig. 6.4 Profile of pile model and sensors distribution

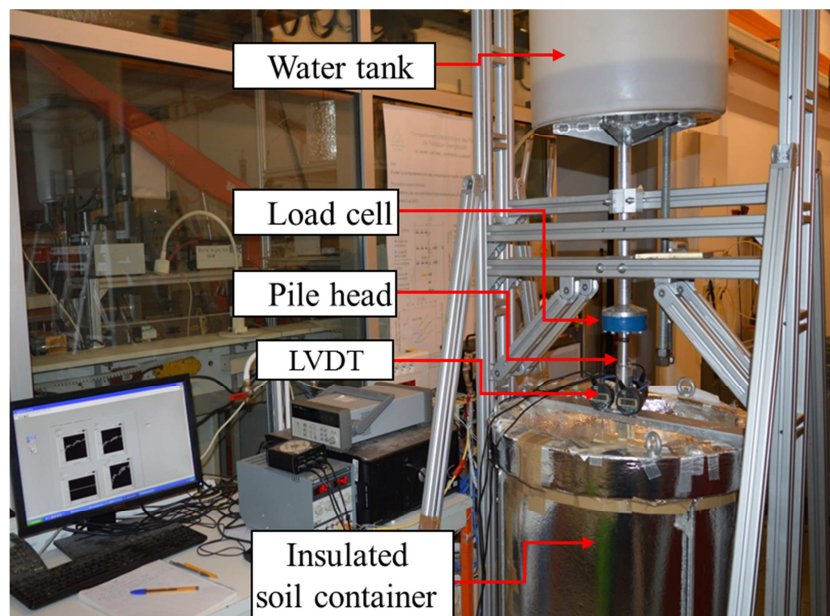


Fig. 6.5 View of the experimental setup

During the compaction, three temperature sensors and two total pressure gauges were installed as showed in Fig. 6.4. The two total pressure gauges (*P1* and *P2*) were located at 50 mm below the pile toe. *P1* measures the horizontal pressure, and *P2* measures the vertical

pressure in the soil. The three soil temperature sensors ( $S2$ ,  $S3$  &  $S4$ ) are placed at 300 mm below the soil surface and at three distances from the pile axis, 20, 40 and 80 mm, respectively. Three displacement transducers (LVDT) are used to measure the pile head displacement, and a load cell records the pile head load, which is controlled by water level in a tank placed above the pile. A metallic U tube, connected to a temperature-controlled bath, is placed inside the pile for heating and cooling the pile. The thermal conductivity of this latter is improved by filling the pile tube with water. A sensor ( $S1$ ) is placed inside the pile to measure its temperature. The soil container is thermally isolated to avoid the heat exchange with the ambient air.

### **6.3.2 Short-term behavior**

#### *6.3.2.1 Test program*

Three experiments have been performed. After each experiment, the pile model was reinstalled according to the process described above. Two experiments  $T1$  and  $T2$  were performed to investigate the load-displacement curve of the pile under mechanical loading. The test procedure follows The French standard NF P 94-150-1 (1999) (Fig. 6.6). In the preparation step, the pile was firstly loaded to  $Q_{max}/10$  for 15 minutes and then unloaded to remove the disturbed settlement component due to soil compaction related to the pile installation process ( $Q_{max}$  is the ultimate load which induced  $D/10$  settlement of pile head,  $D$  being the external diameter of pile). In the experiment, the pile was loaded in steps and subjected to two loading cycles to obtain a load-displacement relationship.

The loading paths of the thermo-mechanical experiment ( $T3$ ) are shown in Fig. 6.7. For this test, the pile was first heated from 22 to 23 °C for 120 min and then cooled to 21 °C for 120 min without head load. Afterward a recovery period of 240 min allows reaching the initial temperature. The total duration of one cycle equals to 8 hours. Once the temperature reached the initial value (22 °C), the pile was loaded to 100 N, when the settlement reached stabilization (after 120 min), one thermal cycle similar to the previous ones was applied. Then, at the end of thermal cycle, the pile was unloaded overnight. The following day, the pile was loaded again to 150 N for 120 min then a thermal cycle was applied to the pile. Similar loading processes were applied until the loading step of 300 N.

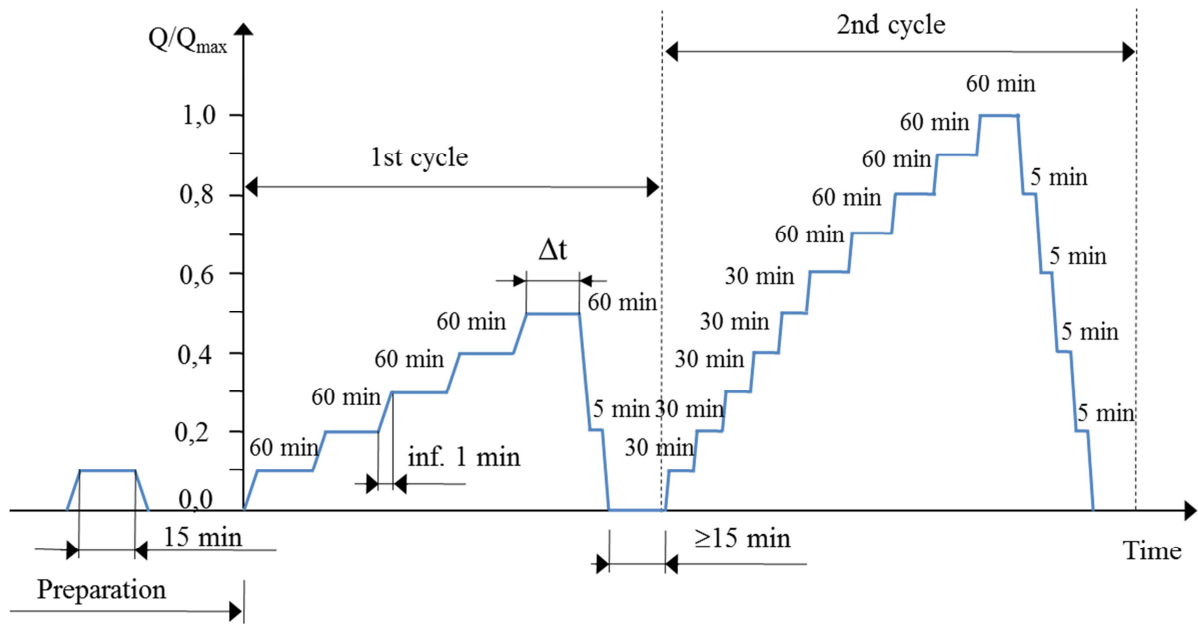


Fig. 6.6 Mechanical loading experiments (Test  $T1$  &  $T2$ )

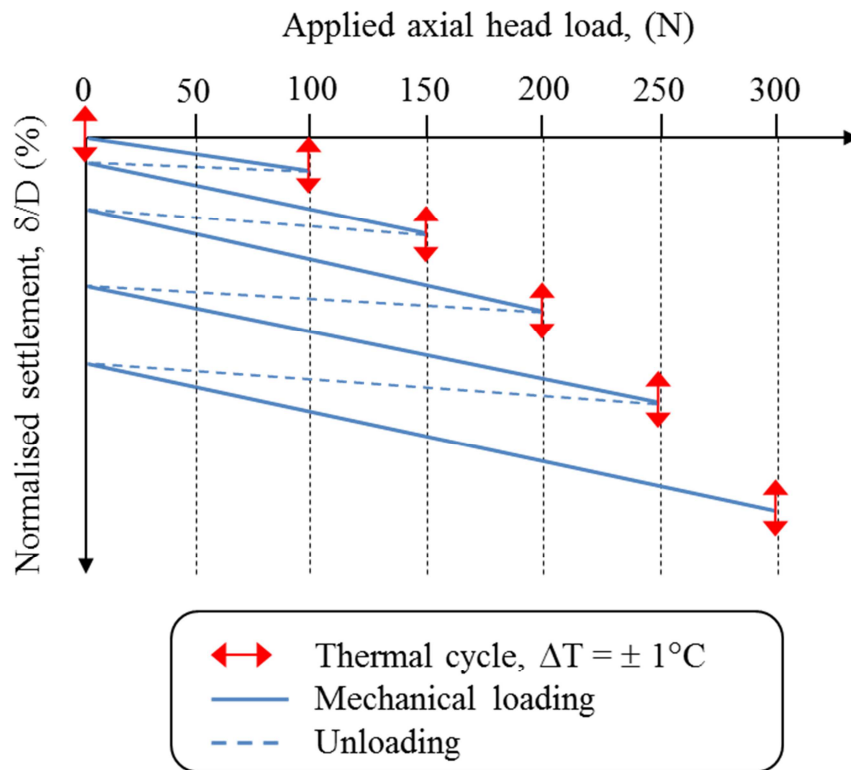


Fig. 6.7 Thermo-mechanical loading of test  $T3$

### 6.3.2.2 Mechanical behavior

In this section, the effects of mechanical loading phase on the pile behavior are shown. Fig. 6.8 shows the time evolution of pile head settlement in logarithmic scale over a 60 min period for test *T1*. In each loading step, the pile settles immediately and then the settlement continues over time but with a lower rate. Creep rate of pile in each loading step can be evaluated from these curves. Following the French standard NF P 94-150-1 (1999), under each loading, creep of pile settlement can be measured by the following index:

$$\alpha_n = (S_{60} - S_{10}) / \log\left(\frac{60}{10}\right) \quad (6.1)$$

where  $\alpha_n$  = creep rate;  $n$  = step number;  $S_{60}$  = settlement of pile head at time  $t = 60$  min;  $S_{10}$  = settlement of pile head at time  $t = 10$  min.

Creep rate results of the three tests are represented in the Fig. 6.9. The creep rate was higher at a higher pile head load and therefore a linear regression line was used to represent the average value of creep rate of all tests.

The settlement obtained in the three tests is illustrated by the load-settlement curve in Fig. 6.10. The pile head settlement value of each loading step in *T3* was measured after 1 hour of each mechanical load step and plus the irreversible settlement of the previous loading steps. From the load-settlement curve, the ultimate bearing capacity of pile (corresponding to 10% of pile diameter) can be approximately estimated at 500 N. In addition, the results of the three tests show a good repeatability of the applied procedure.

Although the test *T3* comprises coupled thermo-mechanical load, the results in Fig. 6.10 show a similar load-settlement curve for all three tests. This result implies that the contribution of thermal cycle in each step of loading to cumulative displacement of pile is negligible when compared to that of mechanical loading.

The axial strains recorded from the strains gauges were used to estimate the axial force along the pile. Fig. 6.11 shows a result of axial force distribution along the pile length obtained at the end of each loading step. Axial load of pile at levels of 100, 200, 300, 400 and 500 mm from the surface were derived from the gauges G5, G4, G3, G2 and G1 respectively.

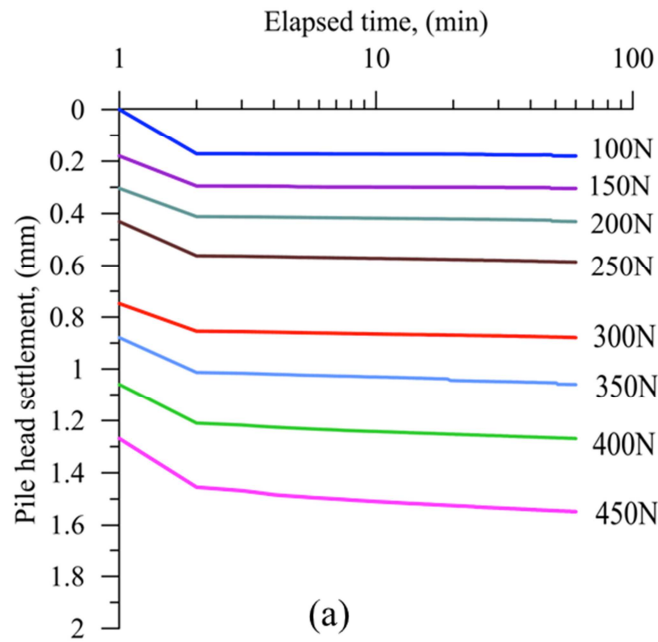


Fig. 6.8 Settlement under constant mechanical load versus logarithm of time in test T1

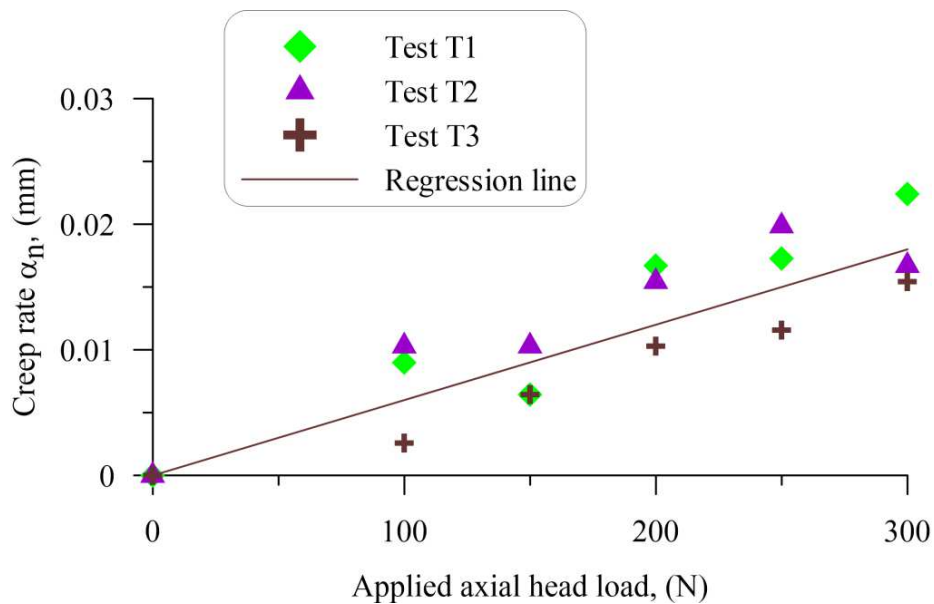


Fig. 6.9 Creep behavior of pile

Axial load value on the surface is used directly from the load cell. This result indicates that most of pile head load is transmitted to the soil via mobilized friction on the pile shaft, while a small amount of head load is transmitted through the pile toe. This latter value could be estimated by extrapolation from the last two measured forces at G1 and G2.

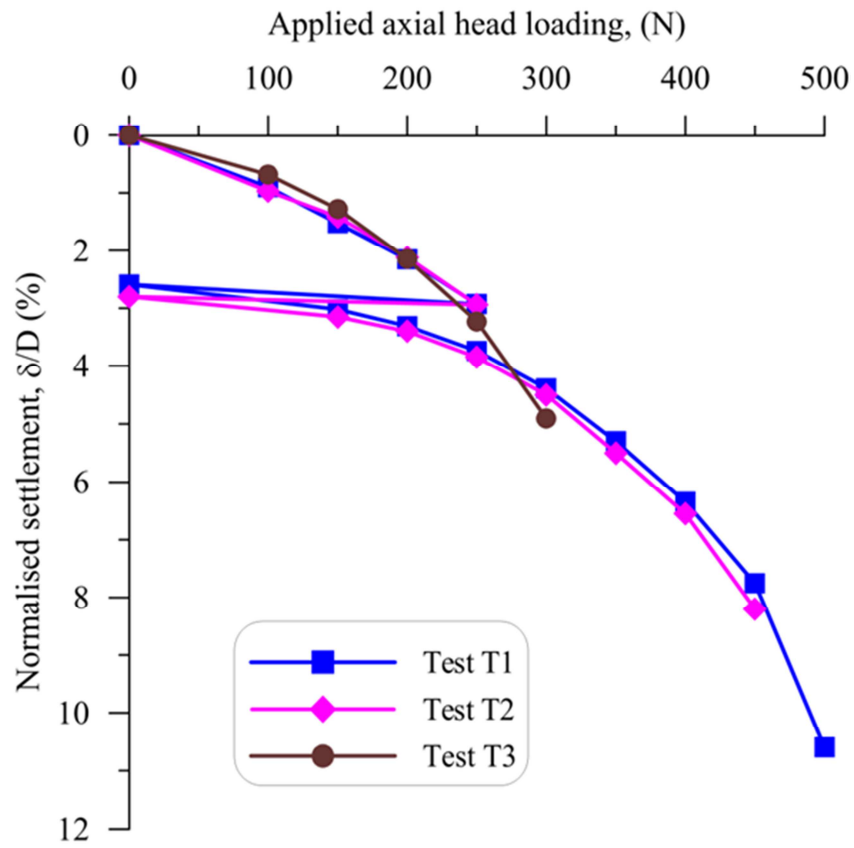


Fig. 6.10 Load-displacement curve

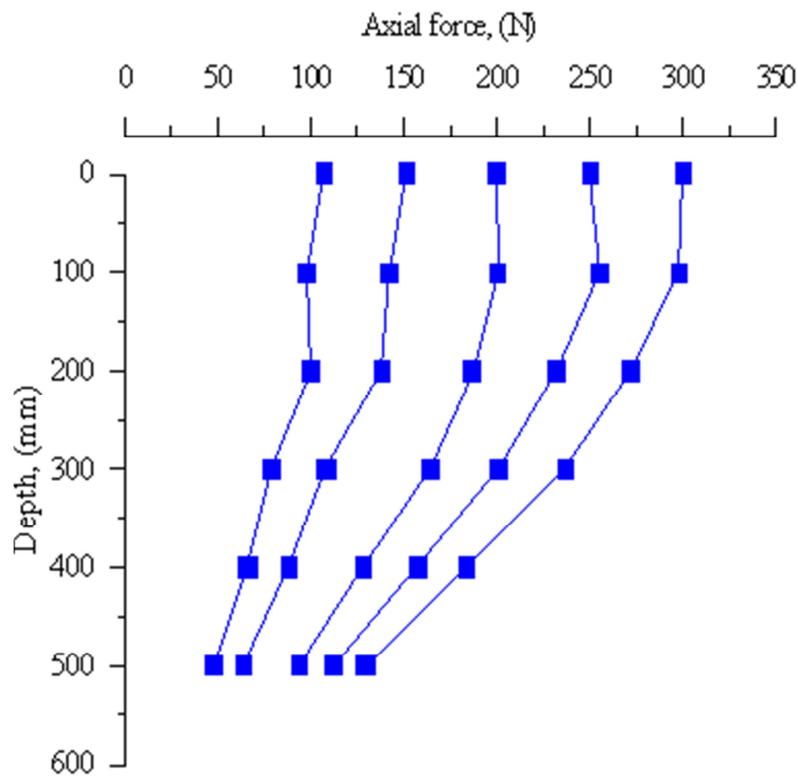


Fig. 6.11 Axial force profile for test T3

### 6.3.2.3 Thermo-mechanical behavior

Fig. 6.12 shows temperature as measured at various locations in the soil and pile for one thermal cycle. Settlement of pile in cooling phase is significant, but in the heating phase the pile head heave is almost negligible.

Fig. 6.13 represents the settlement of pile versus pile temperature during various heating-cooling cycles. Accordingly, the initial point corresponding to the start of each thermal cycle is set at zero. The final point corresponds to the end of the thermal cycle.

The results show that the pile behavior during the thermal cycle phase depends on the mechanical load applied to the pile. When the mechanical loading was null (0 N), the displacement of the pile head curve was almost similar to the pile's thermal expansion curve, which expresses the deformation of a pile restrained at its toe but free in other direction under a temperature change (Fig. 6.13a). The small difference between the free expansion and the observed curve is due to the effect of shaft friction between pile and soil. During the following loading steps, the pile settlement during cooling phase was not compensated by heave during heating so that permanent and cumulating settlement was observed. The slope of the settlement curve under the first cooling phase is similar to the slope of the pile thermal expansion curve. Pile uplift in the second heating phase was observed only in the case of Fig. 6.13b, but it was very small.

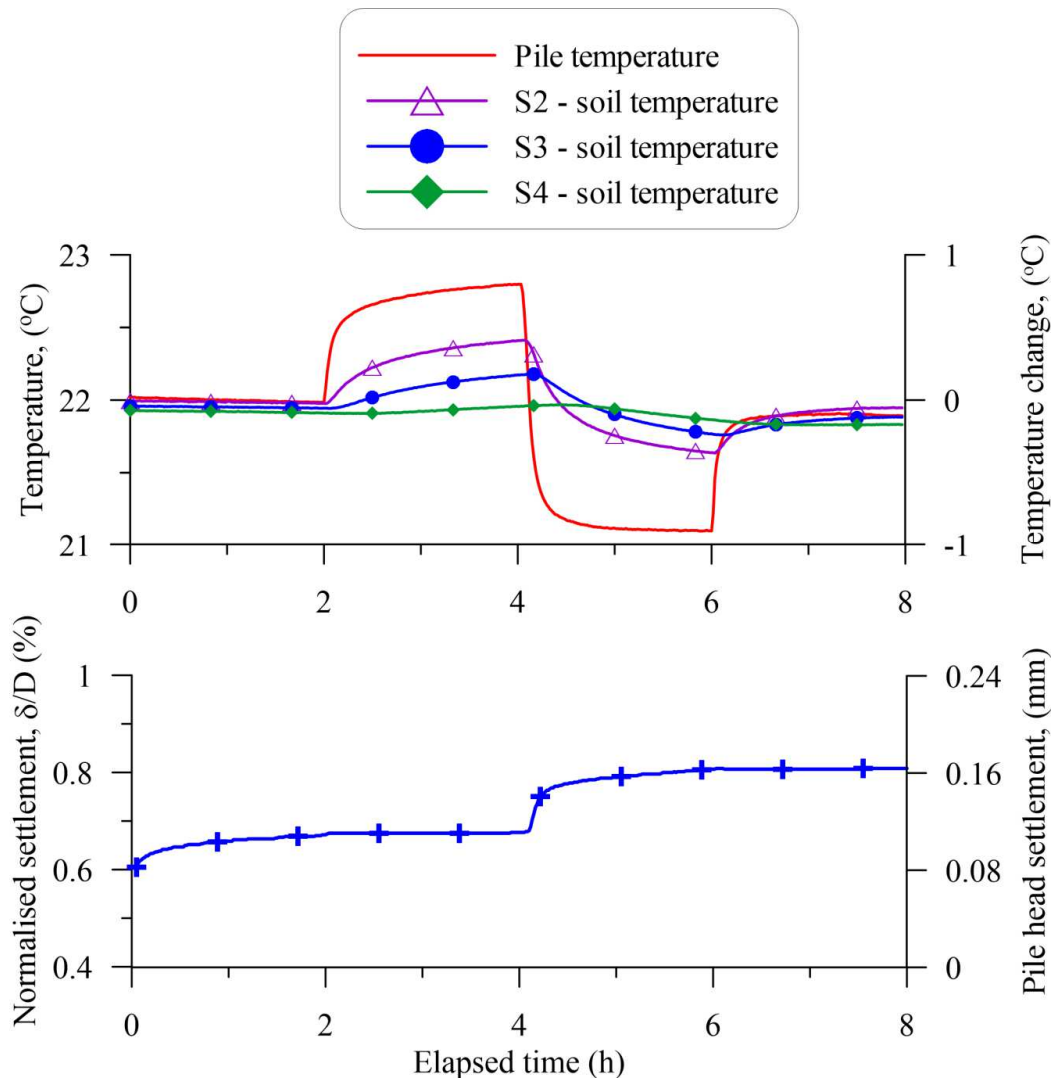


Fig. 6.12 Temperature and settlement versus time at 150-N loading step (test T3)

Axial force measured during test T3 is shown in Fig. 6.14. In the first step, in which pile was heated and cooled without axial loading, the effect of thermal cycle on the axial force along the pile length is not clear. During the following steps the effect of thermal cycles was similar with a small increase of axial force during heating and a decrease during cooling. This result can be seen as reasonable for this floating pile, which transmits most of head load to the soil through skin friction. Actually, this phenomenon is similar to the experimental results on the full-scale energy pile of Bourne-Webb *et al.* (2009), Laloui *et al.* (2011). Besides, the numerical results of Pasten & Santamarina (2014) showed the same tendency (Figure 6.14b).

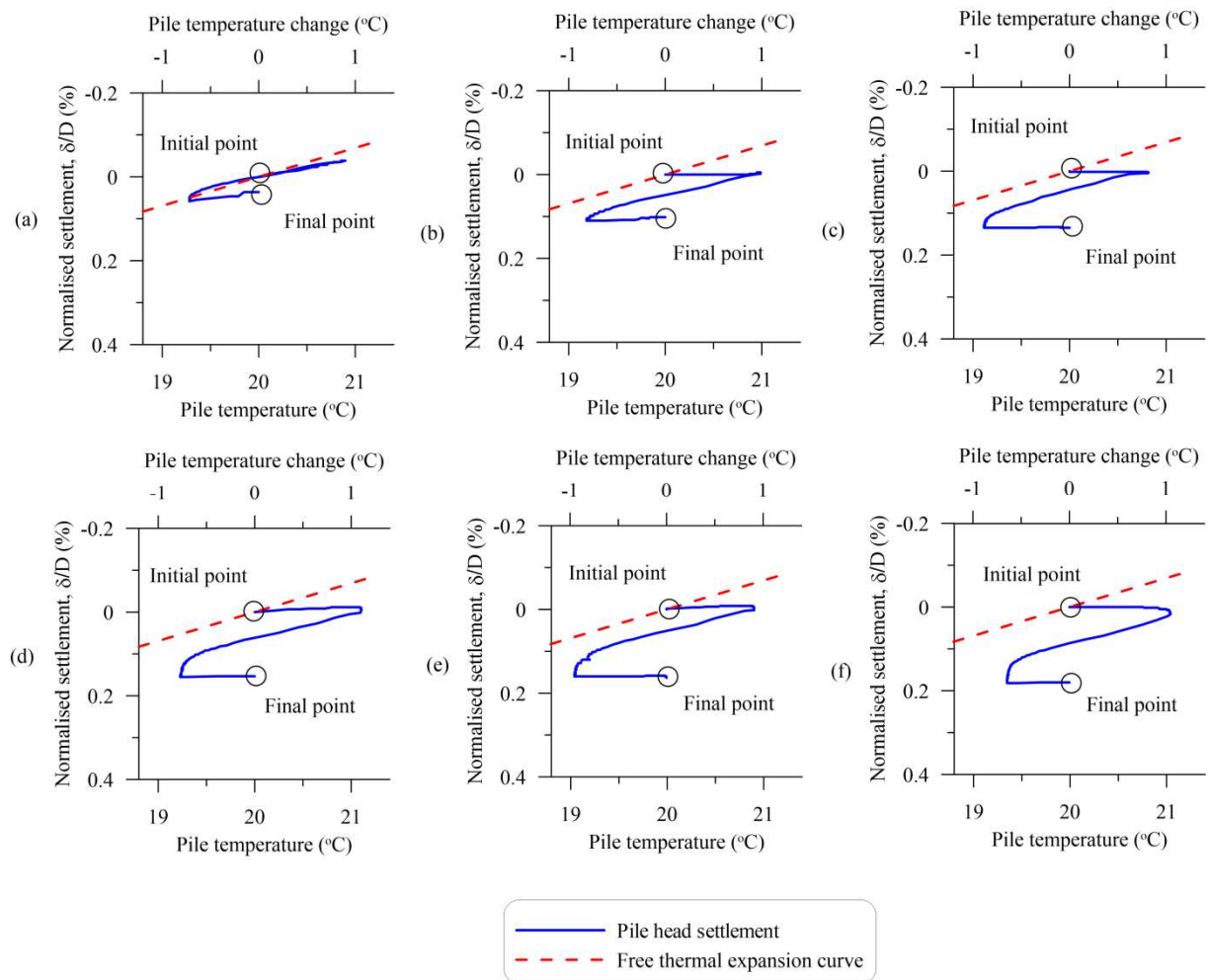


Fig. 6.13 Pile head settlement in T3. Axial loading equals to (a) 0 N; (b) 100 N; (c) 150 N; (d) 200 N; (e) 250 N and (f) 300 N

The irreversible settlement measured at the end of each thermal cycle is plotted versus axial pile head load (Fig. 6.15). Besides, the settlement corresponding to the creep phenomenon was estimated during these cycles by using the creep rate shown in Fig. 6.9. The difference between these two settlements (the measured value and the creep-related value) corresponds to the irreversible settlement directly induced by the thermal cycles. The results show generally a higher irreversible settlement, obtained by a thermal cycle, for a higher pile head axial load.

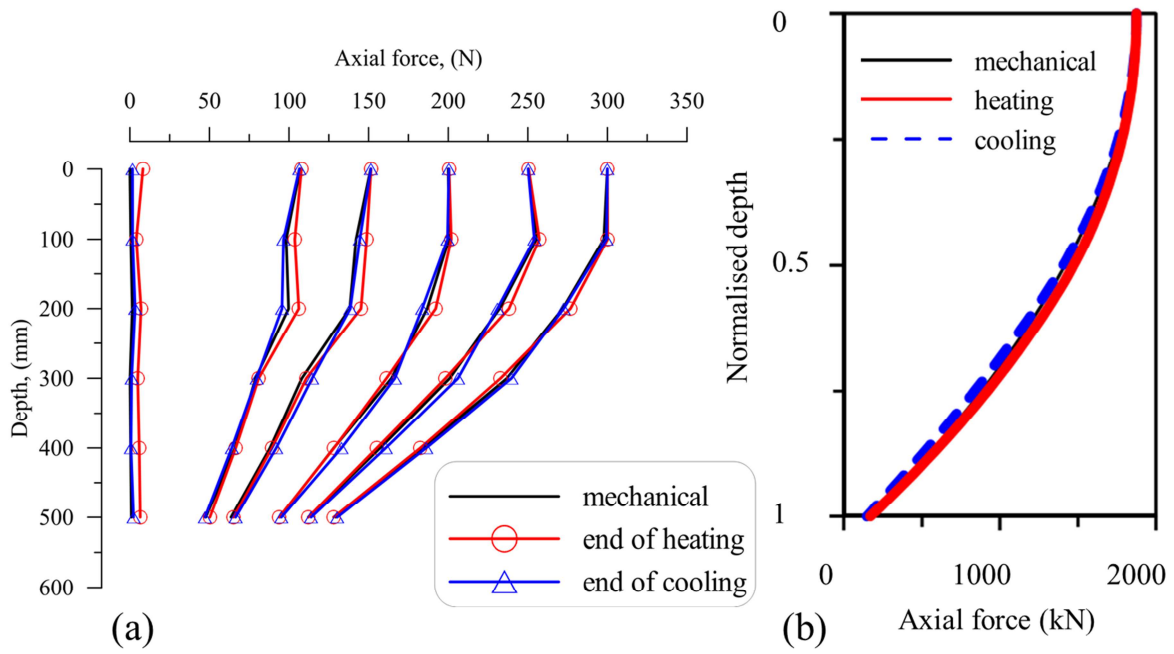


Fig. 6.14 Axial force along the pile length; (a) test T3, (b) results after Pasten & Santamarina (2014)

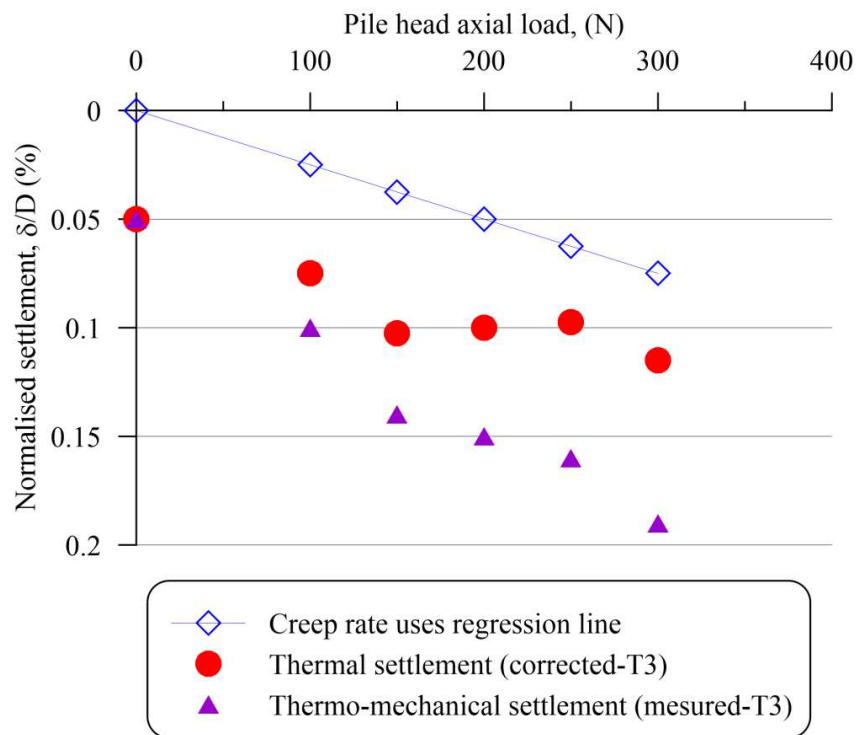


Fig. 6.15 Decoupling thermal and mechanical effects on pile head displacement

### 6.3.3 Long-term behavior

In order to investigate the long-term behavior of energy pile in dry sand, an experiment (test T4) was performed with 30 thermal cycles (representing 30 years of operation) at each pile head load level.

#### 6.3.3.1 Test program

For test T4, after the preparation step as detailed in the section 6.3.1, the pile temperature was fixed at 20 °C (similar to the room temperature) for two days to ensure the homogeneity of the soil and pile temperature at the initial state. After this phase, the pile was first heated from 20 °C to 21 °C for 4 h and then cooled to 19 °C for 4 h. Finally, the initial temperature of 20 °C was imposed to the pile for at least 16 h. Thus, the total duration of one thermal cycle equals to 24 h. Thirty thermal cycles were applied during this first stage. In the subsequent stage, an axial head load of 100 N (20% of the pile capacity) was applied. Thirty thermal cycles were then applied under this pile head load. The same procedure was repeated at pile head loads of 200 and 300 N (40 and 60%, respectively, of the pile resistance). The thermo-mechanical loading path of the test T4 is summarized in Fig. 6.16.

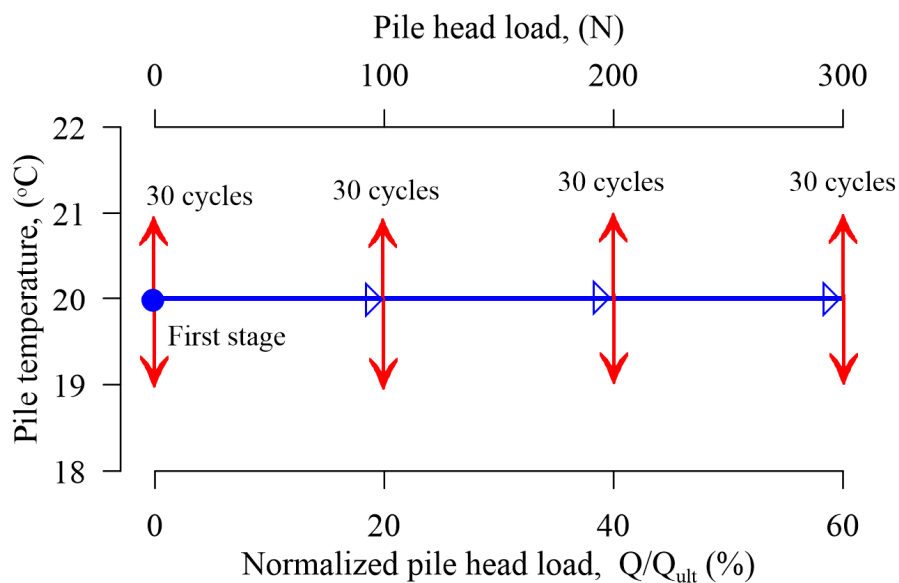


Fig. 6.16 Thermo-mechanical loading path of the test T4

### 6.3.3.2 Results

During the mechanical loading period of test T4, the settlement results of pile head showed a good repeatability of the experimental procedure. And the creep rate was observed similar to the first three tests. In addition, other results concerning the mechanical behavior of the pile under mechanical loading are quite similar to that obtained by Yavari *et al.*, (2014a) by using the same experimental setup and by testing the same sand. For this reason, these results (pile head settlement versus pile head load, pile axial stress profile, *etc.*) are not presented in this chapter.

Pile and ambient temperature is presented in the Fig. 6.17 for the first 30 cycles. The result showed that the room temperature was relatively stable throughout the experiment. Besides, the temperature of pile does not seem to be affected by the external temperature changes.

Pile head displacement under thermal cycles is showed on the Fig. 6.18, when the pile works under vertical load equal to 20% pile's capacity.

In Fig. 6.19, the irreversible pile head settlement and its ratio to the pile diameter (normalized settlement) are plotted versus the number of thermal cycles for all the four axial pile head loads. When pile is free of load, the irreversible settlement is negligible. In the other cases, the higher is the pile head load, the more important is the observed settlement. In addition, for a given pile head load, the irreversible settlement increases with the number of thermal cycles, while tending to stabilize for a high number of cycles.

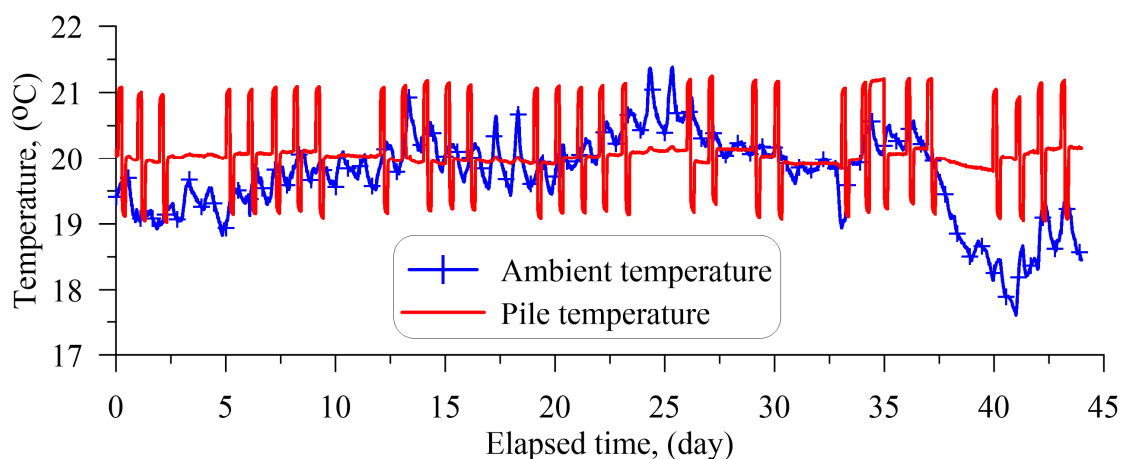


Fig. 6.17 Pile and ambient temperature under 30 cycles

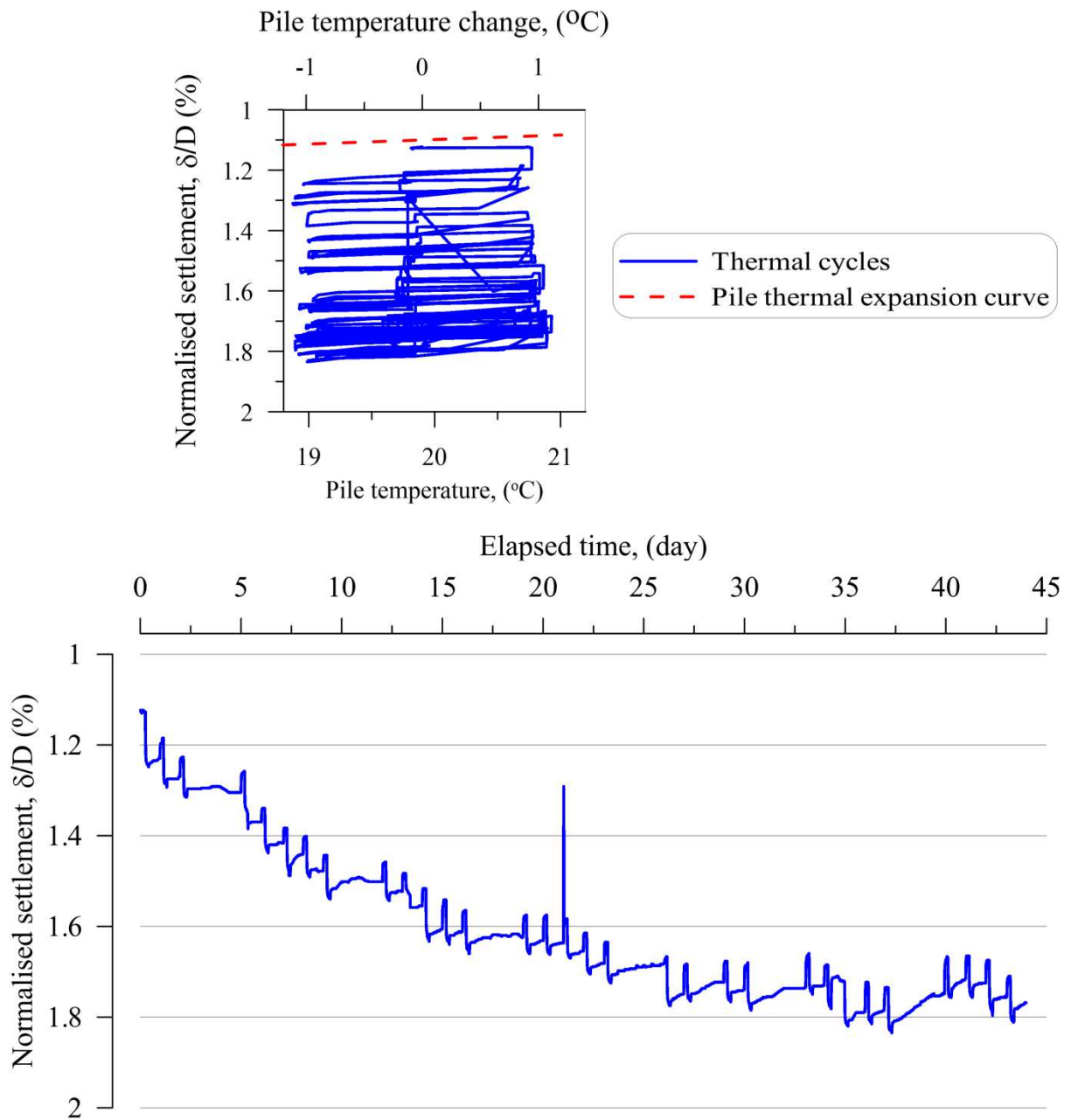


Fig. 6.18 Pile head displacement during 30 thermal cycles under a head load equal 20% pile's capacity

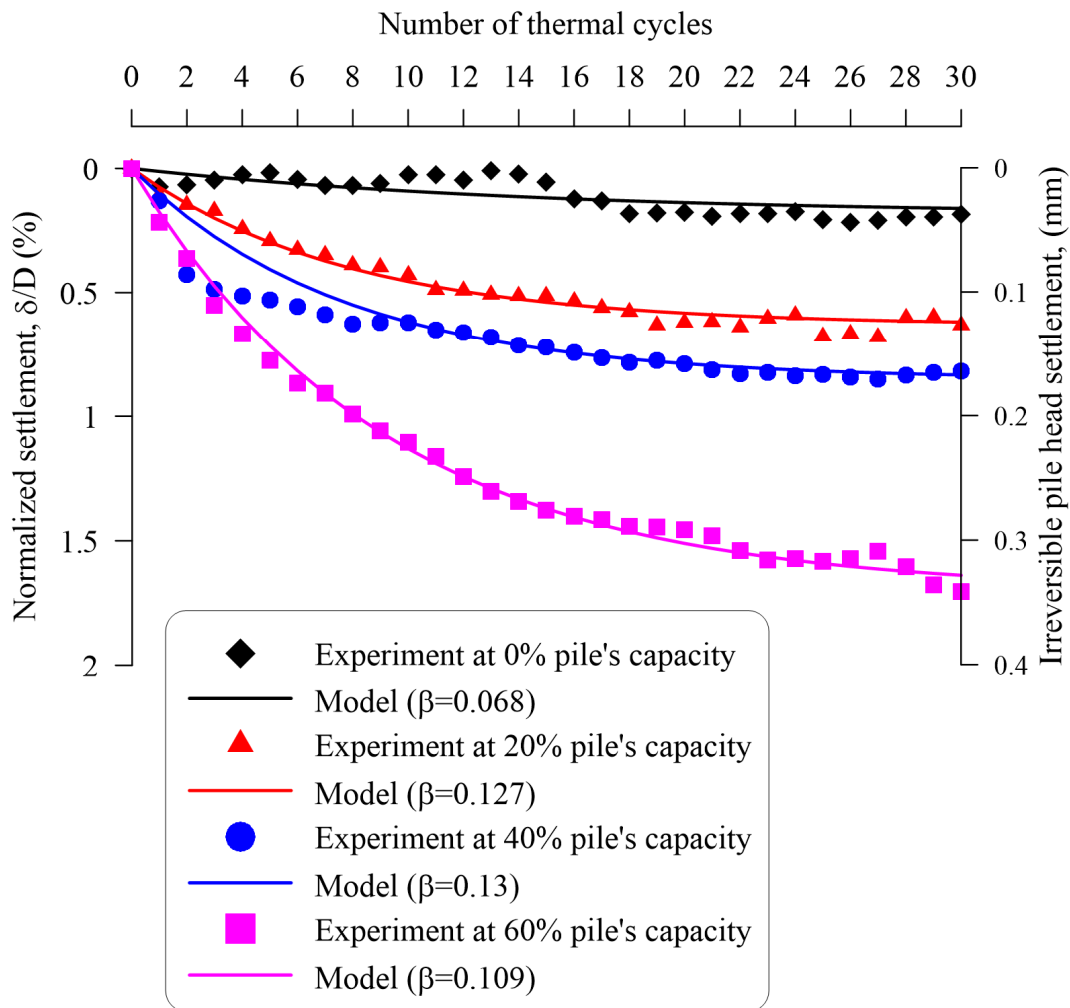


Fig. 6.19 Irreversible pile head settlement versus number of thermal cycles

In addition, while the irreversible pile head settlement tends to stabilize after around 20 cycles for low pile head load (up to 40% of pile resistance), under higher pile head load (60% of pile resistance), it continues to increase at a constant rate over the 30 applied thermal cycles.

For a deeper analysis of the pile head settlement with thermal cycles, the irreversible pile head settlement was calculated using the following equation (Pasten & Santamarina, 2014)

$$\delta_1 = \delta_1|_{N_c \rightarrow \infty} [1 - \exp(-\beta \cdot N_c)] \quad (6.2)$$

Here,  $\delta_1$  is the irreversible pile head displacement;  $N_c$  is the number of cycles;  $\beta$  is a model parameter obtained by fitting the experimental data (one value per pile head load). The result in Fig. 6.19 shows that this equation can fit correctly all the experimental data.

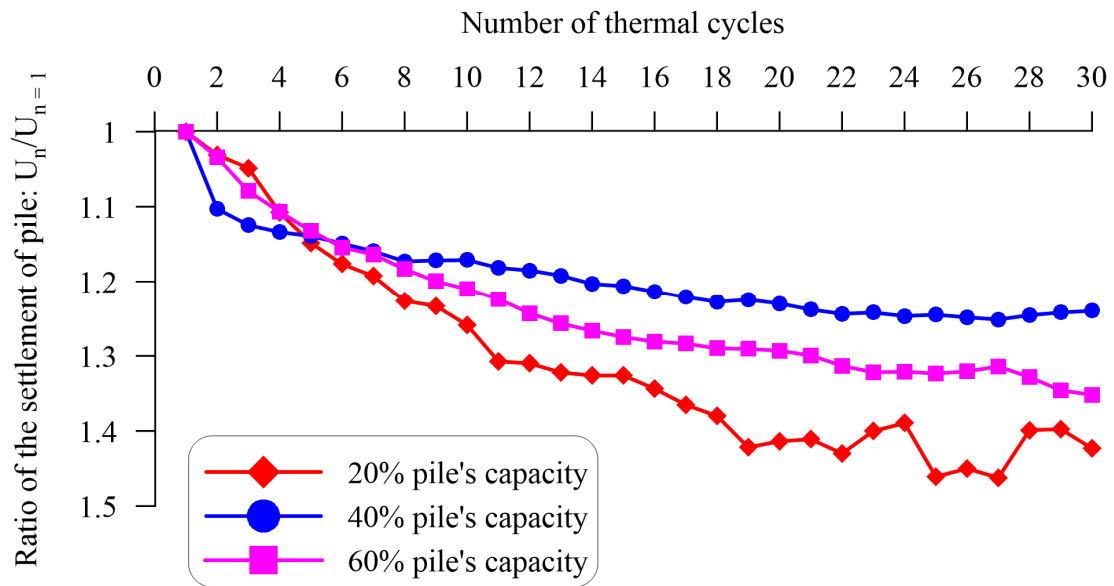


Fig. 6.20 Irreversible pile head settlement normalized to its value after the first thermal cycle versus number of cycles

Besides, irreversible settlement was also normalized with respect to the settlement obtained during the first cycle as suggested by Suryatriyastuti *et al.*, (2014). This ratio of pile settlement is plotted versus the number of cycles in Fig. 6.20 for all the four axial loads. The results show that this ratio increases quickly during the first ten cycles and then tends to stabilize at a high number of cycles. Note that in the study of Suryatriyastuti *et al.*, (2014), at a pile head load of 33% of the pile resistance, 12 heating/cooling cycles induces a ratio of approximately 1.2. This value is similar to the one found in the present work for the case of 40% of the pile resistance.

The results on axial force at different depths of the pile, measured by the strain gages are shown in Fig. 6.21. That evidences that the axial force at depths increases in heating phase and decreases in cooling phase.

The profiles of axial forces along the pile are then plotted in Fig. 6.22, where the axial force values at pile head are measured by the pile head load sensor. The axial force  $Q$  is normalized with respect to the pile resistance  $Q_{ult} = 500$  N, and the depth  $z$  is normalized with respect to the pile length  $H = 600$  mm. At the initial state, when no pile head load is applied, the axial force along the pile remains smaller than 5% of  $Q_{ult}$ . The subsequent thermal cycles do not significantly modify the axial force. When a load of 20% of  $Q_{ult}$  is applied to the pile head, the axial force along the pile also increases. Afterward, the first heating phase leads to a slight increase in the axial force and the subsequent cooling phase leads to a slight decrease. After

30 cycles of heating/cooling, the axial force is higher than the initial one (under mechanical load). Note that the axial force after the 30<sup>th</sup> heating phase is also higher than that after the 30<sup>th</sup> cooling phase. The cases of loads corresponding to 40 and 60% of  $Q_{ult}$  lead to similar observations.

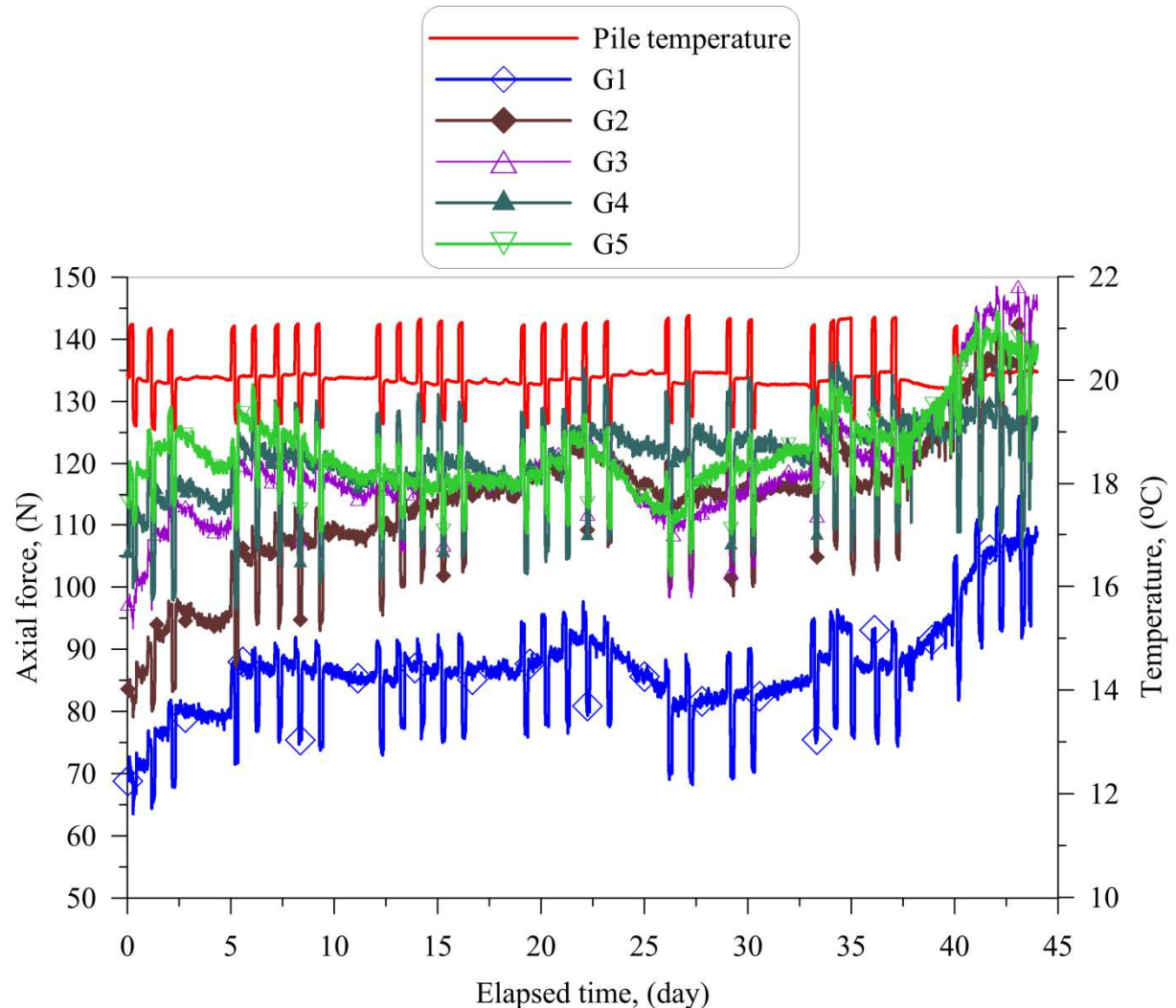


Fig. 6.21 Axial force along the pile length versus 30 thermal cycles with vertical load of 20% pile's capacity (Calculated from five strain gauges)

Fig. 6.23 shows the pile head load, the horizontal and vertical pressures in soil at 50 mm under the pile toe as a function of the number of thermal cycles. The initial stress (10 kPa and 5 kPa for vertical and horizontal ones, respectively) corresponds to the weight of the soil specimen. The coefficient of horizontal pressure at rest of 0.5 is in the usual range for dry sand (Mayne & Kulhawy, 1982; Saggi & Chakraborty, 2015; Yavari *et al.*, 2014a). These pressures increased significantly when the pile head load was increased but the thermal cycles did not influence these values.

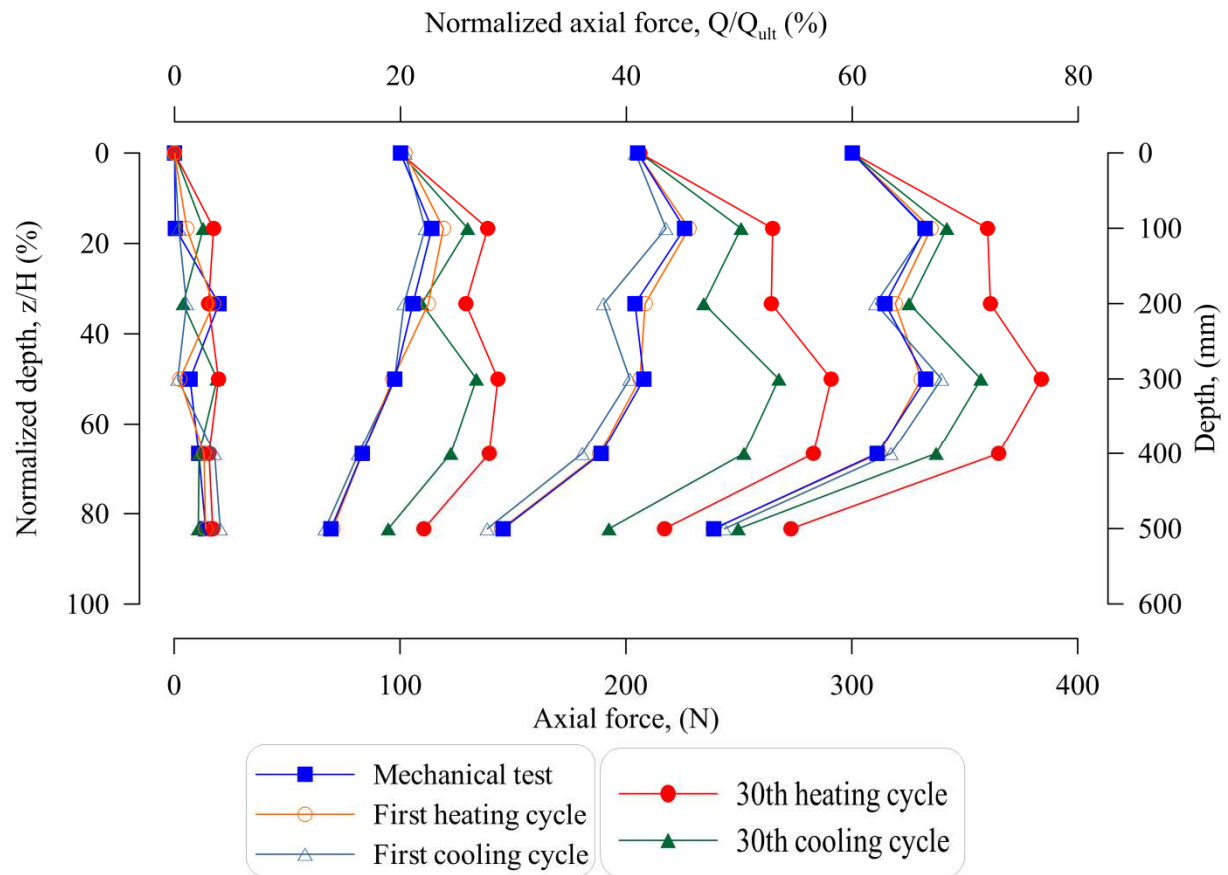


Fig. 6.22 Axial force profile of the pile during thermal cycles

In Fig. 6.24, the irreversible settlement of the pile head measured after 30 thermal cycles is plotted versus the pile head load. In this figure, the pile head settlement, estimated from the creep rate (shown in Fig. 6.9) and the duration of the thermal phase, is also plotted. The difference between these two values can be attributed to the settlement related uniquely to the thermal cycles. It can be seen that the settlement related to thermal cycles is larger than that related to creep, especially when pile works under 20% and 60% of the pile resistance. The higher is the pile head load, the higher is the irreversible settlement.

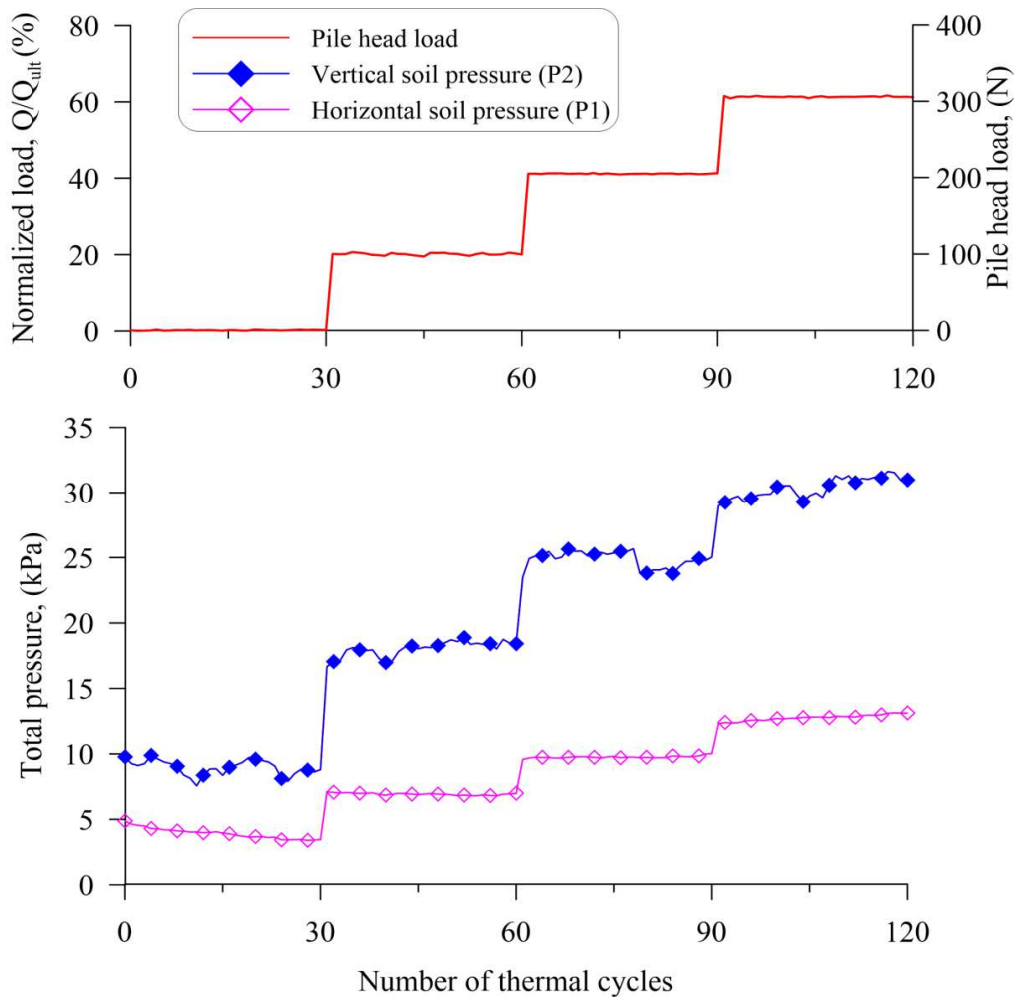


Fig. 6.23 Pile head load and total pressures in soil versus elapsed time

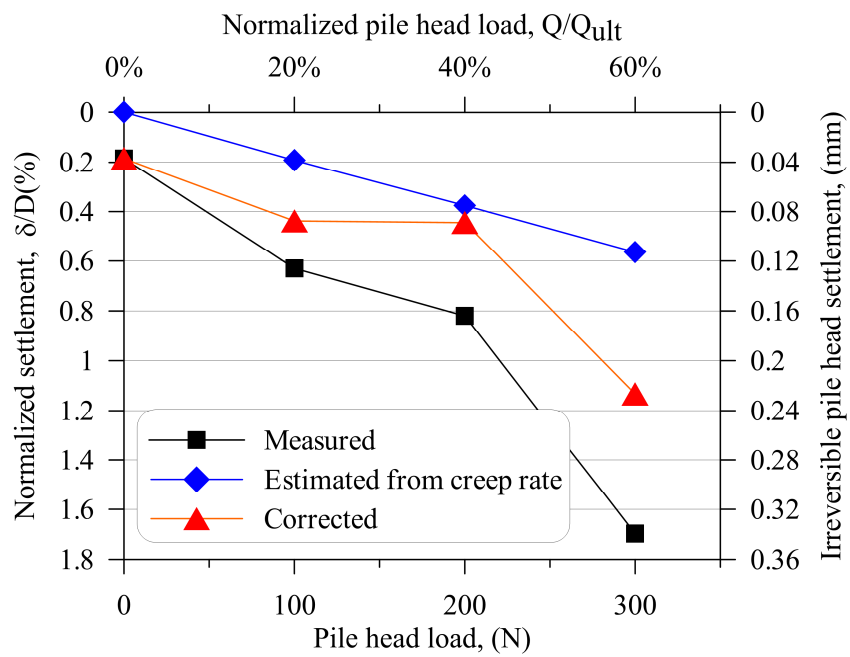


Fig. 6.24 Pile head settlement of pile after 30 cycles versus pile head load

### 6.3.4 Discussion

In the present work, the temperature variation was imposed at  $\pm 1$  °C. This range is much smaller than the temperature variation of the energy piles which can reach up to  $\pm 20$  °C (Bourne-Webb *et al.*, 2009; Laloui *et al.*, 2006; Murphy & McCartney, 2014; Ng *et al.*, 2014; Wang *et al.*, 2014; Yavari *et al.*, 2014a). Actually, in this small-scale model, the dimension of the pile is 20 times smaller than a full-scale pile of 0.4 m in diameter and 12 m length. As a consequence, the strain related to the mechanical load is 20 times smaller than that at the full-scale (Laloui *et al.*, 2006; Murphy *et al.*, 2014; Ng *et al.*, 2015; Wang *et al.*, 2014). For this reason, the temperature variation was reduced 20 times in order to have a thermal dilation of the pile 20 times smaller than that at the full-scale. The thermo-mechanical behavior of the pile observed in the small-scale can then be used to predict the behavior of energy piles at the full-scale.

The irreversible evolution of the pile head settlement with thermal cycles observed in the present work (Fig. 6.19) is similar to that obtained by Ng *et al.*, (2014) on saturated clay using centrifuge modeling. These authors applied five thermal cycles and observed a ratcheting of pile head settlement. A similar behavior can be found in the numerical study of Vieira & Maranha (2016). In the present work, with 30 thermal cycles (which can represent 30 years of seasonal temperature changes of energy piles), the results confirm that the increment of irreversible settlement per cycle is higher during the first cycles but becomes negligible after 20 cycles for the cases of axial loads lower than 40% of the pile resistance (which corresponds to the service load of piles in real cases). The irreversible settlement continues to increase after 20 cycles only when the pile head load is high (60% of the pile resistance).

When comparing the results obtained in the present work to those obtained in the numerical work of Pasten & Santamarina (2014), common trends can be found, as shown in Fig. 6.19. The parameter  $\beta$  represents the shape of the curve. The results obtained does not show a clear trend in the relationship between this parameter and the pile head load. A similar conclusion can be drawn from the Fig. 6.20 where the irreversible pile head settlement is normalized with respect to its value after the first thermal cycle. The mechanisms considered in the work of Suryatriyastuti *et al.*, (2014) can be used to explain the results obtained in the present work. These authors embedded a strain hardening/softening mechanism at the pile-soil interface into the proposed  $t$ - $z$  function to consider cyclic degradation effects during the thermal cycles. The

numerical investigation of Ng *et al.*, (2016) also confirmed the decrease in resistance of pile-soil interface versus number of thermal cycles. In addition, Vargas & McCarthy (2007) show that thermal cycles induce thermal volume change of grains, which can lead to compaction under constant stress. These authors explain this structural rearrangement by the thermal effect generating an increase in the average contact forces between soil particles. In addition, Fityus (2003) studied the behavior of a model footing on expansive clay under wetting/drying cycles and found a similar trend as far as the accumulating irreversible settlement is concerned.

The study of Saggu & Chakraborty (2015) shows an opposite trend compared with the present experiment. Actually, the axial stress decreases after fifty cycles and the pile settlement was observed only in the first thermal cycle. This phenomenon was explained by the stress transfer into the surrounding soil and the progressive heating of pile with thermal cycles. Fig. 6.22 shows an increase in the axial force along the pile when the number of thermal cycles increases. This behavior is similar to that predicted by numerical approaches (Pasten & Santamarina, 2014; Suryatriyastuti *et al.*, 2014; Vieira & Maranhã, 2016). Actually, in these studies, this behavior can be explained by the degradation of the pile-soil interface resistance with the accumulating cycles. In a different case, Pasten & Santamarina (2014) show the axial force profile of pile during fifty cycles. The axial force along the pile was larger in the heating phase than in the cooling phase. However, the axial force in the cooling phase was similar to that at the initial state.

The result in figure 6.24 shows that the thermal settlement response of pile head show a trend similar to the result from the study of Yavari *et al.*, (2016a) and Vieira & Maranhã (2016). In particular, all these studies have investigated the thermal response of pile when it works under different constant head loads. The results showed that the long-term performance of energy piles induced significant irreversible settlement and that the thermal settlement is greater at higher constant head loads.

## 6.4 Experiments in saturated clay

### 6.4.1 Experiment setup

Kaolin clay known as Speswhite China clay was used in this study. The soil parameters are shown in Table 6.1.

Table 6.1 Parameters of Speswhite clay (Yavari *et al.* 2016a)

Soil properties	Quantity	Unit
Liquid limit, $w_L$	57	%
Plastic limit, $w_p$	33	%
Particle density, $\rho_s$	2.60	Mg/m <sup>3</sup>
Plasticity index	24	-

Prior to the compaction, clay powder was mixed with water by soil mixer to achieve a water content of 29%. It is then stored in sealed box for one month for moisture homogenization. Compaction was performed, by layer of 50-mm thick, using an electrical vibratory hammer (see Fig. 6.25). Soil mass used for the compaction of each layer was controlled to obtain a dry density of 1.45 Mg/m<sup>3</sup> (degree of saturation equals 95%; and void ratio equals 0.79). After the compaction of the first six layers, the model pile was installed in place, and upper soil layers were completed. For the position close to the pile model, a small metal hammer was used to avoid damaging the pile. Three temperature gauges were inserted into the soil at depth of 300 mm from the surface to measure the soil temperature.

To control the quality of the compaction procedure, soil samples (20 mm in diameter) was cored from the compacted soil massive for the determination of dry density and water content (see Fig 6.26a). Results show that the dry density and the water content are relatively uniform with depth and they are close to the target values (Fig. 6.26b).

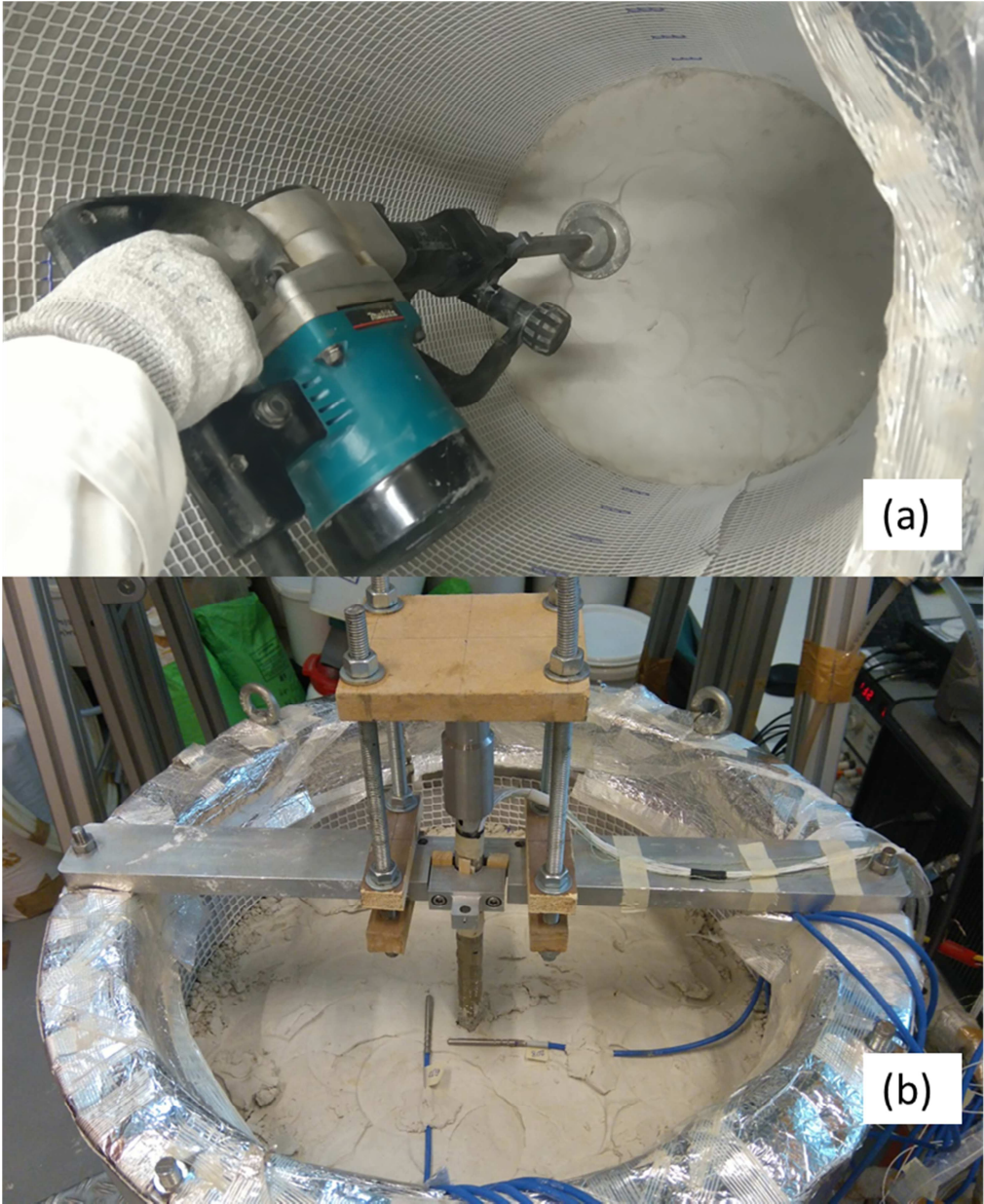


Fig. 6.25 Soil compaction by electrical vibratory hammer

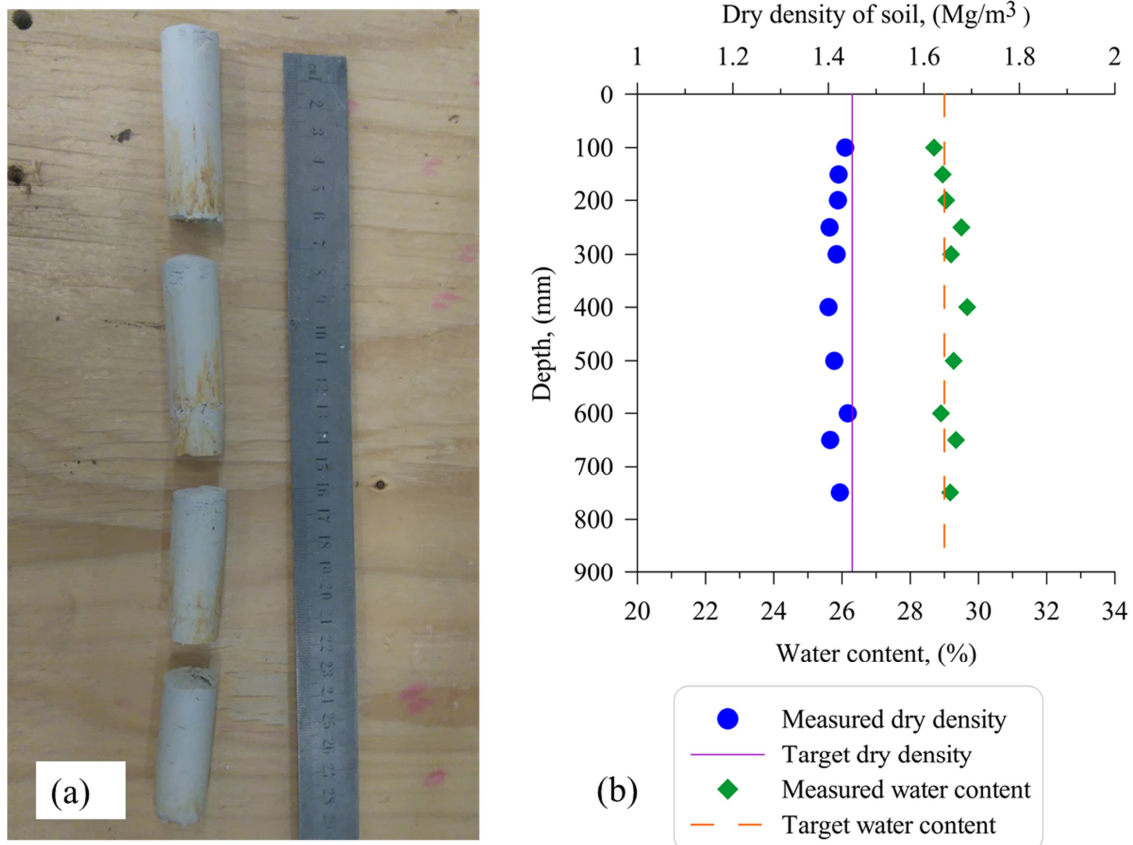


Fig. 6.26 (a) Soil samples after compaction and coring; (b) measured dry density and water content

In the work of Yavari *et al.* (2016a), re-saturating a similar soil massive took several months. In the present work, to speed up this phase, a porous plastic plate was installed at the bottom of the soil container and a thin geotextile layer was installed between the container internal surface and the soil massif (see Fig. 6.27). Thus, water from the container can easily go through the small holes at the bottom of soil container and diffuse into the soil massive via the porous plastic plate and the surrounding geotextile. The water level in the water container was kept 100-mm below the soil surface to avoid water overflow on the soil surface. During the saturation, a tensiometer T8 (T8-UMS, 2008) was used to measure soil suction at 300-mm depth and 110-mm far from the pile's axis.

Result in the Fig. 6.28 shows that after 18 days of saturation the soil at the tensiometer position is almost close to zero. The saturated process was then kept for 45 days to ensure the full saturation of the soil massif. The tensiometer was removed after the saturation process to avoid its influence on the thermo-mechanical behavior of the pile.

It should be noted that, during the saturation, the soil container was covered by a plastic sheet on its surface to avoid water evaporation. Moreover, the saturation system was maintained during the subsequent thermo-mechanical experiment to ensure that the soil is always saturated.

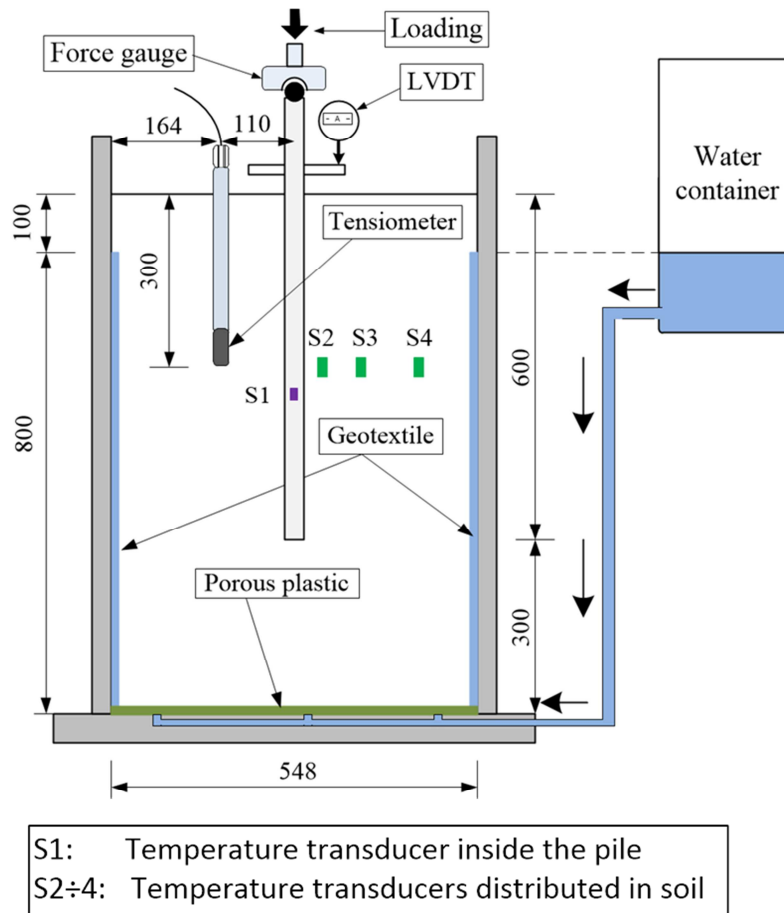


Fig. 6.27 Experiment setup

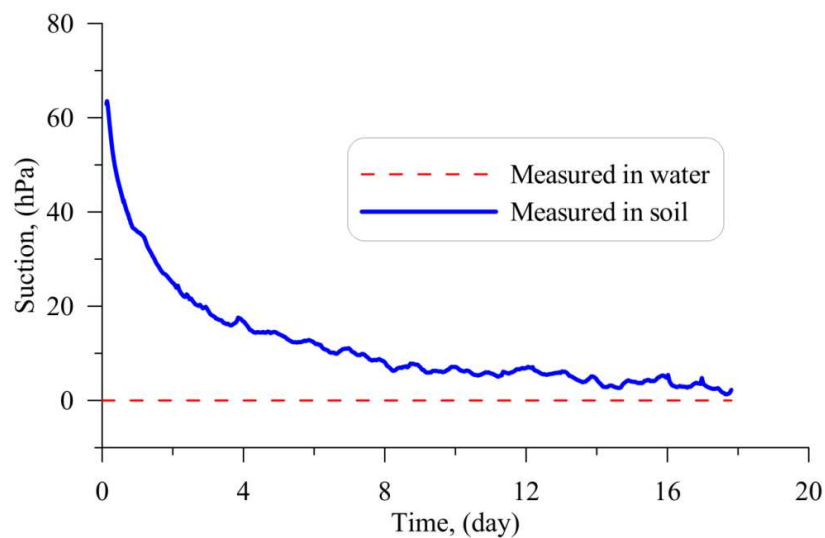


Fig. 6.28 Evolution of soil suction to verify the saturation process (measured by tensiometer)

### 6.4.2 Test program

The experiment is initially subjected to mechanical load (test A1) to determine the pile's ultimate bearing capacity. A series of load steps are applied to the pile head with an increment of 50 N, and each loading step is maintained during one hour, following the French Standard (NF P 94-150-1, 1999). The results, shown in Fig. 6.29, are similar to that obtained by Yavari *et al.*, (2016a). That confirms the repeatability of the applied experimental procedure.

In the test A1, the pile was loaded up to 500 N, which corresponds also to the pile's bearing capacity. After this test, the pile head load was removed. In the test A2, 30 cycles were performed while no load was applied to the pile head. Afterward, the pile head was loaded up to 20% of the pile's capacity prior to the application of 30 thermal cycles (test A3 shown in Fig. 6.29). At the end of these cycles, the pile head load was removed and then a load corresponding to 40% of the pile's capacity was applied. 30 thermal cycles were then performed under this load (test A4). Similar procedure was applied for test A5 corresponding to 60% of pile's capacity.

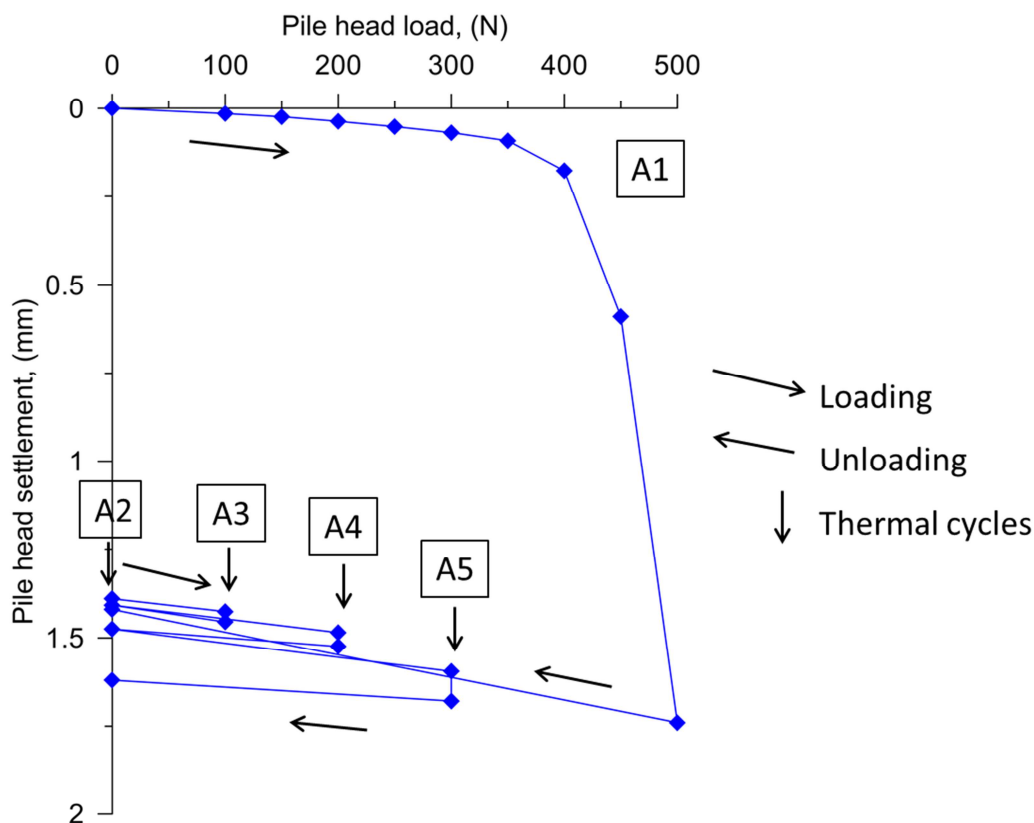


Fig. 6.29 Test programme

For each thermal cycle, the pile temperature is increased and then decreased with a variation of  $\pm 1$  °C around the initial value. Each thermal cycle is completed within 24 hours, which started with a heating period of 4 hours, and followed by a cooling period of 4 hours, finally the remaining time of active heating to return to the initial value.

### 6.4.3 Creep behavior (test A1)

Following the French standard (Afnor, 1999), the creep behavior of pile under mechanical loading steps is measured for each step (see Fig 6.30). The creep rate is then plotted versus the pile head load in Fig 6.30. This function will be used later to estimate the pile settlement related to thermal cycles.

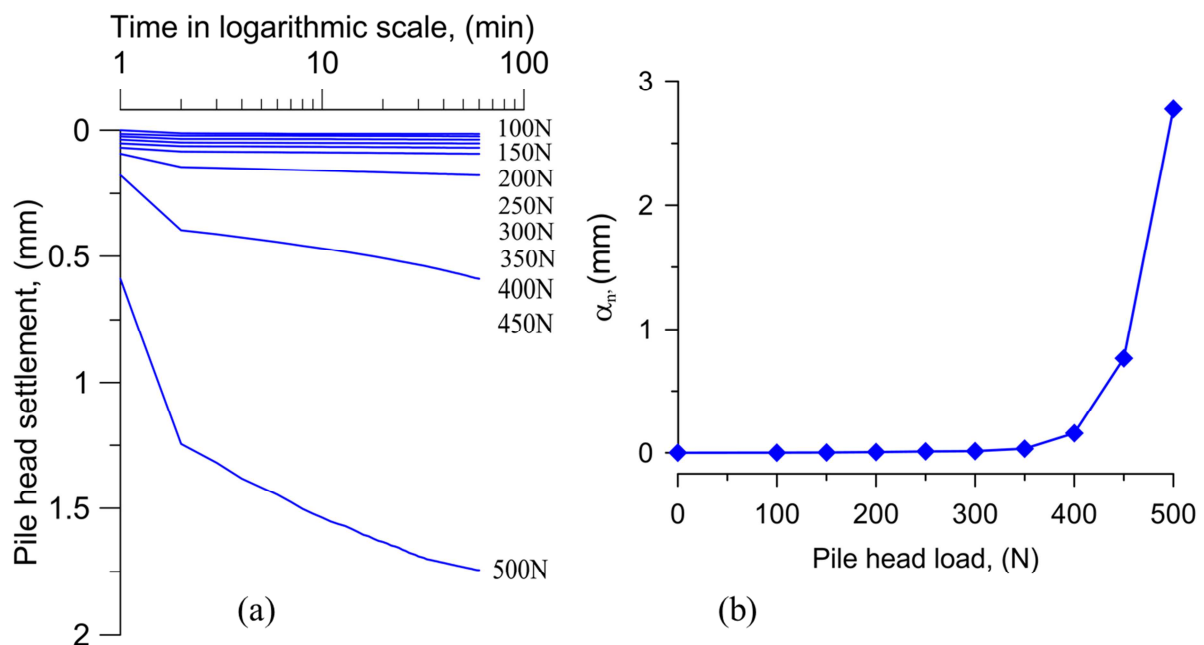


Fig. 6.30 Results under mechanical load test (test A1): (a) pile head settlement versus elapsed time for each loading step, (b) creep rate versus pile head load

### 6.4.4 Thermo-mechanical behavior

In this section, experimental results of the tests from A2 to A5 are presented. In Fig 6.31, the temperature measured in soil and in the pile is plotted versus elapsed time for one thermal cycle. The results of the other cycles are similar.

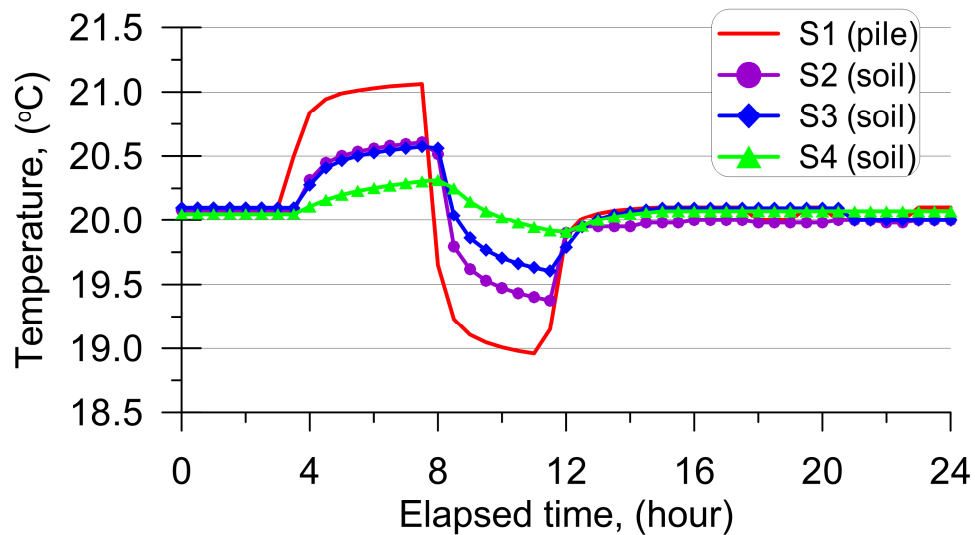


Fig. 6.31 Temperature of pile and soil during one thermal cycle

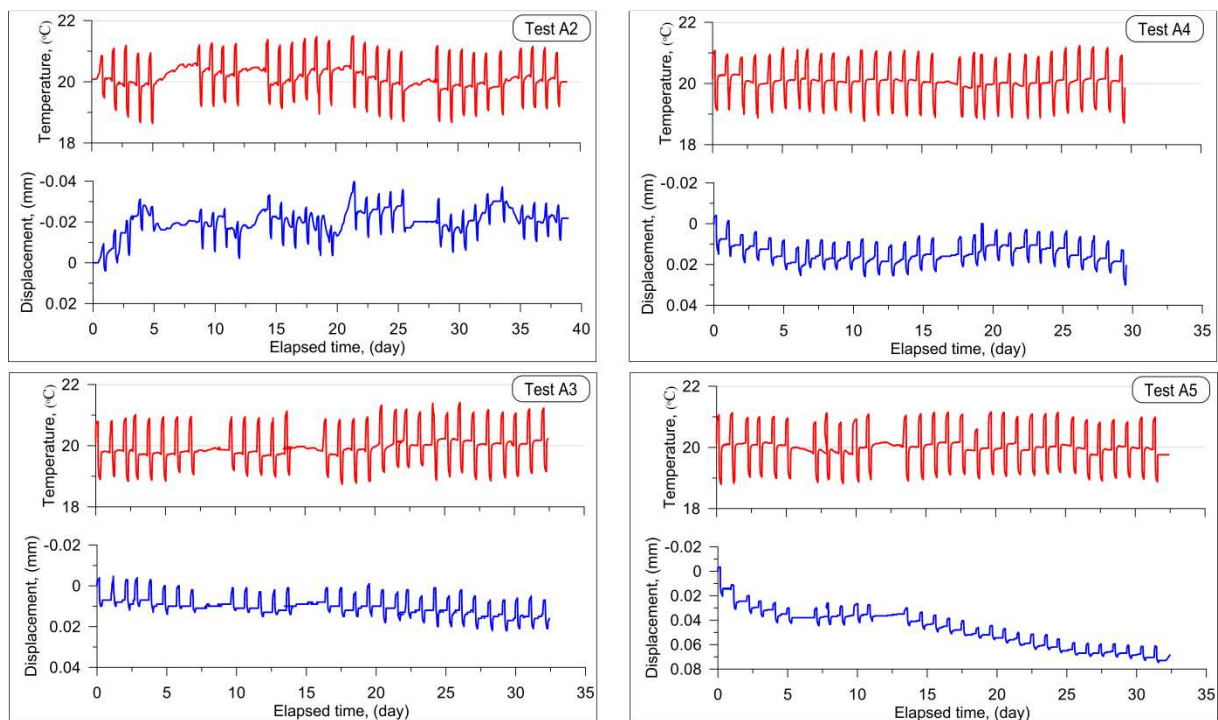


Fig. 6.32 Temperature and displacement of pile with elapsed time

Fig. 6.32 shows temperature and pile head displacement over 30 thermal cycles for all the tests. Note that the pile head displacement was reset to zero at the beginning of the thermal cycles. In the test A2, the pile is progressively moving upward during 30 cycles. This can be explained by the compaction procedure where the pile was fixed during soil compaction. That

would induce high stress at the pile toe, which tends to heave the pile when the fixing system was removed. The thermal cycles, which induce thermal dilation/contraction cycles of the pile, would re-equilibrate the stress state along the pile.

For the other tests (A3, A4, and A5) the first thermal cycle induces an important settlement of the pile head. The subsequent thermal cycles induce equally irreversible settlement but with smaller magnitude.

The displacement of the pile head is plotted versus temperature change in Fig. 6.33. To better show the results, only those corresponding to the first and the last cycles are presented. The free expansion curve, obtained based on the assumption that the pile is restrained at its toe, is also plotted. In each thermal cycle, heating induces pile head heave and cooling induces pile head settlement. However, the slope of pile head displacement versus temperature change is slightly smaller than that of the free expansion curve. That is true for both heating and cooling paths. This phenomenon could be explained by the effect of the cohesion of clay to the dilation/contraction of pile during heating/cooling, respectively.

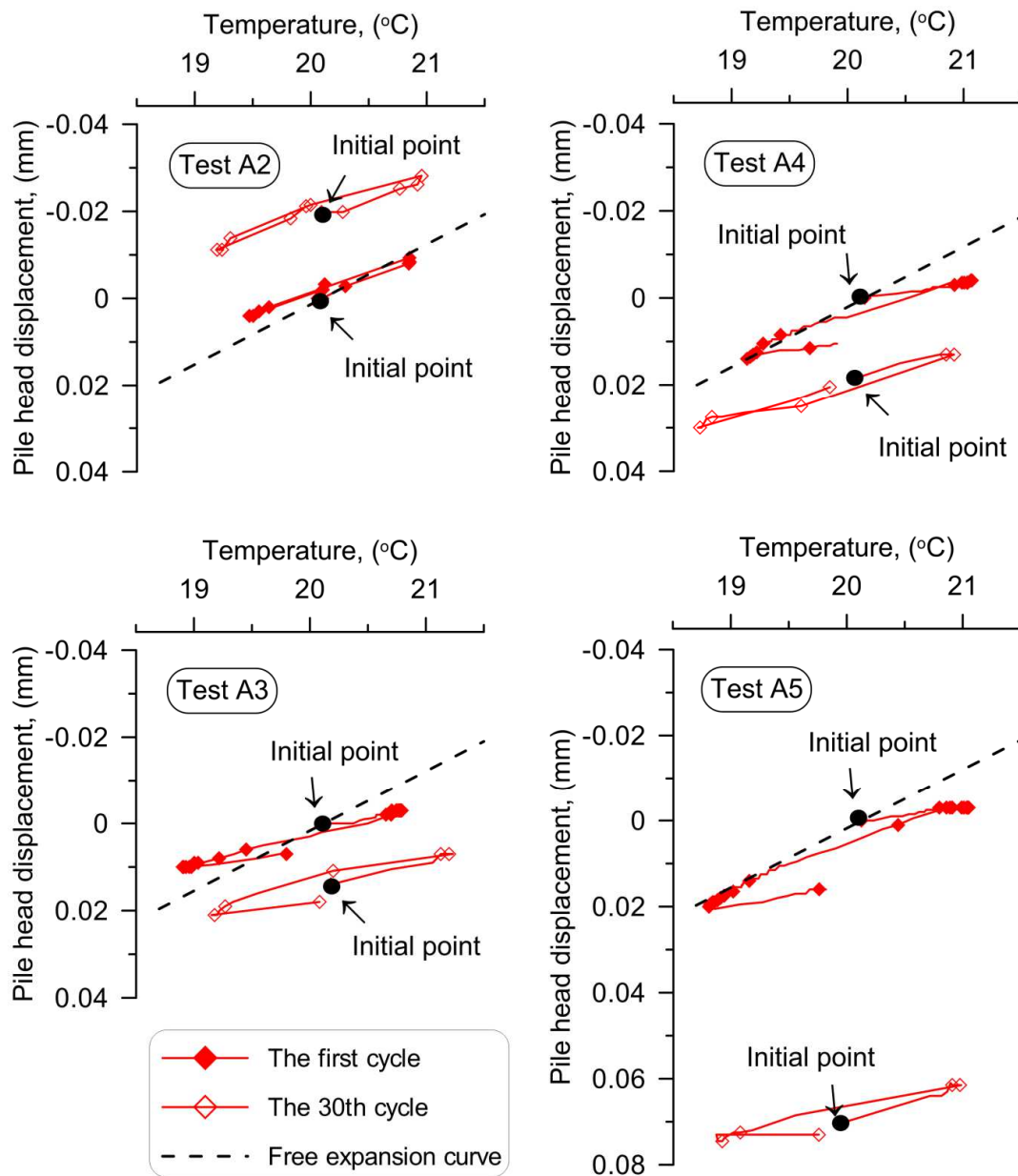


Fig. 6.33 Pile head settlement versus temperature change during the first and the 30th cycle

Fig. 6.34 shows the normalized irreversible settlement of pile head during 30 thermal cycles for all the four tests. The results show that the most important settlement is observed with the highest pile head load (test A5). The two tests A3 and A4 show similar behavior.

Fig. 6.35 presents the irreversible pile head settlement after 30 thermal cycles. The settlement is plotted versus the pile head load for the four tests. Beside the measured settlement, that related to creep is also estimated. That allows determining the pile head settlement that is purely related to the thermal cycles. This value is in the range of 0.1% of the pile's diameter at pile head load of 20% and 40% of pile's capacity.

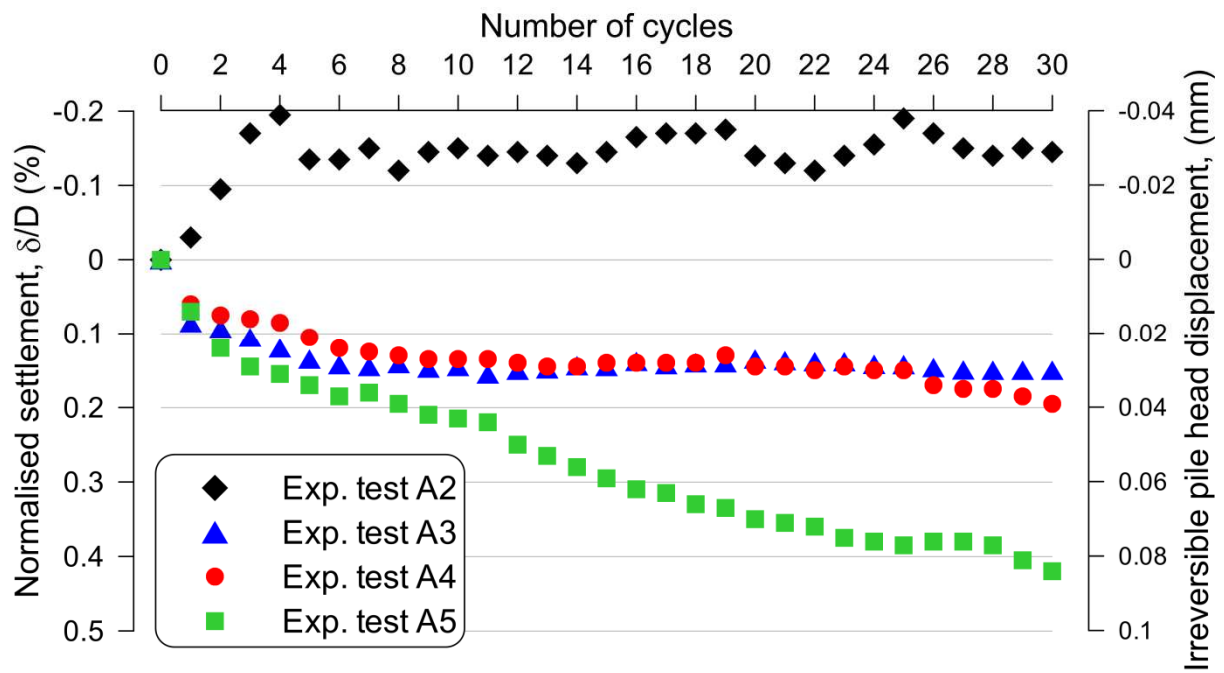


Fig. 6.34 Irreversible normalized displacement of pile versus number of thermal cycles

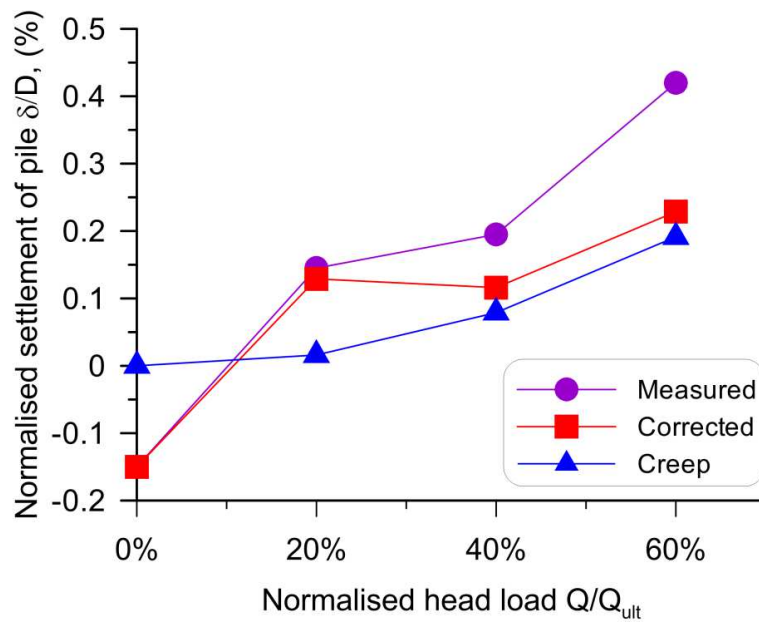


Fig. 6.34 Thermal effect on the normalized settlement of pile after 30 cycles

### 6.4.5 Discussion

In the mechanical test paths (test A1), the slope of the unloading path is nearly parallel with the loading path when the vertical load is smaller than 60% of the ultimate bearing capacity of the pile. In practice, the working load of a pile is usually below this limit. In addition, the creep rate corresponding to this range is very small (see Fig. 6.30*b*). For this reason, the maximum head load value in the subsequent thermo-mechanical tests is selected up to 60% of ultimate bearing capacity in order to avoid large cumulative settlement of the pile.

In the test A2, the upward displacement of pile (as shown in Fig. 6.32) can be explained by the effect of temperature on the thermal behavior of pile and soil. On one hand, temperature of pile tends to rise and results in thermal dilation of pile. On the other hand, temperature change can affect the adhesion force on the pile-soil interface. This means, heating induces increase in excess pore water pressure, then decrease in effective pressure of the soil and also the cohesion force. And vice versa, cooling induces decrease in pore water pressure and increase in cohesion force. Studies of (Bai & Su, 2012; Burghignoli *et al.*, 2000; Campanella & Mitchell, 1968; Fuentes *et al.*, 2016; Hueckel & Pellegrini, 1992) on the effect of temperature change to the behavior of clay soil showed that, under undrained condition testing, heating increased the average pore water pressure of about  $1\div 3$  kPa/°C. The pressure change of pore-water, according to these authors, is related not only to the difference of the expansion coefficient between the water and soil, but also depends on the volumetric stiffness of soil skeleton. In addition, the study of Campanella and Mitchell (1968) pointed out that, the thermal cycles caused accumulation of excess pore water pressure.

In the test A3 and A4, the main irreversible settlement of pile head was observed in the first thermal cycles and then the settlement of pile tends to stabilize. However, in the test A5, the irreversible settlement of pile head tends to stabilize in the first ten thermal cycles but it continues to increase with the thermal cycles.

It should be noted that for model pile in saturated clay, unlike for dry sand, the strain gauges distributed along the pile length did not work. Axial force along the pile could not be therefore analyzed. Thus, in the last chapter, a numerical simulation work is presented to interpret the thermo-mechanical behavior of this small-scale pile in saturated clay.

## 6.5 Conclusions

The long-term behavior of energy piles was investigated by using physical modeling. Thirty heating/cooling cycles (which represent thirty years of seasonal temperature changes of

energy piles) were applied to the model pile under various constant pile head loads varying from 0 to 60% of pile resistance. Temperature variation of pile was reduced 20 times in comparison to the reality in order to simulate the thermo-mechanical behavior of full-scale pile. In the first, the tests were conducted in dry sand. The response of pile is monitored by using temperature, strain and displacement sensors while the response of surrounding soil is monitored by temperature and pressure sensors. The following conclusions can be drawn:

- ❖ Thermal cycles under constant head load induce irreversible settlement of the pile head.
- ❖ The irreversible settlement of the pile head is higher at a higher pile head load.
- ❖ The first thermal cycle induces the highest irreversible pile head settlement. The incremental irreversible settlement, accumulating after each thermal cycle, decreases when the number of cycles increases. It becomes negligible at high number of thermal cycles and/or low pile head load. The evolution of irreversible pile head settlement versus the number of cycles can be reasonably predicted by an asymptotic equation.
- ❖ The axial force measured along the pile increases progressively with the increase of number of thermal cycles. The axial force at the end of a heating phase is higher than that at the end of the subsequent cooling phase.

In a second stage, the pile was tested in saturated clay (Kaolin clay soil). In this case, the pile behavior was only monitored by temperature and displacement sensors while the soil is monitored by temperature sensors. The following conclusions are drawn:

- ❖ Under the working load, cyclic displacement of pile reaches stability after a number of thermal cycles.
- ❖ The thermal effect on the pile head displacement is higher than that induced by creep behavior.
- ❖ After 30 thermal cycles, the largest normalized irreversible settlement of pile reaches 1.02% thus the pile is still working within the safety.

The results obtained in the present work could be helpful to predict the long-term settlement of a building having all the foundation piles equipped with a heat exchanger system. A similar test program should be conducted on full-scale piles, for further researches, in order to confirm quantitatively these observations. In general, the results suggest that the stress/strain behavior of energy piles would continue to evolve even several years after their installation.

## **CHAPTER 7: NUMERICAL MODELING OF ENERGY PILE**

### **7.1 Introduction**

In this chapter, fully coupled thermo-hydro-mechanical (THM) modeling of energy piles is carried out using the finite element software Plaxis. Since its 2015 version, this software supports fully THM analyses for geotechnical applications. It thus appears well suited to model the experimental piles investigated in this work.

Plaxis provides four possibilities to simulate piles in a 2D model: volume elements, plate elements, node to node anchors and embedded pile row. In this study, the pile is modeled by volume elements whose properties correspond to the pile material. This method is suitable for simulating a single pile with circular cross section, provided that the problem can be modeled using axisymmetric conditions.

The small-scale energy pile in saturated clay that was mentioned in Chapter 6 is first investigated by using the aforementioned finite element code. A two dimensional axisymmetric model subjected to thermal cycles is examined. Afterwards, this numerical tool is used to analyze the thermo-mechanical behavior of full-scale energy piles.

### **7.2 Fully coupled analysis of Thermo-Hydro-Mechanical behavior**

In this study, the finite element method with a fully coupled thermo-hydro-mechanical (THM) analysis is used. The effects of temperature change on unsaturated water flow, deformation, and mechanisms of heat transfer in porous media are synthesized and described in the study of Haxaire & Galavi (2009). In that work, the gas pressure is assumed to be constant in the media and therefore the air flow is neglected. The balance equations required to describe the THM problem thus are the water mass balance, the momentum balance and the energy balance in the porous medium. The problem is closed by considering constitutive relations, which include coupled thermal and water flows and the constitutive law describing the mechanical behavior of the materials.

### 7.2.1 Water mass balance

The mass flux of water in liquid phase is governed by Darcy's law as:

$$\underline{J}_w = \rho_w \left( \frac{k_{rel}}{\mu} \underline{\underline{\kappa}}^{int} (\nabla p_w + \rho_w \underline{g}) \right) \quad (7.1)$$

The mass flux of water in vapour phase is given by Rutqvist et al., (2001)

$$\underline{J}_v = -(D_{pv} \nabla p_w + D_{Tv} \nabla T) = - \left( \frac{D_v \rho_v}{\rho_w R T} \nabla p_w + f_{Tv} D_v \left( \theta \frac{\partial \rho_{vS}}{\partial T} - \frac{\rho_v p_w}{\rho_w R T^2} \right) \nabla T \right) \quad (7.2)$$

where  $\rho_w$ ,  $\rho_v$  and  $\rho_{vS}$  are water, vapour and saturated densities, respectively.  $k_{rel}$  is the relative permeability,  $\mu$  is the dynamic viscosity of the fluid,  $\underline{\underline{\kappa}}^{int}$  is tensor of the intrinsic permeability of the porous medium,  $\underline{g}$  is a vector containing the gravity acceleration,  $p_w$  is water pressure,  $T$  is local temperature and  $D_{pv}$  and  $D_{Tv}$  are hydraulic and thermal diffusion coefficients, respectively.  $D_v$  is the vapour diffusion coefficient in a porous medium which depends on temperature,  $R$  is the universal gas constant, and  $f_{Tv}$  is the thermal diffusion enhancement factor which is introduced to control the effect of temperature on the non-advective water mass flux (Phillip & De Vries, 1957).

The equation of mass balance of water is obtained by expanding the form given by *Rutqvist et al.*, (2001):

$$\begin{aligned} & \left[ n(\rho_w - \rho_v) \frac{\partial S}{\partial p_w} - nS\rho_w\beta_{wP0} - n(1-S) \frac{\rho_v}{\rho_w R T} \right] \frac{\partial p_w}{\partial t} + \left[ n(\rho_w - \rho_v) \frac{\partial S}{\partial T} - nS\rho_w\beta_{wT0} + n(1-S) \right. \\ & \left. \left( \theta \frac{\partial \rho_{vS}}{\partial T} - \frac{\rho_v p_w}{\rho_w R T^2} \right) \right] \frac{\partial T}{\partial t} - [(S\rho_w + (1-S)\rho_v(1-n)\beta_{sT})] \frac{\partial T}{\partial t} + (S\rho_w + (1-S)\rho_v) \frac{\partial \varepsilon_v}{\partial t} + \\ & \nabla \cdot (\underline{J}_w - \underline{J}_v) = 0 \end{aligned} \quad (7.3)$$

where  $\rho_s$ ,  $\rho_w$  and  $\rho_v$  are the solid, the water and the vapour densities;  $n$  is porosity;  $S$  is water saturation and  $\varepsilon_v$  is volumetric strain,  $\beta_{wP0}$  and  $\beta_{wT0}$  are the reference compressibility and volumetric expansion of water, respectively.  $\beta_{sT}$  is the volumetric thermal expansion coefficient of soil grains. In case of quasi-saturated states, the term  $(1-S)\rho_v$  can be insignificant in comparison with  $S\rho_w$ .

### 7.2.2 Mechanical behaviour

The linear momentum balance of a representative elemental volume is given by:

$$\nabla \cdot \underline{\underline{\sigma}} + \rho \underline{\underline{g}} = 0 \quad (7.4)$$

In case of multiphase medium,

$$\rho = (1 - n)\rho_s + nS\rho_w + n(1 - S)\rho_g \quad (7.5)$$

$$\underline{\underline{\sigma}} = \underline{\underline{\sigma}}' + P\underline{\underline{m}} \quad (7.6)$$

$\rho_g$  is the gas density,  $\underline{\underline{\sigma}}$  is the total stress tensor,  $\underline{\underline{\sigma}}'$  is the effective stress tensor,  $P$  is the average pore water pressure and  $\underline{\underline{m}}$  is the identity tensor. In the case of unsaturated media, the average fluid pressure is accounted as a weighted sum of the fluid pressures, so that:

$$\underline{\underline{\sigma}} = \underline{\underline{\sigma}}' + (\chi p_w + (1 - \chi)p_g)\underline{\underline{m}} \quad (7.7)$$

$\chi$  is an experimental factor that depends on degree of saturation, porosity and the matric suction.

The mechanical constitutive relation is formally given in incremental form as follows:

$$d\underline{\underline{\sigma}}' = \underline{\underline{M}}: (d\underline{\underline{\varepsilon}} - d\underline{\underline{\varepsilon}}_T) = \underline{\underline{M}}: (d\underline{\underline{\varepsilon}} - \underline{\underline{B}}_{DT} dT) \quad (7.8)$$

$\underline{\underline{M}}$  is stress-strain tensor,  $\underline{\underline{\varepsilon}}$  is the total strain tensor of skeleton and  $\underline{\underline{\varepsilon}}_T$  is thermal strain tensor and  $\underline{\underline{B}}_{DT}$  is the tensor of the drained linear thermal expansion coefficient of soil skeleton.

The governing equation of non-isothermal deformation of the media is then:

$$\nabla \cdot \left[ \underline{\underline{M}}: (d\underline{\underline{\varepsilon}} - \underline{\underline{B}}_{DT} dT) + \chi dp_w \underline{\underline{m}} \right] + d(\rho \underline{\underline{g}}) = 0 \quad (7.9)$$

### 7.2.3 Energy balance

The balance equation of heat energy in porous media can be written as follows:

$$C\rho \frac{\partial T}{\partial t} = \nabla \cdot (\underline{J}_c + \underline{J}_{Aw}) + Q_T \quad (7.10)$$

where  $\underline{J}_c$  and  $\underline{J}_{Aw}$  are tensors of conductive heat flux in the porous medium and the advective internal heat flux in water, respectively.  $Q_T$  is a heat source term,  $C\rho$  is the heat capacity of the porous media.

The heat flux advected by the liquid water is:

$$\underline{J}_{Aw} = C_w T \underline{J}_w = -\rho_w C_w T \left[ \frac{k_{rel}}{\mu} \underline{K}^{int} (\nabla p_w + \rho_w \underline{g}) \right] \quad (7.11)$$

The heat equation in the porous medium, with considering air temperature at the ground surface as boundary condition, can be written as:

$$C\rho \frac{\partial T}{\partial t} + \nabla \cdot (\lambda \nabla T) + \rho_w C_w \left[ \frac{k_{rel}}{\mu} \underline{K}^{int} (\nabla p_w + \rho_w \underline{g}) \right] \cdot \nabla T + \rho_w C_w T \left[ \nabla \cdot \left( \frac{k_{rel}}{\mu} \underline{K}^{int} (\nabla p_w + \rho_w \underline{g}) \right) \right] - Q_T + C_g (T - T_g) = 0 \quad (7.12)$$

where  $T_g$  is the air temperature and  $C_g$  is the convective heat transfer coefficient at the surface in contact with air.

## 7.3 Two dimensions finite element model

### 7.3.1 Modeling of small-scale energy pile in saturated clay

In this section, a two dimensions finite element approach was used to model the thermo-mechanical behavior of the small-scale pile by using Plaxis program (version 2015, thermal and coupled THM analysis). This numerical model will be validated with the experimental works on physical pile model in saturated clay that is presented in Chapter 6.

In the first step of modeling, an axisymmetric pile model is built with dimensions similar to a half of the actual pile model. The empty cylinder aluminium pile is then modeled by an equivalent material with a solid cross section ( $A_{eq}$ ). The elastic modulus of solid cross section pile is determined from the following equation:

$$A_0 E_0 = A_{eq} E_{eq} \quad (7.13)$$

where  $A_0$  is annular area of pipe,  $A_0 = 59.69 \text{ mm}^2$ ;  $E_0 = 69 \text{ GPa}$  and  $A_{eq} = 314.16 \text{ mm}^2$ .

The soil is fully saturated and pore water pressure is hydrostatic. The pile behaves as an elastic non-porous material and the behavior of soil is modeled using a linear elastic-perfectly plastic model, with a Mohr-Coulomb failure criterion. Such a model has been chosen, on the one hand, for its simplicity and small number of parameters, and on the other hand to estimate its applicability in practice to model energy piles subjected to thermal cycles. In the numerical model, the soil parameters are selected from literature on similar compacted clay (Cokca *et al.*, 2004; Muhammed, 2016; Oh *et al.*, 2008; Yavari *et al.*, 2016a). All the model parameters used in the numerical model are summarized in Table 7.1.

Table 7.1 Parameters of pile and soil used in the numerical model

Parameters	Unit	Pile	Saturated clay
Dimension (radius x length)	m	0.01 x 0.6	0.274 x 0.9
Volumetric weight	kN/m <sup>3</sup>	13.2	15.1
Young modulus	MPa	13,000	4
Poisson ratio	-	0.33	0.3
Coefficient of thermal expansion	/°C	2.3 10 <sup>-5</sup>	1 10 <sup>-6</sup>
Hydraulic conductivity	m/min	-	6 10 <sup>-7</sup>
Specific heat capacity	J/kg/°C	900	1269
Thermal conductivity	W/(m °C)	237	1.5
Cohesion	kN/m <sup>2</sup>	-	8.23
Friction angle	°C	-	25
Material model	-	Non-porous	Drained

In the second step, the numerical model is spatially discretized and the convergence of the mesh is investigated: the finite element mesh is refined until no significant variation in the obtained results is observed. The mesh consists of 15-nodded triangular elements for pile and soil. The minimum size of the refined mesh is applied to the soil elements located near the soil-pile interface.

The initial conditions for the model are similar to the physical model shown in Chapter 6: the temperature of pile and soil is assumed homogeneous and equal to 20 °C. Mechanical boundary conditions are fully fixed on the bottom surface, horizontally fixed on the two vertical sides, while the top surface is free to move (Fig. 7.1). The behavior of soil-pile interface is modeled by an interface element.

Regarding the hydraulic boundary conditions, the axis of symmetry is by definition impervious. As mentioned in the section 6.4.1 (Chapter 6), a porous plastic plate was installed at the bottom of the soil container and a thin geotextile was placed at the sides between the container internal surface and the soil massive to speed up the saturation of soil, therefore the water flow is opened at the bottom and the two remaining sides. The pore water pressure in the soil massive increases linear with the depth, and it is not changed during the tests.

The thermal boundary conditions correspond to adiabatic surfaces (no heat flow), either for symmetry reasons or to render the effects of insulation of the physical model.

In the third step, the pile is loaded with the same loading program of the experiment model as shown in the Fig. 6.29 (Chapter 6). Thermal loading is simply simulated by imposing along the pile center the temperature profile considered during the experiment (Table 7.2). In this numerical modeling, only the first two thermal cycles are simulated for each maintained loading step. Each thermal cycle includes three steps which are heating, cooling and heating back to the initial temperature. A fully coupled analysis is used for the mechanical test (test A1), and also for the thermo-mechanical tests (test A2, A3, A4 and A5).

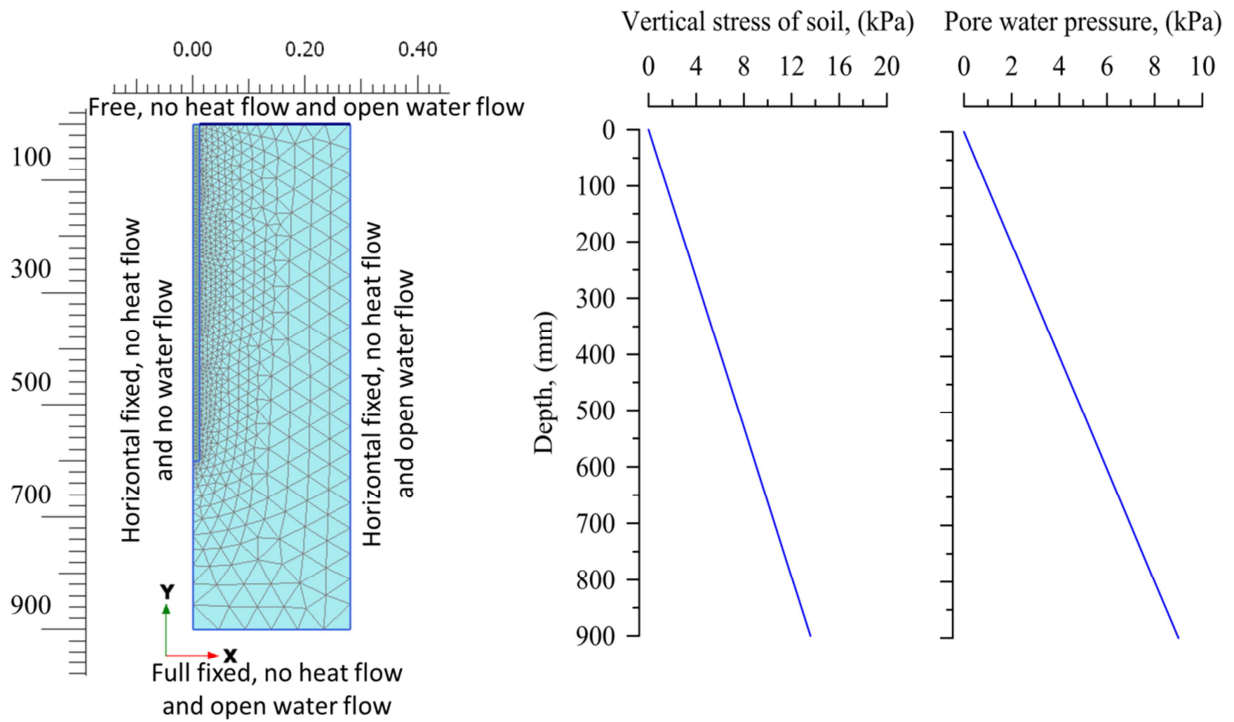


Fig. 7.1 Geometry and boundary conditions of the model

**Table 7.2** Temperature of pile during the first two thermal cycles (°C)

Test	Initial phase	First heating	First cooling	Heating back	Second heating	Second cooling	Heating back
Test A2	20	20.8	19.5	20.1	21.1	19.1	19.9
Test A3	19.9	20.8	19.0	19.8	20.8	19.0	19.8
Test A4	19.8	21.0	19.1	20.2	21.0	19.1	20.3
Test A5	20.3	21.0	18.8	20.1	21.1	18.9	20.1

7.3.1.1 Results

a) Mechanical behavior of pile

The ultimate bearing capacity predicted numerically is similar to the one obtained with the experimental pile. The settlement of the experimental pile head equals 1.74 mm under a head load of 500 N while the numerical pile model settles 1.72 mm (see Figure 7.2). This value approximately corresponds to a settlement of the pile equal to 10% of its diameter,  $D = 20$  mm. It is worth noting that the downward movement of the pile and the compression stress are considered positive.

Fig. 7.3 shows the axial stress distribution along the pile length obtained at the end of each load step. These results indicate that most of pile head load is transmitted to the soil via mobilized friction along the pile shaft, while a small amount of head load is transmitted into the soil through the pile toe. It can be said that the mobilized friction on the pile shaft is significant, and the mobilized resistance of the pile depends mainly on skin friction.

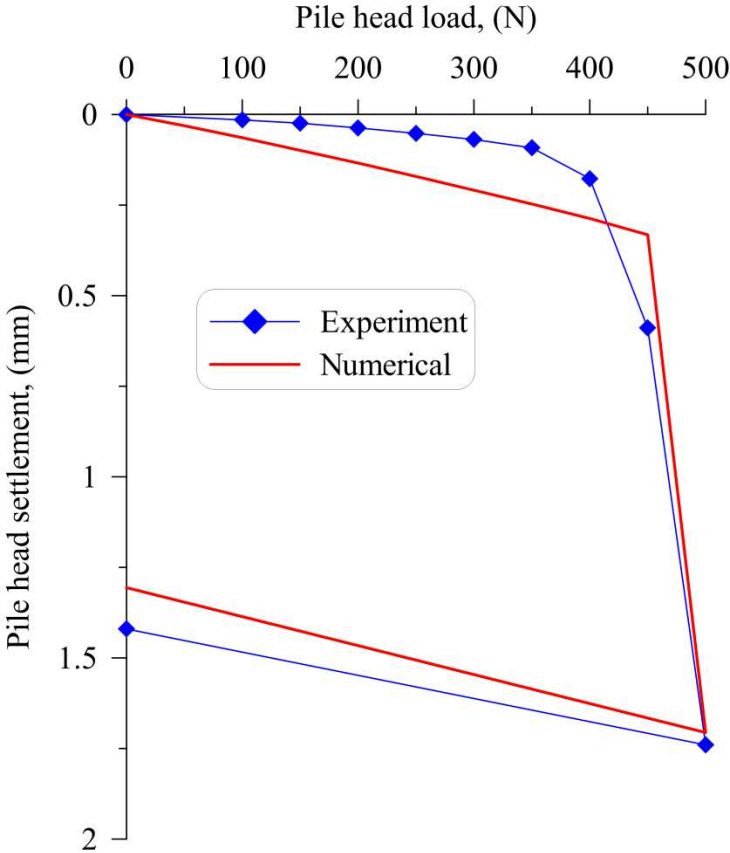


Fig. 7.2 Pile head load displacement curve: experimental curve and numerical prediction

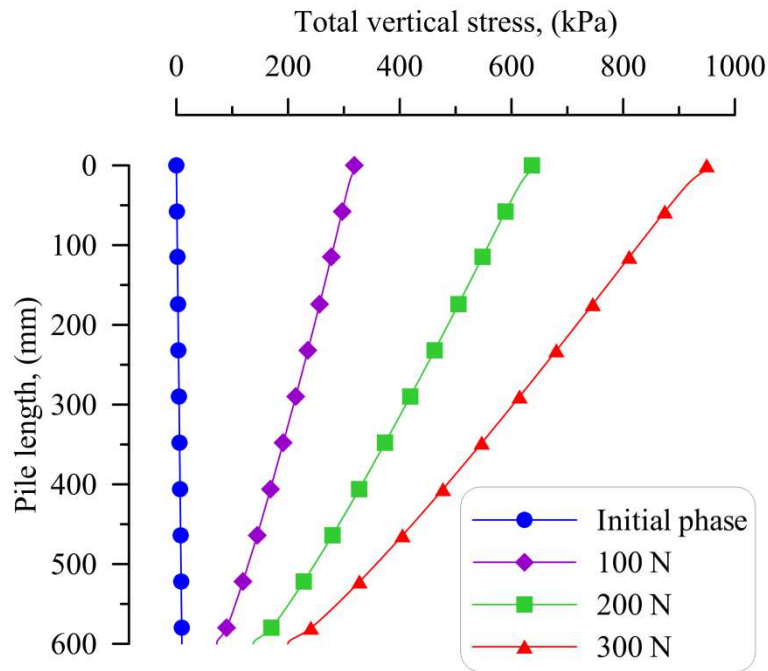


Fig. 7.3 Vertical stress of pile length in the mechanical test A1 (numerical results)

### *b) Thermo-mechanical behavior of pile*

In this section, numerical results for the thermo-mechanical tests A2 to A5 are presented and compared with the experimental data. The distinct thermal phases applied to the pile are modeled as shown in Fig. 7.4.

Fig. 7.5 shows the experimental and numerical results of temperature and displacement of the pile over the first two thermal cycles. It can be observed that the temperatures imposed to the pile precisely correspond to the ones measured during the experiment over the two cycles. Hereafter, we only consider the displacement increment experienced by the pile head during the thermo-mechanical loading phase: this means that the displacement of pile prior to the thermal load is taken as a reference and reset to zero. Physical and numerical results agree relatively well for tests A2 and A3. However, different displacements between the two models are observed for tests A4 and A5.

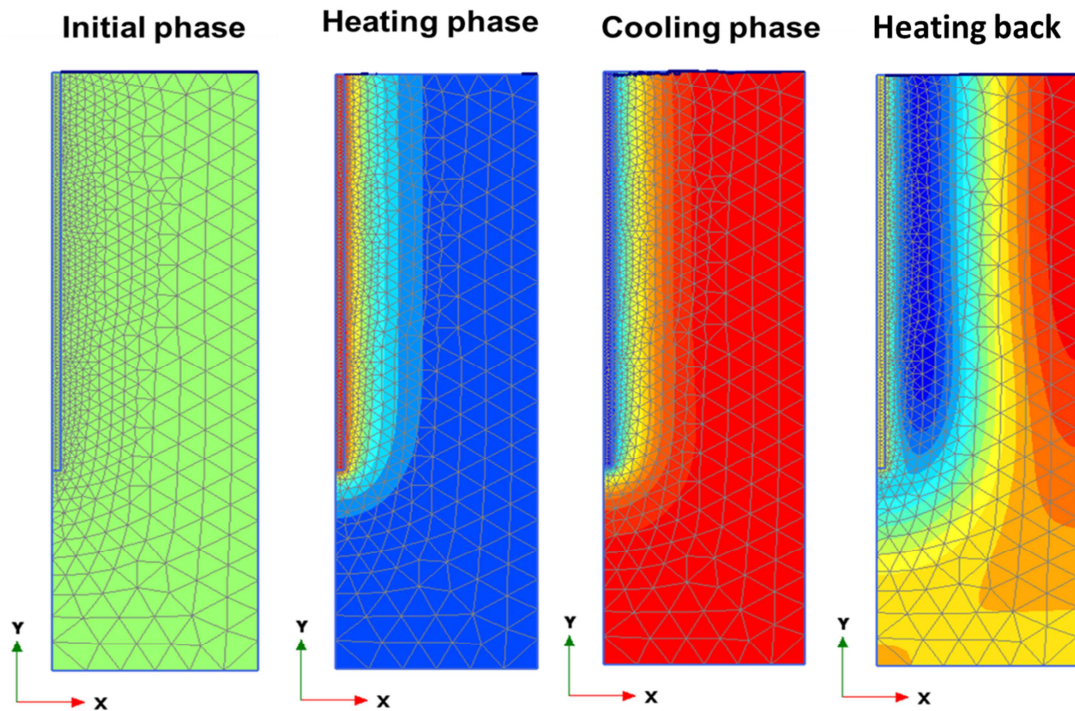


Fig. 7.4 Axisymmetric finite element model

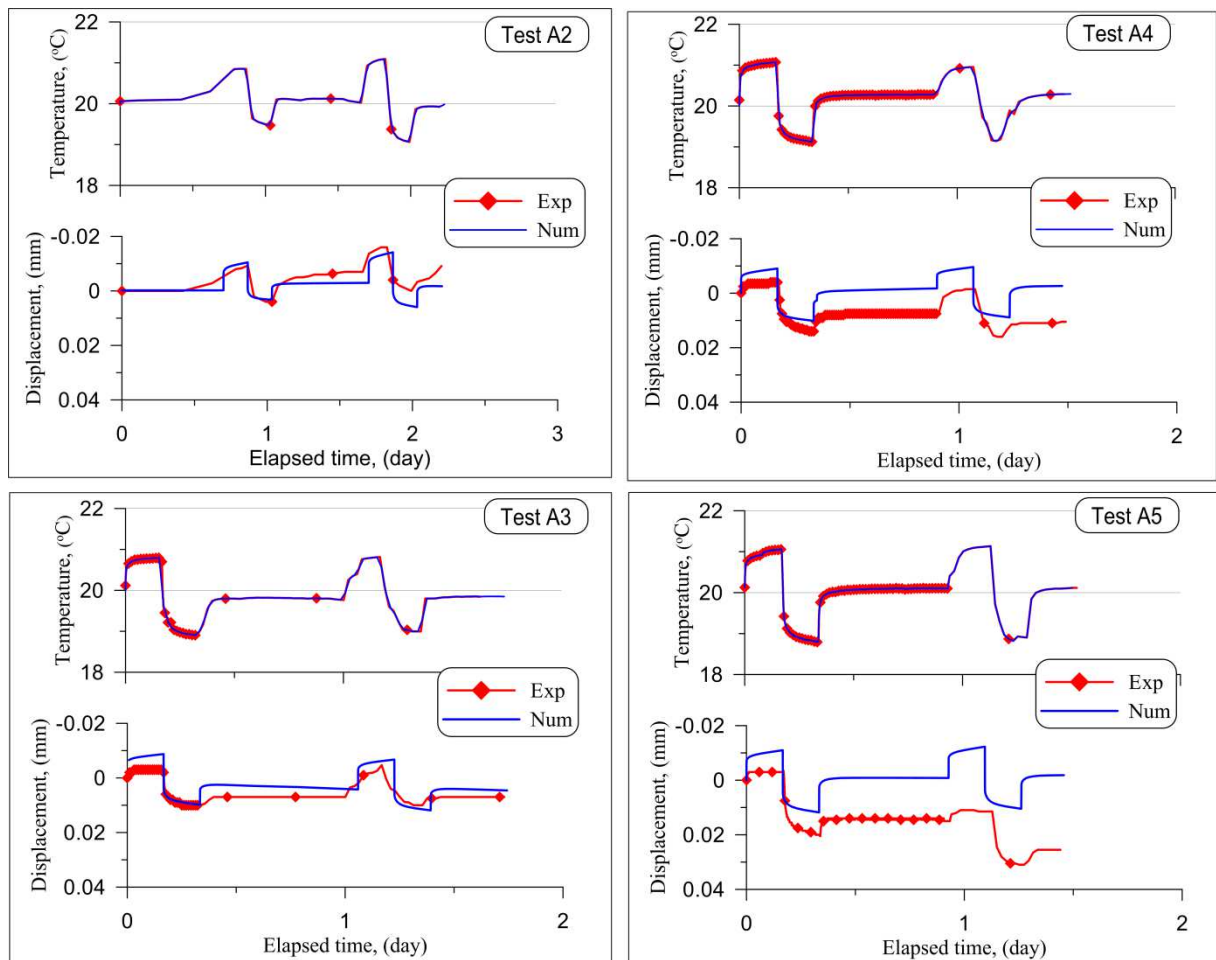


Fig. 7.5 Temperature and displacement of pile

Fig. 7.6 shows the pile head displacement versus temperature changes. It can be said that both numerical and experimental results show the same trend. As mentioned in the previous chapter, the slope of the experimental cyclic curve is smaller than the value corresponding to the free thermal expansion.

It can be seen that the numerical model under-predicts the irreversible settlement of the pile.

In the following parts, numerical simulations are used to analyze the stress-strain behavior of piles subjected to thermal cycles in order to gain a better understanding of the behavior of energy piles. This understanding will also benefit the design work of energy piles in practice.

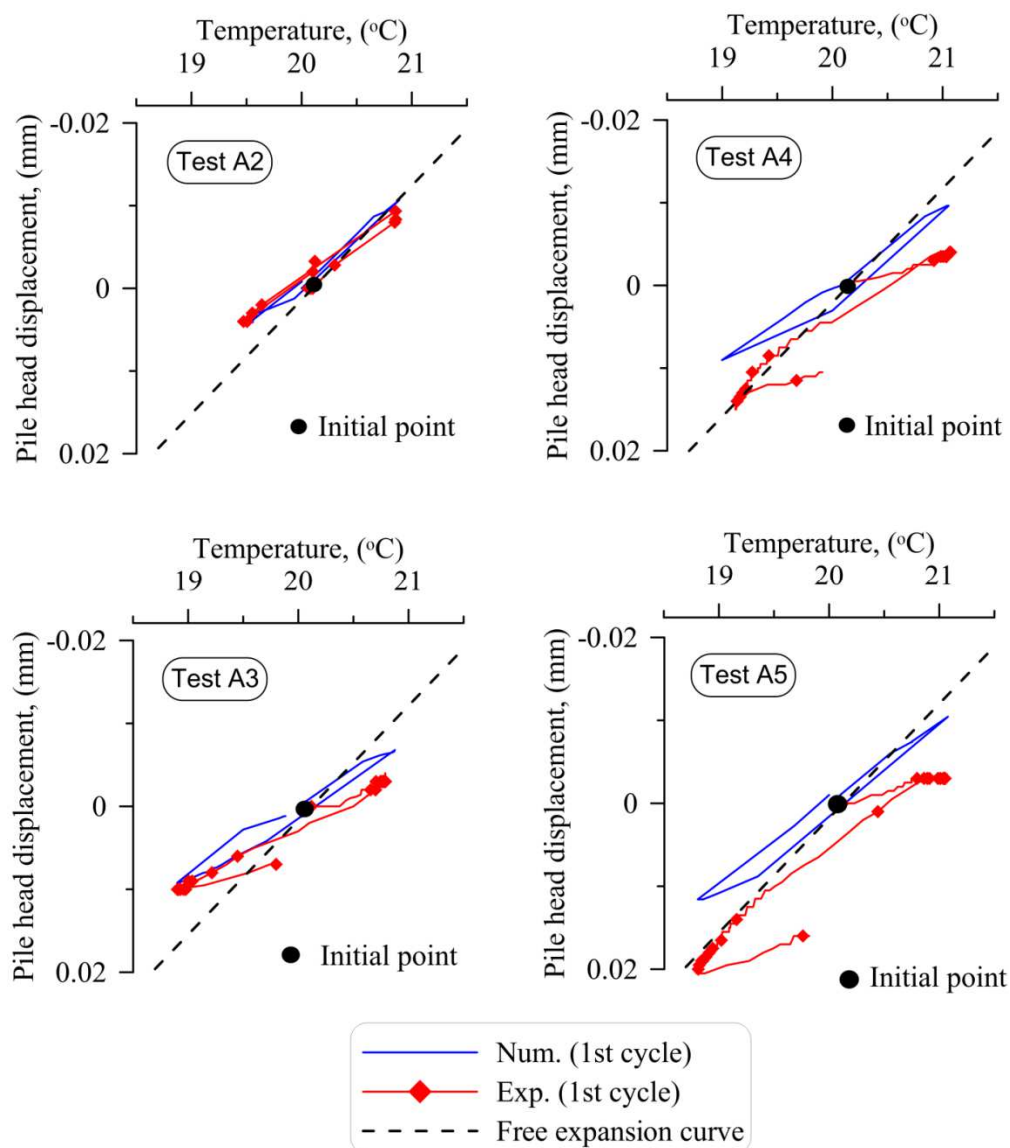


Fig. 7.6 Temperature and displacement of pile

Fig. 7.7 shows the distribution of vertical displacement along the pile length. The displayed profiles correspond to the end of the heating (H phase) and cooling (C phase) phases during the first thermal cycle, respectively. The largest vertical displacement is observed at the pile head, and the point of zero axial displacement (null point) is found near the pile toe.

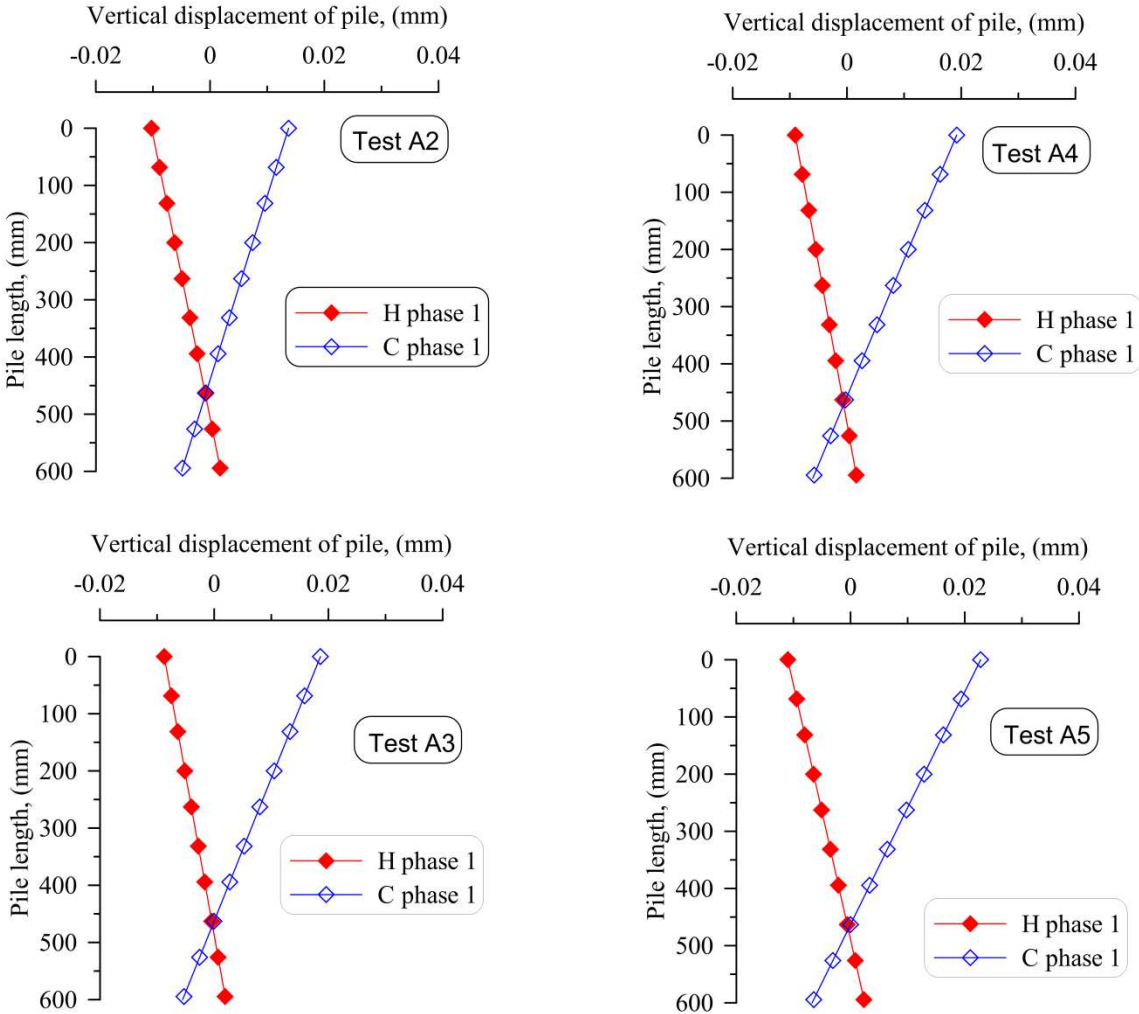


Fig. 7.7 Distributions of the vertical displacement of pile length at the end of heating and cooling phases (numerical modeling)

Numerical results in Fig. 7.8 show the effect of temperature changes on the total axial stress in the pile during the first thermal cycle. The axial stress profiles corresponding to the initial phase (mechanical loading), the heating phase (H phase) and the cooling phase (C phase) are compared. A larger loading stress obviously leads to larger axial stresses along the pile. In the initial phase (mechanical loading), the axial stress is larger at the pile head and decreases with depth for tests A3, A4 and A5. It is increased along the pile depth for test A2. In the thermal

phases, the axial stress increases slightly during heating and decreases during the subsequent cooling phase.

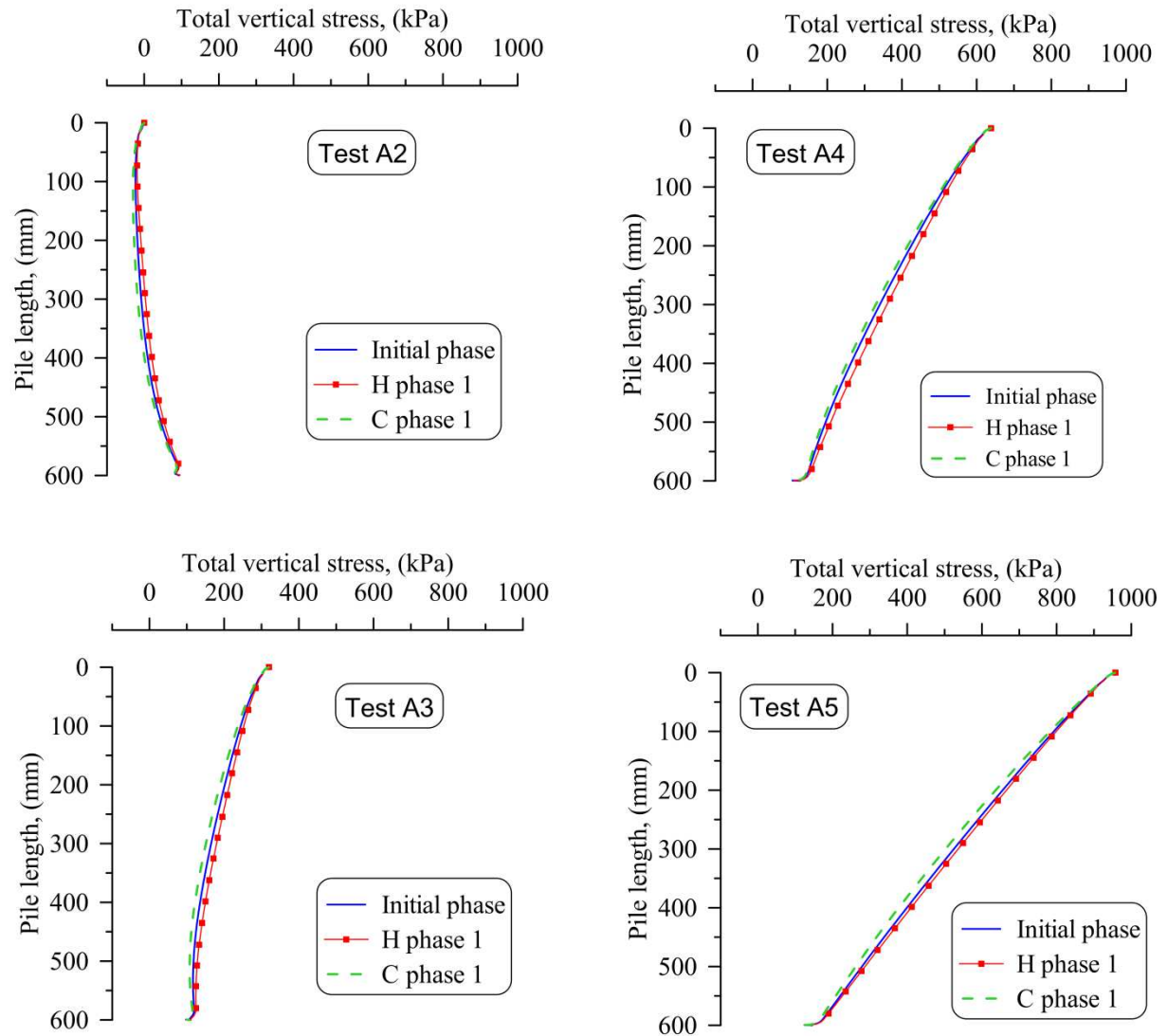


Fig. 7.8 Total axial stress profiles (numerical modeling)

### 7.3.1.2 Discussion

During the test A1, the pile head settlement predicted numerically is larger than the experimental one. The applied load for this test remains within the elastic range, with a load above which irreversible settlements are induced estimated to 300 N. Results in the Fig. 7.2 show that the slope of the unloading curve is almost parallel to the loading curve within the elastic range for both physical and numerical models. It is worth noting that the elastic properties adopted for the soil model come from a fitting process that is a compromise

between the slopes of the elastic parts and the predicted elastic limit. Indeed, choosing a larger elastic modulus would lead to predicted ultimate capacities that strongly underestimate the value observed experimentally. The discrepancies observed between numerical simulations and experimental data could certainly be reduced by adopting more sophisticated constitutive models, including non-linear elasticity and plastic hardening.

Regarding the cyclic behavior, it can be said that the displacement curve for the numerical pile model during the first two cycles is essentially reversible (see Fig. 7.6). Instead, the experimental pile shows irreversible settlement mostly occurring during the first cycles. This is clearly reflected by tests A4 and A5, while for tests A2 and A3, the displacements of the experimental pile are rather elastic during the first two cycles. This is simply due to the fact that the pile worked under small head loads for these two tests. As a result, the numerical and experimental displacement curves match together for these tests.

The analysis of the pile displacement shown in Fig. 7.7 indicates that heating causes an upward movement in the upper part of the pile and a downward movement in the lower one. Reversely, cooling induces a downward (respectively, an upward) movement in the upper (respectively, lower) part of pile. It is also observed that the null point, which corresponds to the equilibrium position where the displacement is zero during a thermal loading, is located close to the pile toe (at depth of 460 mm) while the free thermal expansion curve of the pile is obtained when the null point is hypothesized located at the pile toe. This explains why the slope of the experimental cycle curve is smaller than the one of the free thermal expansion curve. The results in Fig. 7.7 also show that the position of the null point is unlikely to change significantly with the applied head load.

The axial stress increased along the pile depth (Fig. 7.8, test A2) can be explained by the effect of residual stress from previous phases to the axial stress state of the subsequent tests. This can be also used to explain the displacement upward of pile head during the first thermal cycles of the test A2 (Fig. 6.34).

### 7.3.2 Modeling of full-scale energy piles: a case study

This section focuses on the modelling of the thermo-mechanical behavior of the full-scale experimental energy piles mentioned in chapter 3 and Chapter 4, where the thermal behavior of the piles has been investigated experimentally with a heating/cooling load cycle. Hereafter, the thermo-mechanical behavior of an energy pile is investigated numerically. An axisymmetric pile model is built with dimensions corresponding to the half of the actual full-scale pile. This work is done to support the design of an experimental program for two full-scale energy piles being prepared.

The geometry and boundary conditions of the pile are shown in the Fig. 7.9, where the pile-soil interaction is simulated by an interface element.

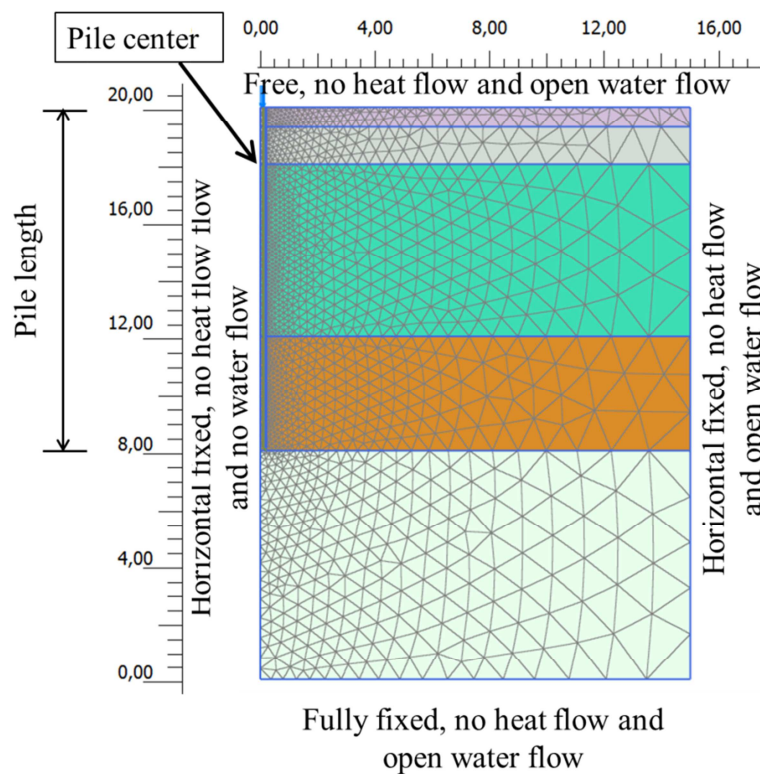


Fig. 7.9 Geometry and boundary conditions of a single energy pile

In a first stage, the pile bearing capacity is tested. In a second stage, head load and temperature are applied simultaneously to the pile to analyze its thermo-mechanical behavior. During this stage, the pile is heated and cooled by imposing a constant inflow/outflow heat rate on a cylindrical surface with a 0.32 m diameter and the pile length. It is worth noting that this diameter corresponds approximately to the radial distance of the fluid circulating pipes

from the pile axis. The constant heat flow rate  $q$  is derived from the field test data that was mentioned in the Chapter 3,  $q = 60 \text{ W/m}$ .

The soil parameters are summarized in the Chapter 3. The parameters of the pile are similar and shown in the table 7.3. The initial temperature of pile and surrounding soil is  $12.5 \text{ }^\circ\text{C}$ .

Two series of numerical simulations were conducted independently of each other to model the thermo-mechanical behavior of the two full-scale energy piles tested in the experimental area of ENPC. Tests corresponding to the pile number 1 are denoted with a  $P$ , while a  $Q$  is used to denote the tests corresponding to the pile number 2. The first pile is tested to investigate its thermo-mechanical behavior under thermal cycles. The second pile is tested to investigate the effects of temperature changes on the pile bearing capacity.

Table 7.3 Parameters of pile

Parameters	Pile
Dimensions: diameter x length (m x m)	0.42 x 12.0
Thermal conductivity $\lambda$ (W/(m.K))	1.5
Specific heat capacity $c$ (kJ/kg/K)	1.1
Density ( $\text{kg/m}^3$ )	2500.0
Initial temperature $T_0$ ( $^\circ\text{C}$ )	12.5

Table 7.4 Tests profile for pile number 1

	Test P1	Test P2	Test P3	Test P4
<b>Step 1</b>	Pile head load to 200 kN and keep constant	Pile head load to 400 kN and keep constant	Pile head load to 600 kN and keep constant	Pile head load to 800 kN and keep constant
<b>Step 2</b>	Imposed a thermal cycle: $1 \text{ }^\circ\text{C}$ to $27 \text{ }^\circ\text{C}$	Imposed a thermal cycle: $1 \text{ }^\circ\text{C}$ to $27 \text{ }^\circ\text{C}$	Imposed a thermal cycle: $1 \text{ }^\circ\text{C}$ to $27 \text{ }^\circ\text{C}$	Imposed a thermal cycle: $1 \text{ }^\circ\text{C}$ to $27 \text{ }^\circ\text{C}$
<b>Step 3</b>	Recovery to initial temperature of pile			
<b>Step 4</b>	Unloading	Unloading	Unloading	Unloading

For the first pile, five tests are performed with a constant pile head load of 200, 400, 600 and 800 kN, respectively. Under each constant head load, the pile is subjected to one thermal cycle with temperatures ranging from 1 °C to 27 °C. To do that, an inflow/outflow heat rate is imposed to the pile during 7 days. Afterwards, the pile temperature is allowed to recover naturally during 40 days to return to the initial temperature. After the thermal cycle, the pile temperature returns to the initial temperature and the pile is then mechanically unloaded (see Table 7.4).

The second pile is first loaded up to 600 kN (equivalent to 50% of its ultimate bearing capacity) by steps of 200 kN, then unloaded (test Q1). In the subsequent test (test Q2), the pile is firstly heated to 27 °C. The pile is then loaded up to 600 kN by steps of 200 kN and finally, unloaded. In test Q3, the pile is firstly cooled to 1 °C, and then loaded up to 600 kN by steps of 200 kN and finally, unloaded (see Table 7.5).

Table 7.5 Tests profile of pile number 2

Steps	Test Q1	Test Q2	Test Q3
<b>Step 1</b>	Pile head load to 200 kN and keep constant	Pile is heated to 27°C	Pile is cooled to 1°C
<b>Step 2</b>	Pile head load to 400 kN and keep constant	Pile head load to 200 kN and keep constant	Pile head load to 200 kN and keep constant
<b>Step 3</b>	Pile head load to 600 kN and keep constant	Pile head load to 400 kN and keep constant	Pile head load to 400 kN and keep constant
<b>Step 4</b>	Unloading	Pile head load to 600 kN and keep constant	Pile head load to 600 kN and keep constant
<b>Step 5</b>	-	Unloading	Unloading

### 7.3.2.1 Results

Results in Fig. 7.10 show that the pile head settlement lies within the range of elastic deformation when the head load is lower than 600 kN (60 tons). Furthermore, it can be observed that the ultimate bearing capacity of the pile is about 1050 kN. This value is estimated conventionally at the moment when the pile head settlement reaches 10% of its diameter. This value is close to the one obtained from the pressiometric method following Eurocode 7.

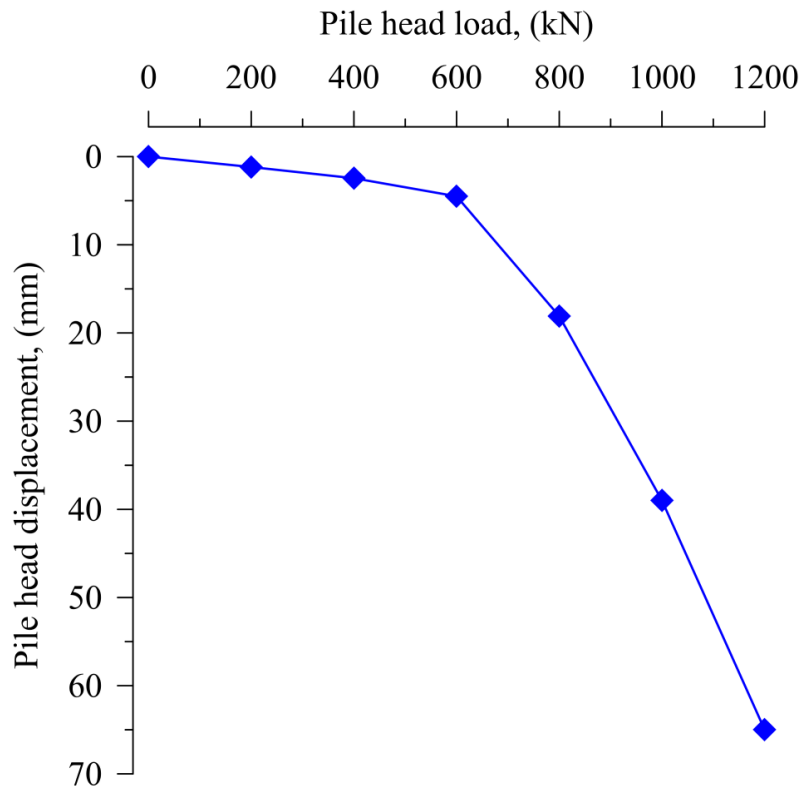


Fig. 7.10 Bearing capacity of pile

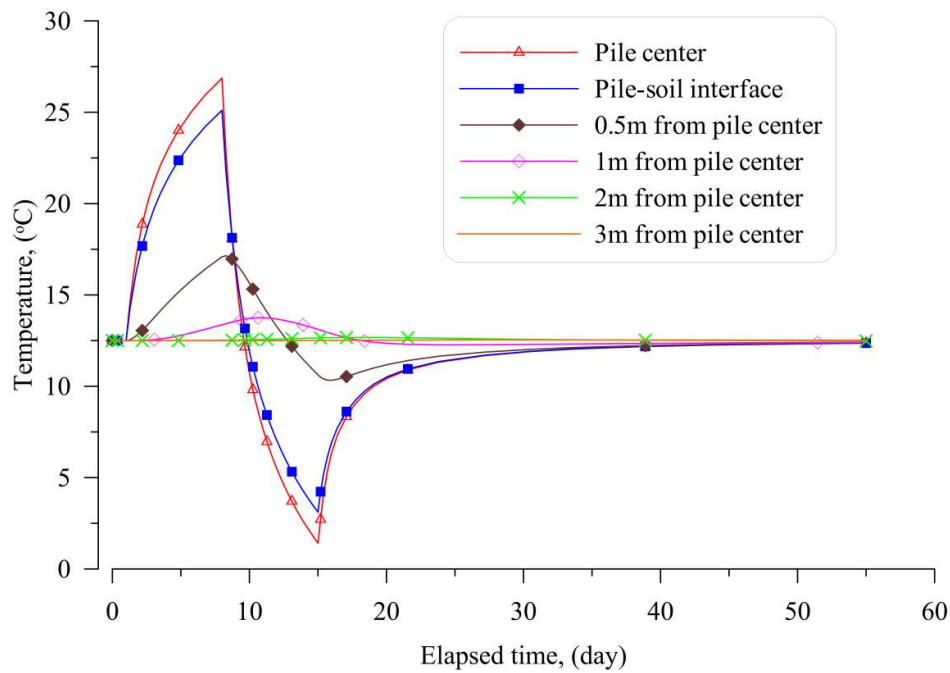


Figure 7.11 Temperature of pile and soil during a thermal cycle

For the first pile, the temperature of pile and surrounding soil during a thermal cycle is shown in Fig. 7.11. Temperature of pile increased to 27 °C after 7 days of heating, and decreased to 1 °C during the next 7 days of cooling. Temperature of soil also changed due to the effect of the thermal cycle, but in a less pronounced manner: the temperature at pile-soil interface reached 25 °C in heating phase and 3 °C in cooling phase, while the soil temperature at the distances of 2 and 3 m from the pile center is not affected by the thermal cycle.

The Fig. 7.12 shows temperature change and displacement of the pile ends during four tests (from P1 to P4). The temperature is measured at the pile center, and the displacements are measured at the pile head and toe. It is observed that thermal cycles induce an irreversible settlement of the pile, and that this irreversible settlement is larger for higher pile head loads. Actually, the irreversible settlement of pile after one thermal cycle is negligible when the pile head load is lower than or equal to 600 kN. Reversely, a significant irreversible settlement occurs when the load is 800 kN.

Fig. 7.13 shows the distribution of the vertical displacement along the pile length during thermal cycles. The figure shows the pile vertical displacement in the mechanical phase (initial phase), and after the heating and cooling phases, each subplot corresponding to a given load. The pile head moves upward in the heating phase and moves downward in the cooling phase, and vice versa for the pile toe as it moves downward in the heating phase and moves upward in the cooling phase. The null point is located in the lower part of the pile.

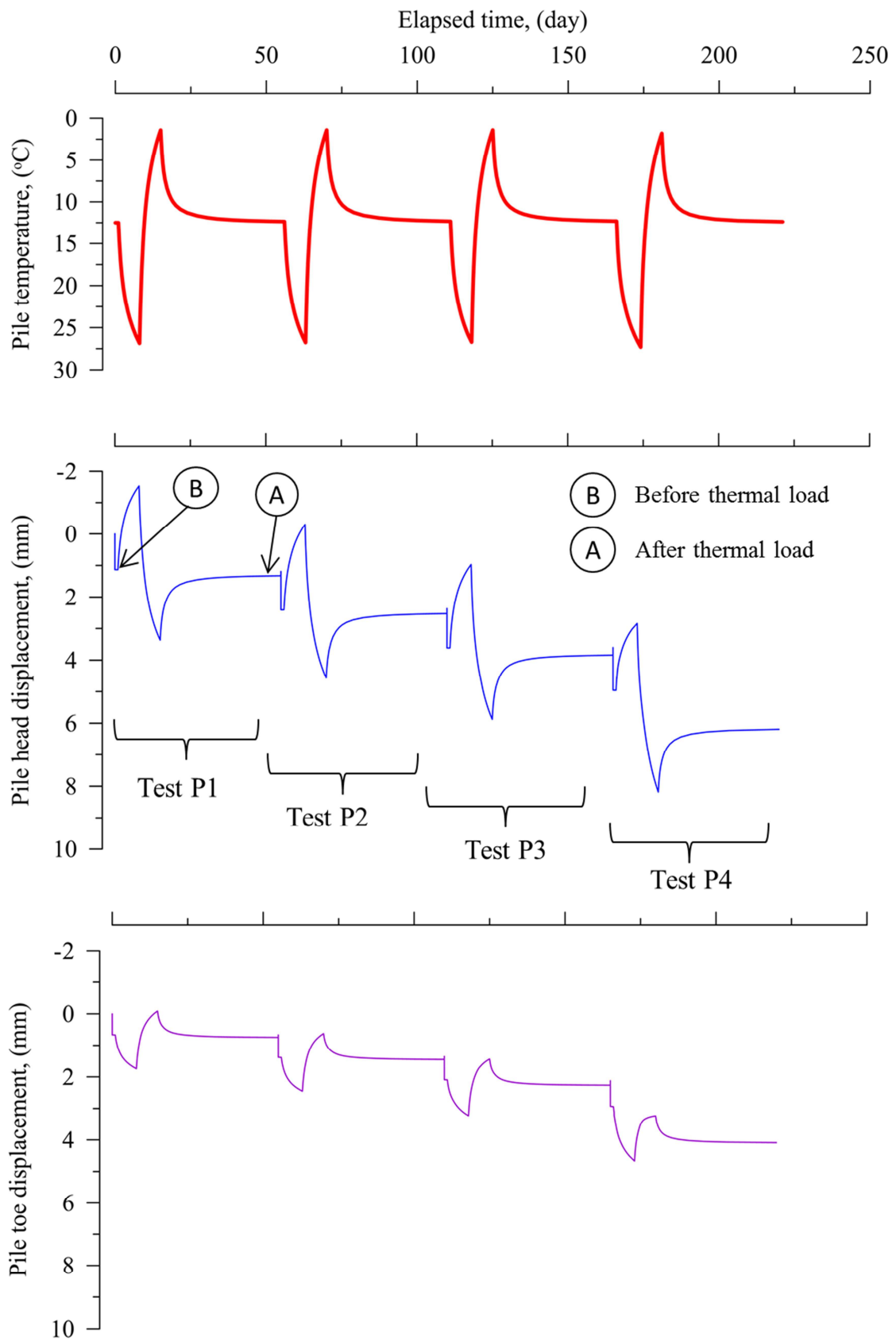


Figure 7.12 Pile head/toe displacement and pile temperature during the four tests P1 to P4

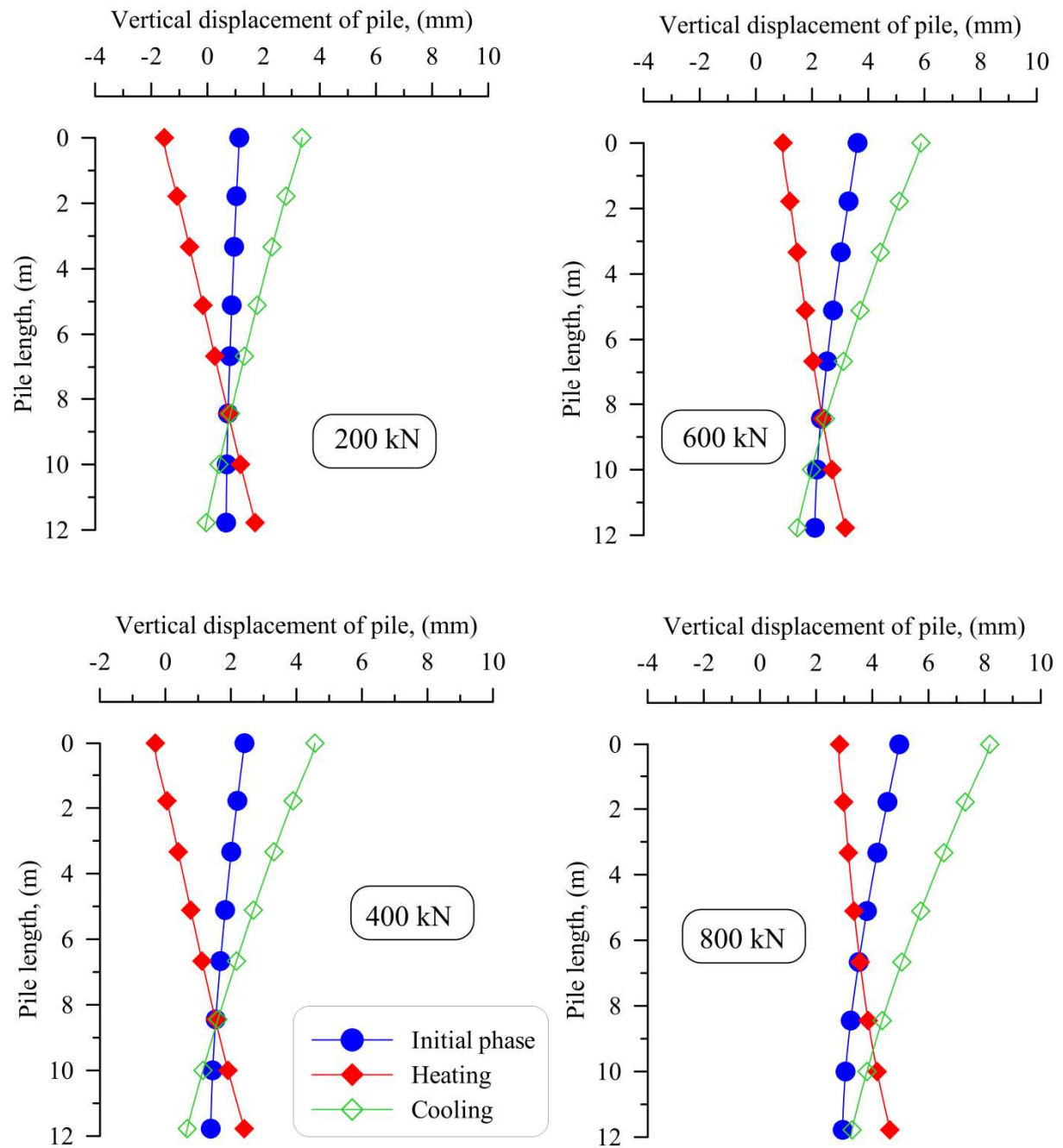


Figure 7.13 Vertical displacement of pile

The results in Fig. 7.14 show that, during a thermal cycle, the axial stress increases during the heating phase and decreases during the cooling phase. The axial stress distribution along the pile length is non-linear, and the axial stress change at the toe of pile is insignificant during the heating/cooling phase comparing with the mechanical phase. In addition, the greatest axial stress is observed near the location of null point.

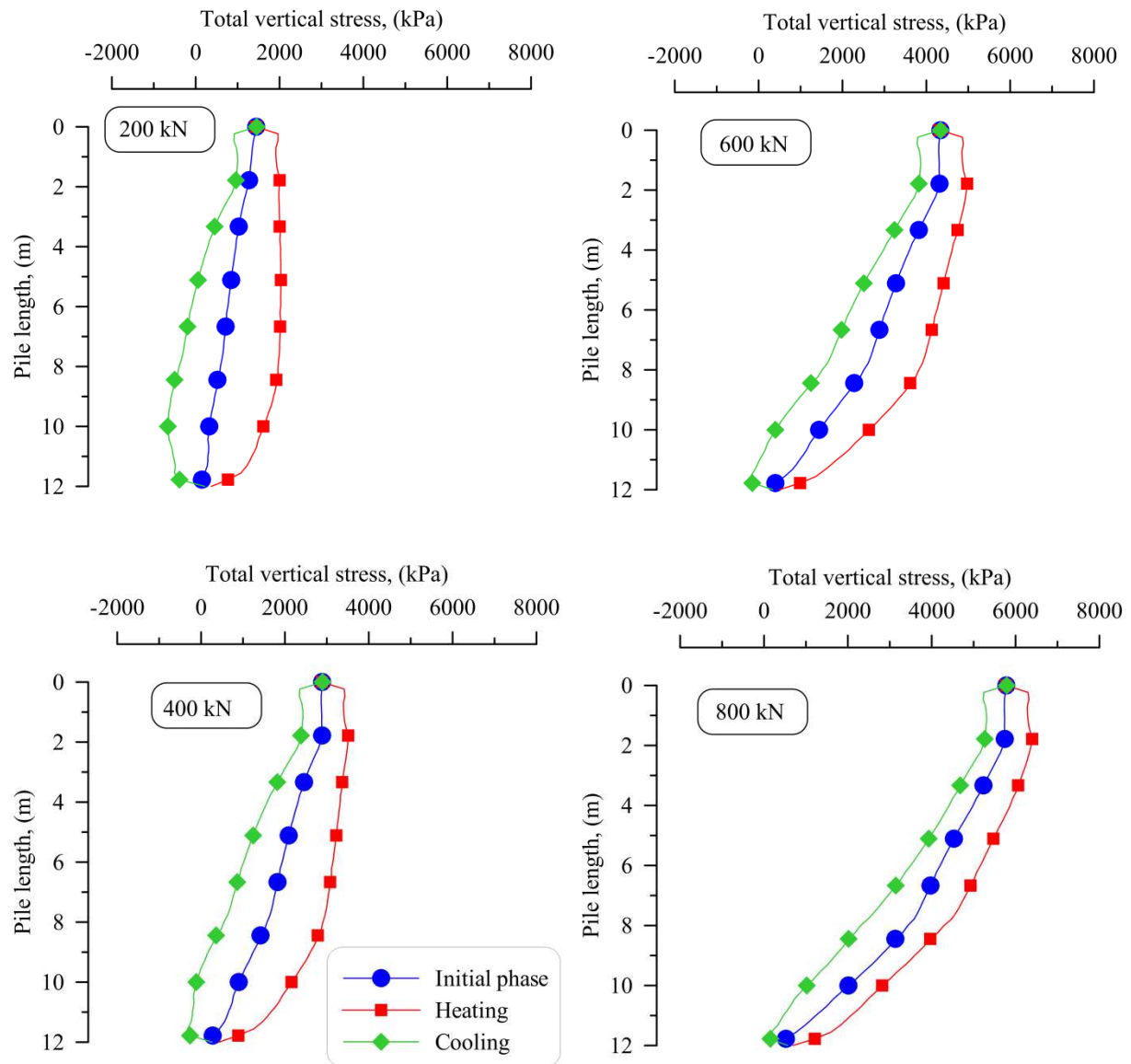


Figure 7.14 Total axial stress of pile

For the second pile, the pile head displacements during the initial phase, the heating and cooling phases are represented in Fig. 7.15. The effect of temperature on the pile head settlement curve is found negligible.

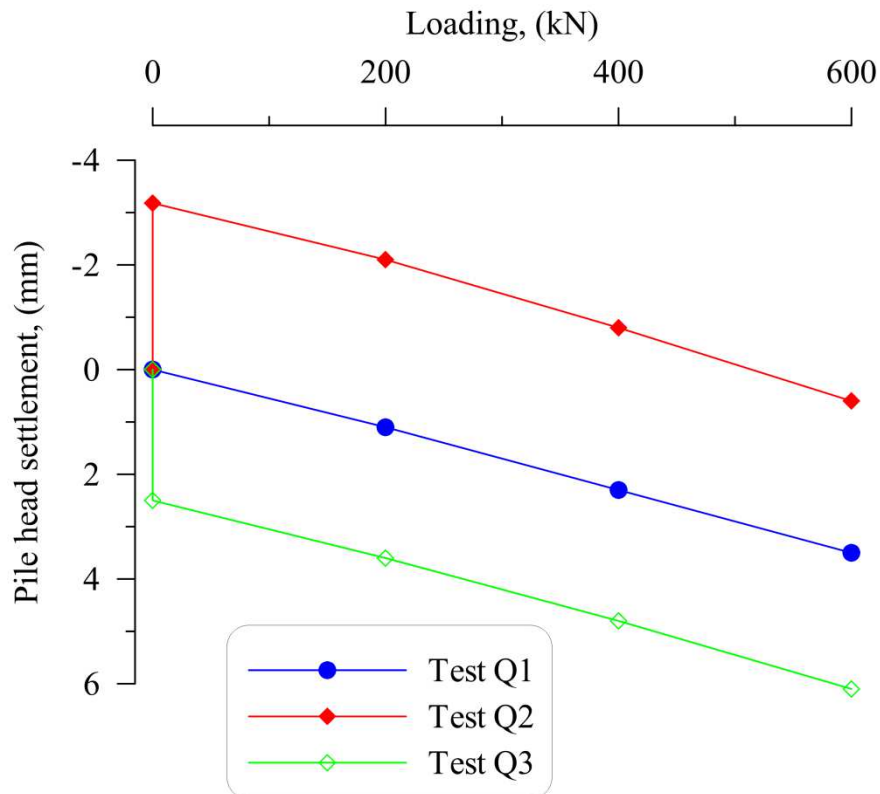


Figure 7.15 Displacement-pile head load curve (pile test 2)

### 7.3.2.2 Discussion

In the practice of pile design, the service load is estimated between 30 to 50% of the ultimate bearing capacity. This value usually lies within the range of elastic deformation of the pile. The results in the Fig. 7.10 show that a service load lower than or equal to 600 kN can be used.

Indeed, it can be seen that the pile behaves thermo-elastically when the pile head load is lower than or equal to 600 kN. The thermally induced irreversible settlement is negligible (Fig. 7.12). Under greater pile head load (head load of 800 kN), irreversible settlements during the thermal cycle becomes significant. This settlement is related to the degradation of the resistance at the soil-pile interface due to the thermal cycle. As showed in the Fig. 7.16, the plastic points on the pile-soil surface extend rapidly in the heating and cooling phase in comparing with the initial phase. In the mechanical phase, plastic points are mainly observed on the interface near the pile toe. In the heating phase, the pile is deformed towards the two pile ends (Fig. 7.13; 800 kN) and so the plastic points developed mainly on the interface towards the two pile ends. In addition, in the cooling phase, the deformation occurs predominantly in the upper half of the pile length in comparing with the mechanical phase, as

a consequence the plastic points developed strongly within this range. Meanwhile, the plastic points in the previous phases are negligible (test P1, P2 and P3).

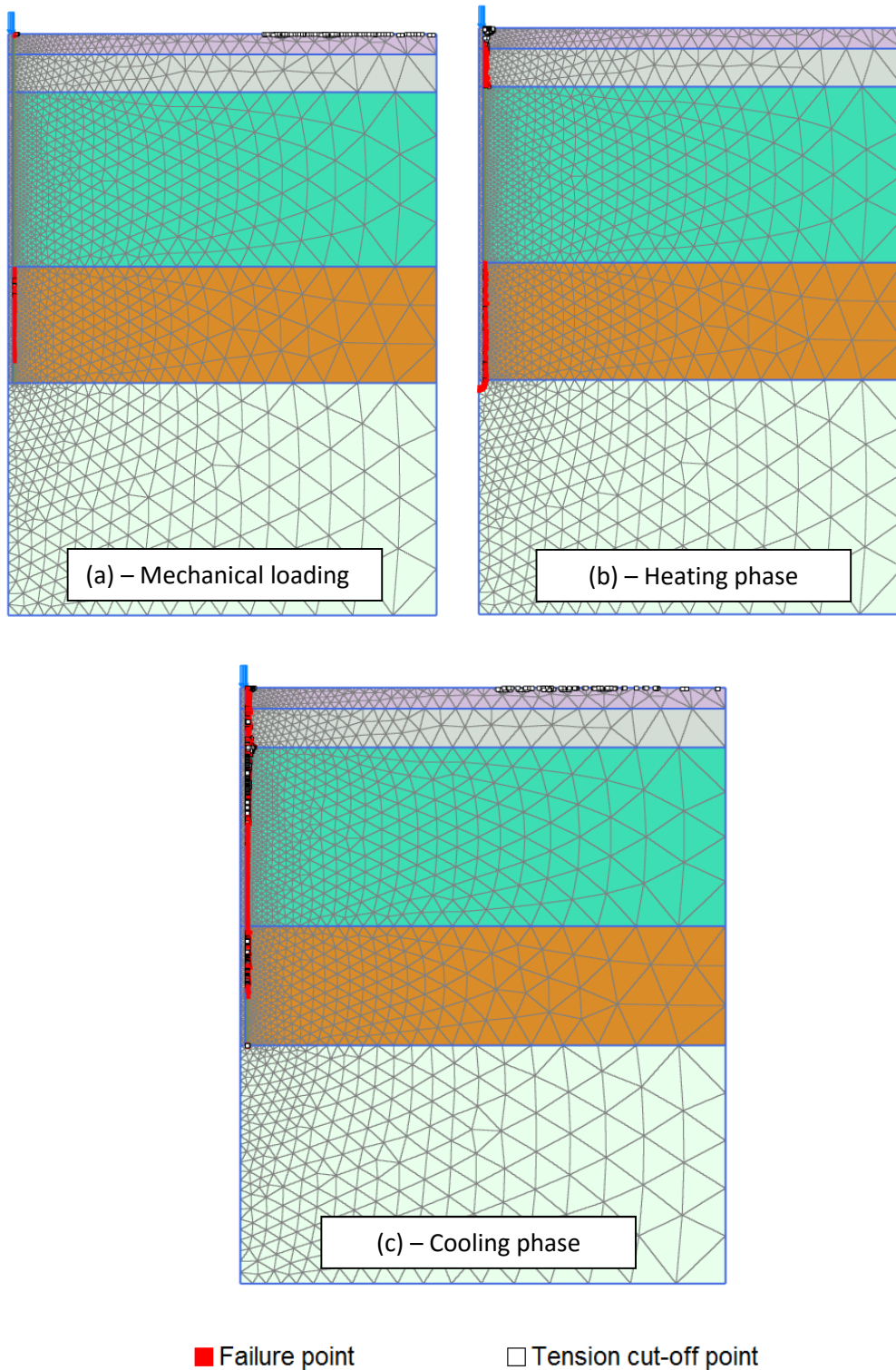


Fig. 7.16 Plastic points on the pile-soil surface (test P4)

The thermo-elastic behavior of the pile is also observable with the distribution of the vertical displacement. It was observed that the null point remains almost unchanged when the pile

works under a small head load ( $\leq 600$  kN; Fig. 7.13). Under a greater head load (800 kN), the displacement of the pile toe is not fully recovered in the cooling phase and results in irreversible settlement of pile toe. Therefore, the null point moves downward: this is consistent with the case of a floating pile.

During the thermal cycle, a greater axial stress change along the pile is observed under a smaller pile head load. Axial stress increases/decreases mainly in the middle of the pile because the bearing capacity of the pile is mainly related to the pile shaft resistance (Fig. 7.14). In addition, the change in axial stress during heating-cooling phases decreases as the pile head load increases. This can be explained by the fact that, as the pile head load increases, the ability of the pile to transmit load to the surrounding soil decreases; this can be related to the degradation of the resistance at the pile-soil surface. Similar results can be found in the studies of Di Donna & Laloui (2015); Olgun *et al.*, (2015) and Vieira & Maranhã (2016);

#### **7.4 Conclusion**

Small-scale energy pile in saturated clay has been examined using two-dimensional finite element method with Plaxis software. This numerical tool allows a fully coupled thermo-hydro-mechanical analysis of energy piles.

In a first stage, the mechanical behavior of experiment small-scale pile is modeled numerically. In a second stage, two thermal cycles are imposed to the pile. These mechanical and thermal loading is similar to the one applied to the experimental pile. The temperature, displacement and also axial stress of the pile are obtained and validated using the experimental data.

The pile head displacement in the numerical model behaves thermo-elastically and the irreversible settlement in the numerical model is smaller than in the experimental model. This is due to the effect of the material model adopted in the modeling. However, the slope of displacement versus temperature change curve from the numerical model is parallel to the experimental curve.

In the second section, this numerical method is used to simulate the thermo-mechanical behavior of full-scale energy piles. Two energy piles are studied. The mechanical and thermal parameters of the full-scale piles are used in the model.

The results indicate that during thermal loading the pile behaves thermo-elastically when the pile works under small head loads. Accordingly, the pile head displacement can be recovered after a thermal cycle. In addition, axial stress of pile increases during a heating phase and decreases during a cooling phase. The maximum/minimum increment of axial stress is observed near the position of null point on the pile length. The same observation can be found in the previous experimental and numerical studies on energy piles.

## GENERAL CONCLUSIONS AND PERSPECTIVES

### Conclusions

In the present work, the thermal and thermo-mechanical behavior of energy piles has been investigated by various approaches: laboratory measurement on small soil samples, physical modeling on small-scale pile, experiments on real-scale pile, and analytical/numerical calculations. The main conclusions are summarized below.

The water retention curve and thermal conductivity of intact silty soil can be obtained by simultaneous measurement of moisture content, suction and thermal conductivity on a single soil sample. During wetting/drying of loess, a unique relationship between the thermal conductivity and the moisture content is observed while the relationship between the suction and the thermal conductivity is characterized by a clear hysteresis loop.

Thermal tests performed on full-scale experimental energy pile show that, within the cryostat used, three weeks are required to heat the pile from its initial temperature (12\_°C) to 32\_°C. This result is important to better define the future experimental program to investigate the behavior of these experimental piles under coupled thermo-mechanical loadings.

An analytical solution is proposed to investigate the heat transfer from the energy pile to the surrounding soil during heating. This solution is based on the approach of Laplace transform and the contour integral methods. The proposed solution is then validated by the finite element method and by the results taken from the full-scale experiments.

The long-term behavior of energy pile is investigated by performing experiments with small-scale pile under thermo-mechanical loading. Tests were performed with dry sand and saturated clay. The most important conclusions of this part can be summarized below:

- Irreversible settlement of the pile after thermal cycles is observed.
- This settlement is the most important after the first cycle and become smaller with the subsequent cycles.
- A higher irreversible settlement is observed at higher pile head load.

- Irreversible settlement of pile tends to stabilize after a high number of thermal cycles.
- The relationship between the irreversible settlement and the number of cycles can be predicted by an asymptotic equation.
- Axial force on the pile length increases progressively with the thermal cycles.

The experimental work with small-scale pile is completed with numerical modeling using the finite element method. The results of numerical modeling are relatively consistent with the experimental results. That allows better interpreting the experimental results. Afterward, the numerical simulation is also performed to predict the thermo-mechanical behavior of full-scale energy pile. These results will be used as scoping calculation for future experimental experiments that will be performed on these piles.

### **Perspectives**

Various futures studies can be expected to investigate the thermal and thermo-mechanical behavior of energy geostructures.

First, heat exchange between different elements (heat transfer fluid, geostructure, and surrounding soil) should be investigated in more details. Actually, various spatial and temporal scales should be considered. That will allow optimizing the design of the energy geostructure and also ensuring its long-term performance.

Secondly, the main findings on the long-term behavior of energy pile under thermo-mechanical loading obtained from experiments on small-scale tests need to be confirmed by full-scale tests. The preliminary thermal tests and the numerical simulations performed in the present study will be used in the design of the test program including thermo-mechanical loadings on the two experimental energy piles at the site of ENPC.

Finally, similar studies can be applied to other types of energy geostructure, such as diaphragm wall or tunnel.

## REFERENCES

- Abramowitz, M. & Stegun, I.A., 1972. *Handbook of Mathematical Functions with Formulas, Graphs and mathematical Tables* 10th ed., National Bureau of Standards Applied Mathematics Series. 55.
- Abuel-Naga, H.M. et al., 2005. Thermal consolidation of soft Bangkok clay. *International journal of Lowland Technology*, 17(1), pp.13–21.
- Abuel-Naga, H.M. et al., 2007. Volume change behaviour of saturated clays under drained heating conditions: experimental results and constitutive modeling. *Canadian Geotechnical Journal*, 44(8), pp.942–956.
- Adam, D. & Markiewicz, R., 2009. Energy from earth-coupled structures, foundations, tunnels and sewers. *Géotechnique*, 59(3), pp.229–236.
- AFNOR, 1999. Essai statique de pieu sous un effort axial. *NF P 94-150*. , pp.1–28.
- AHRI, 1998. Standard for Ground Source Closed-loop Heat Pumps, Arlington,VA22201, USA.
- Akrouch, G.A. & et al, 2013. Energy Geostructures in Cooling Dominated. *Energy Geostructures: Innovation in Underground Engineering*. Book chapter, pp. 175–192. Doi: 10.1002/9781118761809.ch9
- Akrouch, G.A. et al., 2014. Thermo-mechanical behavior of energy piles in high plasticity clays. *Acta Geotechnica*, 9(3), pp.399–412.
- Akrouch, G.A. et al., 2015. An experimental, analytical and numerical study on the thermal efficiency of energy piles in unsaturated soils. *Computers and Geotechnics*, 71, pp.207–220.
- Amatya, B.L. et al., 2012. Thermo-mechanical behaviour of energy piles. *Géotechnique*, 62(6), pp.503–519.
- Antoine, P. et al., 2003. The loess and coversands of northern France and southern England. *Journal of Quaternary Science*, 18(3–4), pp.309–318.
- Bai, B. & Su, Z., 2012. Thermal Responses of Saturated Silty Clay During Repeated Heating - Cooling Processes. *Transport in porous media*, 93(1), pp.1–11.
- Baldi, G. et al., 1988. Thermal volume changes of the mineral-water system in low porosity clay soils. *Canadian Geotechnical Journal*, 25(4), pp.807–825.
- Bandos, T. V. et al., 2009. Finite line-source model for borehole heat exchangers: effect of vertical temperature variations. *Geothermics*, 38(2), pp.263–270.
- Bauer, D. et al., 2011. Transient 3D analysis of borehole heat exchanger modeling. *Geothermics*, 40(4), pp.250-260.
- Bidarmaghz, A. et al., 2016. Geothermal energy in loess. *Environmental Geotechnics*, 3(4),

pp.225-236.

- Bodas Freitas, I.M. et al., 2012. The Kyoto mechanisms and the diffusion of renewable energy technologies in the BRICS. *Energy Policy*, 42, pp.118–128.
- Boennec, O., 2009. Piling on the energy. *Geodrilling international*, 150, pp.8–25.
- Boukelia et al., 2017. Effect of temperautre and initial state on variation of thermal parameters of fine compacted soils. *European Journal of Environmental and Civil Engineering*, Doi: 10.1080/19648189.2017.1344144
- Bourne-Webb, P.J. et al., 2009. Energy pile test at Lambeth College, London: geotechnical and thermodynamic aspects of pile response to heat cycles. *Géotechnique*, 59(3), pp.237–248.
- Bozis, D. et al., 2011. On the evaluation of design parameters effects on the heat transfer efficiency of energy piles. *Energy and Buildings*, 43(4), pp.1020–1029.
- Brandl, H., 1998. Energy piles for heating and cooling of buildings. In *7th International confrence exhibition Piling and deep foundations*. Vienna, pp. 341–346.
- Brandl, H., 2006. Energy foundations and other thermo-active ground structures. *Géotechnique*, 56(2), pp.81–122.
- Burghignoli, A. et al., 2000. A laboratory study on the thermomechanical behaviour of clayey soils. *Canadian Geotechnical Journal*, 37(4), pp.764–780.
- Campanella, R.G. & Mitchell, J.K., 1968. Influence of Temperature Variations on Soil Behavior. *Journal of the Soil Mechanics and Foundation Division, ASCE*, 94(3), pp.609–734.
- Carslaw, H.S. & Jaeger, J.C., 1940. Some two-dimensional problems in conduction of heat with circular symmetry. *Proceedings of the London Mathematical Society*. pp. 361–388. Doi: 10.1112/S2-46.1.361.
- Carslaw, H.S. & Jaeger, J.C., 1947. *Conduction of Heat in Solids* 1st ed., Oxford Science Publications, Clarendon Press.
- Carslaw, H.S. & Jaeger, J.C., 1959. *Conduction of Heat in Solids* 2nd ed., Oxford Science Publications.
- Cekerevac, C. & Laloui, L., 2004. Experimental study of thermal effects on the mechanical behaviour of a clay. *International Journal for Numerical and Analytical Methods in Geomechanics*, 28(3), pp.209–228.
- Cekerevac, C. & Laloui, L., 2010. Experimental analysis of the cyclic behaviour of kaolin at high temperature. *Géotechnique*, 60(8), pp.651–655.
- Choi, J.C. et al., 2011. Numerical simulation of vertical ground heat exchangers: Intermittent operation in unsaturated soil conditions. *Computers and Geotechnics*, 38(8), pp.949–958.
- Cokca, E. et al., 2004. Effects of compaction moisture content on the shear strength of an unsaturated clay. *Geotechnical and Geological Engineering*, 22(2), pp.285–297.
- Coyle, H.M. & Reese, L.C., 1966. Load Transfer for Axially Loaded Piles in Clay. *Journal of*

- the Soil Mechanics and Foundations Division*, 92(2), pp.1–26.
- Cui, Y.J. et al., 2000. A thermomechanical model for saturated clays. *Canadian Geotechnical Journal*, 37, pp.607–620.
- Cui, Y. et al., 2004. A geological and geotechnical characterisation of the loess of Northern France. *Skempton Memorial Conference*, 2004, pp.417-428.
- Curtis, R. et al., 2005. Ground Source Heat Pumps - Geothermal Energy for Anyone , Anywhere : Current Worldwide Activity. *Proceeding World Geothermal Congress 2005*. Antalya, Turkey, pp. 24–29.
- De Moel M. et al., 2010. Technological advances and applications of geothermal energy pile foundation and their feasibility in Australia. *Renewable and Sustainable Energy Reviews*, 14(9), pp.2683-2696.
- Delage, P. et al., 2005. Geotechnical problems related with loess deposit in Northern France. *Proceedings of International Conference on Problematic Soils (Famagusta, North Cyprus)*, pp.517-540.
- Diersch, H.-J.G. et al., 2011. Finite element modeling of borehole heat exchanger systems. *Computers & Geosciences*, 37(8), pp.1136–1147.
- Di Donna, A. & Laloui, L., 2015. Numerical analysis of the geotechnical behaviour of energy piles. *International Journal for Numerical and Analytical Methods in Geomechanics*, 39(8), pp.861–888.
- Di Donna, A. et al., 2016. Experimental investigations of the soil – concrete interface : physical mechanisms , cyclic mobilization , and behaviour at different temperatures. *Canadian Geotechnical Journal*, 53(4), pp.659–672.
- Di Donna, A. et al., 2016. Numerical study of the response of a group of energy piles under different combinations of thermo-mechanical loads. *Computers and Geotechnics*, 72(2016), pp.126–142.
- Dong, Y. et al., 2015. Critical review of thermal conductivity models for unsaturated soils. *Geotechnical and Geological Engineering*, 33(2), pp.207-221.
- Duong, T.V. et al., 2013. Development of a large-scale infiltration column for studying the hydraulic conductivity of unsaturated fouled ballast. *Geotechnical Testing Journal*, 36(1), pp.54-63.
- Eskilson, P., 1987. Thermal Analysis of Heat Extraction Boreholes. *Doctoral Dissertation, University of Lund, Department of mathematical Physics, Lund, Sweden*.
- Farouki, O.T., 1986. *Thermal properties of soils*, Trans Tech Publications.
- Fityus, S., 2003. Behaviour of a model footing on expansive clay. *Proceedings of the 2nd Asian Unsaturated Soils Conference*. Osaka, pp. 181–186.
- Florides, G. & Kalogirou, S., 2005. Annual ground temperature measurements at various depths. *The 8th REHVA World Congress*. Clima, Lausanne, Switzerland.
- Fondasol, 2010. *Etude d'avant projet geotechnique: Rapport d'etude géotechnique IPE 10 00221 Mission G2*,

- Franzius, J.N. & Pralle, N., 2011. Turning segmental tunnels into sources of renewable energy. *Proceedings of the ICE - Civil Engineering*, 164(1), pp.35–40.
- Fromentin, A. et al., 1998. *Pieux échangeurs – QN EPFL Etude préliminaire de faisabilité technique et économique*,
- Fuentes, R. et al., 2016. Effect of temperature induced excess porewater pressures on the shaft bearing capacity of geothermal piles. *Geomechanics for Energy and the Environment*. 8 (2016), pp.30-37
- Ghasemi-Fare, O. & Basu, P., 2013. A practical heat transfer model for geothermal piles. *Energy and Buildings*, 66 (2013), pp.470–479.
- Graham, J. et al., 2001. Modified Cam-Clay modelling of temperature effects in clays. *Canadian Geotechnical Journal*, 38(3), pp.608–621.
- Grosch, J.J. & Reese, L.G., 1980. Field tests of small-scale pile segments in a soft clay deposit under repeated axial loading. *Offshore Technology Conference, 5-8 May, Houston, Texas*. Stockholm, pp. 211–214.
- GSHP Association, 2012. Thermal Pile Design , Installation & Materials Standards, *Ground source Heat Pump Association National Energy Centre*.
- Guan, X. et al., 2009. Variability of soil moisture and its relationship with surface albedo and soil thermal parameters over the Loess Plateau. *Advances in Atmospheric Sciences*, 26(4), pp.692-700.
- Haxaire, A. et al., 2009. Fully coupled thermo-hydro-mechanical analysis for unsaturated soils in Plaxis.
- He, M.M. & Lam, H.N., 2006. Study of geothermal seasonal cooling storage system with energy piles. *Proceedings of the EcoStock conference, Richard Stockton College; Atlantic city, NJ, USA, New Jersey*.
- Hicher, P.Y., 1974. *Etude des propriétés mécaniques des argiles à l'aide d'essai triaxiaux, influence de la vitesse et de la température*, Paris.
- Hong, P.Y. et al., 2015. A two-surface thermomechanical model for saturated clays. *International Journal for Numerical and Analytical Methods in Geomechanics*. 40 (7), pp.1059-1080
- Hueckel, T. & Baldi, G., 1990. Thermoplasticity of Saturated Clays: Experimental Constitutive Study. *Journal of Geotechnical Engineering*, 116(12), pp.1778–1796.
- Hueckel, T. & Pellegrini, R., 1992. Effective Stress and Water-Pressure in Saturated Clays during Heating-Cooling Cycles. *Canadian Geotechnical Journal*, 29(6), pp.1095–1102.
- Hueckel, T. et al., 2009. Explaining thermal failure in saturated clays. *Géotechniqueotechnique*, 59(3), pp.197–212.
- Inalli, M. & Esen, H., 2005. Seasonal cooling performance of a ground-coupled heat pump system in a hot and arid climate. *Renewable Energy*, 30(9), pp.1411–1424.
- Jaeger, J.G., 1944. Some problems involving line sources in conduction of heat. *The London, Edinburgh, and Dublin Philosophical Magazine and Journal of Science*, 35(242),

pp.169–179.

- Jeong, S. et al., 2014. Thermally induced mechanical response of energy piles in axially loaded pile groups. *Applied Thermal Engineering*, 71(1), pp.608–615.
- Johansen, O. 1975. Thermal conductivity of soils. *Ph.D. thesis*, Trondheim, Norway. (CRREL Draft Translation 637, 1977). ADA 044002.
- Kalantidou, A. et al., 2012. Preliminary study on the mechanical behaviour of heat exchanger pile in physical model. *Géotechnique*, 62(11), pp.1047–1051.
- Karam, J. et al., 2009. Experimental study on the Cyclic Resistance of A Natural Loess from Northern France. *Soils and Foundations*, 49(3), pp. 421-429.
- Knellwolf, C. et al., 2011. Geotechnical Analysis of Heat Exchanger Piles. *Journal of Geotechnical and Geoenvironmental Engineering*. ASCE, 137(10), pp.890–902.
- Laloui, L. et al., 2003. Comportement d'un pieu bi-fonction, fondation et échangeur de chaleur. *Canadian Geotechnical Journal*, 40, pp.388–402.
- Laloui, L. et al., 2006. Experimental and numerical investigations of the behaviour of a heat exchanger pile. *International Journal for Numerical and Analytical Methods in Geomechanics*, 30(8), pp.763–781.
- Laloui, L., 2011. In Situ Testing of a Heat Exchanger Pile. *Geo-Frontiers 2011 - Advances in Geotechnical Engineering*. ASCE, pp.410–419.
- Laloui, L. et al., 2014. Issues involved with thermoactive geotechnical systems : characterization of thermomechanical soil behavior and soil-structure interface behavior. *DFI-The journal of the Deep Foundation Institute*, 8(2), pp.108–120.
- Lamarche, L. & Beauchamp, B., 2007. New solutions for the short-time analysis of geothermal vertical boreholes. *International Journal of Heat and Mass Transfer*, 50(7–8), pp.1408–1419.
- Li, M. & Lai, A.C.K., 2012a. New temperature response functions (G functions) for pile and borehole ground heat exchangers based on composite-medium line-source theory. *Energy*, 38(1), pp.255–263.
- Li, M. & Lai, A.C.K., 2012b. Heat-source solutions to heat conduction in anisotropic media with application to pile and borehole ground heat exchangers. *Applied Energy*, 96, pp.451–458.
- Loveridge F., 2012. The thermal Performance of foundation Piles used as heat exchangers in Ground energy systems. Ph.D. thesis, University of Southampton, England.
- Loveridge, F., Powrie, W., 2013a. Pile heat exchangers : thermal behaviour and interactions. *Journal of Geotechnical Engineering* 166(2), pp.178-196.
- Loveridge, F. & Powrie, W., 2013b. Temperature response functions ( G -functions ) for single pile heat exchangers. *Energy*, 57, pp.554–564.
- Lu, N. & Dong, Y. 2013. Closed-form equation for thermal conductivity of unsaturated soils at room temperature. *Journal of Geotechnical and Geoenvironmental Engineering*,

ASCE 141, No. 6, 04015016.

- Man, Y. et al., 2009. Study on hybrid ground-coupled heat pump system for air-conditioning in hot-weather areas like Hong Kong. *Applied Energy*, 87(9), pp.2826–2833.
- Man, Y. et al., 2010. A new model and analytical solutions for borehole and pile ground heat exchangers. *International Journal of Heat and Mass Transfer*, 53(13–14), pp.2593–2601.
- Man, Y. et al., 2011. Feasibility study on novel hybrid ground coupled heat pump system with nocturnal cooling radiator for cooling load dominated buildings. *Applied Energy*, 88(11), pp.4160–4171.
- Mattsson, N. et al., 2008. Advanced compact device for the in situ determination of geothermal characteristics of soils. *Energy and Buildings*, 40(7), pp.1344–1352.
- Mayne, P.W. & Kulhawy, F.H., 1982. K<sub>0</sub> - OCR Relationships in Soil. *Journal of the Geotechnical Engineering Division*, 108(6), pp.851–872.
- Mccartney, J.S. & Murphy, K.D., 2012. Strain Distributions in Full-Scale Energy Foundations ( DFI Young Professor Paper Competition 2012 ). *DFI Journal: The Journal of the Deep Foundations Institute*, 6(2), pp.26–38.
- Mimouni, T. et al., 2013. Heat Exchanger Anchors for Thermo-active Tunnels. *EPFL\_Report-21453\_1417*, 70 pages, Ecole Polytechnique Fédérale de Lausanne, Switzerland
- Mimouni, T. & Laloui, L., 2014. Towards a secure basis for the design of geothermal piles. *Acta Geotechnica*, 9(3), pp.355–366.
- Modaressi, H. & Laloui, L., 1997. A Thermo-Viscoplastic Constitutive Model for Clays. *Numerical and Analytical methods in Geotechnics*, 21(5), pp.313–335.
- Muñoz-Castelblanco, J. et al., 2011. Some aspects of the compression and collapse behaviour of an unsaturated natural loess. *Géotechnique Letters*, 1(2), pp.17-22.
- Muñoz-Castelblanco, J. et al., 2012a. The water retention properties of a natural unsaturated loess from northern France. *Géotechnique*, 62(2), pp.95-106.
- Muñoz-Castelblanco, J. et al., 2012b. On-sample water content measurement for a complete local monitoring in triaxial testing of unsaturated soils. *Géotechnique*, 62(7), pp.595-604.
- Muhammed, R.D., 2016. Etude en chambre d'étalonnage du frottement sol-pieu sous grands nombres de cycles. Application au calcul des fondations profondes dans les sols fins saturés. *Ph.D. thesis, Université Paris-Est, France*.
- Murphy, K.D. et al., 2013. Evaluation of thermo-mechanical and thermal behavior of full-scale energy foundations. *Acta Geotechnica*, 10 (2), pp.179-195
- Murphy, K.D. et al., 2014. Thermo-Mechanical Characterization of a Full-Scale Energy Foundation. In *From Soil Behavior Fundamentals to Innovations in Geotechnical Engineering Conference*. Atlanta, Georgia, United states, pp. 617–628.
- Murphy, K.D. & McCartney, J.S., 2014. Seasonal Response of Energy Foundations During Building Operation. *Geotech Geol Eng*, 33(2), pp.343–356.

- NF P 94-110-1, Essai pressiométrique Ménard. , 33(0), pp.38–39.
- Ng, C.W.W. et al., 2014. Centrifuge modelling of energy piles subjected to heating and cooling cycles in clay. *Géotechnique Letters*, 4, pp.310–316.
- Ng, C.W.W. et al., 2015. Centrifuge modelling of heating effects on energy pile performance in saturated sand. *Canadian Geotechnical Journal*, 52(8), pp.1045–1057..
- Ng, C.W.W. et al., 2016a. Water retention and volumetric characteristics of intact and re-compacted loess. *Canadian Geotechnical Journal*, 53(08), pp.1258-1269.
- Ng, C.W.W. et al., 2016b. Horizontal stress change of energy piles subjected to thermal cycles in sand. *Computers and Geotechnics*, 78, pp.54–61.
- Nguyen, V.T. et al., 2017a. Water retention and thermal conductivity of a natural unsaturated loess. *Géotechnique Letters*, 7(4): pp.286-291.
- Nguyen, V.T. et al., 2017b. Long-term thermo-mechanical behavior of energy pile in dry sand. *Acta Geotechnica*, 12(4): pp.729-737.
- Nicholson, D.P. et al., 2013. Developments in thermal piles and thermal tunnel lining for city scale GSHP systems. *Thirty-Eighth Workshop on Geothermal Reservoir Engineering*. Stanford University, Stanford, California.
- Oh, W.T. et al., 2008. Shear strength characteristics of statically compacted kaolin. *Canadian Geotechnical Journal*, 45(7), pp.910–922.
- Olgun, C.G. & McCartney, J.S., 2014. Outcomes from International Workshop on Thermoactive Geotechnical Systems for Near-Surface Geothermal Energy: from research to practice. *DFI Journal-The Journal of the Deep Foundation Institute*, 8(2), pp.59–73.
- Olgun, C.G. et al., 2015. Long-term performance of heat exchanger piles. *Acta Geotechnica*, 10(5), pp.553–569.
- Omer, A.M., 2008. Ground-source heat pumps systems and applications. *Renewable and Sustainable Energy Reviews*, 12(2), pp.344–371.
- Ozgener, O. & Hepbasli, A., 2007. A review on the energy and exergy analysis of solar assisted heat pump systems. *Renewable and Sustainable Energy Reviews*, 11(3), pp.482–496.
- Ozudogru, T.Y. et al., 2015. Numerical Modeling of Vertical Geothermal Heat Exchangers Using Finite Difference and Finite Element Techniques. *Geotechnical and Geological Engineering*, 33, pp.291–306.
- Pahud, D. & Hubbuch, M., 2007. Measured Thermal Performances of the Energy Pile System of the Dock Midfield at Zürich Airport. *Proceeding European Geothermal Congress 2007* (Unterhaching, Germany), pp. 1–7.
- Pao, H.-T. & Tsai, C.-M., 2010. CO2 emissions, energy consumption and economic growth in BRIC countries. *Energy Policy*, 38(12), pp.7850–7860.
- Pasten, C. & Santamarina, J.C., 2014. Thermally Induced Long-Term Displacement of Thermoactive Piles. *Journal of Geotechnical and Geoenvironmental Engineering*,

140(5), p.6014003.

- Payne, K. et al., 2010. Squeezing the heat out of London's Tube. *Proceedings of the ICE - Civil Engineering*, 163(3), pp.114–122.
- Permchart, W. & Tanatvanit, S., 2009. Study on Using the Ground as A Heat Sink for A 12,000-Btu/h Modified Air Conditioner. *World Academy of Science, Engineering and Technology*, (51), pp.15–18.
- Pham Q.H. et al., 2005. A study of hysteresis models for soil-water characteristic curves. *Canadian Geotechnical Journal*, 42(6), pp.1548-1568.
- Phillip, J.R. & De Vries, D.A., 1957. Moisture Movement in Porous Materials under Temperature Gradients. *EOS Trans*, 38, pp.222–232.
- Popiel, C.O. et al., 2001. Measurements of temperature distribution in ground. *Experimental Thermal and Fluid Science*, 25(5), pp.301–309.
- Poulos, H.G., 1982. Influence of Cyclic Loading on Axial Pile Response. *Proc. 2<sup>nd</sup> Conference on Numerical Methods in Offshore Piling*, Austin, Texas, pp.419-440.
- Pouloupatis, P.D. et al., 2011. Measurements of ground temperatures in Cyprus for ground thermal applications. *Renewable Energy*, 36(2), pp.804–814.
- Rees, S.W. et al., 2000. Ground heat transfer effects on the thermal performance of earth-contact structures. *Renewable and Sustainable Energy Reviews*, 4, pp.213–265.
- Resch, G. et al., 2008. Potentials and prospects for renewable energies at global scale. *Energy Policy*, 36(11), pp.4048–4056.
- Riederer, A.P. et al., 2007. Conception de fondations géothermiques. *Rapport final\_CSTB, Département Energie Santé Environnement, Pole Energie Renouvelables*. France
- Rotta Loria, A.F. & Laloui, L., 2016. The interaction factor method for energy pile groups. *Computers and Geotechnics*, 80, pp.121–137.
- Rutqvist, J. et al., 2001. Thermohydromechanics of partially saturated geological media: Governing equations and formulation of four finite element models. *International Journal of Rock Mechanics and Mining Sciences*, 38(1), pp.105–127.
- Sadorsky, P., 2009. Renewable energy consumption and income in emerging economies. *Energy Policy*, 37(10), pp.4021–4028.
- Saggu, R. & Chakraborty, T., 2015. Cyclic Thermo-Mechanical Analysis of Energy Piles in Sand. *Geotechnical and Geological Engineering*, 33(2), pp.321–342.
- Sagia, Z. et al., 2012. Cooling dominated Hybrid Ground Source Heat Pump System application. *Applied Energy*, 94, pp.41–47.
- Singh, R.M. et al., 2011. Geothermal Energy Pile: Thermal cum Static Load Testing. *Australian Geothermal Energy Conference 2011*. pp. 245–248.
- Smits et al., 2013. Temperature dependence of thermal properties of sands across a wide range of temperatures (30-70°C). *Vadose Zone Journal*, 12 No.1.

- Stewart, M.A. et al., 2014. Centrifuge Modeling of Soil-Structure Interaction in Energy Foundations. *Journal of Geotechnical and Geoenvironmental Engineering*, 140 (4) , pp.1–11.
- Stewart, M.A. & McCartney, J.S., 2013. Centrifuge Modeling of Soil-Structure Interaction in Energy Foundations. *Journal of Geotechnical and Geoenvironmental Engineering*, 140(4), p.4013044.
- Sultan, N. et al., 2002. Temperature effects on the volume change behaviour of Boom clay. *Engineering Geology*, 64 (2002), pp.135–145.
- Suryatriyastuti, et al., 2012. Understanding the temperature-induced mechanical behaviour of energy pile foundations. *Renewable and Sustainable Energy Reviews*, 16(5), pp.3344–3354.
- Suryatriyastuti, et al., 2014. A load transfer approach for studying the cyclic behavior of thermo-active piles. *Computers and Geotechnics*, 55, pp.378–391.
- Tang A.M. et al., 2008. A study on the thermal conductivity of compacted bentonites. *Applied Clay Science*, 41(3-4), pp.181-189.
- The World Bank, 2007. Growth and CO2 Emissions: How do Different Countries Fare, Washington, DC.
- Thomas, H.R. & Rees, S.W., 2009. Measured and simulated heat transfer to foundation soils. *Géotechnique*, 59(4), pp.365–375.
- Uchida, Y. et al., 2011. Subsurface Temperature Survey in Thailand for Geothermal Heat Pump Application. *Journal of the Geothermal Research society of Japan*, 33(2), pp.93–98.
- Usowicz, B. et al., 2016. The effect of biochar application on thermal properties and albedo of loess soil under grassland and fallow. *Soil and Tillage Research*, 164, pp.45-51.
- Vargas, W.L. & McCarthy, J.J., 2007. Thermal expansion effects and heat conduction in granular materials. *Physical Review E - Statistical, Nonlinear, and Soft Matter Physics*, 76(4 pt 1): 041301.
- Vieira, A. & Maranha, J.R., 2016. Thermoplastic Analysis of a Thermoactive Pile in a Normally Consolidated Clay. *International journal of Geomechanics*, 17(1), 2017:4016030. Doi:10.1061/(ASCE)GM.1943-5622.0000666.
- Wang, B. et al., 2014. Posttemperature Effects on Shaft Capacity of a Full-Scale Geothermal Energy Pile. *Journal of Geotechnology and Geoenvironmental Engineering*, 141(4), 04014125. Doi: 10.1061/(ASCE)GT.1943-5606.0001266.
- Wang, H. & Qi, C., 2008. Performance study of underground thermal storage in a solar-ground coupled heat pump system for residential buildings. *Energy and Buildings*, 40(7), pp.1278–1286.
- Yang, C. et al., 2008. A constitutive model for unsaturated cemented soils under cyclic loading. *Computer and Geotechnics*, 35(6), pp.853-859.
- Yasukawa, K. et al., 2009. Groundwater Temperature Survey for Geothermal Heat Pump Application in Tropical Asia. *Bulletin of the Geological Survey of Japan*, 60(9/10),

pp.459–467.

- Yavari, N. et al., 2014a. Experimental study on the mechanical behaviour of a heat exchanger pile using physical modelling. *Acta Geotechnica*, 9(3), pp.385–398.
- Yavari, N. et al., 2014b. A simple method for numerical modelling of mechanical behaviour of an energy pile. *Géotechnique Letters*, 4(2), pp.119–124.
- Yavari, N. 2014. Aspects géotechniques des pieux de fondation énergétiques. *Ph.D. thesis*, Université Paris-Est, France.
- Yavari, N. et al., 2016a. Mechanical behaviour of a small-scale energy pile in saturated clay. *Geotechnique*, 66(11), pp.878–887.
- Yavari, N. et al., 2016b. Effect of temperature on the shear strength of soils and soil/structure interface. *Canadian Geotechnical Journal*, 53(7), pp.1186–1194.
- Yavuzturk, C. & Spitler, J.D., 1999. A Short Time Step Response Factor Model for Vertical Ground Loop Heat Exchangers. *ASHRAE transactions*, 105(2), pp.475–485.
- Yun T.S. and Santamarina J.C., 2008. Fundamental study of thermal conductivity in dry soils. *Granular Matter*, 10(3), pp.197–207.
- Zeng, H.Y., et al., 2002. A finite line-source model for boreholes in geothermal heat exchangers. *Heat Transfer Asian Research*, 31(7), pp.558–567.
- Zhang, H. et al., 2011. Comparison of renewable energy policy evolution among the BRICs. *Renewable and Sustainable Energy Reviews*, 15(9), pp.4904–4909.